

Validation and Documentation of Tensile Strain Limit Design Models for Pipelines

Contract PR-ABD-1 – Project 1

Final Report

**Prepared for the
Design, Materials, and Construction Technical Committee
of
Pipeline Research Council International, Inc**

**Prepared by
Center for Reliable Energy Systems
Yong-Yi Wang, Ming Liu, and Xin Long**

**C-FER Technologies (1999) Inc.
Mark Stephens and Randy Petersen**

**Microalloying International
Robin Gordon**

August 2, 2011

Version	Date of Last Revision	Date of Uploading	Comments
1.1	October 12, 2010	October 12, 2010	
1.2	May 31, 2011	May 31, 2011	
1.3	August 2, 2011	August 2, 2011	Final

Notice

This report is furnished to Pipeline Research Council International, Inc. (PRCI) under the terms of PRCI contract PR-ABD-1-Project 1, between PRCI and ABD-1 contractors: Center for Reliable Energy Systems ("CRES"), C-FER Technologies (1999) Inc. ("C-FER"), and Microalloying International.

The contents of this report are published as received from the ABD-1 contractors. The opinions, findings, and conclusions expressed in the report are those of the authors and not necessarily those of PRCI, its member companies, or their representatives. Publication and dissemination of this report by PRCI should not be considered an endorsement by PRCI of the ABD-1 contractors, or the accuracy or validity of any opinions, findings, or conclusions expressed herein.

In publishing this report, PRCI and the ABD-1 contractors make no warranty or representation, expressed or implied, with respect to the accuracy, completeness, usefulness, or fitness for purpose of the information contained herein, or that the use of any information, method, process, or apparatus disclosed in this report may not infringe on privately owned rights. PRCI and the ABD-1 contractors assume no liability with respect to the use of, or for damages resulting from the use of, any information, method, process, or apparatus disclosed in this report. By accepting the report and utilizing it, you agree to waive any and all claims you may have, resulting from your voluntary use of the report, against PRCI and the ABD-1 contractors.

©2010, Pipeline Research Council International, Inc., all rights reserved. The contents of this publication, or any part thereof, may not be reproduced or transmitted in any form by any means, electronic or mechanical, including photocopying, recording, storage in an information retrieval system, or otherwise, without the prior, written approval of PRCI.

Pipeline Research Council International Catalog No. L5XXXX

All Rights Reserved by Pipeline Research Council International, Inc.

PRCI Reports are Published by Technical Toolboxes, Inc.

3801 Kirby Drive, Suite 520

Houston, Texas 77098

Tel: 713-630-0505

Fax: 713-630-0560

Email: info@ttoolboxes.com



List of Funding Partners

BP
Chevron
Spectra Energy
El Paso
Enbridge
ExxonMobil
Gaz de France
Petrobras
Southern California Gas Company
TransCanada
Williams
Lincoln Electric
Tenaris
Evraz Inc NA
ConocoPhillips Company
JFE
NSC
Sumitomo Metal Industries
PHMSA
PRCI

Responsibilities and Acknowledgement

The work reported here reflects the joint efforts of principally three organizations, Center for Reliable Energy Systems, C-FER Technologies, and Microalloying International. The lead organizations responsible for the sections of this report are listed below.

Section 1	CRES,
Section 2	Microalloying International,
Section 3	CRES,
Section 4	CRES,
Section 5	C-FER,
Section 6	CRES and C-FER,
Section 7	CRES,
Section 8	CRES.

Many individuals provided valuable contributions throughout this multi-year effort. The project team is particularly grateful to the guidance and encouragement of Mr. David Horsley of BP for the entire duration of this project. Mr. David Horsley, Dr. Joe Zhou of TransCanada, and Dr. Laurie Collins of Evraz NA served as the project technical managers during various phases of this project. Mr. Chris McLaren of PHMSA served as the technical manager from the US Department of Transportation. He has provided many insightful inputs to the project. Mr. Ken Lorang of PRCI, who was the project manager from PRCI, was a constant and persistent driving force behind all project activities.

Representatives of project funding partners have provided constructive suggestions throughout the course of this project. Of particular note, in recognition of their active participation, are Dr. Paulo Gioielli of ExxonMobil, Dr. Pedro Vargas of Chevron, and Dr. V. B. Rajan of Lincoln. The project team is grateful to Dr. Tom Zimmerman of Enbridge for his central role in the preliminary development of the large-scale experimental test program.

The project team wishes to dedicate this work to the late Ms. Marina Smith whose enthusiasm and support for this project were evident whenever and wherever she was present.

Finally, we wish to thank the line pipe manufacturers for their donation of the pipe materials.



Validation and Documentation of Tensile Strain Limit Design Models for Pipelines

Executive Summary

Pipelines may experience significant longitudinal strains in areas subject to large ground movements. Such movements may result from frost heave and thaw settlements in arctic regions, seismic activities, mine subsidence, and other natural occurrences. *Strain-based design* (or SBD), can be advantageous both technically and economically for pipelines that are expected to experience high levels of longitudinal strain. In North America, the need for SBD is primarily driven by the anticipated pipeline projects in the far north where the pipeline routes will traverse regions of discontinuous permafrost. In other parts of the world, SBD is playing an increasingly important role in the design of pipelines passing through areas of seismic activity and mine subsidence. Existing pipelines world-wide also face ground movement hazards such as landslides and seismic events. SBD is also applicable to integrity maintenance and risk assessment.

SBD encompasses both strain demand (applied strain) and strain capacity (strain limit). At least two limit states are associated with SBD: *tensile rupture* and *compressive buckling*. This project deals specifically with the tensile rupture limit state. This limit state is an ultimate limit state, and exceeding this limit results in the loss of product containment and the potential for loss of life and property, damage to the environment, and disruption of service.

A major focus of the large-scale test program carried out within this project was to assess the effect of internal pressure on tensile strain capacity. Preliminary work carried out prior to the start of the project indicated that the tensile strain capacity could be reduced by the application of internal pressure. However, no conclusive public domain test data was available to substantiate this concern. Previously, curved-wide-plate (CWP) tests had been relied on as the benchmark for determining the tensile strain capacity. If the detrimental effects of internal pressure were substantiated, strain capacity estimates based on CWP test data would be shown to be non-conservative.

A large number of paired tests, involving full-scale pipe specimens with and without pressure, were conducted within this project to investigate the effects of internal pressure. To ensure that high-quality, consistent, and useful test results were obtained, extensive pre-test analysis was conducted to determine the proper specimen dimensions, flaw placement location, flaw size, and internal pressure level. Careful consideration was also given to instrumentation plan and post-test data analysis and interpretation. The large-scale tests were accompanied by extensive small-scale material characterization tests. An exhaustive post-test physical examination of the full-scale specimens was also conducted to provide corroborative evidence of the behavior of the flaws. The large-scale tests were also simulated numerically to establish the correlation between the small and large-scale behavior.

The large-scale experimental test results conclusively demonstrated that the internal pressures consistent with Classes 1 and 2 designs can reduce the strain capacity of pipelines with circumferential planar flaws by 50% or more. While the large-scale test results provide the basis for some general findings, regarding the effect of internal pressure and other key parameters on strain capacity, the variability in the results obtained from duplicate tests involving effectively identical flaws serves to highlight the high sensitivity of strain capacity to small changes in the inelastic stress-strain response of pipe body, weld metal, and heat-affected zone (HAZ).

Based on the work completed thus far, following practical considerations are recommended for strain-based design.

- (1) *Reduce strain demand.* This may be accomplished through judicious selection of pipeline routes which impose low strain demands, using specially designed trenches and backfill, and other strain reduction methods.
- (2) *Select appropriate line pipe.* A few characteristics that are beneficial to strain capacities are (1) high strain hardening and (2) an upper bound to the strength distribution that is as low as possible for manufacturing and yet high enough to meet the minimum specification requirements. Suitable specifications and verifications throughout the line pipe manufacturing processes are necessary to ensure the expected properties are achieved.
- (3) *Minimize the likelihood of gross strain concentration at welds.* This can be achieved by controlling the high-low misalignment at the girth welds and having sufficient weld metal strength overmatching.
- (4) *Ensure upper-shelf toughness behavior.* The materials need to behave in a ductile manner at the lowest expected service temperature.
- (5) *Balance the selection of pipe grade and pipe wall thickness.* Thicker-walled pipe of a lower grade may be more appropriate in areas of high strain demand. Lower grade pipe material does not automatically lead to high strain capacity, but it offers the potential for higher strain capacity, since the resulting thicker wall provides greater design flexibility.
- (6) *Control flaw size and distribution.* Girth weld flaws need to be controlled using appropriate welding and NDT procedures. However, overly restrictive flaw size limits may lead to excessive repairs, which can be counterproductive with respect to the overall pipeline quality and economy.
- (7) *Follow a rigorous program of material qualifications, including consistent and robust test procedures.* It is necessary to ensure all test data are generated using a consistent set of test procedures among all labs, including specimen fabrication, instrumentation, data reduction, and reporting.

Although this work is the product of a large multi-year effort, there are certain limitations associated with the work scope which was carried out. Anticipated strain-based design projects would most likely involve pipes of larger diameters manufactured to different material

specifications. In addition, girth weld high-low misalignment, a parameter not directly explored in the large-scale test program, is being increasingly considered to have a significant influence on the tensile strain capacity. Lastly, the inherent variability in the strain capacity, as exhibited in the testing of the duplicate specimens, highlights the need for more tests to further examine the sources of this variability and to provide a statistically sound basis for its quantification.



Table of Contents

Notice	i
List of Funding Partners	ii
Responsibilities and Acknowledgement	iii
Executive Summary	iv
1 Introduction	1
1.1 Incentives of the Project	1
1.2 Overview of Strain-Based Design	1
1.3 Strain Demand on Pipelines	1
1.3.1 Strain Demand under Seismic Activities	2
1.3.2 Strain Demand in Arctic Region	3
1.4 Tensile Strain Capacity (TSC)	3
1.4.1 Overview	3
1.4.2 Status of Current Technology in TSC	3
1.5 Compressive Strain Capacity	7
1.6 Incentives for This Work - Effects of Internal Pressure	8
1.7 Objectives	10
1.8 Overall Work Plan of the Consolidated Program	11
2 Line Pipe Procurement and Welding	13
2.1 Introduction	13
2.2 Pipe Materials	14
2.2.1 General	14
2.2.2 Grade X65 Pipe Material (Low Y/T)	14
2.2.3 Grade X65 Pipe Material (High Y/T)	15
2.2.4 Grade X80 Pipe Material	15
2.3 Parent Pipe Tensile Properties	16
2.3.1 Grade X65 Pipe Materials	16
2.3.2 Grade X80 Pipe Material	18
2.4 Grade X65 Girth Weld Fabrication	19
2.4.1 General	19
2.4.2 Grade X65 Weld Procedure Development Trials	20
2.4.3 Grade X65 Weld Procedures	22
2.4.4 Grade X65 Girth Weld Fabrication	22
2.5 Grade X80 Girth Weld Fabrication	28
2.5.1 Weld Procedure Development Trials	28
2.5.2 Grade X80 Weld Procedures	30
2.5.3 Grade X80 Girth Weld Fabrication	30
3 Small-scale Material Characterization Tests	32
3.1 Background and Objectives	32
3.1.1 Overview of the Welds	32

3.1.2	Sources of Data	32
3.1.3	Scope of the Small-scale Tests	34
3.2	Weld Macro	34
3.3	Hardness Map	34
3.4	Line pipe Tensile Properties	39
3.4.1	Tensile Properties of X65 12-Inch High Y/T Pipe	39
3.4.2	Tensile Properties of X65 12-Inch Low Y/T Pipe	39
3.4.3	Tensile Properties of X80 24-Inch Pipes	42
3.5	Girth Weld Tensile Properties and Weld Strength Mismatch	46
3.5.1	Tensile Properties of 1 st Production Girth Welds	46
3.5.2	Tensile Properties of 2 nd Production Girth Weld	46
3.5.3	Tensile Properties of Girth Welds for 12-Inch Low Y/T Pipe	50
3.5.4	Tensile Properties of Girth Welds for 24-Inch X80 Pipe	50
3.6	Summary of Tensile Properties	52
3.7	Girth Weld Toughness	54
3.7.1	Charpy Transition Curves	54
3.7.2	CTOD Transition Curves from SENB Specimens	55
3.7.3	Toughness Transition from SENT Specimens	55
3.8	Major Observations from the Small-Scale Toughness Tests	55
4	Pre-Test Analysis	63
4.1	Objectives and Scope	63
4.2	Curved Wide Plate Tests	64
4.2.1	Specimen Geometry and Strain Measurement Procedure	64
4.2.2	Initial Flaw Size	65
4.2.3	Unloading Magnitude	66
4.3	Full Scale Pipe Tests	70
4.3.1	Specimen Geometry and Strain Measurement Procedure	70
4.3.2	Flaw Size	71
4.3.3	Pressure	71
4.4	Pre-Test Analysis Summary	74
5	Large-Scale Tests	76
5.1	Overview	76
5.2	Test Program Design	77
5.2.1	Pipe Tests	77
5.2.2	Curved Wide Plate Tests	84
5.3	Test Results	90
5.3.1	Pipe Tests	90
5.3.2	Curved Wide Plate Tests	92
5.4	Results Summary and Discussion	97
5.4.1	Specimens Fabricated from 12.75-inch Diameter Pipe	97
5.4.2	Specimens Fabricated from 24-inch Diameter Pipe	107

5.5	Appendix 5A - 5D	108
6	Post-Test Physical Examination	109
6.1	Background and Objectives	109
6.2	Flaws Subjected to Detailed Examination	109
6.3	Flaw Examination Results	109
6.3.1	Non-Breaching Flaws	109
6.3.2	Wall-Breaching Flaws	126
6.4	Summary of Post-Test Examination Results and Observations	133
6.5	Appendix 6A	134
7	Post-Test Data Summary and Correlation	136
7.1	Objectives and Work Scope	136
7.2	Variation of Test Results under “Identical” Conditions	136
7.2.1	Load vs. Remote Strain	136
7.2.2	CMOD versus Remote Strain	136
7.3	Stress-Strain Curves Used in FEA	136
7.4	Introduction to FEA Model	140
7.5	Overall Trend in the Comparison of Test and FEA Results	140
7.6	Effect of Test Parameters	141
7.6.1	Internal Pressure	141
7.6.2	Specimen Type – Full-Scale Pipe vs. CWP	141
7.6.3	Flaw Size	141
7.6.4	Temperature	141
7.7	Effect of Stress-Strain Curves on Simulation Results	151
7.8	Effect of Flaw Growth on Simulation Results	151
7.9	Summary of Post-Test Analysis	154
8	Concluding Remarks	157
8.1	Overview of the Project	157
8.2	Major Observations of the Tests	157
8.3	Discussion of a Few Important Features	158
8.3.1	Effects of Test Temperature	158
8.3.2	Tensile Property Variations	159
8.4	Practical Considerations for SBD	162
8.5	Limitation of the Current Project	163
8.6	Future Work	163
9	References	165

1 Introduction

1.1 Incentives of the Project

Pipelines may experience large longitudinal strains in areas subjected to significant ground movements. Such movements may come from frost heave and thaw settlements in arctic regions, seismic activities, mine subsidence, and other natural occurrences. For offshore pipelines, large longitudinal strains may be induced within certain spans by thermal expansion or displacement of pipelines due to underwater landslides. *Strain-based design* or SBD is often necessary technically and economically for pipelines expected to experience high longitudinal strains.

SBD refers to pipeline design methodologies with a specific goal of maintaining pipeline service and integrity under large longitudinal plastic deformation (often defined as longitudinal strain greater than 0.5%). Such deformation is frequently displacement-controlled, although combined displacement- and load-controlled events are possible. In contrast, traditional pipeline design is stress-based, in which the applied stress is kept below the specified minimum yield stress (SMYS). As the SMYS is typically defined as the yield strength measured at 0.5% total strain, the stress-based design limits the longitudinal strain to less than 0.5%.

In North America, the need for SBD is primarily driven by the anticipated pipeline projects in the far north where pipelines traverse regions of discontinuous permafrost. In other parts of the world, SBD is playing an increasingly important role for pipelines going through areas of seismic activities and mine subsidence. One such example is the Second West-East Pipeline in China for which SBD was applied to several hundred kilometers of the pipeline. Many in-service pipelines world-wide also face ground movement hazards such as landslides and seismic events. SBD may be employed for maintenance and risk assessment.

1.2 Overview of Strain-Based Design

SBD encompasses both strain demand (applied strain) and strain capacity (strain limit). At least two limit states are associated with SBD: *tensile rupture* and *compressive buckling*. The consequence of the two limit states could be quite different. *Tensile rupture* is an ultimate limit state which leads to the breach of pressure boundary. The consequence of exceeding the limit state could be very serious, including potential loss of life and property, contamination of environment, and interruption of service. *Compressive buckling* could be either a service limit state or an ultimate limit state. If a rupture occurs due to compressive buckling, the consequence is the same as for tensile rupture. In many cases, compressive buckling does not lead to immediate rupture. However, delayed rupture can occur from cyclic loads and high risk of corrosion damage.

1.3 Strain Demand on Pipelines

Determining the strain demand can be a very complex undertaking, with the exception of offshore pipe reeling, in which the strain demand can be easily computed from the geometry of

the lay vessel. For onshore pipelines, estimating strain demand involves multiple disciplines such as geology, seismology, soil mechanics, and soil-pipe interaction.

Large longitudinal strains may be generated by a number of sources. The most relevant events for onshore pipelines are seismic activities, slope movements, and arctic hazards.

1.3.1 Strain Demand under Seismic Activities

Seismic activities (earthquakes) can cause permanent ground deformation (PGD) and transient ground deformation (TGD). PGD is irrecoverable ground movement from liquefaction, surface-faulting, and landslides. TGD is from wave propagation of earthquake induced ground shaking.

1.3.1.1 Strain Demand from Surface Faulting

Surface faulting could occur in one plane or in all three dimensions. Large tensile and compressive strains can be generated from surface faulting. Initially, the strains imposed on the pipelines increase with the amount of fault movement. The strains would typically saturate after a certain amount of fault movement, as the pipes start to shear through the soil, assuming the pipes are strong enough to withstand the loads up to the saturated strain levels.

Estimating the amount of fault movement at the specific fault crossings requires geological assessment, field trenching surveys, and seismo-tectonic models [1]. Empirical relations based on past seismic events may be used to estimate the amount of fault movement [2].

Pipe-soil interaction models play a critical role in determining the strain level imposed on the pipelines. Soil springs representing the soil's resistance in the axial, lateral, and vertical directions are used in the pipe-soil interaction models [3]. Field survey of soil conditions can provide appropriate soil data of a specific fault crossing.

It should be recognized that the amount of strain imposed on the pipeline is the result of the interaction between pipe and surrounding soil. Consequently, the characteristics of the pipelines also affect the strains on the pipes. The “strain demand” is intrinsically related to the strain capacity of the pipes. For instance, internal pressure affects the stiffness of the pipelines, and therefore, the response of the pipelines to the ground movements.

1.3.1.2 Strain Demand from Lateral Spreading

In an event of earthquake, soils beneath the surface layer could liquefy. A buried pipeline could move down-slope due to gravity and inertial effects as the pipeline loses the soil support. This event is called lateral spreading, which can occur theoretically in any direction. Past earthquakes have generated lateral spreading as high as several meters. Consequently, large longitudinal straining can occur by lateral spreading.

1.3.1.3 Strain Demand from Seismic Wave Propagation

The amount of ground displacement from seismic wave propagation is generally much smaller than those by fault crossing and lateral spreading. However, seismic wave can affect a

large area, thus a long section of a pipeline. The amount of strain generated in a pipeline depends on the magnitude of the ground strain and transmission of the ground strain to the pipeline. Shallow burial in less stable soils enables relative slip between the pipe and ground. Consequently, a lower level of strains is transmitted to these pipelines than the pipelines with deep burial and dense soils.

1.3.2 Strain Demand in Arctic Region

1.3.2.1 Strain Demand from Frost Heave and Thaw Settlement

Buried pipelines may experience high longitudinal strains due to frost heave and thaw settlement. In the case of frost heave, the pipeline is pushed upward by the expansion of the soil beneath it. As the deformation is restrained by the frozen soil on either side of the heaving span, both tensile and compressive strains can be generated. These strains generally grow over time if no mitigation is performed. Similarly, pipelines can settle downward if the pipelines are installed in frozen soil and operated at a temperature above that of the surrounding soil.

1.3.2.2 Strain Demand from Ice Scouring

A floating iceberg may drag its keel along the sea bottom, with portions digging into the sea floor. Buried pipelines beneath the sea floor may be pushed by the keel of the iceberg, thereby generating high strains in the pipelines. This event is termed ice scouring.

Estimating strain demand from ice scouring requires special knowledge and tools. An in-depth treatment of ice scouring is given by Kenny [4].

1.4 Tensile Strain Capacity (TSC)

1.4.1 Overview

The tensile strain capacity of a pipeline is controlled by the tensile strain capacity of its girth welds. The girth welds here refer to the entire weld region, including the weld metal, fusion boundary, and the heat-affected zone (HAZ). Girth welds tend to be the weakest link due to the possible existence of weld defects and often deteriorative metallurgical and/or mechanical property changes from welding thermal cycles. Certain base metal (pipe material) properties are a critical part of the girth weld strain capacity, as they affect the metallurgical and mechanical properties of the weld region. For instance, the chemical composition of the base metal plays a critical role in the propensity of hydrogen cracking and HAZ softening, which can have a significant impact on the tensile strain capacity of the pipeline.

1.4.2 Status of Current Technology in TSC

1.4.2.1 Wide Plate Test as a Design and Validation Tool

Wide plate testing has been one of the most recognized tools for determining girth weld tensile strain capacity. The test specimen is a curved piece of pipe with a nominal gauge width of 200 to 450 mm and is loaded in longitudinal tension. The specimen is often termed curved wide plate or CWP. The girth weld in the middle of the specimen has a machine-notched or

fatigue sharpened flaw. The strain across the weld is monitored while the specimen is pulled longitudinally until failure occurs. Many organizations now have CWP testing capabilities, including the University of Gent, C-FER, Stress Engineering Services, National Institute of Standards and Technology (NIST), Evraz, JFE, Nippon Steel Corporation, and POSCO.

Wide plate testing has been used as a tool for material and weld procedure qualification [5]. It has also been used for project-specific design validation. A large database of the failure strains of girth welded pipes has been established from wide plate tests [6].

A few noted shortcomings of the past CWP tests are:

- (1) There are no universally accepted test standards governing the specimen dimensions, instrumentation, data acquisition and post-test processing. A study has shown that the specimen width, weld strength mismatch, and specimen length have strong impacts on the reported failure strains when the failure strains are measured in the most commonly used form [7].
- (2) The effects of internal pressure on tensile strain capacity cannot be readily evaluated from wide plate tests.
- (3) As noted in later sections, girth weld high-low misalignment can affect the tensile strain capacity. When a wide plate specimen with high-low misalignment is pulled longitudinally, the two halves of the specimens on either side of the girth weld are more easily aligned with the loading path than the same girth weld in the full-circumference pipe. The relative motion (to align the weld with the loading path) of the two halves on either side of the pipe is restrained by the entire pipe circumference. Consequently, the effects of the misalignment in a full pipe may not be fully represented by a CWP specimen.

The shortcomings No. (2) and No. (3) are associated with the particular CWP specimen geometry and there is little one can do to overcome them. The shortcoming No. (3) is associated with prior wide plate test data.

With respect to the shortcoming No. (1), significant progress has been made in recognizing the importance of the test specimen and procedure consistency [7]. Denys, et al., has published a recommended testing procedure of CWP specimens [8]. The research team of a joint US DOT and PRCI project is also working on a “standard” CWP testing procedure [9].

Much of the recommended practices from References [8,9] have been implemented in this project.

1.4.2.2 Extension of Stress-Based Design Procedures for Strain-Based Design

Section G100 of DNV OS-F101 [10] provides guidance on the determination of girth weld defect acceptance criteria for strain-based design conditions. It states that the unstable fracture assessment method in Level 3 of BS 7910 [11] is formulated for stress-based assessments and is therefore, not directly applicable for strain-based design. Guidelines on input parameters are given in F101 so the format of BS 7910 can still be used. A number of key input parameters are

covered in the guidelines, including (1) the selection of appropriate stress-strain curves for flaws located in the weld metal and HAZ, (2) the treatment of strain concentration, and (3) the treatment of residual stress. The guidelines also caution that the confirmation of predominantly displacement-controlled loading is necessary to safely use strain-based design. Extensive guidance is provided on the fracture toughness testing. The suggested test method is using shallow-cracked SENB (single-edge-notched bend) specimens, although tension loaded specimens are also allowed.

DNV OS RP F108 [12] provides further guidance on the engineering critical assessment (ECA) of girth welds for installation by reeling. The recommended toughness testing procedure is a multiple-specimen SENT (single-edge-notched tension) procedure with further qualification and validation. The resistance curve obtained by the SENT testing is to be used in BS 7910 Level 3 assessment. An integral part of RP F108 is the requirement for the confirmation test in the form of so-called “Sector” specimen. This specimen is similar to a miniature CWP specimen. The defect acceptance criteria are adjusted based on the outcome of the confirmation test. Due to the needs for the compressive loading of the Sector specimen, the specimen’s length-to-width ratio in the reduced-gage section is kept small. However, such a small aspect ratio does not allow the development of uniform strain within the reduced gage section [7]. The transferability of the measured strain within the reduced section to the full-scale pipe is therefore, compromised.

DNV F101 and F108 collectively provide insightful comments related to many complex factors affecting TSC. The implementation of those comments is, in many instances, not prescribed. Therefore, the application of F101 and F108 requires the involvement of well-seasoned experts. The outcome from the application is expected to be different, even among these experts, as the implement of those comments are frequently subjected to different interpretations. Another difficulty with the implementation is the use of Level 3 BS 7910 procedures for strain-based applications. One of the fundamental bases of the Level 3 approach is the existence of a limit load (or plastic collapse load). While the limit load is a good measure of a structure’s load bearing capacity, it is a poor measure of the strain capacity. When the material response is in the plastic range, a small change in the stress can result in a large change in the strain. This is particularly true for modern high-strength line pipe materials which typically exhibit low strain hardening.

DNV F101 and F108 are excellent reference documents for strain-based design. However, the platform of ECA, i.e. Level 3 of BS 7910, is not the most suitable format for strain-based design. It does serve as a useful intermediate step before more suitable formats are developed and validated. In addition, the full implementation of F101 and F108 may be prohibitively expensive for small onshore projects.

1.4.2.3 Crack Driving Force Approach for Strain-Based Design

Since the late 1990’s, PRCI has funded a number of research projects aimed at developing quantitative tensile strain-based design procedures. These projects have utilized the crack

driving force approach, which relied on the relation between the crack driving force (as measured by crack tip opening displacement, or CTOD driving force) and the remote longitudinal strain, taking into account defect size, defect location, material tensile properties, weld strength mismatch, and weld geometry [13,14,15,16]. The crack driving force approach is a modern and more specific version of the CTOD design curve approach [17]. It shares some similarity with the crack driving force (CDF) curve approach of SINTAP [18]. The crack driving force approach eliminates the use of “limit load” and thus overcomes the fundamental difficulties associated with the use of the FAD approach. The tensile strain limit state is assumed to be reached when the crack driving force reaches the apparent toughness of the material.

The most challenging aspect of using the crack driving force approach is the determination of the apparent toughness. The apparent toughness is the toughness measured from specimens with similar constraint conditions as those of pipeline girth welds. There are no codified test standards to measure the toughness of low constraint specimens. Attempts have been made to estimate the apparent toughness from the database generated using standard CTOD specimens (high constraint) [19,20]. Recent work at CRES demonstrated that the apparent toughness may be obtained from small-scale low-constraint specimens [21].

The CTOD driving force approach has been implemented in Annex C of CSA Standard Z662 [22]. Some of the earlier validation against CWP test data is given by Wang, et al. [23]. The implied safety factor against mini-wide plate (without pressure) is shown to be 2-3 [24].

1.4.2.4 Resistance-Curve Approach

The resistance-curve approach is based on instability analysis of ductile failure process. The crack driving forces in terms of CTOD or J -integral are derived from finite element analysis for various material properties and pipe and flaw sizes. Empirical driving force equations are obtained by curve-fitting the finite element results. The resistance curve (R -curve) is directly measured from test specimens. The failure point or the unstable ductile tearing point is determined by the traditional tangency criteria. The representative models based on the R -curve and tangent criteria are the ones developed independently by SINTEF [25,26,27] and ExxonMobil [28,29,30,31]. In the SINTEF's model, the crack driving force curves are developed in the form of CTOD and then converted to J_{app} -integral. The R -curves were presented in the form of J_R -integral. In the ExxonMobil's model, both crack driving force curves and R -curves are presented in the form of CTOD. The SINTEF's driving force equations were published and available to the public. The ExxonMobil's driving force equations are proprietary at this moment.

1.4.2.5 Osaka University and JFE Approach

The Osaka/JFE approach relies on the failure loci relating stress triaxiality to equivalent plastic strain at a crack tip. The so-called two-parameter approach has been applied to a wide variety of fracture mechanics applications [32,33]. The usual route of application is first establishing the failure loci from a combination of small-scale testing and finite element analysis. The ductile initiation is observed at the crack tip from small-scale test specimens. This test is

simulated using finite element analysis. By equating the condition at the point of ductile initiation between the finite element simulation and experimental testing, the failure loci is established from the local crack-tip conditions in the finite element model. The same failure loci are then applied to large-scale structures using finite element analysis. Igi and Suzuki applied this methodology for the prediction of tensile strain limit of X80 pipes [34]. The SENT and CWP specimens were tested to establish the failure loci. Since both of the specimens are considered low constraint, the triaxiality parameter drops out of consideration. The failure condition is effectively determined by the equivalent plastic strain at the ductile initiation. This equivalent plastic strain is then used as the failure criteria in large-scale finite element models to estimate tensile strain limits. Igi and Suzuki demonstrated the effects of internal pressure and Y/T on tensile strain limits using this method. The reduction of tensile strain limits were shown to be a factor of 1.8 for low Y/T material ($Y/T=0.76$) and over 5.0 for high Y/T material ($Y/T=0.95$). A similar method was also applied to X80 and X100 pipes by Sadasue et al. [35].

1.5 Compressive Strain Capacity

The compressive strain capacity of a pipeline is dominated by the diameter to wall thickness ratio (i.e. D/t), design factor (internal pressure), and the shape of the stress-strain curves. In addition, geometric imperfections such as wall thickness and diameter variations, play an important role in the compressive strain capacity.

Pipelines subjected to sufficient compressive or bending strains may fail by either global or local buckling. Local buckling is of most interest to onshore pipelines, and is most likely where displacement controlled loads are present. Equations to predict critical local buckling, defined as the strain at a peak moment, have been developed and adopted by codes such as CSA and DNV. The equations consider factors that influence the buckling limit state, such as pipe diameter, wall thickness, internal pressure, yield strength, and elastic modulus. Often, additional factors are used to account for decreased resistance, such as the presence of a girth weld and the associated material variations, misalignment, and change in diameter due to the contraction of the girth weld. One of the earliest useful equations, developed by Gresnigt [36], considers diameter, thickness, elastic modulus, and the effect of internal pressure. It has been used in codes, including the 2003 edition of CSA Z662. A revised form of the equation is included in the 2007 edition of CSA Z662. DNV OS-F101 uses a different equation, with a weaker dependence on internal pressure, and provides lower estimates of buckling strain than the Gresnigt equation.

The recent interest in high strength pipeline steels has initiated a review of the existing equations in light of the different properties of the high strength steels. It appears that the existing equations behave reasonably well for lower grades of materials (with the exception of over-predicting the pressure effects), but their ability to predict the behavior for high strength pipe has been inconsistent. Several studies are looking at this, with focus on material properties [37] (including anisotropy), and accurate consideration of geometry imperfections in the specimens [38]. Also of concern are the effects of cold bends, which can change pipe properties and create ripples [39, 40].

In addition to the determination of critical buckling strain, there is a keen interest in the behavior in the post buckling region, as it is recognized that the onset of a buckle is not a true limit state, as the pipeline may be safe to operate for some time after the initial onset of the formation of a buckle [41]. For example, a long-term research program on the post-wrinkling behavior of buried pipelines, under various loading conditions, was initiated at the University of Alberta in 1999 [42, 43, 44].

The D/t ratio is widely accepted as a dominant factor in determining the compressive strain capacity of a pipeline. Suzuki found that the finite element analysis tends to overestimate the compressive strain capacity of a pipe, if the geometric imperfections are not modeled [45]. The compressive strain capacity is also affected by the shape of the stress-strain curves. Generally speaking, high strain hardening and round-house stress-strain curves promote high compressive strain capacity [45,46]. The existence of Lüders extension could significantly reduce the compressive strain capacity [46].

1.6 Incentives for This Work - Effects of Internal Pressure

Tensile rupture represents one of the most severe limit states in pipeline service. It is critical to understand the TSC of a pipeline. The TSC of a pipeline is often governed by the TSC of its girth welds. Consequently, the TSC of girth welds has been the subject of intense research activities in the recent years. Experimentally measured TSC can vary from under 0.5% to pipe's uniform elongation (>6%). This is attributable to the large number of factors affecting the TSC. The following factors are known to affect TSC.

- Line pipe material
 - Longitudinal tensile property (strength level, strain hardening, and the shape of the stress-strain curve)
 - Transverse (hoop) tensile property (strength level, strain hardening, and the shape of the stress-strain curve)
 - Steel chemical composition
- Girth weld
 - Weld metal tensile property (strength level or mismatch level with respect to the base pipe, strain hardening, and the shape of the stress-strain curve)
 - Weld metal toughness
 - Weld bevel geometry
 - High-low misalignment
- Interface between the line pipe and weld
 - HAZ toughness
 - HAZ softening
- Weld flaws
 - Flaw location (weld vs. HAZ)

- Flaw orientation
- Flaw size (length and height)
- Flaw position in thickness direction (for buried flaws)
- Pipe geometries
 - Pipe diameter
 - Pipe wall thickness
- Loading
 - Internal pressure
 - Accumulation of plastic strain (low cycle fatigue)
 - Loading rate

Examination of all these factors is nearly impossible in a single project. The stated focus of this project at the start, was the possible detrimental effects of internal pressure on TSC. Research performed in the early to mid 2000's indicated that a softened HAZ and the presence of internal pressure can potentially reduce the TSC of pipeline girth welds [47,48,49]. The possible reduction in tensile strain capacity, due to internal pressure, is a major concern, since previous project-specific experimental studies have all been conducted under uniaxial loading. Preliminary models, which existed at the time, assumed that the TSC is dominated by the longitudinal loading. The model prediction was validated against CWP test results obtained under uniaxial tension. There were no validated models which accounted for the effect of internal pressure. The development of such models was hampered by the lack of experimental test data.

Figure 1.1 shows the effect of the hoop stress (induced by internal pressure) on the CTOD driving force of a girth weld flaw. The solid line shows the case of a 2-mm wide and 15% softened HAZ, and the dotted line shows the case without a HAZ. In the analysis, the hoop stress was applied first by imposing an internal pressure on the pipe, followed by applying a uniform longitudinal displacement. The results show that the CTOD driving force is significantly increased by the hoop stress. The driving force is more sensitive to hoop stress than it is to HAZ softening.

The detrimental effects of internal pressure on TSC were demonstrated by experimental tests since the start of this project in 2006. Østby reported full-scale pipe bend tests intended to verify the effects of internal pressure on tensile strain capacity [50]. The seamless pipes had a nominal outside diameter of 12.75" (323.9 mm) and a nominal wall thickness of 14.9 mm. The nominal surface-breaking flaws were 3 mm deep and 100 mm long. The material had an average yield strength of 484.4 MPa, an ultimate tensile strength of 559.5 MPa, and a uniform elongation of 7.6%. The pipes failed by compressive buckling, without internal pressure, at a nominal strain value of 3.5-4.0%. The application of internal pressure shifted the failure mode to the tension side. The failure strain by tensile rupture was in the range of 1.5-2.0%. Since tensile failures did not occur at the nominal strain value of 3.5-4.0% without internal pressure, it can be argued that

the tensile failure strains would have been greater than 3.5-4.0%. It may be concluded, therefore, that the tensile strain capacity was reduced by at least a factor of 2 or more. Other experimental tests have reported similar results. More extensive coverage of these tests will be provided in Project 2 report.

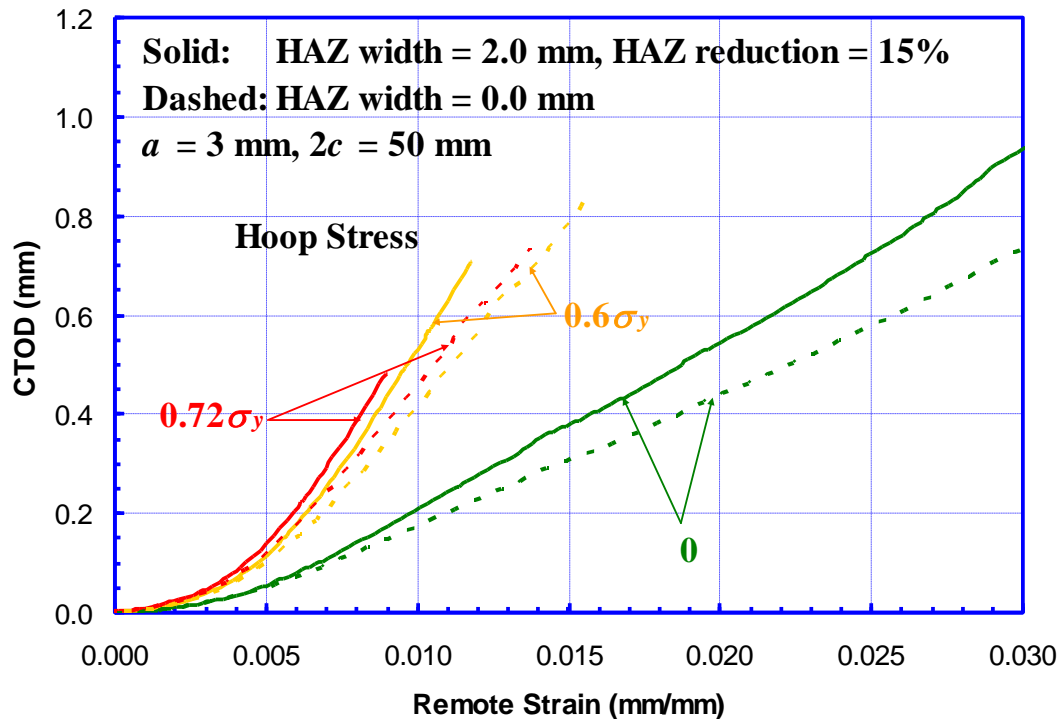


Figure 1.1 Effect of hoop stress on crack driving force (CTOD). Solid lines are cases with 15% HAZ softening. The dashed lines are cases without HAZ softening

1.7 Objectives

The overall objective of this consolidated program is to provide the industry with a tensile strain design procedure in a form that is suitable for citing by pipeline design standards. The objective is accomplished through the execution of two technical projects, namely, Project 1 and Project 2.

The objectives of Project 1 are:

- (1) Obtain high quality test data to demonstrate the effects of internal pressure on TSC
- (2) Using the test data and building on previous work, determine the factors to be included in finite element (FE) models for the prediction of large-scale test results
- (3) Determine revisions needed to improve model accuracy and identify requirements for second generation model developments
- (4) Prepare initial recommendation for tensile strain design.

The objectives of Project 2 are:

- (1) Using the test data of Project 1, develop second generation tensile strain models that incorporate the effects of internal pressure
- (2) Provide practical and comprehensive guidelines on the use of the second generation models.

1.8 Overall Work Plan of the Consolidated Program

The overall work plan is schematically shown in Figure 1.2. One of the major focuses of this program is the large-scale tests, i.e. full scale pipe tests and curved wide plate tests. Significant preparation work was done to ensure the best possible quality data could be generated from the tests [51]. The large-scale test results are then used to evaluate the first generation (existing) models and develop the understanding for the necessary features in the second generation models. The final product of the program is a set of guidelines for tensile strain design and the second generation models.

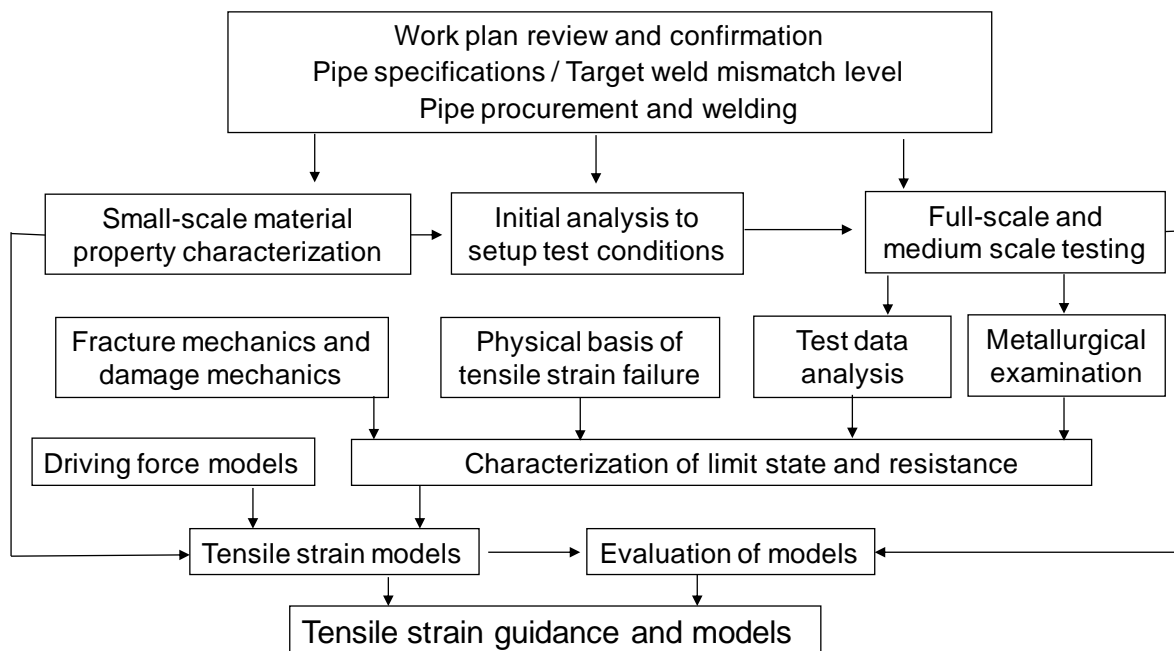


Figure 1.2 Overall work flow plan

The overall work plan followed the steps and sequence below:

1. Review and agree on an overall work approach. This was accomplished at the project launch meeting.
2. Develop line pipe procurement specifications.
3. Procure pipes per the line pipe specifications.
4. Develop girth welding procedures that would procedure welds with target mismatch level. This process involved the initial testing of line pipe tensile properties, so the target weld strength can be developed.
5. Fabricate procedure qualification welds.
6. Conduct mechanical tests to confirm the weld strengths from the qualification welds.

7. Conduct initial analysis to determine the spacing of multiple welds in a single test specimen and the overall specimen length.
8. Perform girth welding of test pipes with the qualified welding procedures.
9. Allocate girth welds for various planned small-scale and large-scale tests.
10. Conduct initial analysis to determine the number of flaws that may be installed in a single girth weld.
11. Conduct small-scale material property characterization tests.
12. Conduct initial analysis to determine the instrumentation plan of the large-scale tests.
13. Conduct initial analysis to determine the initial flaw size to be notched into the welds.
14. Fabricate the large-scale test specimens.
15. Install instrumentation on the large-scale test specimens.
16. Conduct tests of the large-scale specimens.
17. Conduct post-test physical examination of the large-scale test specimens.
18. Conduct post-test numerical analysis of the full-scale tests in conjunction with the small-scale test data.
19. Evaluate the first generation (existing) models.
20. Develop features to be included in the second generation models.
21. Develop the second generation models.
22. Evaluate the second generation models against test data.
23. Develop guidance document for tensile strain design.
24. Provide documentation of the work.

This is the approximate order of the work flow, over the entire consolidated program. Some of the work items listed above were conducted simultaneously to shorten the project execution time. In some cases, multiple iterations were necessary as more data became available. For instance, the determination of initial flaw size was first conducted with the qualification weld properties and later conducted with production weld properties.

The current report covers Project 1, which includes work up to Item No. 18, as well as some initial coverage of the subsequent items. However, the Project 2 report will cover Item Nos. 19 to 24 in their entirety.

2 Line Pipe Procurement and Welding

2.1 Introduction

To enable the SBD Models developed in this Program to be evaluated over a range of pipe grades with different material properties, particularly work hardening capacity, the experimental Test Program was developed to include the following nominal pipe materials:

- API 5L Grade X65 (Low Work Hardening)
- API 5L Grade X65 (High Work Hardening)
- API 5L Grade X80

Pipe Specifications were developed for each pipe material to assist in discussions with pipe mills / pipe suppliers. The original Pipe Specifications are presented in Table 2.1.

Table 2.1 Original Pipe Specification

Description	Requirements		
	Grade X65 Low Y/T	Grade X65 High Y/T	Grade X80
Pipe Diameter	12 inch	12 inch	24 inch
Wall Thickness	0.50 – 0.60 inch	0.50 – 0.60 inch	0.50 – 0.60 inch
Pipe Manufacture	ERW Single Heat	ERW Single Heat	UOE DSAW Single Heat
Maximum Carbon	< 0.08%	< 0.08%	< 0.08%
Axial Y/T Ratio	< 0.85	$0.90 < Y/T \leq 0.95$	< 0.95
Stress Strain Curve (Axial)	No Discontinuous Yielding	Continuous Yielding Preferred	No Discontinuous Yielding
Uniform Elongation	> 8%	> 6%	> 6%
Pipe Body Charpy Energy	> 200J	> 150J	> 200J
DWTT 85% Shear	< -20 deg C	< -20 deg C	< -20 deg C
Pipe Quantity	4 x 40-foot joints	7 x 40-foot joints	4 x 40-foot joints
Minimum Section Lengths	12 feet	12 feet	12 feet
Max Yield (Axial)	75 ksi	75 ksi	80-85 ksi

2.2 Pipe Materials

2.2.1 General

The task of procuring pipe material was more difficult than expected, due to a combination of the reasonably tight Pipe Specifications and strong backlogs at the pipe mills. Following discussions with different pipe mills / pipe suppliers the following materials were eventually procured for the experimental Test Program:

Table 2.2 Pipe Suppliers

Pipe Grade	Nominal Y/T Ratio	Diameter (inch)	Wall Thickness (inch)	Supplier
X65*	Low	12.75	0.500	1
X65	High	12.75	0.500	2
X80	-	24.0	0.500	3

2.2.2 Grade X65 Pipe Material (Low Y/T)

The X65 pipe material supplied by Pipe Mill 1 was originally made as part of a special order. The supplier indicated at the time of placing the order, that the pipe would be slightly understrength. The chemical composition of the X65 Low Y/T pipe is summarized in Table 2.3 together with the calculated Carbon Equivalent and Pcm values:

Table 2.3 Chemical Analyses of Grade X65 Low Y/T Pipe

C	Mn	P	S	Si	Cu	Ni	Cr
0.06	0.88	0.011	0.007	0.10	0.022	0.006	0.027

Mo	V	Nb	Ti	Al	B	Ceq	Pcm
0.003	0.000	0.029	0.000	0.030	0.0000	0.215	0.109

$$Ceq = C + \frac{Mn}{6} + \frac{(Cr + Mo + V)}{5} + \frac{(Ni + Cu)}{15}$$

$$Pcm = C + \frac{Si}{30} + \frac{Mn}{20} + \frac{Cu}{20} + \frac{Ni}{60} + \frac{Cr}{20} + \frac{Mo}{15} + \frac{V}{10} + 5B$$

2.2.3 Grade X65 Pipe Material (High Y/T)

Pipe Supplier 2 supplied seven pipe joints all from a single Heat of steel. The chemical composition of the High Y/T pipe is summarized in Table 2.4 together with the calculated Carbon Equivalent and Pcm values:

Table 2.4 Chemical Analysis of Grade X65 High Y/T Pipe

C	Mn	P	S	Si	Cu	Ni	Cr
0.070	1.36	0.013	0.005	0.18	0.04	0.10	0.03

Mo	V	Nb	Ti	Al	B	Ceq	Pcm
0.01	0.001	0.035	0.016	-	-	0.314	0.148

$$C_{eq} = C + \frac{Mn}{6} + \frac{(Cr + Mo + V)}{5} + \frac{(Ni + Cu)}{15}$$

$$P_{cm} = C + \frac{Si}{30} + \frac{Mn}{20} + \frac{Cu}{20} + \frac{Ni}{60} + \frac{Cr}{20} + \frac{Mo}{15} + \frac{V}{10} + 5B$$

2.2.4 Grade X80 Pipe Material

Pipe Supplier 3 provided four joints of X80 pipe. Each joint was from a different Heat of Steel as highlighted in Table 2.5.

Table 2.5 Grade X80 Plate and Heat Numbers

Manufacturing Number	Plate Number	Heat Number	Length (mm)	Remarks
67-04674	MD426-02	5-2771	15000	CSA-Z245.1-G550-CAT3
67-04720	LJ041-01	5-1766	15500	CSA-Z245.1-G550-CAT3
68-00082	LL472-04	5-1764	16300	CSA-Z245.1-G550-CAT3
68-00158	MD431-01	5-2775	15000	CSA-Z245.1-G550-CAT3

The chemical composition of the Grade X80 pipes is summarized in Table 2.6 together with the calculated Carbon Equivalent and Pcm values:

Table 2.6 Chemical Analysis of Grade X80 Pipe

Heat	C	Mn	P	S	Si	Cu	Ni	Cr
5-2771	0.057	1.84	0.008	0.0013	0.11	0.24	0.14	0.021
5-1766	0.055	1.86	0.01	0.0013	0.11	0.25	0.14	0.022
5-1764	0.058	1.82	0.013	0.0013	0.10	0.25	0.15	0.021
5-2775	0.058	1.86	0.006	0.0012	0.11	0.25	0.14	0.027

Heat	Mo	V	Nb	Ti	Al	B	Ceq	Pcm
5-2771	0.17	0.002	0.043	0.010	0.028	0.0002	0.428	0.180
5-1766	0.17	0.002	0.045	0.012	0.03	0.0002	0.430	0.179
5-1764	0.17	0.003	0.046	0.010	0.031	0.0002	0.427	0.180
5-2775	0.18	0.002	0.044	0.009	0.024	0.0001	0.436	0.182

$$Ceq = C + \frac{Mn}{6} + \frac{(Cr + Mo + V)}{5} + \frac{(Ni + Cu)}{15}$$

$$Pcm = C + \frac{Si}{30} + \frac{Mn}{20} + \frac{Cu}{20} + \frac{Ni}{60} + \frac{Cr}{20} + \frac{Mo}{15} + \frac{V}{10} + 5B$$

2.3 Parent Pipe Tensile Properties

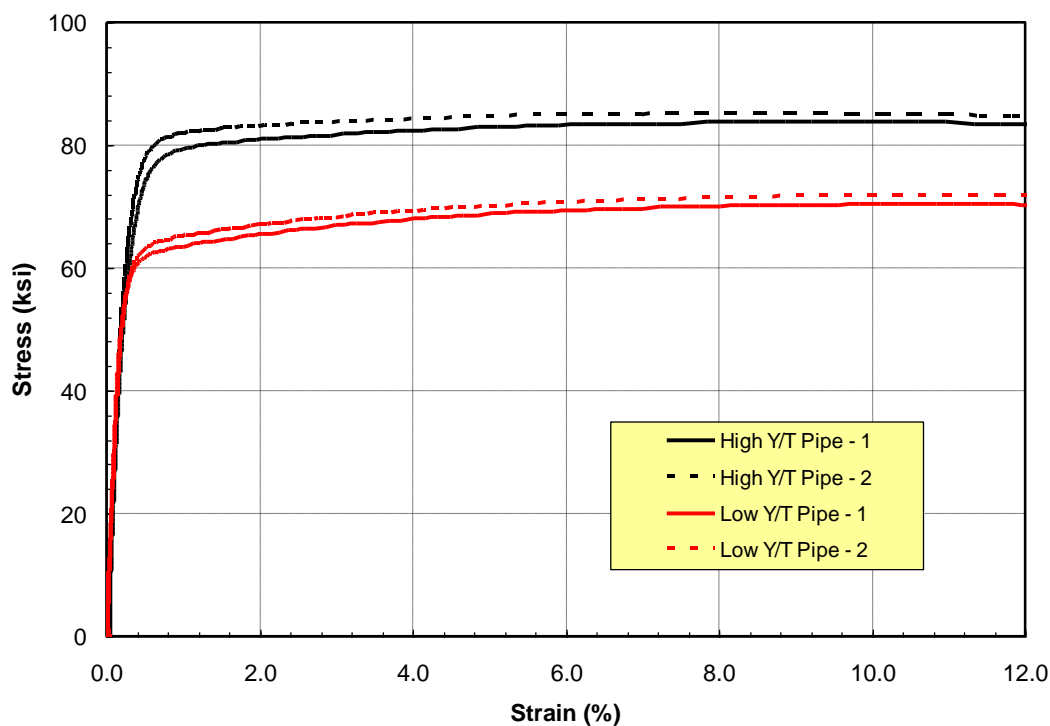
2.3.1 Grade X65 Pipe Materials

On receipt of the Grade X65 pipe materials, a series of longitudinal (axial) round bar tensile tests were performed to characterize the axial tensile properties of the pipe materials and develop target all weld metal tensile properties to ensure overmatched girth welds.

The results of the tensile tests are summarized in Table 2.7 and presented as stress-strain curves in Figure 2.1. It can be seen from Table 2.7 and Figure 2.1 that although the intent was to procure pipe with a high and a low Y/T ratio, both pipes have very similar Y/T ratios. The Y/T ratio of the Low Y/T pipe was 0.86, which is slightly higher than the target Y/T ratio (< 0.85). Similarly, the Y/T ratio for the High Y/T pipe ranged from 0.87 – 0.90, which is below the target Y/T ratio (0.90 – 0.95). Nevertheless, since the intent was to test low and high Y/T pipe materials, the terms Low Y/T and High Y/T were retained, despite the fact that the spread in the Y/T ratios was less than planned.

Table 2.7 Grade X65 Pipe Tensile Properties

Pipe Supplier	Yield Strength (ksi)	Tensile Strength (ksi)	Y/T Ratio
1	60.9	70.7	0.86
	62.0	71.7	0.86
2	73.1	83.7	0.87
	77.0	85.2	0.90

Parent Pipe Axial Stress Strain Curves**Figure 2.1 Grade X65 Parent Pipe Axial Stress Strain Curves**

It can be seen from Table 2.7 and Figure 2.1 that the Low Y/T Grade X65 pipe had an average Yield Strength closer to 60 ksi and the High Y/T Grade X65 pipe had a Yield Strength around 75 ksi. Both pipe materials exhibited uniform strains in the range of 8 – 10%.

2.3.2 Grade X80 Pipe Material

A series of axial tensile tests were also performed on the X80 pipe. Two tensile tests were performed on each of the four joints of pipe. The axial tensile properties are summarized in Table 2.8 and presented as stress strain curves in Figure 2.2

Table 2.8 Grade X65 Pipe Tensile Properties

Specimen	YS (ksi)	TS ksi	YS (MPa)	TS (MPa)	Y/T Ratio
801395-1	93.5	100.4	645	692	0.93
801395-2	93.0	101.0	641	697	0.92
801396-1	92.6	103.9	639	717	0.89
801396-2	95.3	102.5	657	707	0.93
801397-1	96.9	104.6	668	721	0.93
801397-2	95.1	108.5	656	748	0.88
801398-1	89.7	101.2	619	698	0.89
801398-2	93.6	102.5	646	707	0.91

X80 Parent Pipe Stress Strain Curves

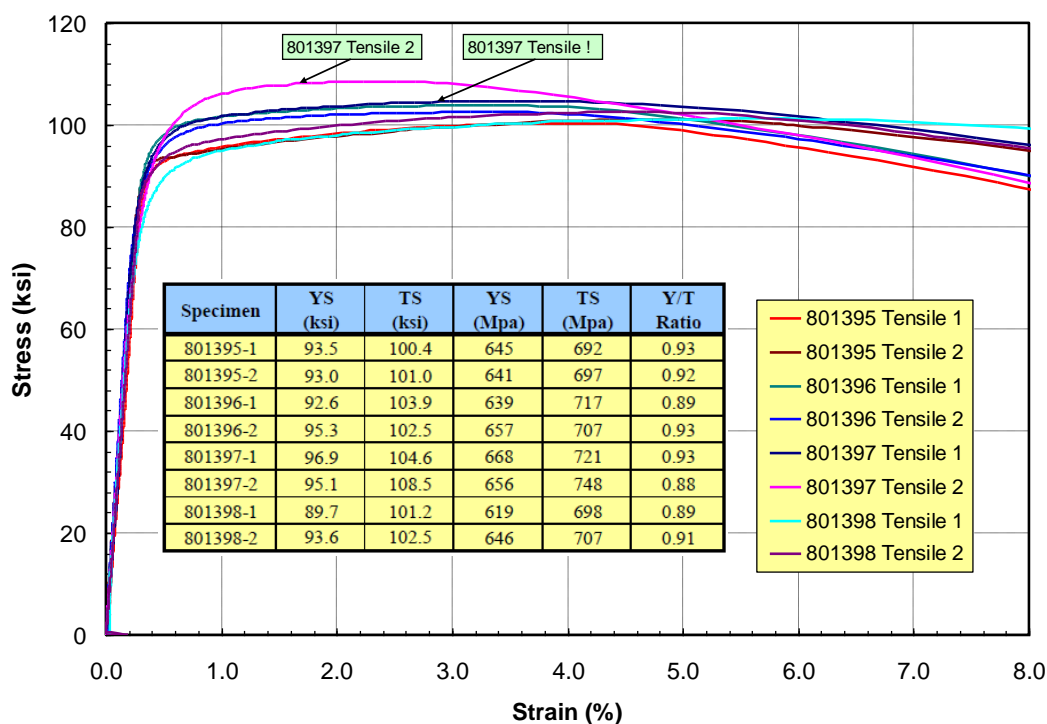


Figure 2.2 Grade X80 Parent Pipe Axial Stress Strain Curves

It can be seen that Pipe Joint 801397 exhibited higher tensile properties than the other three pipe joints. Since the Test Program only required three Joints for small scale and large scale specimen fabrication, Pipe Joint 801397 was set aside and the other three joints, which exhibited consistent properties, were used for specimen fabrication

The axial tensile stress strain curves for the three Pipe Joints selected for specimen fabrication are compared in Figure 2.3.

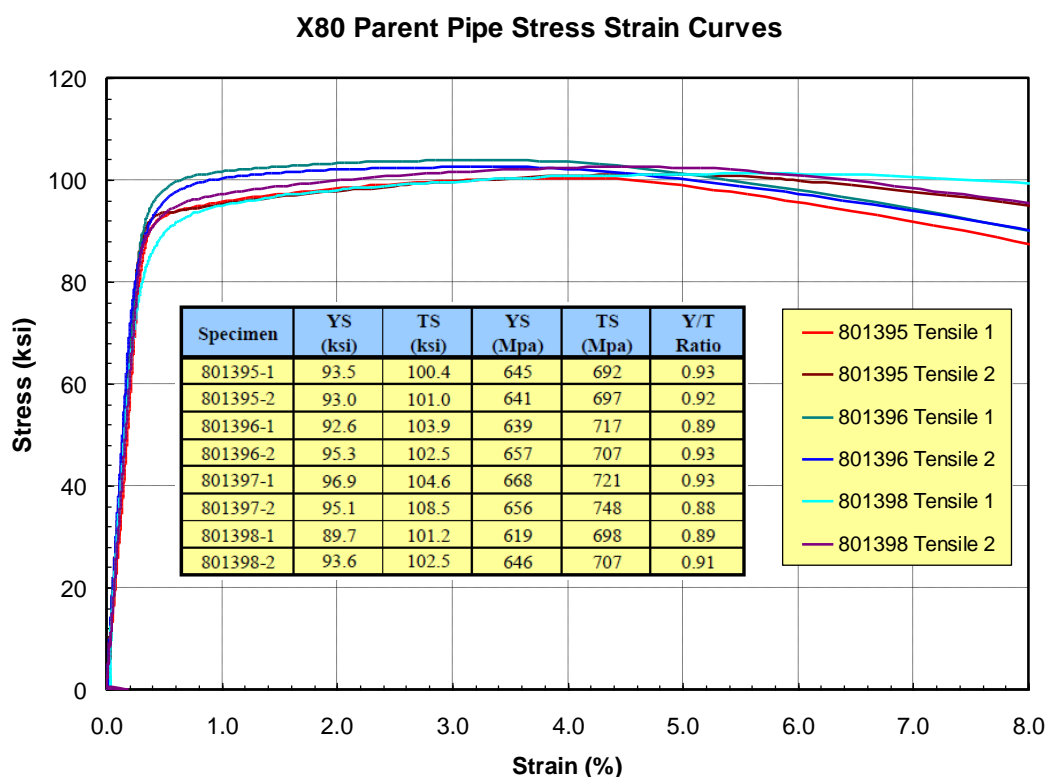


Figure 2.3 Grade X80 Parent Pipe Axial Stress Strain Curves

2.4 Grade X65 Girth Weld Fabrication

2.4.1 General

Since the objective of this Project was to develop and validate SBD assessment models, the girth welds were all fabricated as 1G roll out welds, i.e., the welding torch was fixed and the pipe was rotated. This ensured that the girth weld properties were consistent around the pipe circumference, thus avoiding any significant circumferential variation in weld metal properties. Although the 1G roll out girth welds are not representative of mechanized girth welds in the 5G position, the consistency in weld metal properties around the circumference was considered critical to validate the SBD models.

The target levels of weld metal overmatch for the Grade X65 pipe samples can be summarized as follows:

- Low Y/T Pipe : 10% Overmatch
- High Y/T Pipe : 10 and 25% Overmatch

Based on the tensile results presented in Table 2.7 the target all weld metal tensile properties were as follows:

- Low Y/T Pipe
 - 10% Overmatch : YS ~ 70 ksi, TS ~ 80 ksi
- High Y/T Pipe
 - 10% Overmatch : YS ~ 85 ksi, TS ~ 95 ksi
 - 25% Overmatch : YS ~ 95 ksi, TS ~ 105 ksi

2.4.2 Grade X65 Weld Procedure Development Trials

A series of welding trials were performed to evaluate different welding processes / welding consumables, to determine welding procedures which could provide the target all weld metal tensile properties and the target levels of overmatch. The initial welding trials included the following welding combinations:

Table 2.9 Grade X65 Pipe Weld Procedure Combinations

Welding Process	Welding Consumable	Transfer Mode	Shielding Gas
GMAW	Lincoln LH56	Short Arc	100% CO ₂
GMAW	Lincoln LH56	Spray	85% Argon / 15% CO ₂
GMAW	K Nova Ni	Short Arc	100% CO ₂
GMAW	K Nova Ni	Spray	85% Argon / 15% CO ₂

The results of the all weld metal tensile tests are summarized in Table 2.10 and presented as all weld metal stress strain curves in Figure 2.4. The all weld metal tensile tests were performed on round bar samples. Also included in Figure 2.4, are the parent pipe axial tensile stress strain curves for the Low Y/T and High Y/T pipes.

Table 2.10 X65 All Weld Metal Tensile Results (Procedure Development)

Welding Consumable	Transfer Mode	Shielding Gas	Yield Strength (ksi)	Tensile Strength (ksi)
Lincoln LH56	Short Arc	100% CO ₂	68.3	84.3
Lincoln LH56	Spray	85% Argon / 15% CO ₂	85.6	94.7
K Nova Ni	Short Arc	100% CO ₂	88.3	97.3
K Nova Ni	Spray	85% Argon / 15% CO ₂	96.4	103.9

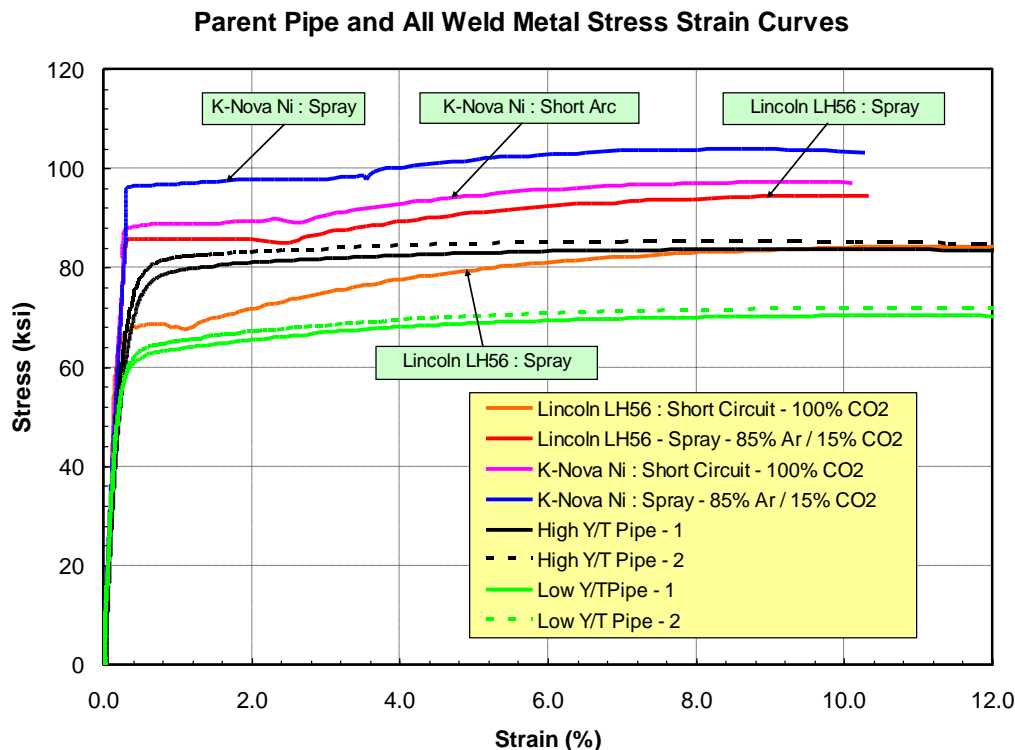


Figure 2.4 X65 All Weld Metal Stress Strain Curves (Procedure Development)

Based on the results presented in Figure 2.4, the following welding combinations were selected for Grade X65 girth weld fabrication:

- Low Y/T Pipe
 - 10% Overmatch : Lincoln LH56 Short Arc
- High Y/T
 - 10% Overmatch : K Nova Ni – Short Arc
 - 25% Overmatch : K Nova Ni – Spray

The welding combinations outlined above provide the following levels of overmatch based on the average parent pipe Yield and Tensile Strengths.

Table 2.11 X65 All Weld Metal Tensile Results (Procedure Development)

Welding Consumable	Transfer Mode	Shielding Gas	Parent Pipe	Overmatch	
				Yield Strength (%)	Tensile Strength (%)
Lincoln LH56	Short Arc	100% CO ₂	Low Y/T	11.1	18.4
K Nova Ni	Short Arc	100% CO ₂	High Y/T	17.7	15.2
K Nova Ni	Spray	85% Argon / 15% CO ₂	High Y/T	28.4	23.0

2.4.3 Grade X65 Weld Procedures

The Grade X65 weld procedures are summarized in Tables 2.12 to 2.14:

- Low Y/T : Table 2.12
- High Y/T – 10% Overmatch : Table 2.13
- High Y/T – 25% Overmatch : Table 2.14

2.4.4 Grade X65 Girth Weld Fabrication

A detailed Fabrication Plan was developed, which laid out all the welded pipe sections required to support the small, medium and large scale Test Programs. Prior to cutting any of the pipe joints, a reference line was marked along each pipe joint to assist with alignment after cutting and prior to welding. To minimize girth weld Hi-Lo misalignment, each girth weld was fabricated by cutting a section of pipe and then mating the cut surface back together with the reference line aligned. Although this procedure resulted in the long seam welds being aligned, which is not standard practice, it did provide a method of minimizing and controlling Hi-Lo misalignment.

The Fabrication Plan also permitted full traceability of each girth weld, with respect to initial pipe joints, in the event that there was a need to explain or investigate anomalous results and evaluate material property variability in specific pipe joints.

A total of 10 Low Y/T girth welds and 33 High Y/T (10% overmatch) girth welds were fabricated and shipped to a lab (Lab 2) for detailed small scale testing. Lab 2 performed six parent pipe axial tensile tests on the High Y/T pipe (5 different pipe joints) and obtained yield strengths in the range of 74.4 to 92.2 ksi with an average yield strength of 79.3 ksi. These results compare to the average axial yield strength of 75.1 ksi, determined from the initial tensile tests performed at the other lab (Lab 1), to establish target weld metal properties. Lab 2 also recorded all weld metal yield strengths which, on average, were approximately 10% lower than the 88.3 ksi value obtained during the Weld Procedure Development Trials. In comparison, the parent pipe and all weld metal tensile results obtained by Lab 2 for the Low Y/T pipes, were consistent with the results obtained during the weld procedure development trials.

A detailed review of the welding records for the 33 production Grade X65 High Y/T welds was undertaken to determine the cause of the lower strength weld metal results. From the review it was concluded that the only significant difference between the original welds made during the Weld Procedure Development Trails and the production welds was the interpass temperature. During weld procedure development, welding was stopped after each pass to allow the welder to inspect the weld and make any necessary adjustments. In comparison, during Production welding, with the weld procedure fully dialed in, the welding was performed on a continuous basis or with short hold periods between passes to maximize productivity. Due to the small diameter of the Grade X65 pipe (12.75 inch), welding continuously or with short hold periods resulted in the interpass temperature reaching 220 deg C (430 deg F), which is well above the

300 deg F specified in the Weld Procedure. The increased interpass temperature in the Production welds is considered to be the primary reason for the reduced all weld metal yield strength, although the magnitude of the reduction is larger than expected. To further explore the effect of interpass temperature a series of trial welds were fabricated with different interpass temperatures. These results confirmed that welding continuously (high interpass temperature) as opposed to stopping between passes (low interpass temperature), produces a 3-4 ksi reduction in weld metal yield strength. This indicates that although interpass temperature contributed to the lower weld metal yield strength, it did not fully explain the 10% reduction. Weld metal chemical analyses were performed on both the Low Y/T and High Y/T girth welded samples to determine the Nickel content. These results confirmed that the High Y/T girth welds had a Nickel content of 0.66%, which is consistent with K-Nova Ni. In comparison, the Low Y/T girth welds had zero Nickel in the weld metal. This confirms that the High Y/T welds were made with K-Nova Ni. It should also be noted that K-Nova Ni is not available as a 70 ksi welding wire and consequently there was no possibility of using a lower strength K-Nova Ni wire. Finally, hardness surveys were performed on the original weld fabricated during weld procedure development, as well as several production welds. The hardness surveys were consistent.

Another possible contributing factor to the variable all weld metal tensile results is related to the test method itself. When performing all weld metal tensile tests on small diameter pipe, the tensile specimens sample the weld root region, due to the curvature of the pipe, as illustrated in Figure 2.5. This means that the test is sensitive to parent pipe dilution in the weld root region and accurate placement of the tensile specimen so that it intersects the center of the weld root region.

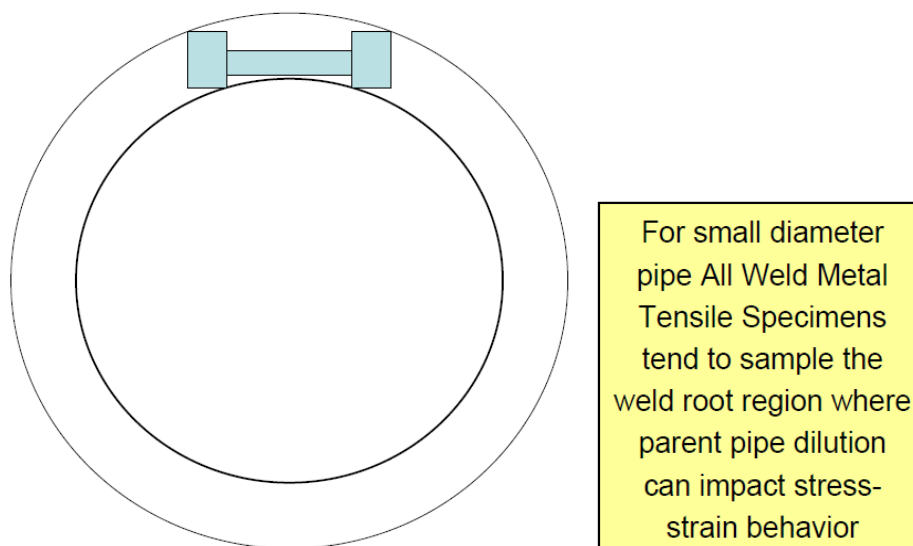


Figure 2.5 All Weld Metal Tensile Sample Location in Small Diameter Pipe

In summary, although the reason for the low weld metal strength in the High Y/T girth welds is not fully understood, the most significant contributing factor is considered to be the high

interpass temperature. This, in combination with the higher measured average yield strengths of the High Y/T pipe obtained by Lab 2 from a larger and more representative set of tests, resulted in High Y/T Grade X65 girth welds that were even matched or slightly under matched, as opposed to the target 10% overmatch. Note, the effect of interpass temperature would have been more significant with the High Y/T pipe than the Low Y/T pipe, since the High Y/T Grade X65 pipe had a yield strength approximately 15 ksi higher than the Low Y/T pipe. Since weld metal tensile and toughness properties are highly dependent on cooling rate at higher strength levels, the effect of interpass temperature would be expected to be more significant for the High Y/T pipe, which also had a Yield Strength around 75 ksi.

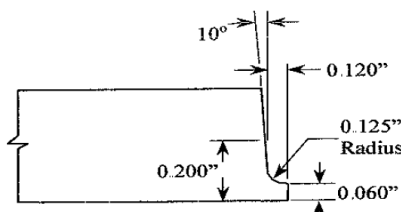
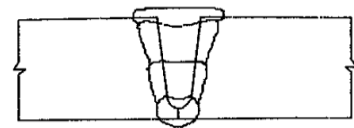
Although overmatching is normally a requirement for pipelines that may experience high strains during installation or operation, it was concluded that there was some value in performing a limited number of tests on pipe samples with even matched (or slightly under matched) girth welds. Due to material property variability, this situation could potentially arise in a Pipeline Project.

Ultimately, six even matched High Y/T girth welds were tested by C-Fer and the remainder of the even matched High Y/T welded pipe samples was returned to CRC Evans for re-fabrication. The re-fabricated pipe samples were welded with the weld procedure originally developed for the high (25%) overmatch condition. Several trial welds were made with the high overmatch weld procedure to confirm the weld metal properties and the degree of overmatch. It was found that the yield strengths were approximately 5 ksi lower than the values obtained during the original weld procedure development trials, presumably due to the increased interpass temperature in the pre-production verification welds, which were deliberately fabricated under production representative conditions. With the increased average parent pipe yield strength measured by Lab 2, the pre-production verification trials produced a 12% overmatch based on yield strength and more than 20% based on tensile strength.

The high overmatch procedure was used to re-fabricate the even matched welds that were returned to Lab 2. At this point it was decided to drop the target 25% overmatch girth welds from the Test Program.

Table 2.12 Welding Procedure for Low Y/T Grade X65 Pipe

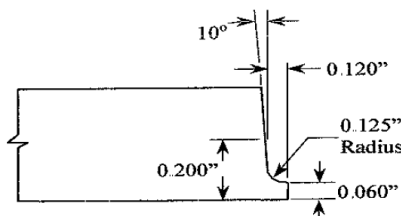
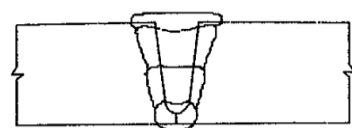
Project: ABD-1 Material Grade: API 5L X65 Material & Heat #: Low Y/T, Ht# 88-1924 Diameter: 12.75" Wall Thickness: 0.500" Preheat: 50 deg C Min Interpass Temperature: 300 deg F Max Clamps Released: After 100% Root Bead Location of Seams: Aligned Method of Heating: Propane				Electrode Trade Name: L-56 Electrode Manufacturer: Lincoln Electrode Class: ER70S-6 Electrode Heat: 698-L Shielding Gas: See Below Electrical Current: Direct Current Polarity: DCEP Position: 5G Root / 1G Others Grinding: Power Grinding as needed Cleaning: Power Brushing as needed			
Pass Number	Root	Hot	Fill 1	Cap			
Travel	Downhill	Downhill	Downhill	Downhill			
Electrode Dia	1.0 mm	1.0 mm	1.0 mm	1.0 mm			
Gas Flow Rate	50 CFH	50 CFH	50 CFH	50 CFH			
Shielding Gas	50Ar / 50CO ₂	100 CO ₂	100 CO ₂	75Ar / 25CO ₂			
CTWD	0.250"-0.375"	0.250"-0.375"	0.500"-0.625"	0.500"-0.625"			
Oscillate RPM	N.A.	165	160	110			
Oscillate Width	N.A.	0.160"-0.190"	0.200"-0.220"	0.270"-0.340"			
Head Angle	0 ⁰ -7 ⁰ Lead	0 ⁰ -7 ⁰ Lead	0 ⁰ -7 ⁰ Lead	0 ⁰ -7 ⁰ Lead			
Equipment	P450 CMT	P260 GMAW	P260 GMAW	P260 GMAW			
Max Amps	214	294	251	224			
Min Amps	193	172	215	149			
Max Volts	17.4	24.1	24.1	19.5			
Min Volts	14.5	17.5	2.9	17.9			
Max WFS	370 in/min	403 in/min	403 in/min	282 in/min			
Min WFS	270 in/min	393 in/min	393 in/min	276 in/min			
Max TS	20.4 in/min	15.2 in/min	19.9 in/min	19.9 in/min			
Min TS	17.0 in/min	14.7 in/min	12.9 in/min	9.8 in/min			
Max Heat Input	13.1 kJ/in	28.9 kJ/in	28.1 kJ/in	26.7 kJ/in			
Min Heat Input	8.2 kJ/in	11.9 kJ/in	14.8 kJ/in	8.0 kJ/in			

<div><p><u>Joint Design</u></p></div>	<div><p><u>Pass Sequence</u></p></div>
---	---

Power Supplies used: Fronius 3200 CMT Root / Fronius TransPuls Synergic 3200 pipe Hot, Fill and Cap
Fronius Program: Root run on Program CMT 1055 / Hot, Fill and Cap run on Program 1

Table 2.13 Welding Procedure for High Y/T Grade X65 Pipe – 10% Overmatch

<div><div>Project: ABD-1</div><div>Material Grade: API 5L X65</div><div>Material & Heat #: High Y/T, Ht# ZY2948</div><div>Diameter: 12.75"</div><div>Wall Thickness: 0.500"</div><div>Preheat: 50 deg C Min</div><div>Interpass Temperature: 300 deg F Max</div><div>Clamps Released: After 100% Root Bead</div><div>Location of Seams: Aligned</div><div>Method of Heating: Propane</div></div>				<div><div>Electrode Trade Name: K-Nova Ni</div><div>Electrode Manufacturer: Thyssen</div><div>Electrode Class: ER80S-G</div><div>Electrode Heat: 6030</div><div>Shielding Gas: See Below</div><div>Electrical Current: Direct Current</div><div>Polarity: DCEP</div><div>Position: 5G Root / IG Others</div><div>Grinding: Power Grinding as needed</div><div>Cleaning: Power Brushing as needed</div></div>			
Pass Number	Root	Hot	Fill 1	Cap			
Travel	Downhill	Downhill	Downhill	Downhill			
Electrode Dia	1.0 mm	1.0 mm	1.0 mm	1.0 mm			
Gas Flow Rate	50 CFH	50 CFH	50 CFH	50 CFH			
Shielding Gas	50Ar / 50CO ₂	100 CO ₂	100 CO ₂	75Ar / 25CO ₂			
CTWD	0.250"-0.375"	0.250"-0.375"	0.500"-0.625"	0.500"-0.625"			
Oscillate RPM	N.A.	165	160	110			
Oscillate Width	N.A.	0.160"-0.190"	0.200"-0.220"	0.230"-0.340"			
Head Angle	0 ⁰ -7 ⁰ Lead	0 ⁰ -7 ⁰ Lead	0 ⁰ -7 ⁰ Lead	0 ⁰ -7 ⁰ Lead			
Equipment	P450 CMT	P260 GMAW	P260 GMAW	P260 GMAW			
Max Amps	219	277	272	216			
Min Amps	195	206	208	143			
Max Volts	17.4	25.8	24.3	19.4			
Min Volts	14.4	22.1	22.7	18.6			
Max WFS	385 in/min	406 in/min	404 in/min	284 in/min			
Min WFS	280 in/min	393 in/min	393 in/min	275 in/min			
Max TS	20.4 in/min	18.5 in/min	18.5 in/min	14.5 in/min			
Min TS	17.0 in/min	14.7 in/min	11.0 in/min	9.8 in/min			
Max Heat Input	13.4 kJ/in	29.2 kJ/in	36.1 kJ/in	25.7 kJ/in			
Min Heat Input	8.3 kJ/in	14.8 kJ/in	15.3 kJ/in	11.0 kJ/in			

<div><div>Joint Design</div><div></div></div>	<div><div>Pass Sequence</div><div></div></div>
--	--

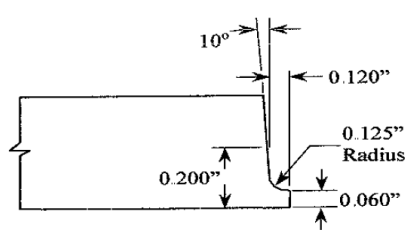
Power Supplies used: Fronius 3200 CMT Root / Fronius TransPuls Synergic 3200 pipe Hot, Fill and Cap

Fronius Program: Root run on Program CMT 1055 / Hot, Fill and Cap run on Program 1

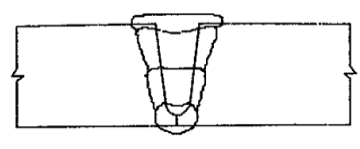
Table 2.14 Welding Procedure for Nippon Pipe – 25% Overmatch

<div><div>Project: ABD-1</div><div>Material Grade: API 5L X65</div><div>Material & Heat #: High Y/T, Ht# ZY2948</div><div>Diameter: 12.75"</div><div>Wall Thickness: 0.500"</div><div>Preheat: 50 deg C Min</div><div>Interpass Temperature: 300 deg F Max</div><div>Clamps Released: After 100% Root Bead</div><div>Location of Seams: Aligned</div><div>Method of Heating: Propane</div></div>				<div><div>Electrode Trade Name: K-Nova Ni</div><div>Electrode Manufacturer: Thyssen</div><div>Electrode Class: ER80S-G</div><div>Electrode Heat: 6030</div><div>Shielding Gas: See Below</div><div>Electrical Current: Direct Current</div><div>Polarity: DCEP</div><div>Position: 5G Root / 1G Others</div><div>Grinding: Power Grinding as needed</div><div>Cleaning: Power Brushing as needed</div></div>			
Pass Number	Root	Hot	Fill 1	Cap			
Travel	Downhill	Downhill	Downhill	Downhill			
Electrode Dia	1.0 mm	1.0 mm	1.0 mm	1.0 mm			
Gas Flow Rate	50 CFH	50 CFH	50 CFH	50 CFH			
Shielding Gas	50Ar / 50CO ₂	85Ar / 15CO ₂	85Ar / 15CO ₂	85Ar / 15CO ₂			
CTWD	0.250"-0.375"	0.250"-0.375"	0.500"-0.625"	0.500"-0.625"			
Oscillate RPM	N.A.	165	160	110			
Oscillate Width	N.A.	0.160"-0.190"	0.200"-0.220"	0.270"-0.340"			
Head Angle	0 ⁰ -7 ⁰ Lead	0 ⁰ -7 ⁰ Lead	0 ⁰ -7 ⁰ Lead	0 ⁰ -7 ⁰ Lead			
Equipment	P450 CMT	P260 GMAW	P260 GMAW	P260 GMAW			
Max Amps	214	294	251	224			
Min Amps	193	172	215	149			
Max Volts	17.4	24.1	24.1	19.5			
Min Volts	14.5	17.5	2.9	17.9			
Max WFS	370 in/min	403 in/min	403 in/min	282 in/min			
Min WFS	270 in/min	393 in/min	393 in/min	276 in/min			
Max TS	20.4	15.2	19.9	19.9			
Min TS	17.0	14.7	12.9	9.8			
Max Heat Input	13.1 kJ/in	28.9 kJ/in	28.1 kJ/in	26.7 kJ/in			
Min Heat Input	8.2 kJ/in	11.9 kJ/in	14.8 kJ/in	8.0 kJ/in			

Joint Design



Pass Sequence



Power Supplies used: Fronius 3200 CMT Root / Fronius TransPuls Synergic 3200 pipe Hot, Fill and Cap

Fronius Program: Root run on Program CMT 1055 / Hot, Fill and Cap run on Program 6

2.5 Grade X80 Girth Weld Fabrication

2.5.1 Weld Procedure Development Trials

Given the issues experienced with the Grade X65 weld procedure development trials, a comprehensive set of welding trials were undertaken to develop a weld procedure for the 24 inch diameter Grade X80 pipe. Since the X80 pipe was 24 inches in diameter, as opposed to the 12.75 inch Grade X65 pipe materials, the issue of interpass temperature was less problematic from a welding heat input perspective, since the weld had more time to cool between successive passes. However, as weld metal strength increases, weld metal tensile properties become increasingly dependent on the weld cooling rate. Consequently, although interpass temperature is less of an issue from a welding heat input perspective, interpass temperature and its effect on cooling rate, is an important parameter when welding X80 pipe and higher strength grades.

The following weld procedure combinations were evaluated as part of the X80 weld procedure development trials:

Table 2.15 Grade X80 Welding Procedure Development Trials

Weld Consumable	Bevel Angle (deg)	Heat Input (kJ/inch)	Maximum Interpass Temp (deg C)
K Nova Ni-HHI	10	19.9	130
K Nova Ni-LHI	10	16.4	120
NiMo80-LHI	10	15.5	120
NiMo80-HHI	10	19.5	200
NiMo80-HHI	5	19.5	130
NiMo80	5	18.3	170
NiMo80	5	18.3	50

The results of the weld procedure development trials are summarized in Table 2-16 and presented as stress strain plots in Figure 2.6.

Table 2.16 Results from Grade X80 Welding Procedure Development Trials

Description	Bevel Angle (deg)	Specimen	YS (ksi)	TS (ksi)	YS Over-match (%)	TS Over-match (%)	Interpass Temperatures & Heat Inputs
Parent Pipe	N.A.	Average Parent	92.9	101.9	N/A	N/A	N/A
K Nova Ni-HHI	10	776-1-A (1)	92.7	107.2	-0.22	5.20	19.9 kJ/in heat input fills, 50deg. C preheat, max interpass 130deg. C, Slight delay between fills.
		776-1-A (2)	90.2	107.9	-2.91	5.89	
K Nova Ni-LHI	10	776-1-B (1)	91.4	105.7	-1.61	3.73	16.4 kJ/in heat input fills, 50deg. C preheat, max interpass 120deg. C, Slight delay between fills.
		776-1-B (2)	89.4	103.1	-3.77	1.18	
NiMo80-LHI	10	776-1-C (1)	114.8	129.1	23.57	26.69	15.5 kJ/in heat input fills, 50deg. C preheat, max interpass 120deg. C, Slight delay between fills.
		776-1-C (2)	117.9	126.2	26.91	23.85	
NiMo80-HHI	10	776-1-D (1)	94.7	111.9	1.94	9.81	19.5 kJ/in heat input fills, 120deg. C preheat, max interpass 200deg. C, No time delay between fill passes.
		776-1-D (2)	97.3	115.4	4.74	13.25	
		776-1-D (3)	93.3	118.5	0.43	16.29	
NiMo80-HHI	5	776-1-E (1)	98	120.1	5.49	17.86	19.5 kJ/in heat input fills, 50 deg. C preheat, max interpass 130deg. C, Slight delay between fill passes.
		776-1-E (2)	98.4	116.6	5.92	14.43	
NiMo80 Intermediate	5	776-1-F (1)	98.1	121.3	5.60	19.04	18.3 kJ/in heat input fills 1 and 2 Continuous welding no time delay between passes, 50deg. C preheat. Max Interpass temp 170 deg C
		776-1-F (2)	100.8	120.3	8.50	18.06	
NiMo80 Intermediate	5	776-1-G (1)	104.7	126.6	12.70	18.00	18.3 kJ/in heat input fills 1 and 2 Time delay between passes cooled to 50deg. c before welding re-started
		776-1-G (1) Retest	110	120.3	18.41	18.06	
		776-1-G (2)	101.9	124.1	9.69	21.79	

Based on the results presented in Table 2.16 and Figure 2.5, the NiMo80 Weld Procedure with Intermediate Heat Input and a Low Interpass Temperature, was selected for the Grade X80 girth weld sample fabrication.

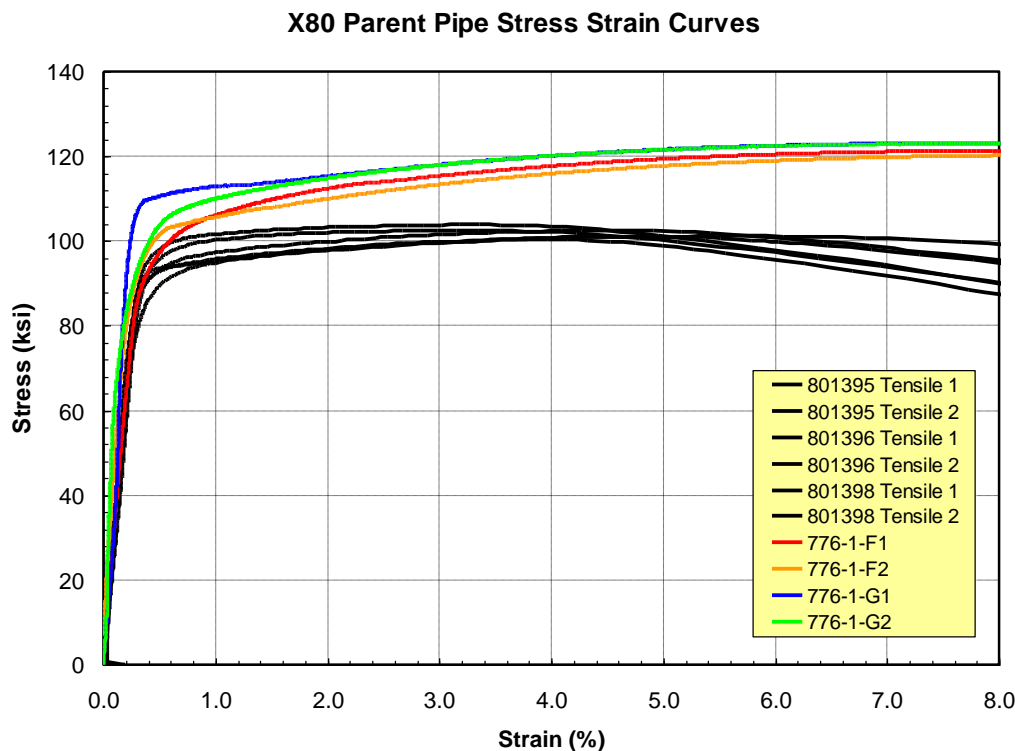


Figure 2.6 Stress Strain Plots from Grade X80 Welding Procedure Development Trials

2.5.2 Grade X80 Weld Procedures

The Grade X80 weld procedure is summarized in Tables 2.17.

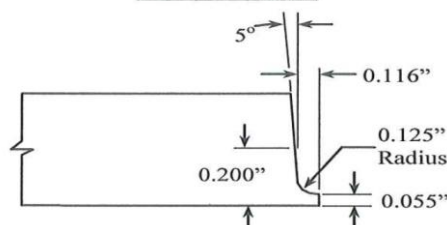
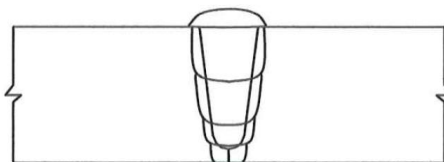
2.5.3 Grade X80 Girth Weld Fabrication

A detailed Fabrication Plan was developed for the X80 pipe which laid out all the welded pipe sections required to support the small, medium and large scale Test Programs. Prior to cutting any of the pipe joints, a reference line was marked along each pipe joint to assist with alignment after cutting and prior to welding. To minimize girth weld Hi-Lo misalignment, each girth weld was fabricated by cutting a section of pipe and then mating the cut surface back together with the reference line aligned. Although this procedure resulted in the long seam welds being aligned, which is not standard practice, it did provide a method of minimizing and controlling Hi-Lo misalignment. The Fabrication Plan also permitted full traceability of each girth weld with respect to initial pipe joints, in the event that there was a need to explain or investigate anomalous results and evaluate material property variability in specific pipe joints.

A total of 2 Grade X80 girth welds were fabricated and shipped to CRES for detailed small-scale testing. An additional 12 Grade X80 girth weld samples were fabricated and shipped to C-Fer for medium and large-scale tests.

Table 2.17 Grade X80 Welding Procedure

<div><div>Project: ABD-1</div><div>Material Grade: API 5L X80</div><div>Material & Heat #: Heat# 68-00158</div><div>Diameter: 24"</div><div>Wall Thickness: 0.500"</div><div>Preheat: 50 deg C Min</div><div>Interpass Temperature: 100 deg C Max</div><div>Clamps Released: After 100% Root Bead</div><div>Location of Seams: Aligned</div><div>Method of Heating: Propane</div></div>				<div><div>Electrode Trade Name: NiMo80</div><div>Electrode Manufacturer: Thyssen</div><div>Electrode Class: ER90S-G</div><div>Electrode Heat: 6030</div><div>Shielding Gas: See Below</div><div>Electrical Current: Direct Current</div><div>Polarity: DCEP</div><div>Position: 5G Root / 1G Others</div><div>Grinding: Power Grinding as needed</div><div>Cleaning: Power Brushing as needed</div></div>			
Pass Number	Root	Hot	Fill 1	Fill 2	Cap		
Travel	Downhill	Downhill	Downhill	Downhill	Downhill		
Electrode Dia	0.9 mm	0.9 mm	0.9 mm	0.9 mm	0.9 mm		
Gas Flow Rate	78 CFH	65 CFH	65 CFH	65 CFH	65 CFH		
Shielding Gas	75Ar / 25CO ₂	85Ar / 15CO ₂	85Ar / 15CO ₂	85Ar / 15CO ₂	85Ar / 15CO ₂		
CTWD	0.250"-0.500"	0.250"-0.500"	0.250"-0.500"	0.250"-0.500"	0.250"-0.500"		
Oscillate RPM	N.A.	220	220	220	180		
Oscillate Width	N.A.	0.170"	0.220"	0.220"	0.180"		
Head Angle	0 ⁰ -7 ⁰ Lead	0 ⁰ -7 ⁰ Lead	0 ⁰ -7 ⁰ Lead	0 ⁰ -7 ⁰ Lead	0 ⁰ -7 ⁰ Lead		
Equipment	P260 GMAW	P260 GMAW	P260 GMAW	P260 GMAW	P260 GMAW		
Max Amps	274	218	222	220	194		
Min Amps	239	209	218	218	192		
Max Volts	22.4	24.2	24.1	24.1	25.6		
Min Volts	22.0	20.7	22.7	22.9	24.4		
Max WFS	521 in/min	524 in/min	541 in/min	541 in/min	481 in/min		
Min WFS	514 in/min	514 in/min	534 in/min	534 in/min	475 in/min		
Max TS	40.0	21.5	17.1	17.0	18.6		
Min TS	39.7	21.2	16.8	16.8	18.3		
Max Heat Input	9.2 kJ/in	14.2 kJ/in	18.7 kJ/in	18.7 kJ/in	16.1 kJ/in		
Min Heat Input	8.0 kJ/in	12.7 kJ/in	17.7 kJ/in	17.8 kJ/in	15.4 kJ/in		

<div><div>Bevel Design</div><div></div></div>	<div><div>Pass Sequence</div><div></div></div>
--	--

Power Supplies used: Fronius 3200 CMT Root / Fronius TransPuls Synergic 3200 pipe Hot, Fills and Cap

Fronius Program: Root run on Program 1 / Hot, Fills and Cap run on Program 11

3 Small-scale Material Characterization Tests

3.1 Background and Objectives

The small-scale material characterization tests serve multiple purposes, including:

- (1) initial assessment of the weld strength mismatch level,
- (2) input for the pre-test analysis for the determination of a number of critical test parameters,
- (3) correlation with large-scale test data, and
- (4) determination of requirements of small-scale tests for tensile strain design.

Although the major focus of this project is the large-scale testing, it should be recognized that in actual pipeline applications, most of the material qualification tests are done in small-scale specimens. Therefore, understanding the correlation between the small-scale and large-scale test results is a critical requirement for tensile strain design.

3.1.1 Overview of the Welds

The line pipe procurement and girth welds fabrication are covered in Section 2.0. A brief summary of these welds is provided below for continuity.

Four girth welds from three pipes were fabricated in this project. The two ERW (electric resistance welded) X65 pipes were of 12.75 inch (324 mm) diameter and 0.5 inch (12.7 mm) wall thickness, supplied by two manufacturers. These pipes were designated as high Y/T and low Y/T pipes, where Y and T refer to the yield and ultimate tensile strength, respectively. The remaining one UOE X80 pipe had 24 inch (610 mm) diameter and 0.5 inch (12.7 mm) wall thickness, manufactured by a third manufacturer.

Girth welds in all three pipes were made with mechanized GMAW processes. The root pass was deposited from the OD side in a 5G position. The hot, fill, and cap passes were deposited in a 1G position, by rolling the pipe while holding the welding head steady, with the intent to produce as uniform of weld properties around the circumference as possible.

Two distinctively different girth welding procedures were applied to the X65 high Y/T pipe, resulting in two girth weld strength levels. These two welds are referred to as the first production and second production welds. One girth welding procedure was applied to the X65 low Y/T pipe and another procedure was applied to the X80 pipe.

3.1.2 Sources of Data

Multiple labs were involved in the generation of the small-scale material property data. A list of data type and the labs that generated those data are given in Table 3.1. Lab 1 was primarily involved in the tests surrounding the welding procedure qualification. Labs 2 and 3 were primarily involved in the testing of production welds.

Table 3.1 List of test labs for small-scale material characterization tests

Data Type	Material	Attribute	Data Source
Tensile Properties	12" high Y/T pipe body	Longitudinal	Lab 1 and Lab 2
	12" high Y/T pipe body	Hoop	Lab 2 and Lab 3
	12" low Y/T pipe body	Longitudinal	Lab 1 and Lab 2
	12" low Y/T pipe body	Hoop	Lab 2 and Lab 3
	24" pipe body	Longitudinal	Lab 1 and Lab 3
	24" pipe body	Hoop	Lab 1 and Lab 3
	12" high Y/T weld	1st qualification	Lab 1
	12" high Y/T weld	1st production	Lab 2
	12" high Y/T weld	2nd qualification	Lab 1
	12" high Y/T weld	2nd production	Lab 3
	12" low Y/T weld	qualification	Lab 1
	12" low Y/T weld	production	Lab 3
	24" weld	qualification	Lab 1
	24" weld	production	Lab 3
Charpy	12" low Y/T pipe	Pipe body	Lab 2
		Weld centerline	Lab 2
		HAZ	Lab 2
	12" high Y/T pipe	Pipe body	Lab 2
		1st pro. weld centerline	Lab 2
		1st pro. HAZ	Lab 2
	12" high Y/T pipe	Pipe body	Lab 2
		2nd pro. weld centerline	Lab 3
		2nd pro. HAZ	Lab 3
CTOD	12" low Y/T pipe	Weld centerline	Lab 3
		HAZ	Lab 3
	12" high Y/T pipe	1st pro. weld centerline	Lab 3
		1st pro. HAZ	Lab 3
	12" high Y/T pipe	2nd pro. weld centerline	Lab 3
		2nd pro. HAZ	Lab 3
	24" pipe	Weld centerline	Lab 3
		HAZ	Lab 3
SENT R-Curves	Matrix the same as CTOD		NIST
Hardness Map	Selected welds		A project sponsor
Macro	All welds		Lab 2 and Lab 3

3.1.3 Scope of the Small-scale Tests

The scope of the small-scale testing includes the qualification of the following features / parameters:

- (1) Weld macro
- (2) Microhardness map
- (3) Pipe tensile properties at room temperature and -20C.
 - a. Longitudinal properties
 - b. Hoop properties
- (4) All weld metal tensile properties
- (5) Charpy transition curves
- (6) CTOD transition curves with standard deeply notched SENB specimens
- (7) J-resistance curves with low-constraint SENT (SE(T) in ASTM notation) specimens

Details of the testing are fully described in the following sections.

3.2 Weld Macro

The sample macros of the X65 welds are shown in Figure 3.1 and Figure 3.2 for high Y/T and low Y/T girth welds, respectively. The overall weld geometry is consistent with the expected profiles of narrow groove mechanized GMAW welds. However, there are variations of the shape and the width of the deposited weld metal. It may be noted that the deposited weld metal near the cap passes can be highly non-symmetrical. Therefore, using the weld cap as a reference for HAZ flaw notch location can be problematic.

3.3 Hardness Map

Microhardness maps of selected samples were produced by the Lincoln Electric Company as a part of its contribution to this project. The microhardness of the 1st production weld of the X65 high Y/T pipe is shown in Figure 3.3. The hardness of the base pipe material is in the range of 190-230 Hv. The hardness of the deposited weld metal is in the same range. There is a narrow band of softened HAZ with the hardness in the 150-190 range. The width of this softened zone varies from approximately 0.5 mm to 1.5 mm. It may be noted by comparing the indentation map (left) and the hardness map (right), that the softened zone is on the outer boundary of the visible HAZ.

The microhardness map of the 2nd production weld is shown in Figure 3.4. In this case, the hardness of the deposited weld metal is mostly in the range of 230-250 Hv, with isolated zones at 250-270 Hv. The softened HAZs with a hardness of 170-190 Hv are visible on both sides of the weld. The width of the softened zone is approximately 1.5 mm.

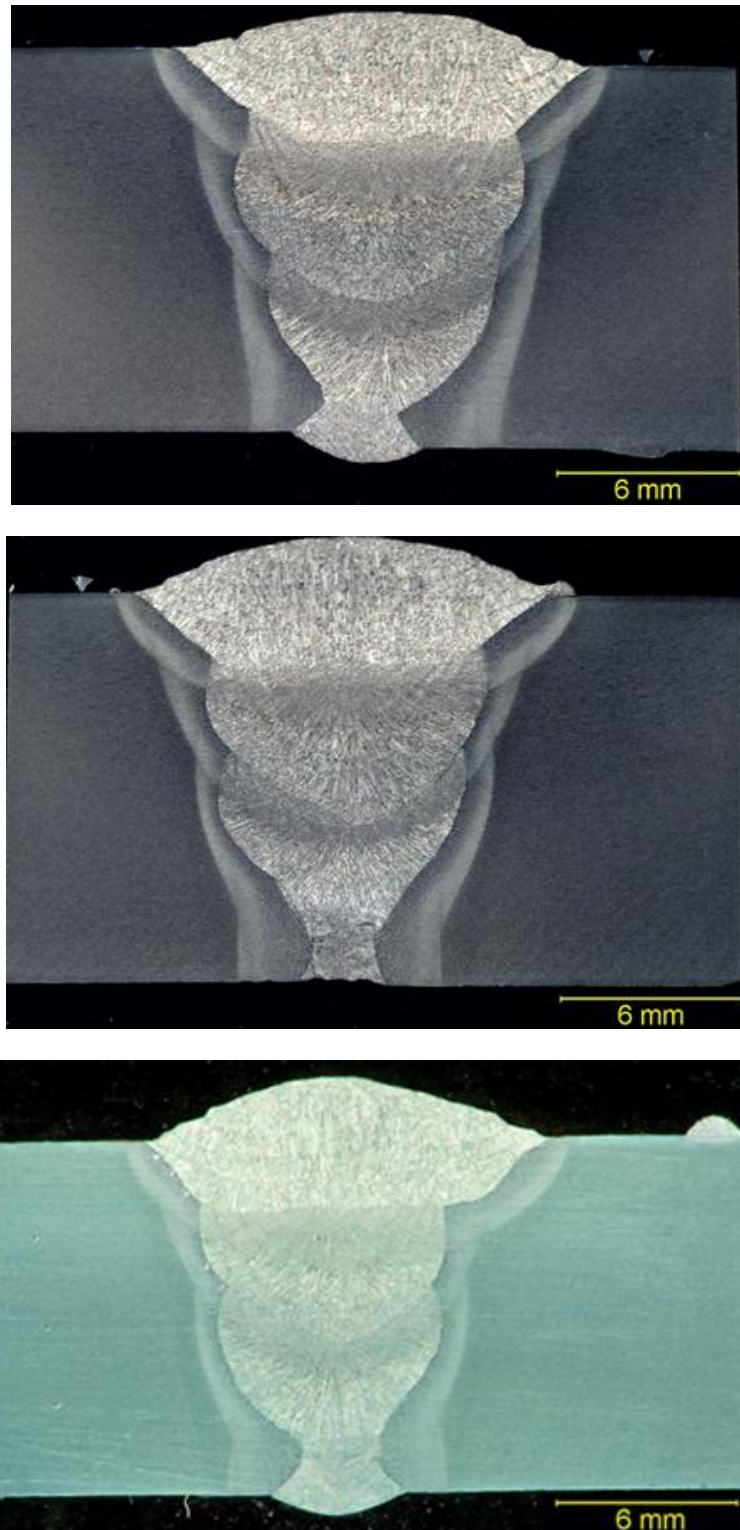


Figure 3.1 Girth weld macro of the 1st production weld of high Y/T X65 pipe

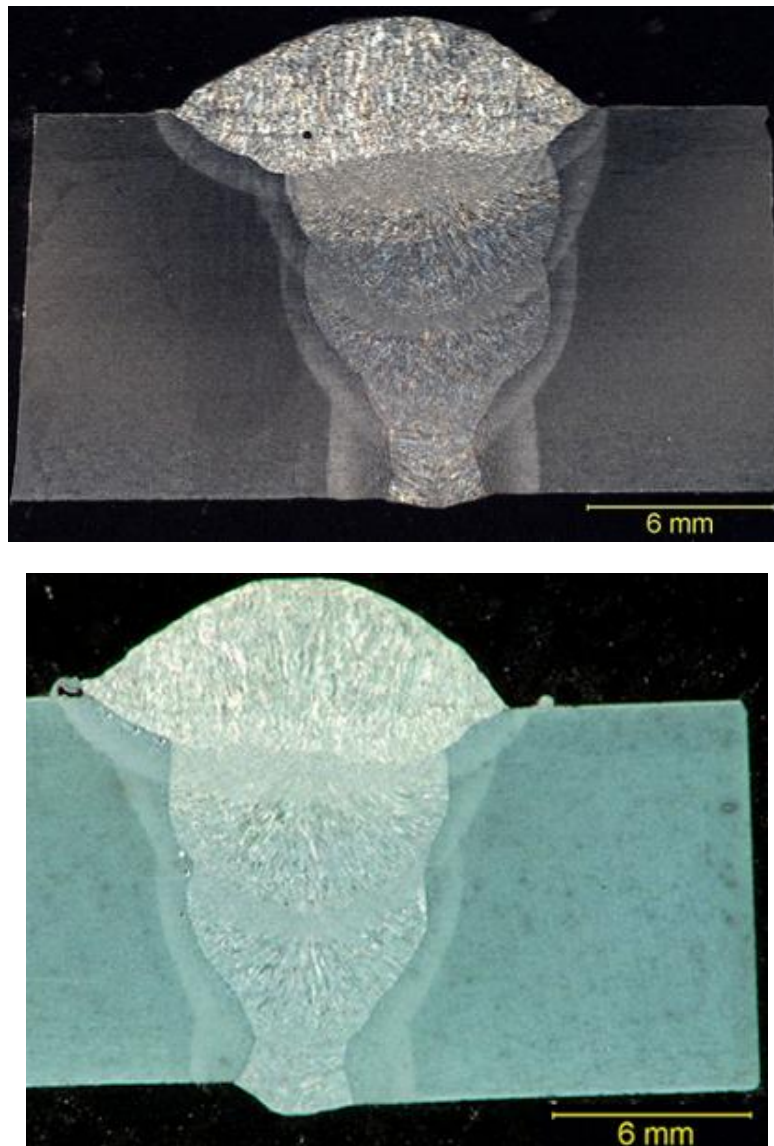


Figure 3.2 Girth weld macro of the low Y/T X65 pipe

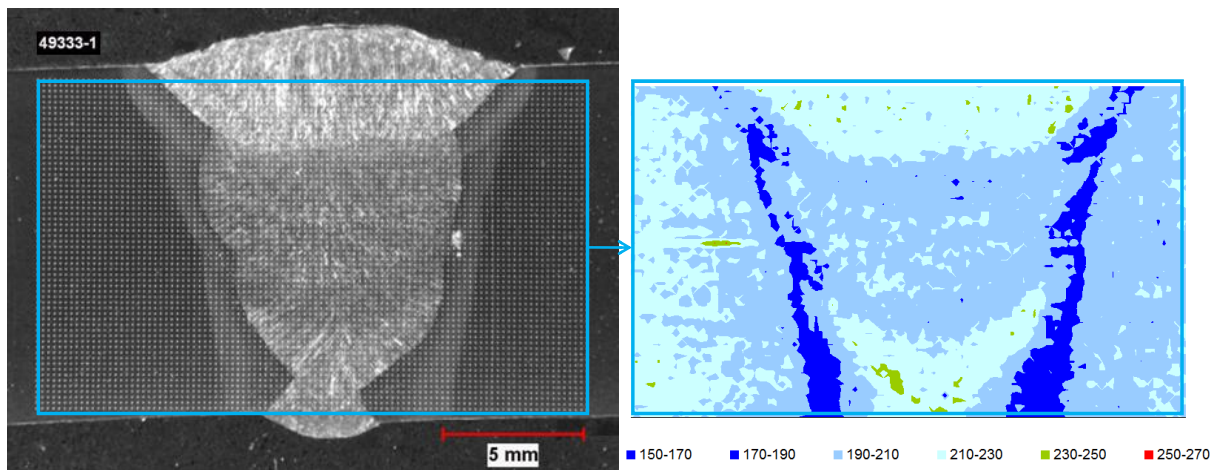


Figure 3.3 Indentation map (left) and microhardness map of the 1st production weld of the X65 high Y/T pipe. The hardness scale is in Vickers

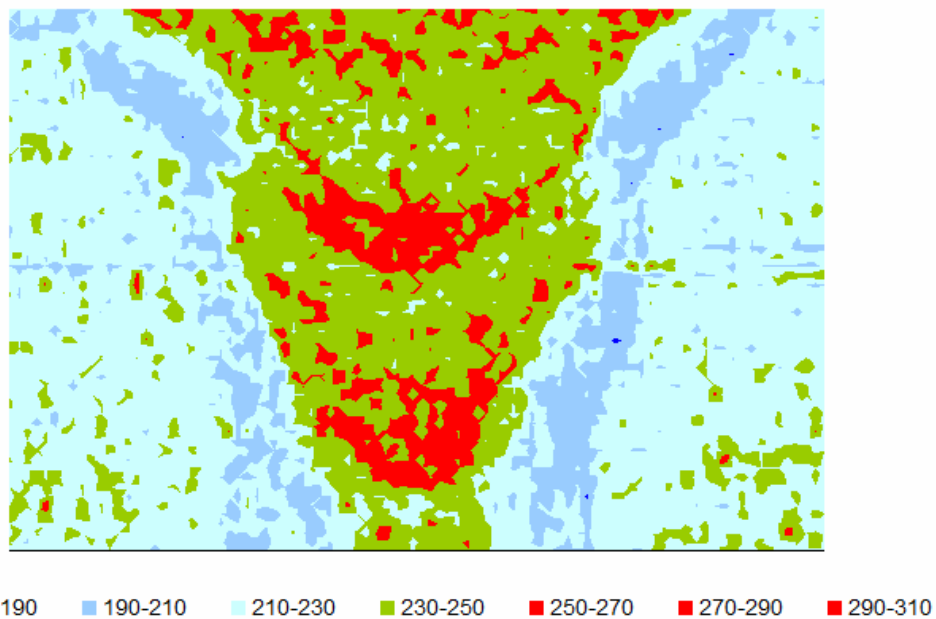


Figure 3.4 Microhardness map of the 2nd production weld of the X65 high Y/T pipe

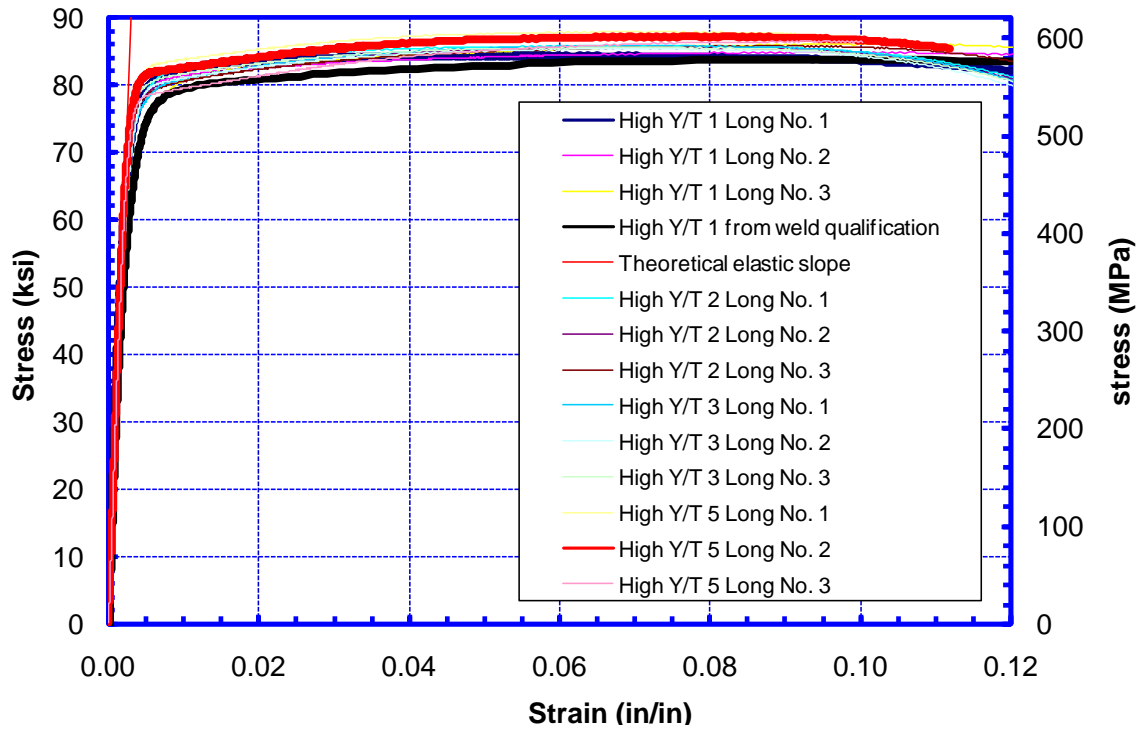


Figure 3.5 Longitudinal tensile properties of the 12" high Y/T ratio pipe

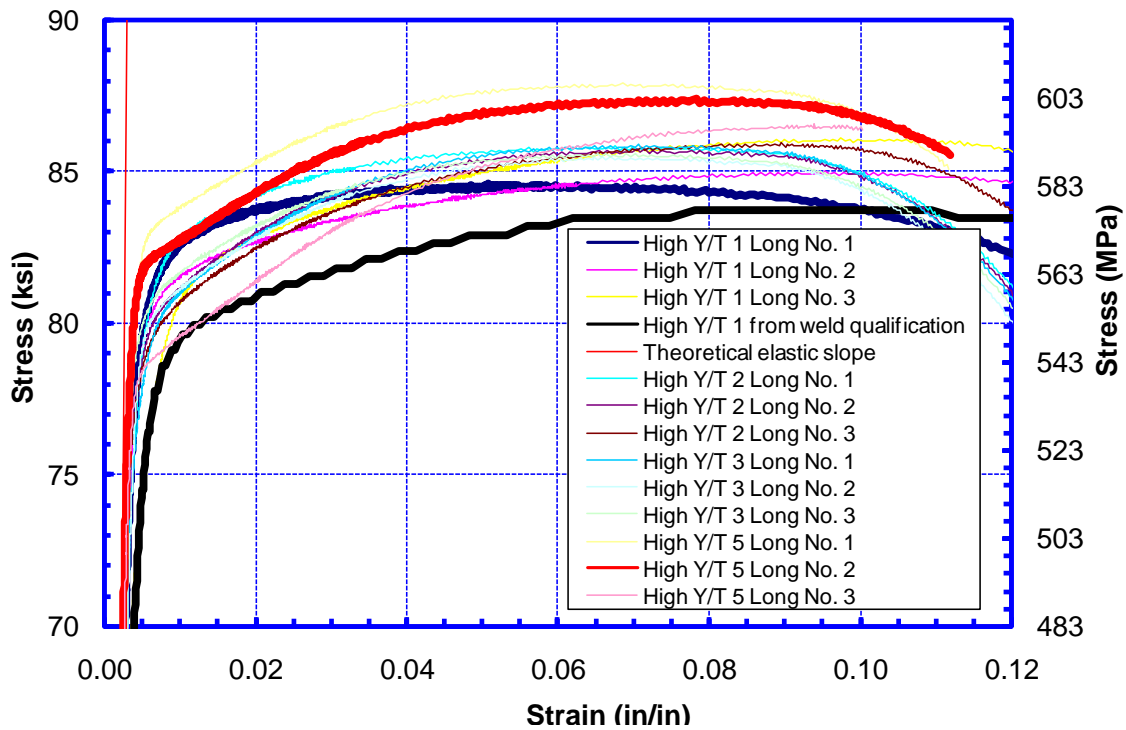


Figure 3.6 Top portion (high strength) of Figure 3.5

3.4 Line pipe Tensile Properties

Extensive tensile tests were done to characterize the line pipe tensile properties. All tests were done in round bar form with the gage diameter of 0.25 inch (6.35 mm). The tests involved three labs. Initial results were produced from Lab 1 during the weld procedure qualification. More results were produced in Lab 2 and Lab 3 at a later time.

3.4.1 Tensile Properties of X65 12-Inch High Y/T Pipe

3.4.1.1 High Y/T Pipe Longitudinal Properties

A selected set of longitudinal stress-strain curves of the X65 high Y/T pipe are shown in Figure 3.5. One of the curves was obtained from Lab 1 during the initial testing as a part of the welding procedure qualification. The rest of the curves were from Lab 2. To illustrate the range of the stress-strain curves, the top portion of Figure 3.5 is shown in Figure 3.6. There are considerable variations in the plastic part of the stress-strain curves, indicating different levels of strain hardening. The strength variation in the plastic part of the stress-strain curves is in the range of 4-5 ksi (28-34 MPa).

3.4.1.2 High Y/T Pipe Hoop Properties

A selected set of hoop stress-strain curves of the X65 high Y/T pipe are shown in Figure 3.7. The top portion of Figure 3.7 is shown in Figure 3.8, which demonstrates the variations of the plastic part of the stress-strain curves. The high strength portion of the stress-strain curve is further focused to a small strain range in Figure 3.9. At the customary definition of yield strain, at 0.5% of total engineering strain, the report yield strength could have varied from 60 ksi to 83 ksi.

To illustrate the effects of test temperature, the four stress-strain curves produced by Lab 3 are shown in Figure 3.10. The increase of the strength at -20°C over that at room temperature is evident. More interestingly, the strain hardening rate and the uniform elongation are higher at -20°C than those at room temperature.

3.4.1.3 Comparison of Longitudinal and Hoop Properties

The comparison of the longitudinal and hoop properties is given in Figure 3.11. Given the scatters in both longitudinal and hoop properties, curves at the middle of the variation ranges were selected for the comparison.

3.4.2 Tensile Properties of X65 12-Inch Low Y/T Pipe

3.4.2.1 Low Y/T Pipe Longitudinal Properties

A selected set of longitudinal stress-strain curves of the X65 low Y/T pipe are shown in Figure 3.12. One of the curves was obtained from Lab 1 during the initial testing as a part of the welding procedure qualification. The rest of the curves were from Lab 2. The portion of the curves at high strength and low strain is given in Figure 3.13. Even with the relatively small number of curves, the yield strength at 0.5% strain varies from 56 ksi to 64 ksi.

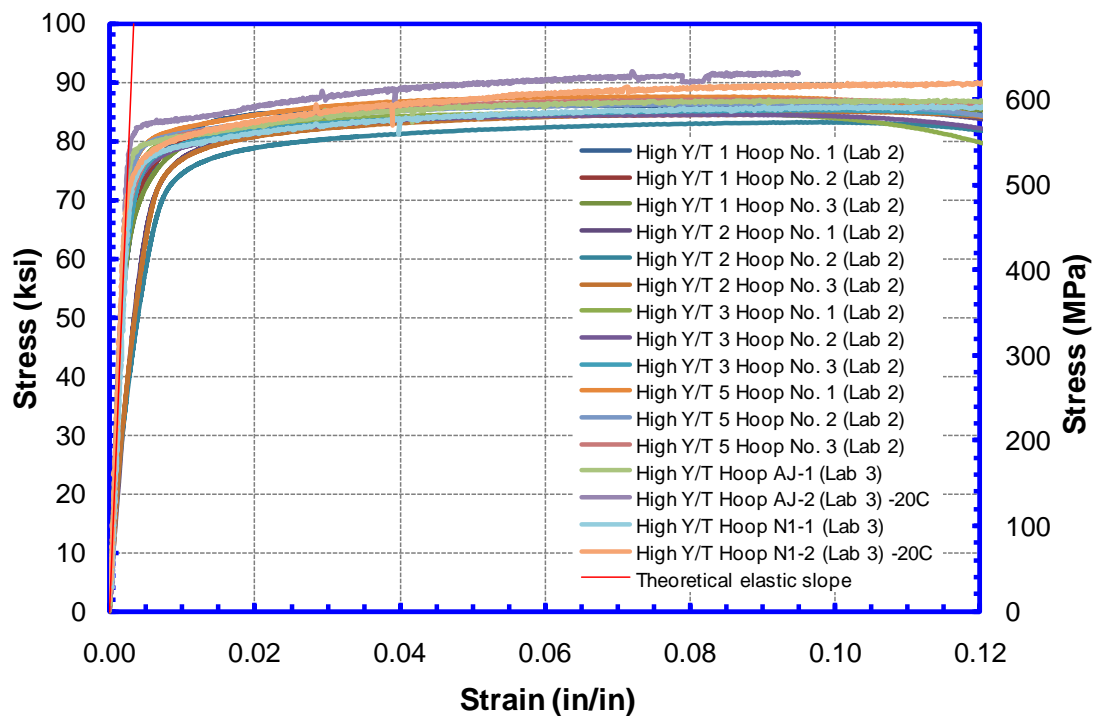


Figure 3.7 Hoop tensile properties of the 12" high Y/T ratio pipe

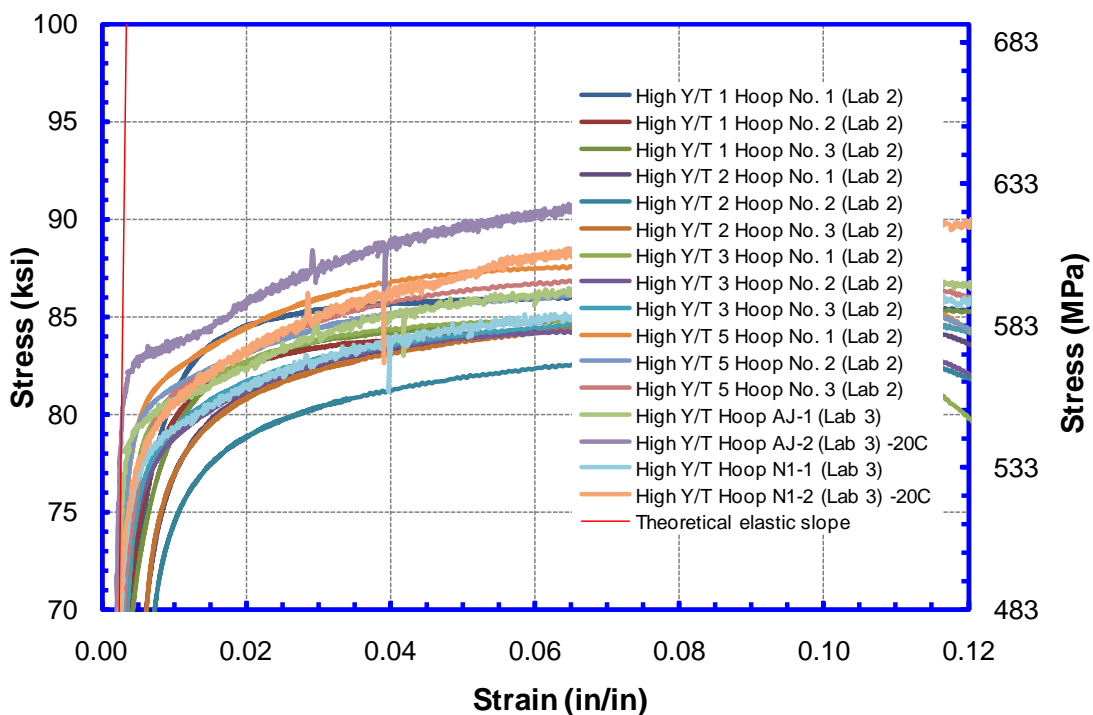


Figure 3.8 Top portion (high strength) of Figure 3.7

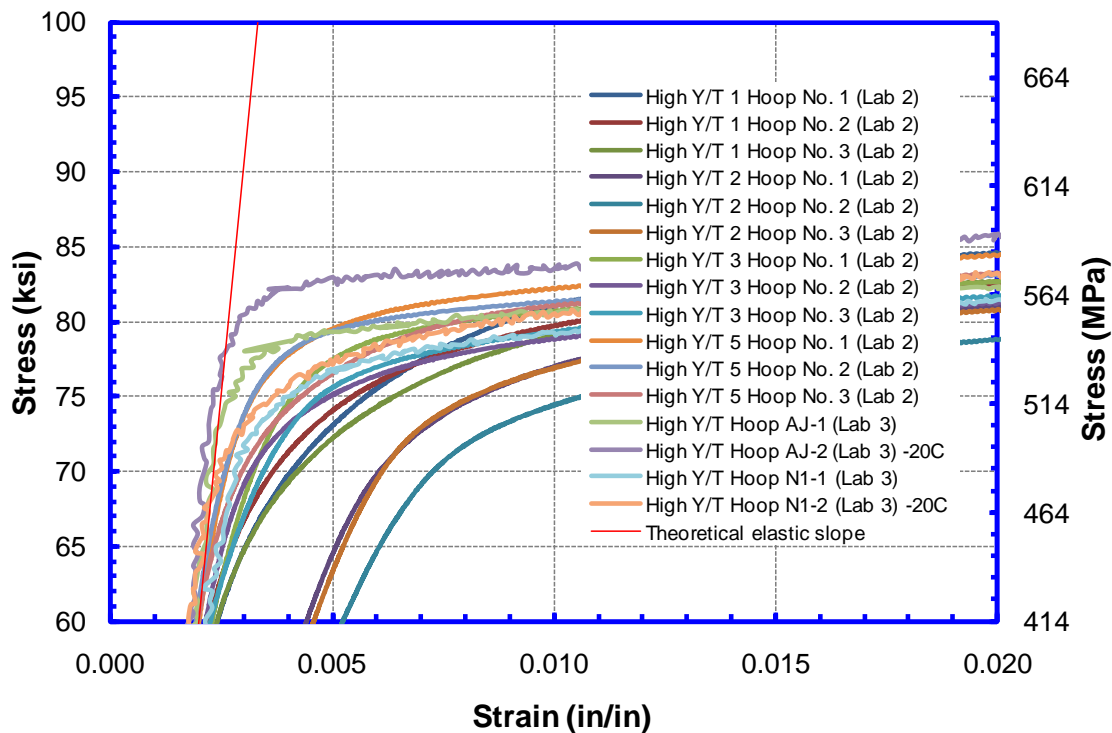


Figure 3.9 Top left (high strength and low strain) portion of Figure 3.7

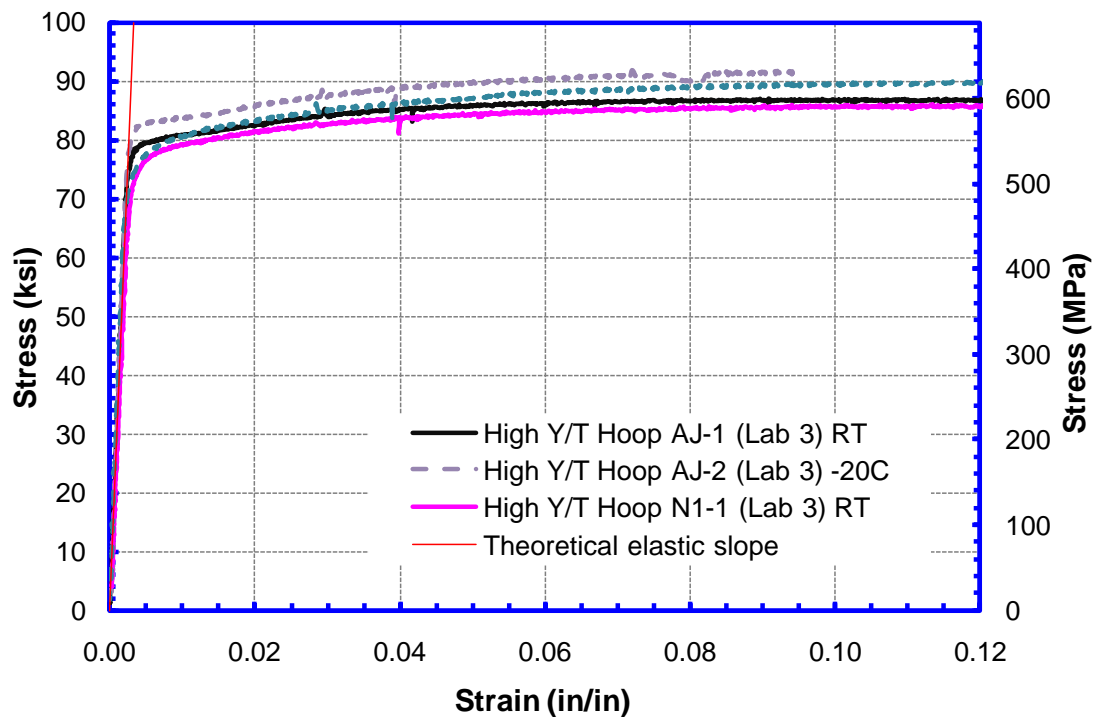


Figure 3.10 Comparison of hoop tensile properties of 12 inch high Y/T pipe at different temperatures

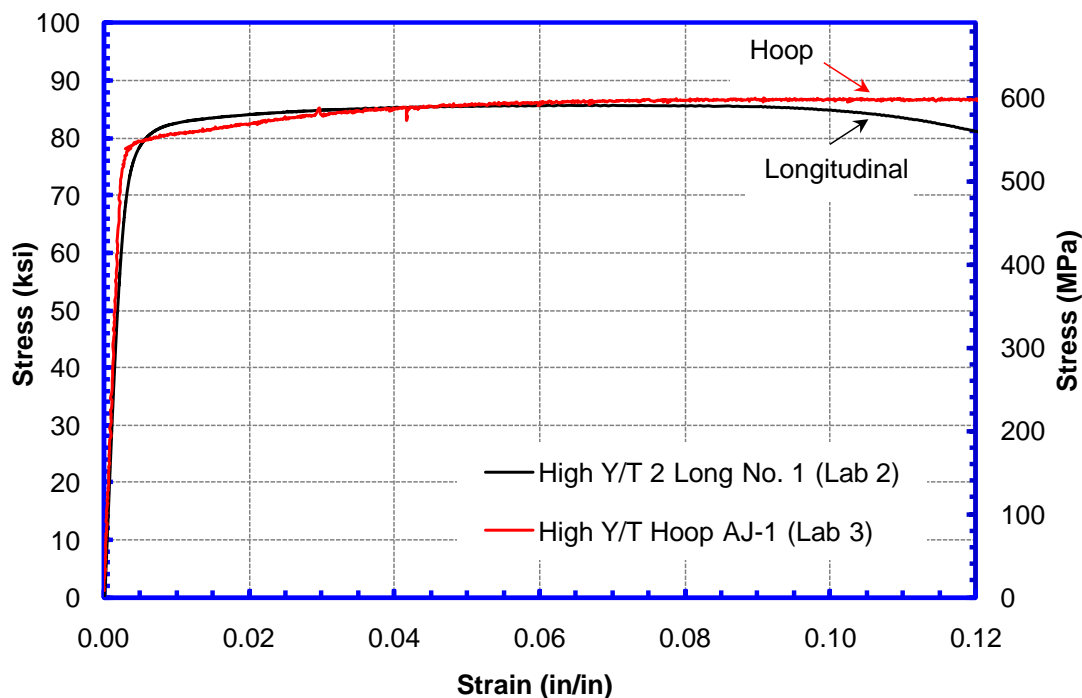


Figure 3.11 Comparison of selected longitudinal and hoop tensile properties of the 12" high Y/T pipe

3.4.2.2 Low Y/T Pipe Hoop Properties

A selected set of hoop stress-strain curves of the X65 low Y/T pipe are shown in Figure 3.14. The top portion of Figure 3.14 at small strain is shown in Figure 3.15. At the customary definition of yield strain, at 0.5% of total engineering strain, the report yield strength could have varied from 58 ksi to 68 ksi. The increased strain hardening and uniform elongation at -20°C over those at room temperature is quite dramatic, as shown in Figure 3.14.

3.4.2.3 Comparison of Longitudinal and Hoop Properties

The comparison of the longitudinal and hoop properties is given in Figure 3.16. Given the scatters in both longitudinal and hoop properties, curves at the middle of the variation ranges were selected for the comparison.

3.4.3 Tensile Properties of X80 24-Inch Pipes

3.4.3.1 Longitudinal Properties of 24-inch Pipe

The longitudinal stress-strain curves of the X80 pipe at two different temperatures are shown in Figure 3.17. There is a marked increase in both strength and uniform elongation at -20°C .

3.4.3.2 Hoop Properties of 24-inch Pipe

The hoop stress-strain curves of the X80 pipe at two different temperatures are shown in Figure 3.18. There is a marked increase in the strength at -20°C . The increase in uniform elongation is particularly dramatic, from approximately 1.5-2.0% to over 5%.

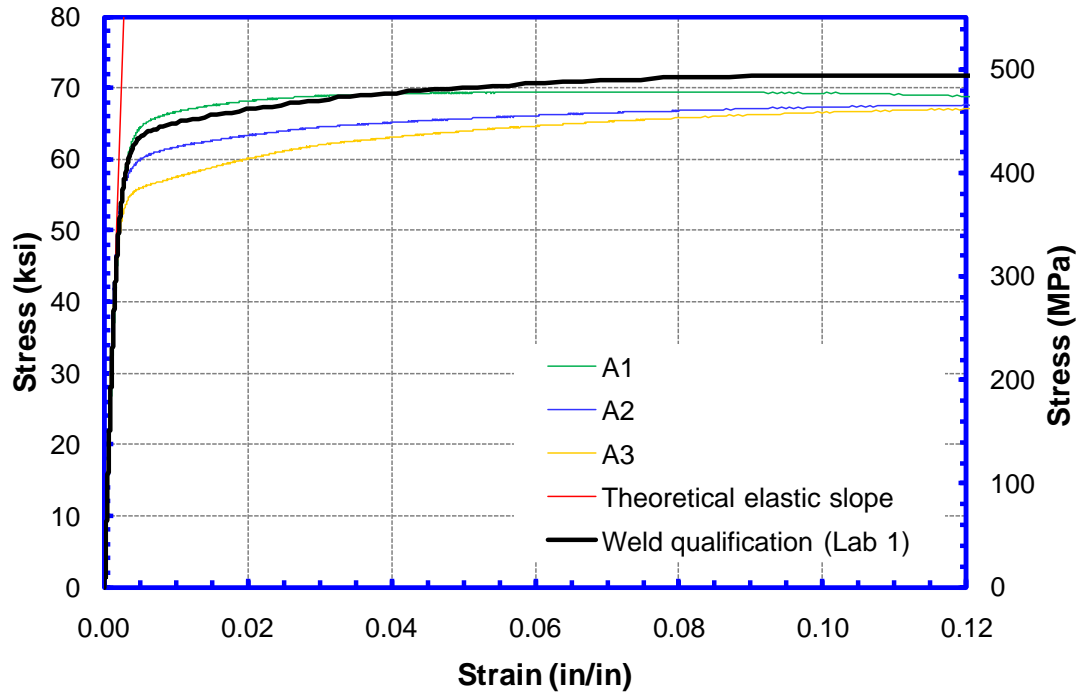


Figure 3.12 Longitudinal tensile properties of the 12" low Y/T ratio pipe

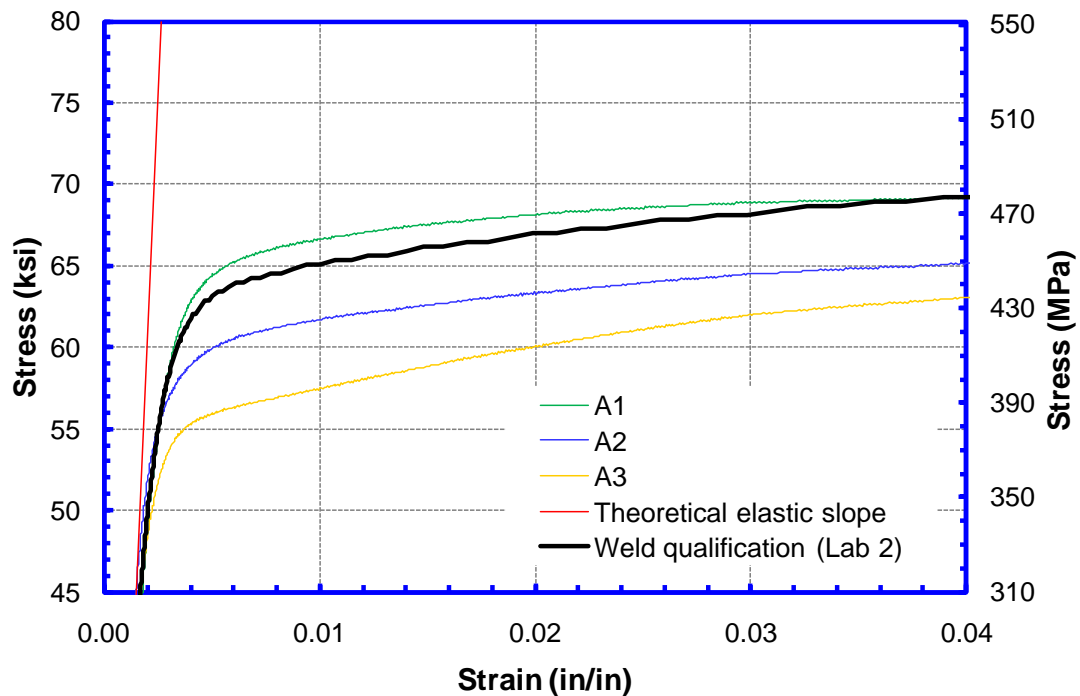


Figure 3.13 Top left portion (high strength and low strain) of Figure 3.12

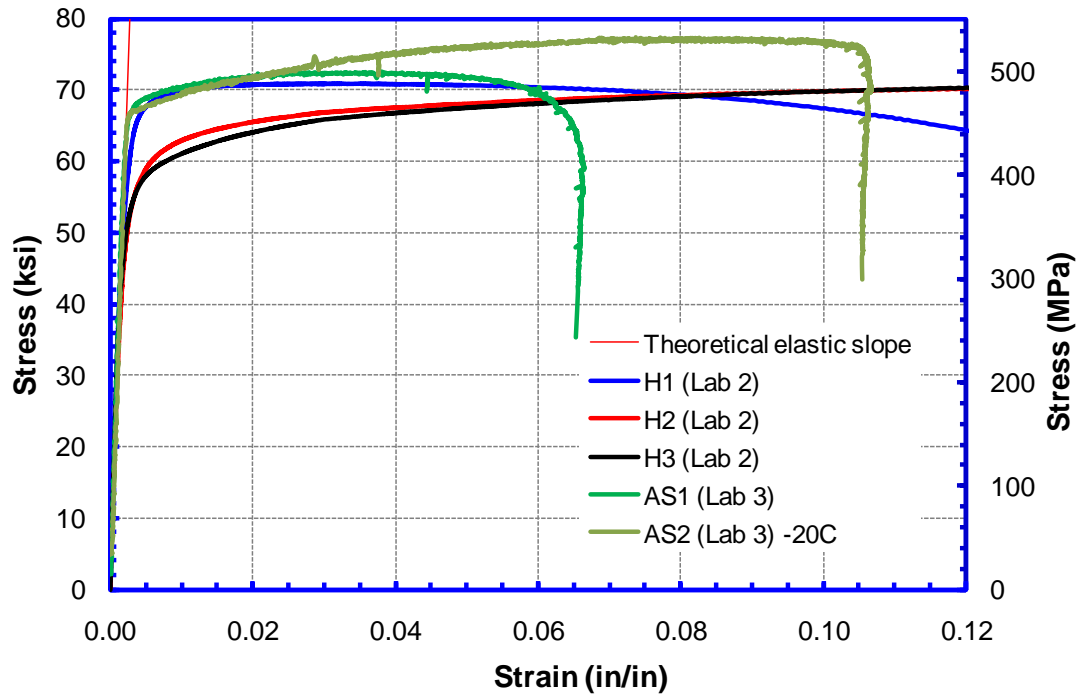


Figure 3.14 Hoop tensile properties of the 12" low Y/T pipe

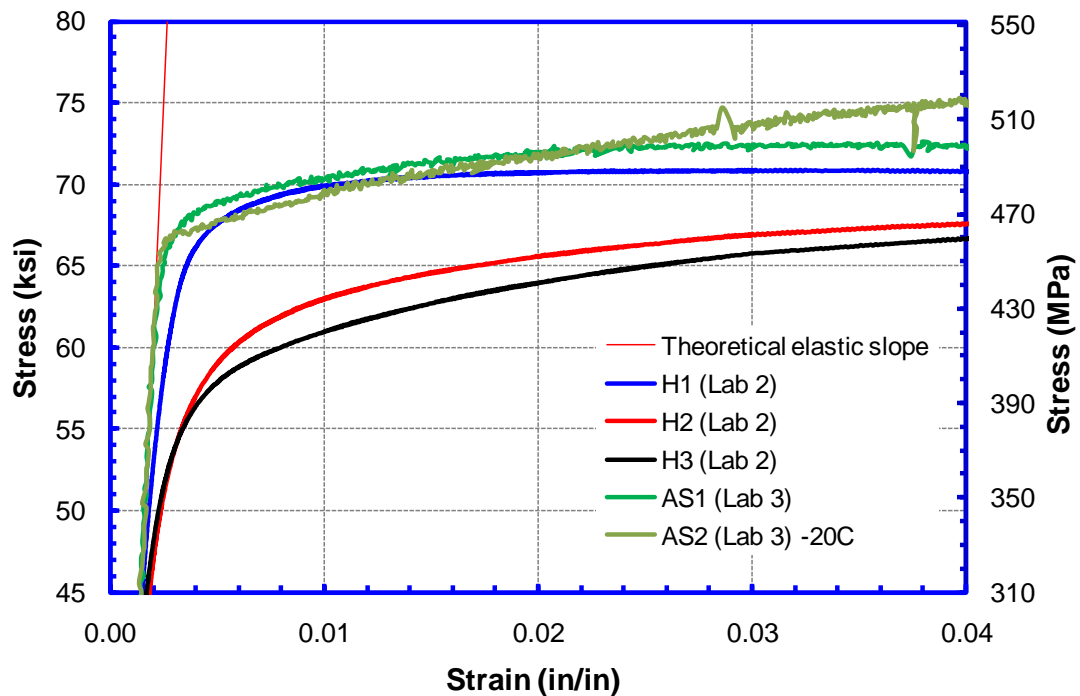


Figure 3.15 Top left portion (high strength and low strain) of Figure 3.14

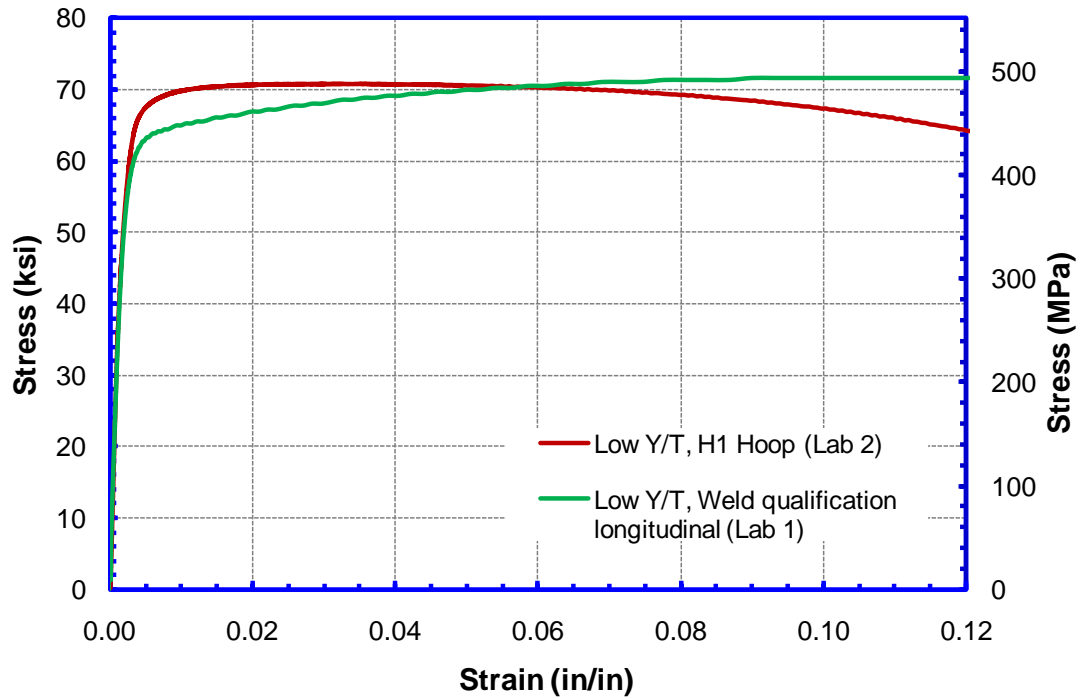


Figure 3.16 Comparison of longitudinal and hoop properties of the 12" low Y/T pipe

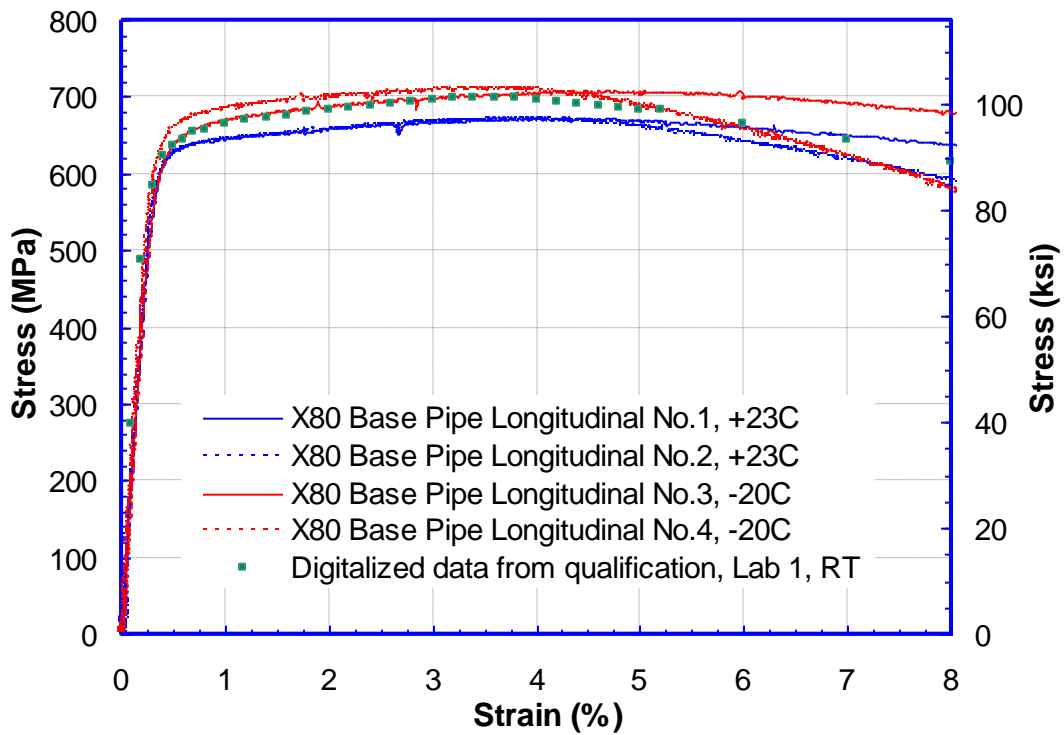


Figure 3.17 Longitudinal tensile properties of 24" pipe

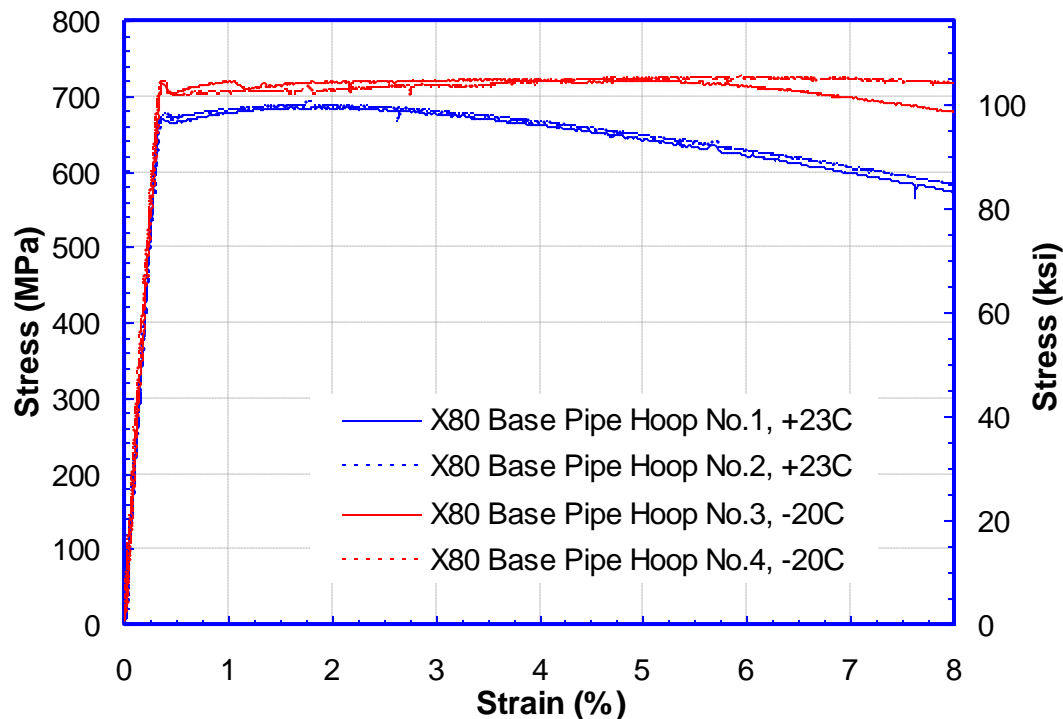


Figure 3.18 Hoop tensile property of the 24" pipe

3.5 Girth Weld Tensile Properties and Weld Strength Mismatch

3.5.1 Tensile Properties of 1st Production Girth Welds

A selected set of all-weld metal tensile properties are shown in Figure 3.19. A longitudinal base pipe property is plotted on the same figure for reference. Two stress-strain curves from the welding procedure qualification are also plotted for reference. Additional weld metal tensile properties are shown in Figure 3.20. For a clear illustration of the range of the all-weld metal properties and the weld strength mismatch levels with respect to the base pipe properties, selected curves are shown in Figure 3.21 and Figure 3.22. The weld metal stress-strain curves were selected to present the upper and lower bounds of the stress-strain curves. It is evident from those curves that on average, the weld metal yield strength is lower than that of the base pipe. The weld metal UTS is higher than that of the base pipe.

The effects of test temperature on all-weld metal tensile properties are shown in Figure 3.23. There is a marked increase in the strength, strain hardening, and uniform elongation at -20°C.

3.5.2 Tensile Properties of 2nd Production Girth Weld

The all-weld metal tensile properties of the 2nd production weld, at two different test temperatures, are shown in Figure 3.24. A longitudinal base pipe property is plotted on the same figure for reference. The weld metal overmatches the base pipe at both yield and UTS. The weld metal exhibits higher strength and uniform elongation at -20°C than those at room temperature.

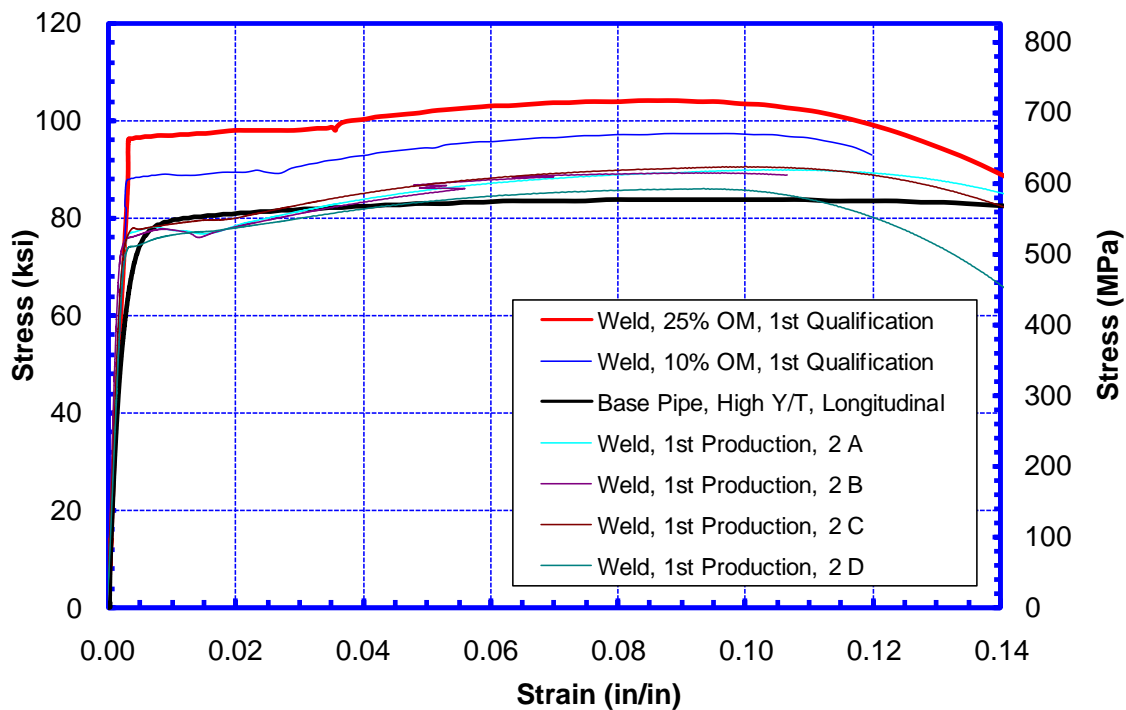


Figure 3.19 Tensile properties of the 1st production welds and the comparison with the properties from the qualification welds

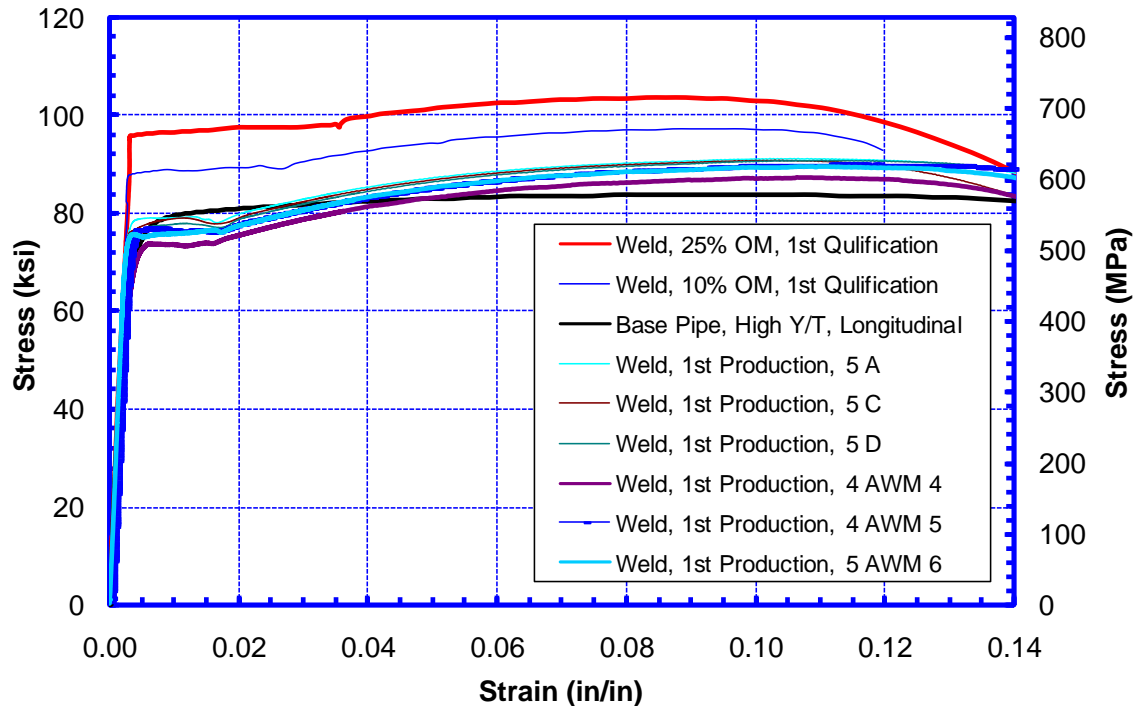


Figure 3.20 Additional tensile properties of the 1st production welds and the comparison with the properties from the qualification welds

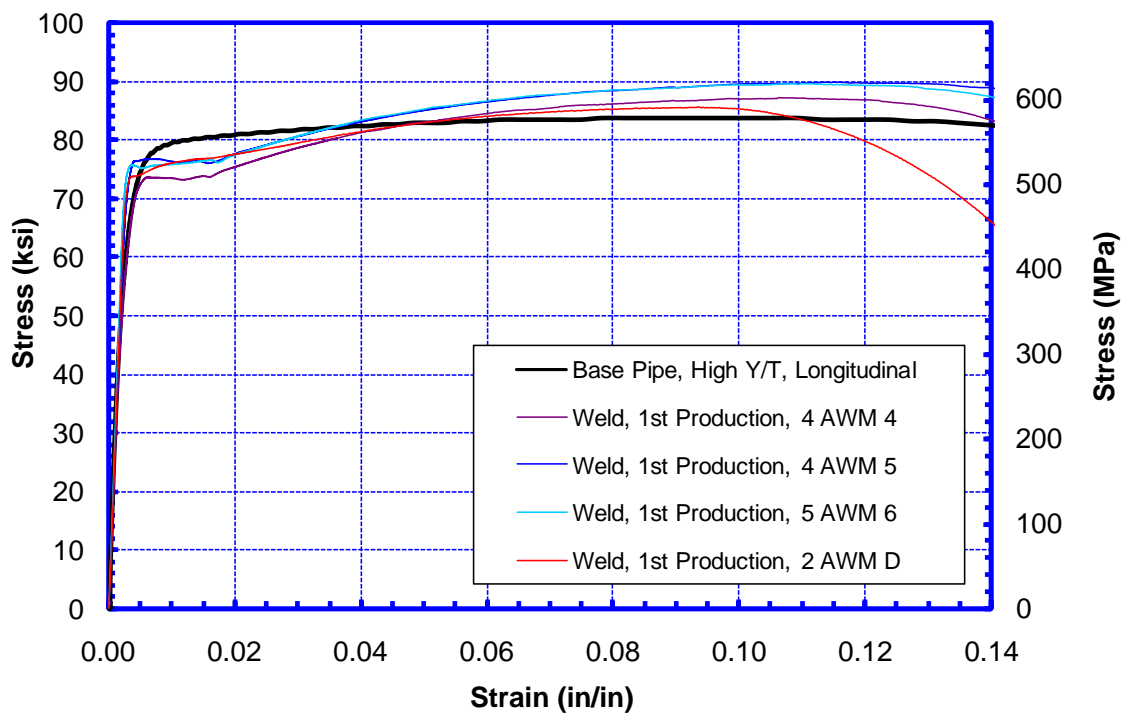


Figure 3.21 Comparison of 1st production weld properties with a typical longitudinal property of high Y/T pipe

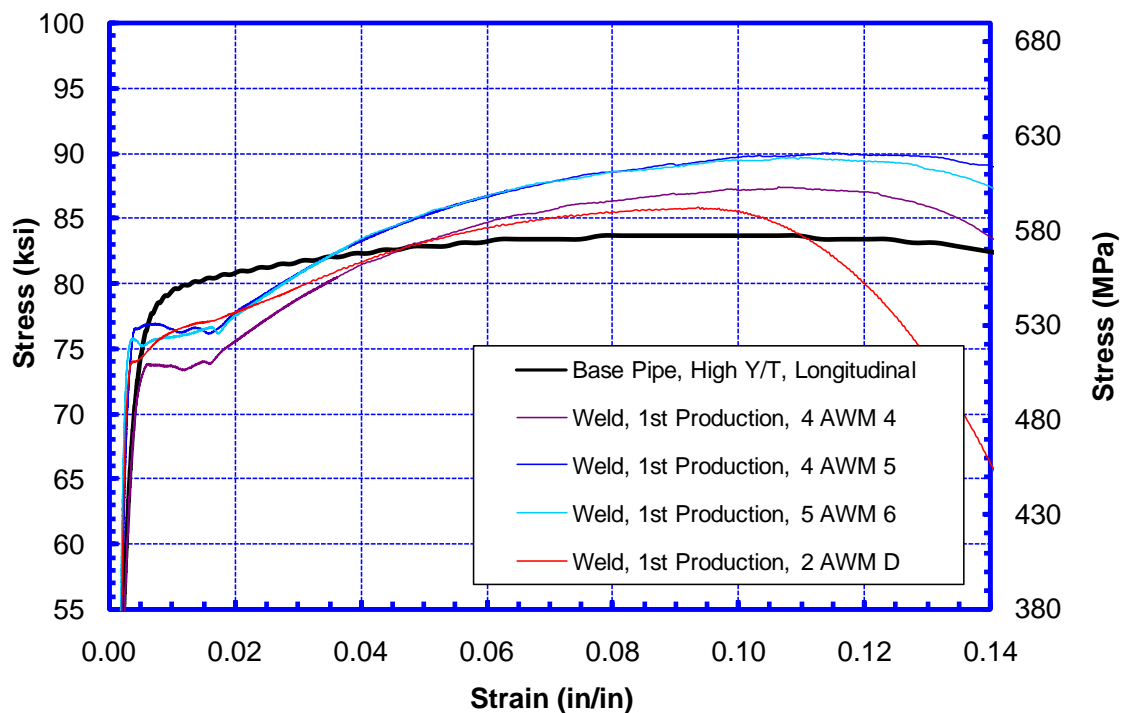


Figure 3.22 Top portion (high strength) of Figure 3.21

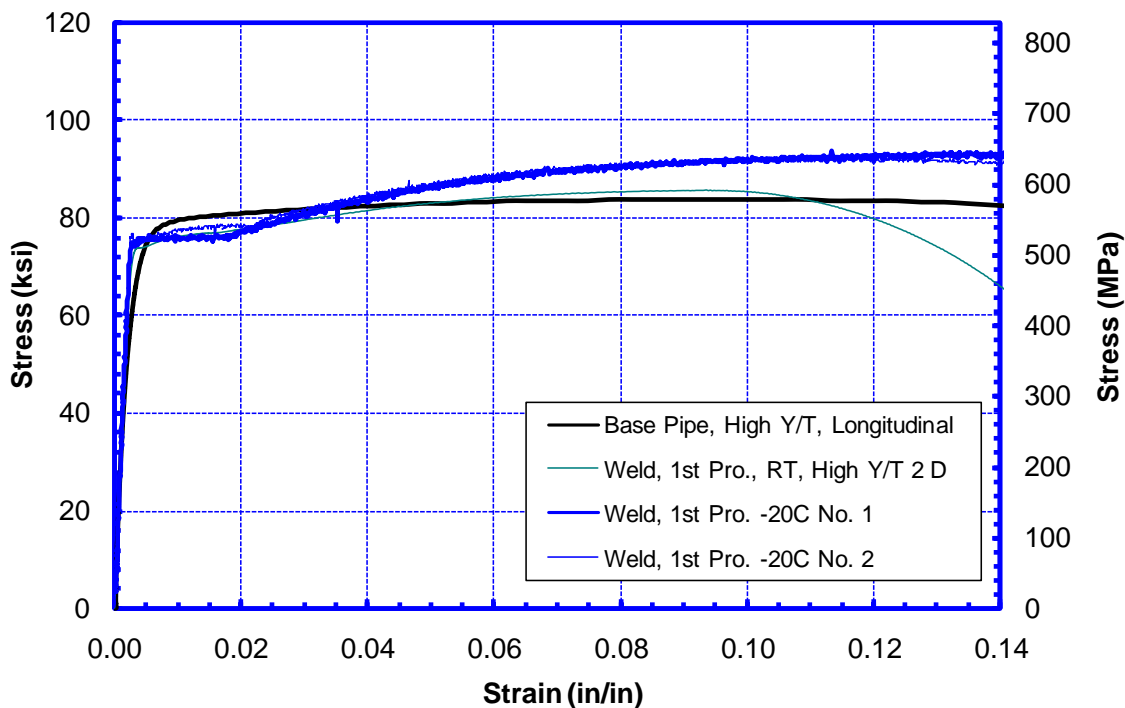


Figure 3.23 Comparison of weld tensile properties at two different temperatures with the high Y/T pipe property as a reference

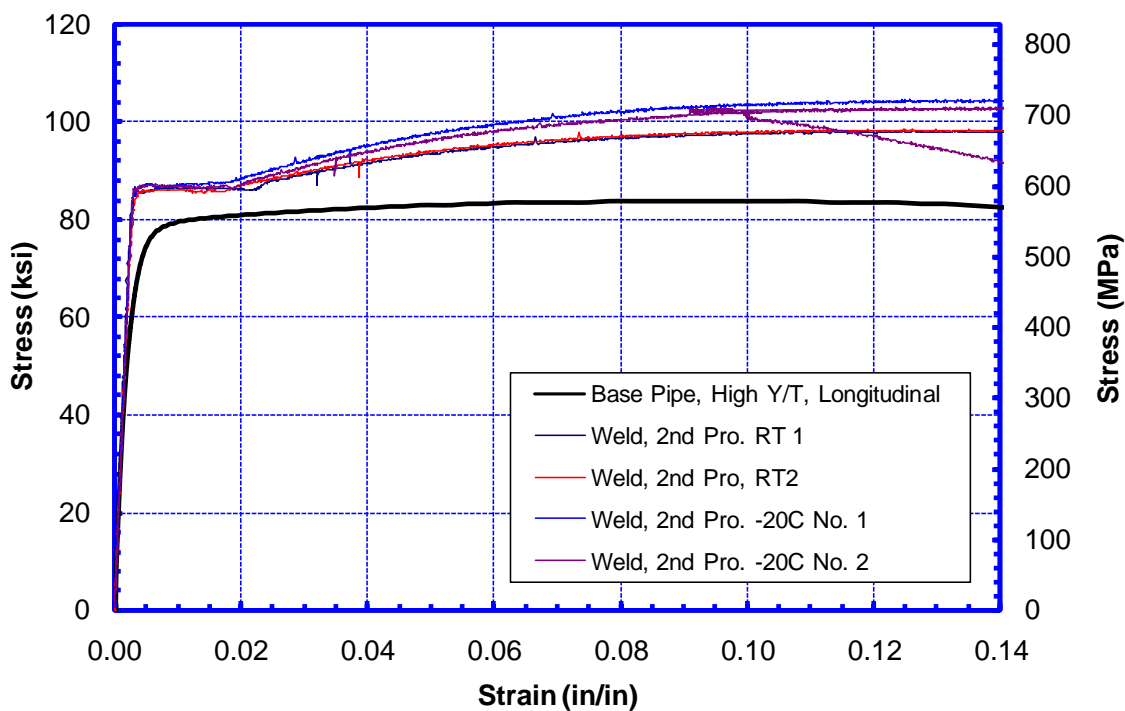


Figure 3.24 Tensile properties of 2nd production welds at two different temperatures with the tensile property of high Y/T pipe as a reference

3.5.3 Tensile Properties of Girth Welds for 12-Inch Low Y/T Pipe

The all-weld metal tensile properties of the low Y/T pipe, at two different test temperatures, are shown in Figure 3.25. A longitudinal base pipe property is plotted on the same figure for reference. The weld metal overmatches the base pipe at both yield and UTS. The weld metal exhibits higher strength and uniform elongation at -20°C than those at room temperature.

3.5.4 Tensile Properties of Girth Welds for 24-Inch X80 Pipe

The all-weld metal tensile properties of the X80 pipe, at two different test temperatures, are shown in Figure 3.26. Four of the five curves were obtained from Lab 3 with the production welds. The remaining curve was from Lab 1 as a part of welding procedure qualification (room temperature). There are some appreciable differences between the curve from the welding procedure qualification and the curves of the production welds. The curves of the production welds all exhibit Lüder's extension, whereas the qualification curve does not show any Lüder's extension. For the production welds, there is an appreciable increase in strength and strain hardening at the low temperature. The qualification curve, tested at room temperature, shows higher strength than the curves from the production welds tested at the same temperature.

The comparison of the pipe properties in both longitudinal and hoop directions, and the weld properties at room temperature, is given in Figure 3.27. A similar comparison at -20°C is shown in Figure 3.28.

The summary of the X80 tensile properties by individual tests is given in Table 3.2.

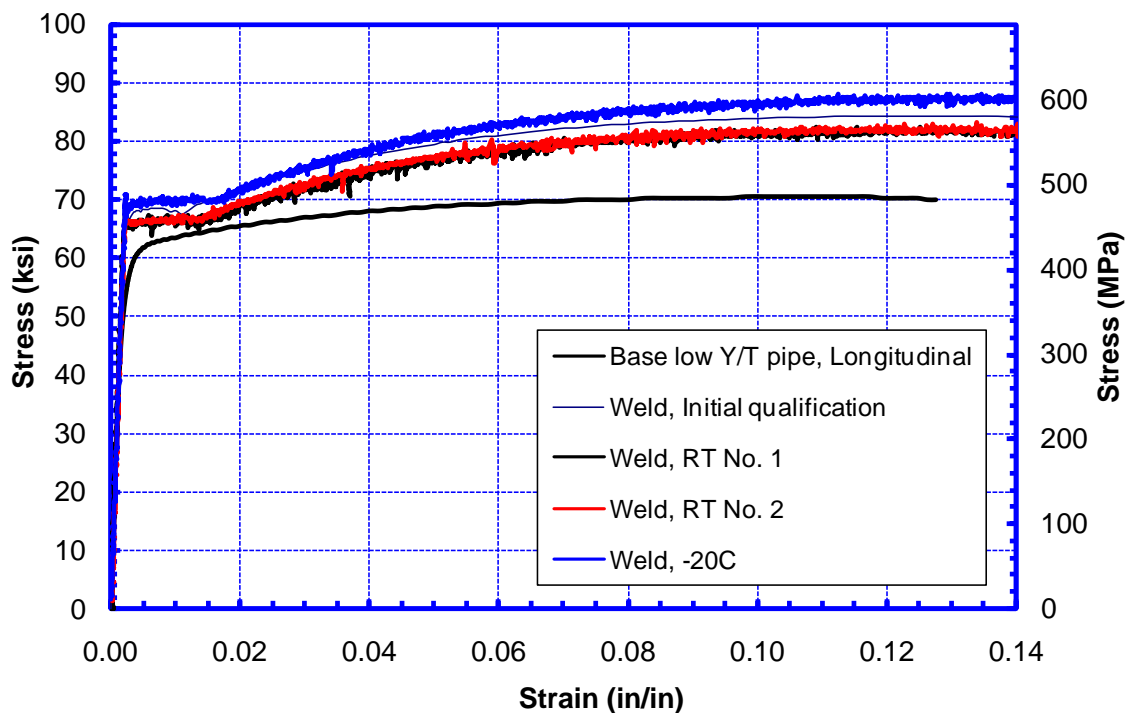


Figure 3.25 Tensile properties of the weld of the low Y/T pipe

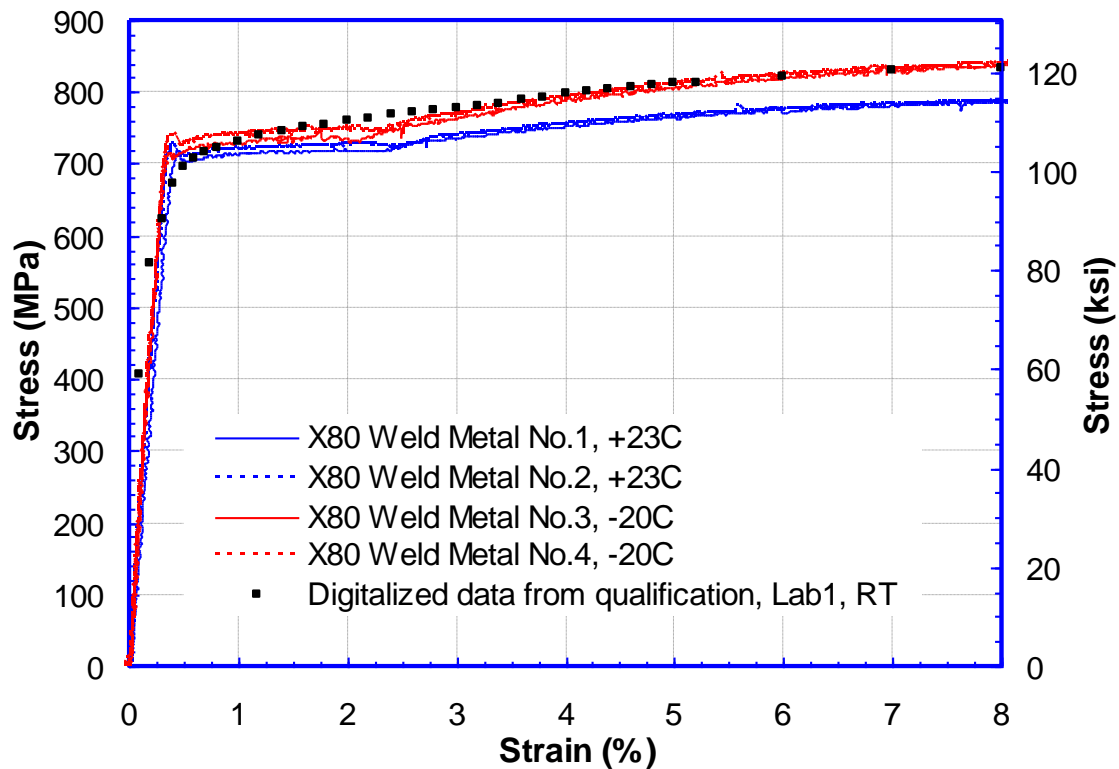


Figure 3.26 Tensile properties of the weld at two different temperatures to the 24" pipe

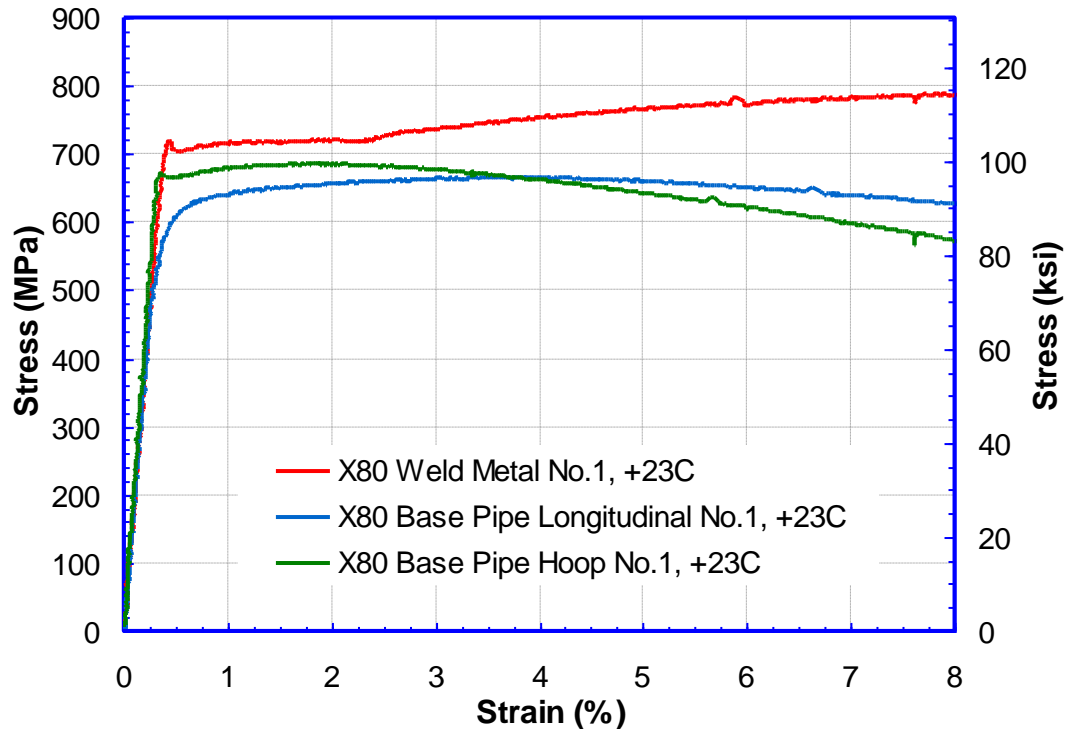


Figure 3.27 Comparison of the weld, pipe longitudinal, and pipe hoop tensile properties at room temperature

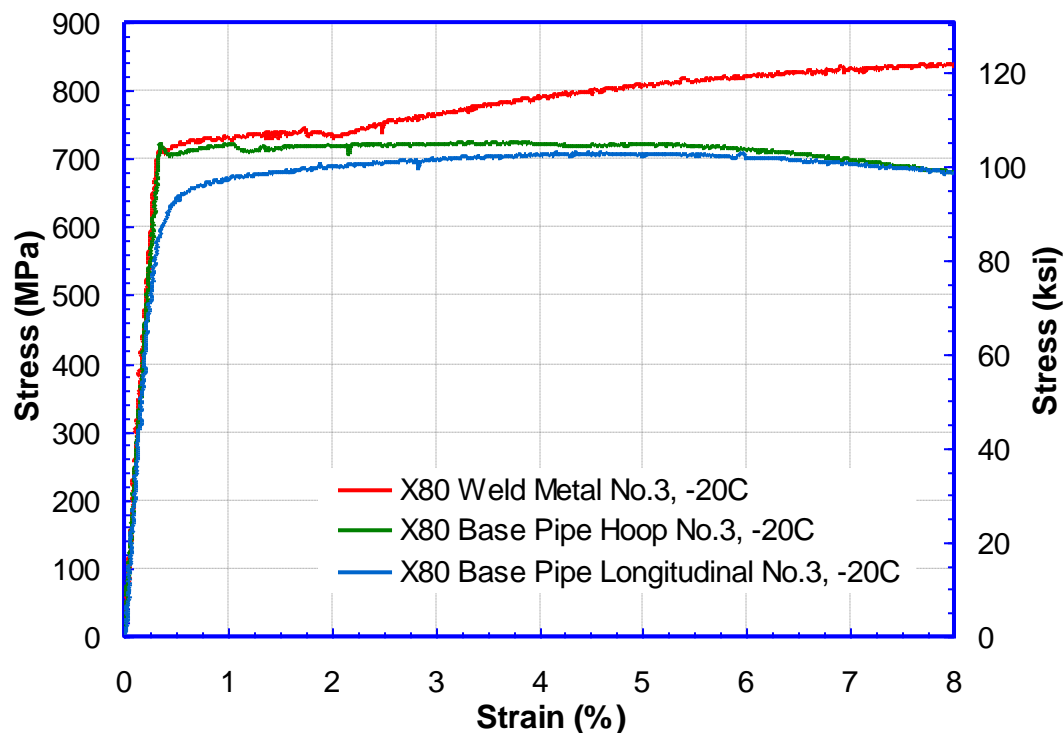


Figure 3.28 Comparison of the weld, pipe longitudinal, and pipe hoop tensile properties at -20°C

3.6 Summary of Tensile Properties

The summary of the tensile properties in customary measures, such as yield strength and UTS, is given in

Table 3.3. A few major features of the tensile properties that can be observed are:

- (1) Variations in UTS are typically smaller than in yield strength.
- (2) Hoop properties tend to have greater variations than longitudinal properties.
- (3) In most cases, when comparable tests exist, there were marked increases in the strength, strain hardening, and uniform elongation of the materials at -20°C, over the same properties at room temperature.
- (4) With a large number of tests of the high Y/T pipe and the first production welds, the yield strength exhibited large variations. Such large variations were not observed when only a small number of tests were conducted for other pipes and welds. It may be postulated that large variations of yield strength could exist, but a small number of tests may not capture such variations.
- (5) For the 1st production weld, the tensile strength of the weld metal from the qualification weld was much higher than that from the production welds. The difference in tensile strength between the qualification weld and production weld is also evident for the X80 weld. The tests were done at different labs so it's not clear if the different labs contributed to the different properties obtained from the tests.

Table 3.2 Summary of X80 tensile properties

Specimen ID	Temp. C	YS (0.2%) MPa	YS (0.5%) MPa	UTS MPa	Uniform Strain %	Total Elongation %	Y/T
BML-1	23	612.7	606.3	665.8	3.99	19.91	0.91
BML-2	23	630.2	625.2	672.7	3.90	N/A	0.93
BML-3	-20	641.1	639.4	709.5	5.95	20.45	0.90
BML-4	-20	664.6	654.5	712.4	3.68	N/A	0.92
Average	23	621.5	615.7	669.3	3.95	19.91	0.92
Average	-20	652.8	647.0	710.9	4.82	20.45	0.91

Specimen ID	Temp. C	YS (0.2%) MPa	YS (0.5%) MPa	UTS MPa	Uniform Strain %	Total Elongation %	Y/T
BMC-1	23	666.3	665.7	686.0	1.84	14.70	0.97
BMC-2	23	670.9	670.2	690.9	1.78	15.47	0.97
BMC-3	-20	707.0	706.7	723.3	3.33	18.69	0.98
BMC-4	-20	699.2	700.6	724.7	5.98	22.79	0.97
Average	23	668.6	667.9	688.5	1.81	15.08	0.97
Average	-20	703.1	703.7	724.0	4.65	20.74	0.97

Specimen ID	Temp. C	YS (0.2%) MPa	YS (0.5%) MPa	UTS MPa	Uniform Strain %	Total Elongation %	Y/T
WM-1	23	705.7	706.0	793.6	10.63	24.07	0.89
WM-2	23	711.4	710.8	796.9	9.68	23.32	0.89
WM-3	-20	718.9	718.9	853.2	9.22	N/A	0.84
WM-4	-20	730.2	725.8	851.1	9.51	24.94	0.85
Average	23	708.5	708.4	795.2	10.15	23.70	0.89
Average	-20	724.6	722.3	852.2	9.37	24.94	0.85

Table 3.3 Summary of tensile properties

Material	Attribute	Total Number of Tests at Room Temperature	Availability of -20C Data	Yield (ksi, MPa)			UTS (ksi, MPa)			Y/T	Mismatch Ratio	Mismatch Ratio
				Min	Max	Average	Min	Max	Average	Using Averaged Values	Using Averaged Yield Values	Using Averaged UTS Values
High Y/T pipe	Pipe Long	15		74.6 (514.4)	82.2 (566.8)	79.3 (547.0)	84.6 (583.3)	87.9 (606.1)	86.1 (593.4)	0.92	N/A	N/A
	Pipe Hoop	17	Yes	58.3 (402.0)	79.5 (548.2)	73.8 (508.7)	80.4 (554.4)	87.6 (604.0)	85.2 (587.7)	0.87	N/A	N/A
	Weld, 1st Prod	10	Yes	72.5 (499.9)	79.1 (545.4)	76.3 (526.2)	85.8 (591.6)	91.4 (630.2)	89.6 (617.6)	0.85	0.96	1.04
	Weld, 2nd Prod	2	Yes	85.9 (592.3)	85.9 (592.3)	85.9 (592.3)	98.4 (678.5)	98.6 (679.8)	98.5 (679.2)	0.87	1.08	1.14
Low Y/T pipe	Pipe Long	5		55.9 (385.4)	64.4 (444.0)	61.0 (420.5)	67.7 (466.8)	71.7 (494.4)	69.5 (478.9)	0.88	N/A	N/A
	Pipe Hoop	4	Yes	57.9 (399.2)	68.7 (473.7)	63.3 (436.5)	70.5 (486.1)	72.6 (500.6)	71.2 (490.9)	0.89	N/A	N/A
	Weld	2	Yes	66.0 (455.1)	66.4 (457.8)	66.2 (456.4)	82.3 (567.5)	83.2 (573.7)	82.8 (570.6)	0.80	1.09	1.19
X80 Pipe	Pipe Long	2	Yes	87.9 (606.3)	90.7 (625.2)	89.3 (615.7)	96.6 (665.8)	97.6 (672.7)	97.1 (669.3)	0.92	N/A	N/A
	Pipe Hoop	2	Yes	96.5 (665.7)	97.2 (670.2)	96.9 (667.9)	99.5 (686.0)	100.2 (690.9)	99.9 (688.5)	0.97	N/A	N/A
	Weld	2	Yes	102.4 (706)	103.1 (710.8)	102.7 (708.4)	115.1 (793.6)	115.6 (796.9)	115.3 (795.2)	0.89	1.15	1.19

3.7 Girth Weld Toughness

3.7.1 Charpy Transition Curves

Weld centerline and HAZ (heat-affected zone) Charpy transition curves were generated for all girth welds, as shown in Figure 3.29 to Figure 3.32. The transition curves of the base pipes were also generated for the X65 pipes. The upper shelf energy of the X65 pipes are very high, nearly 300 ft-lbf or 400 J. The upper shelf energy of the HAZ varies but all are greater than 150 ft-lbs or 200 J. The upper shelf energy of the weld metal is lower than that of the HAZ. For the X65 welds, the weld metals also have higher transition temperatures than the HAZ. For the X80 weld, the transition temperature of the weld is slightly lower than that of the HAZ.

3.7.2 CTOD Transition Curves from SENB Specimens

CTOD transition curves were generated for all girth welds. All data shown in Figure 3.33 to Figure 3.40 are individual test data. All CTOD tests were conducted in BX2B deeply-notched SENB configurations following test standard BS 7448. In general, there is greater scatter at the same test temperature in the HAZ transition curves than that in the weld metal transition curves.

The data scatter, particularly in the HAZ specimens, makes it difficult to precisely draw transition curves. It is apparent for all welds that the upper-shelf HAZ CTOD toughness is higher than that of the corresponding welds. For the X65 welds, the transition temperature of the welds is higher than that of the HAZ. For the X80 weld, the transition temperature of the weld is slightly lower than that of the HAZ, consistent with the trend of the Charpy transition curves.

3.7.3 Toughness Transition from SENT Specimens

SENT testing is becoming increasingly accepted as a more representative small-scale toughness test than the traditional three-point bend CTOD testing [52,53]. All the welds described in the previous section were subjected to SENT testing at NIST and the test results were extensively covered in an IPC paper [54]. The tests followed a single-specimen procedure developed by CANMET [55]. For the comparison of toughness, and particularly the transition temperature, the summary results from the SENT specimens are given in Figure 3.41 and Figure 3.42. Using the J -integral values at the maximum load as a reference, the difference in the toughness behavior between the HAZ and weld metal is quite dramatic. There is no appreciable drop in toughness at temperatures as low as -100°C for the HAZ specimens. In contrast, the toughness of the weld metal starts to drop at temperatures around -30°C. For some of the tested welds, the difference in the transition temperatures between the weld metal and HAZ is greater with the SENT specimens than those with Charpy and CTOD specimens.

3.8 Major Observations from the Small-Scale Toughness Tests

The following observations may be made from the small-scale toughness tests:

1. On the upper shelf, the three forms of tests, Charpy, SENB, and SENT, provide consistent rank of the relative toughness for specimens with notches into the weld, HAZ, and base metal.
2. The toughness values tend to have greater scatter for specimens with notches into the HAZ than those with notches into the weld centerline.
3. The welds tend to have higher transition temperatures than the HAZ of the same girth welds. The difference is most significant from the SENT specimens.
4. The HAZ transition temperature from SENT specimens can be significantly lower than that from Charpy and deeply-cracked (high-constraint) CTOD specimens.

The significance of the toughness data from the small-scale tests is further analyzed in Project 2 and will be reported at a later time.

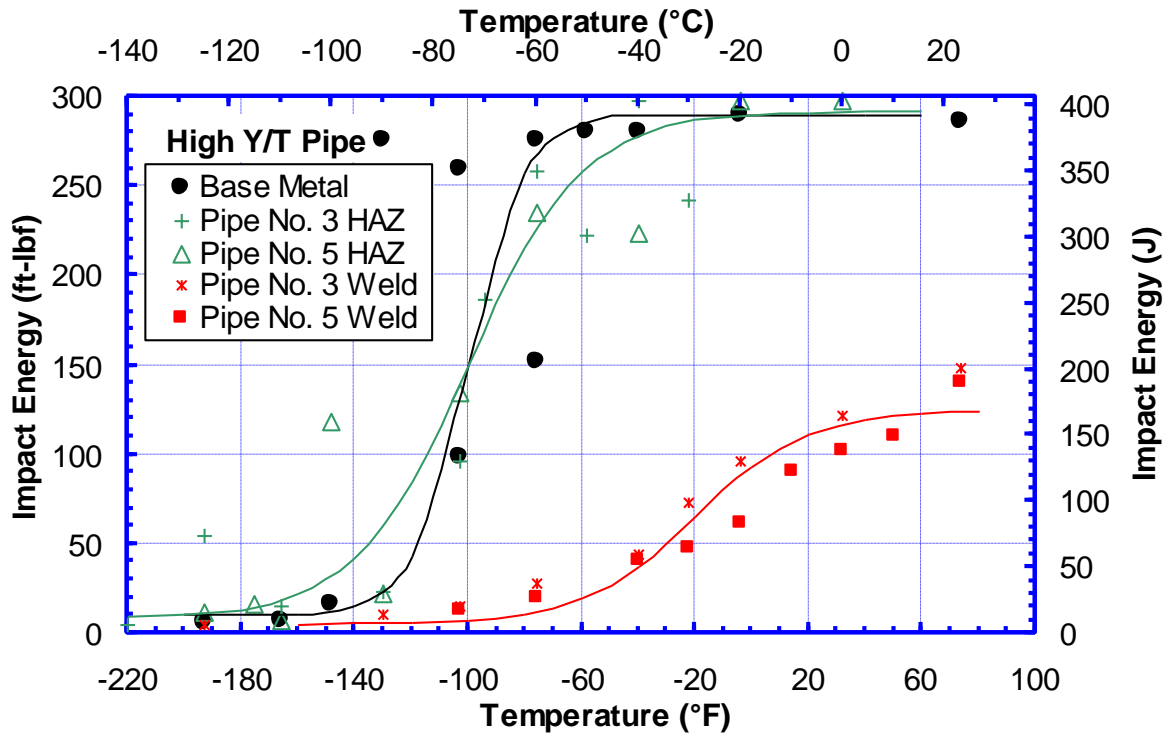


Figure 3.29 Charpy transition curves of the pipe and evenmatched weld of high Y/T X65 pipe

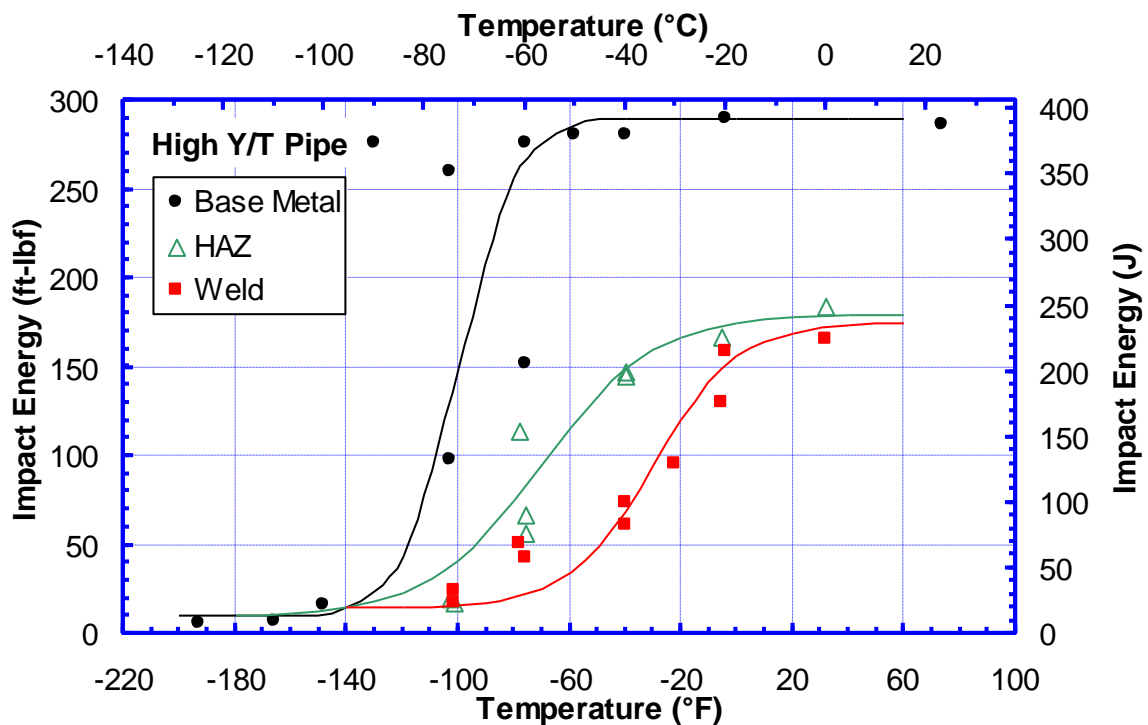


Figure 3.30 Charpy transition curves of the pipe and overmatched weld of high Y/T X65 pipe

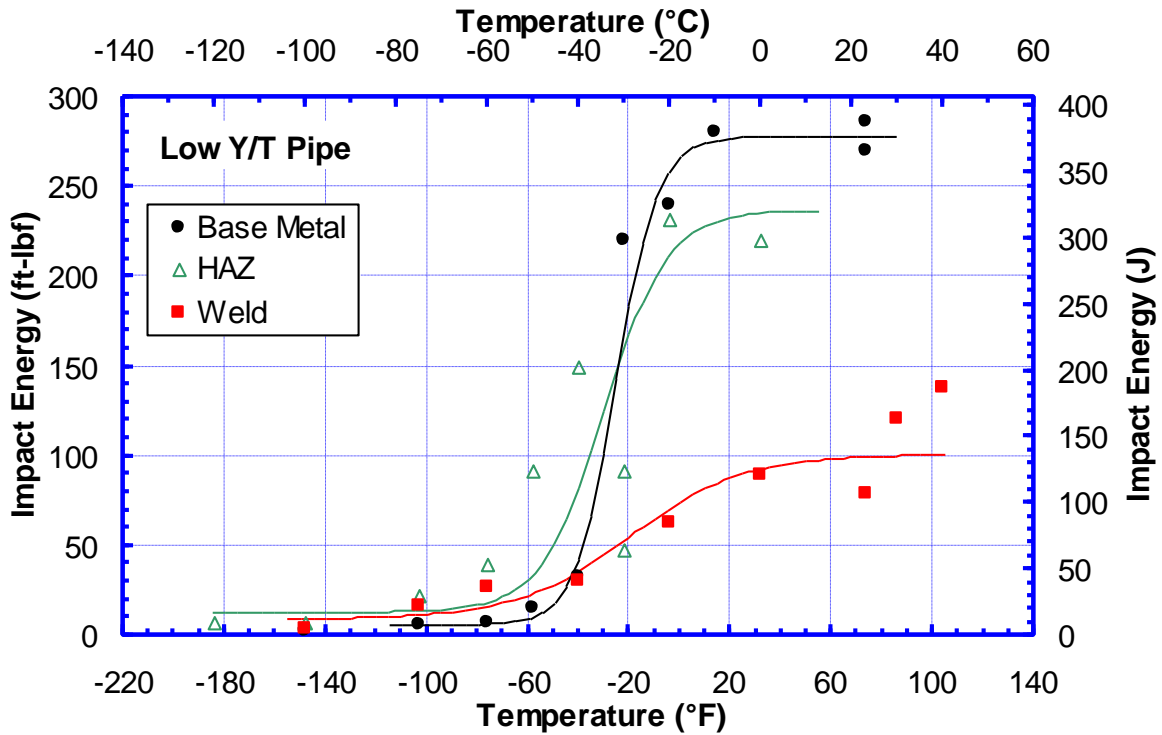


Figure 3.31 Charpy transition curves of the pipe and weld of low Y/T X65 pipe

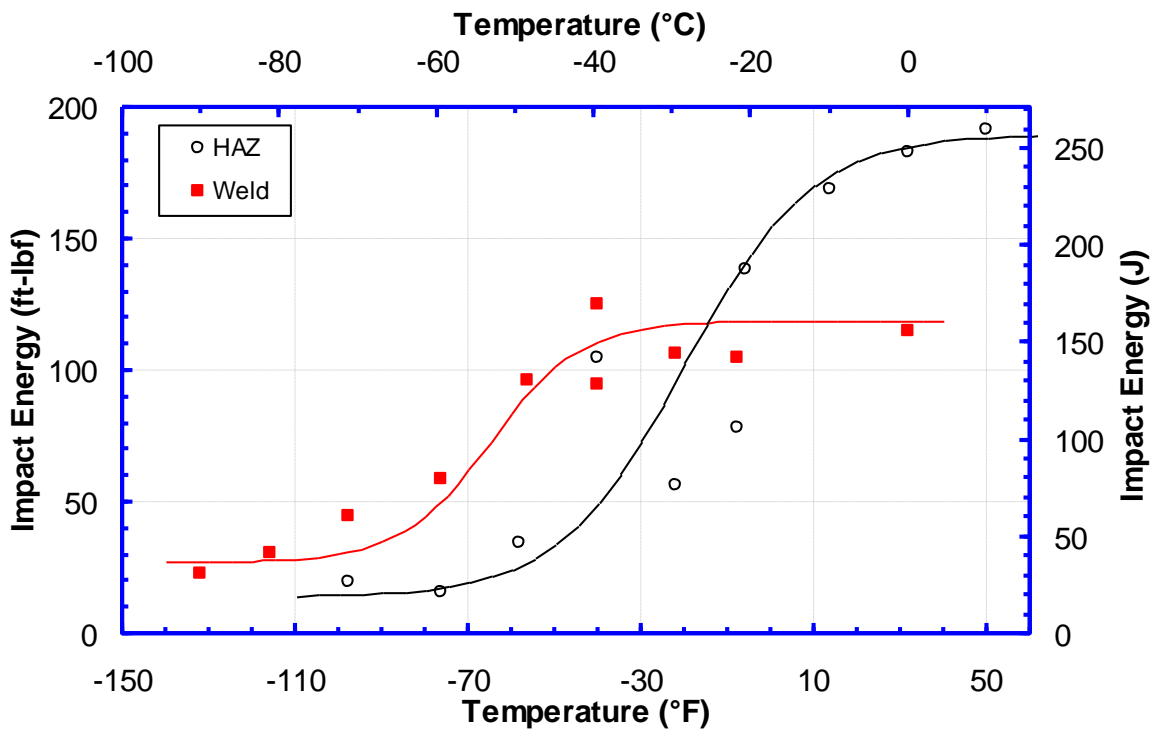


Figure 3.32 Charpy transition curves of the X80 weld

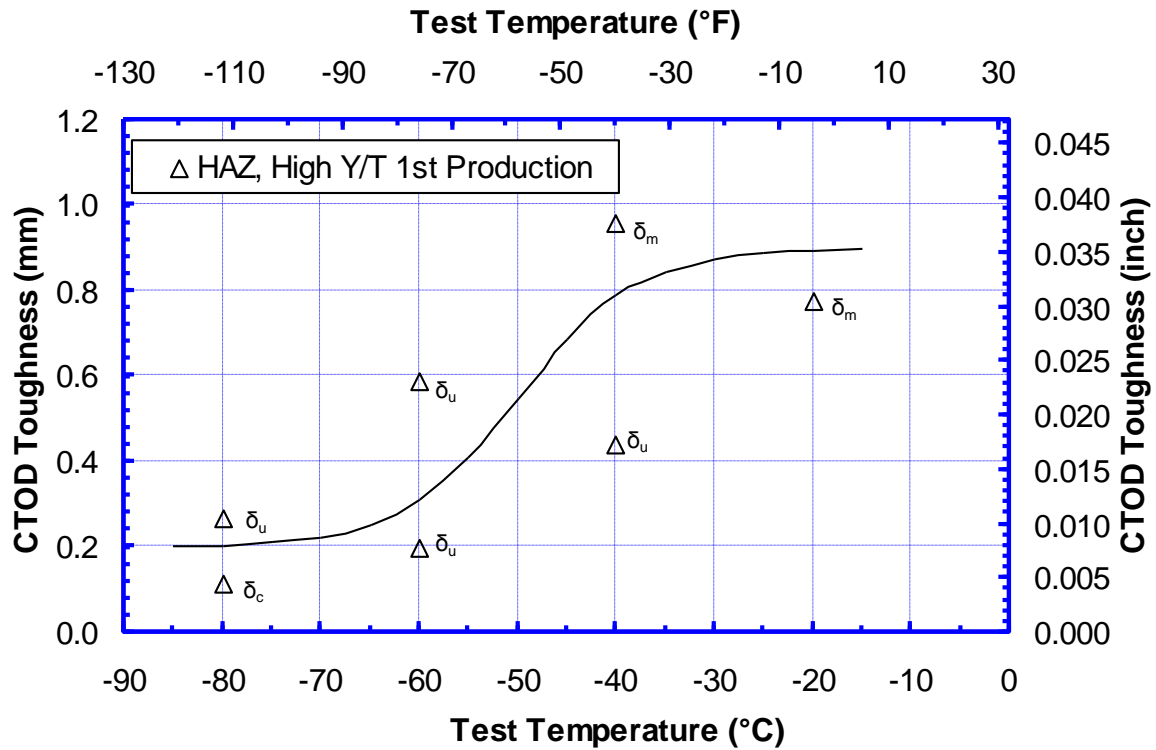


Figure 3.33 HAZ CTOD transition curve of the evenmatched weld of high Y/T X65 pipe

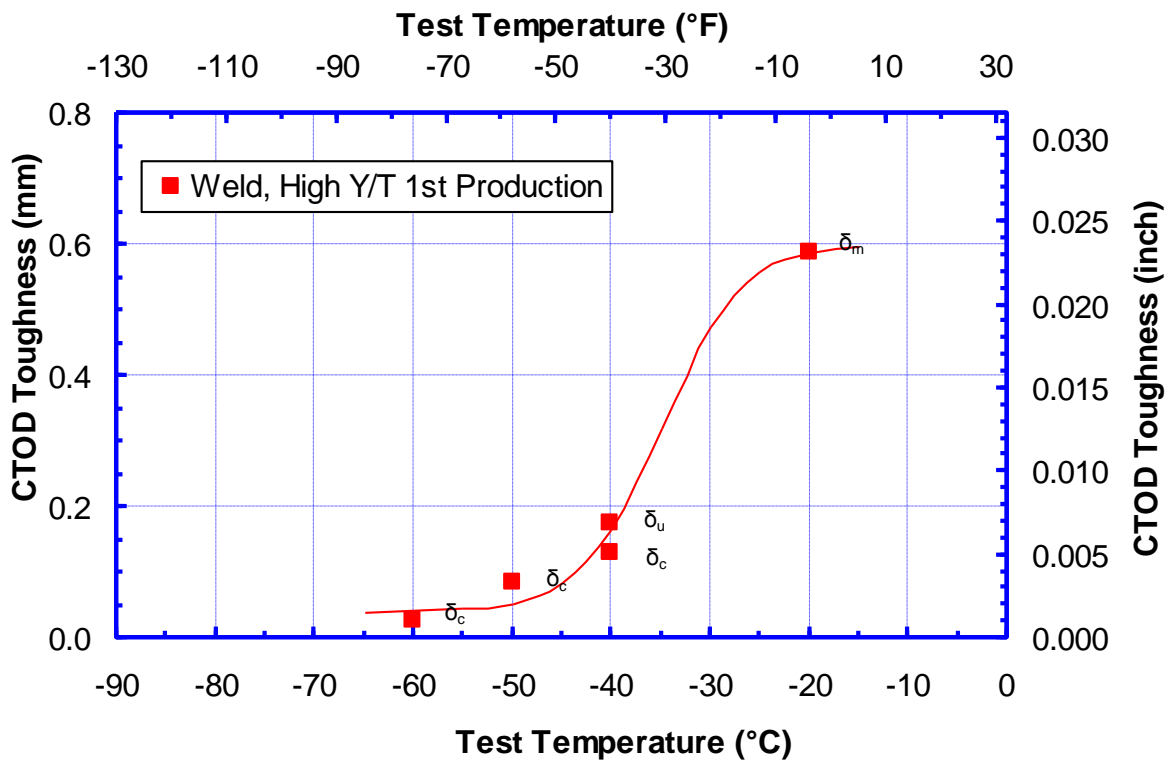


Figure 3.34 Weld metal CTOD transition curve of the evenmatched weld of high Y/T X65 pipe

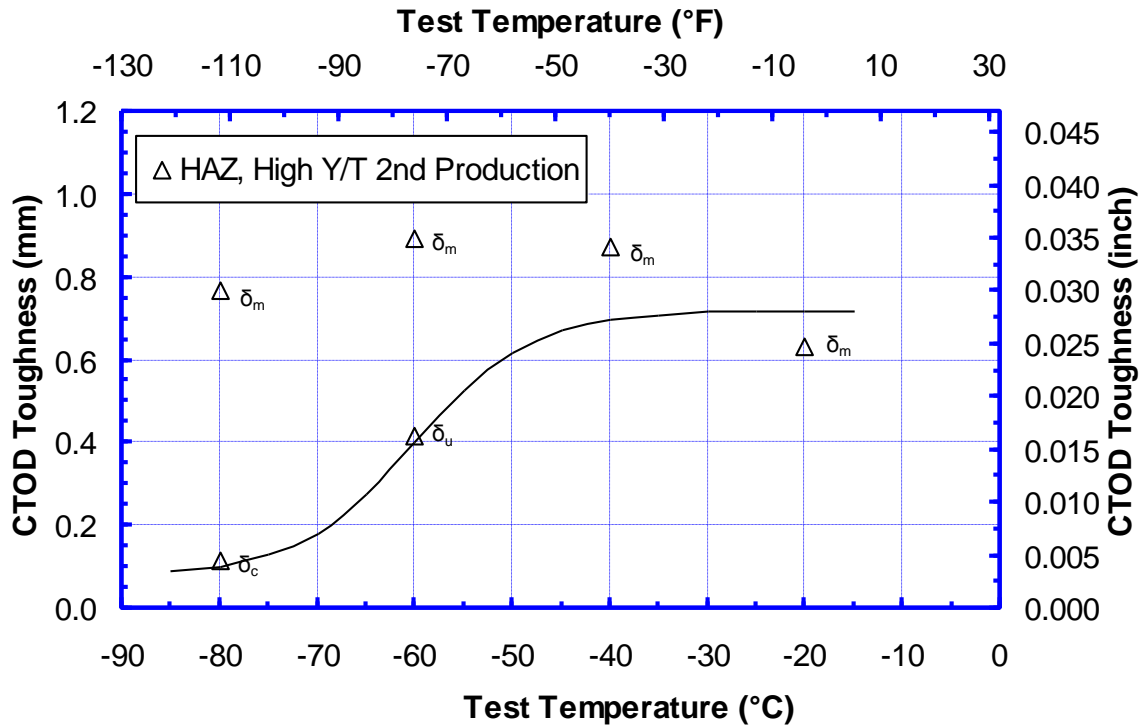


Figure 3.35 HAZ CTOD transition curve of the overmatched weld of high Y/T X65 pipe

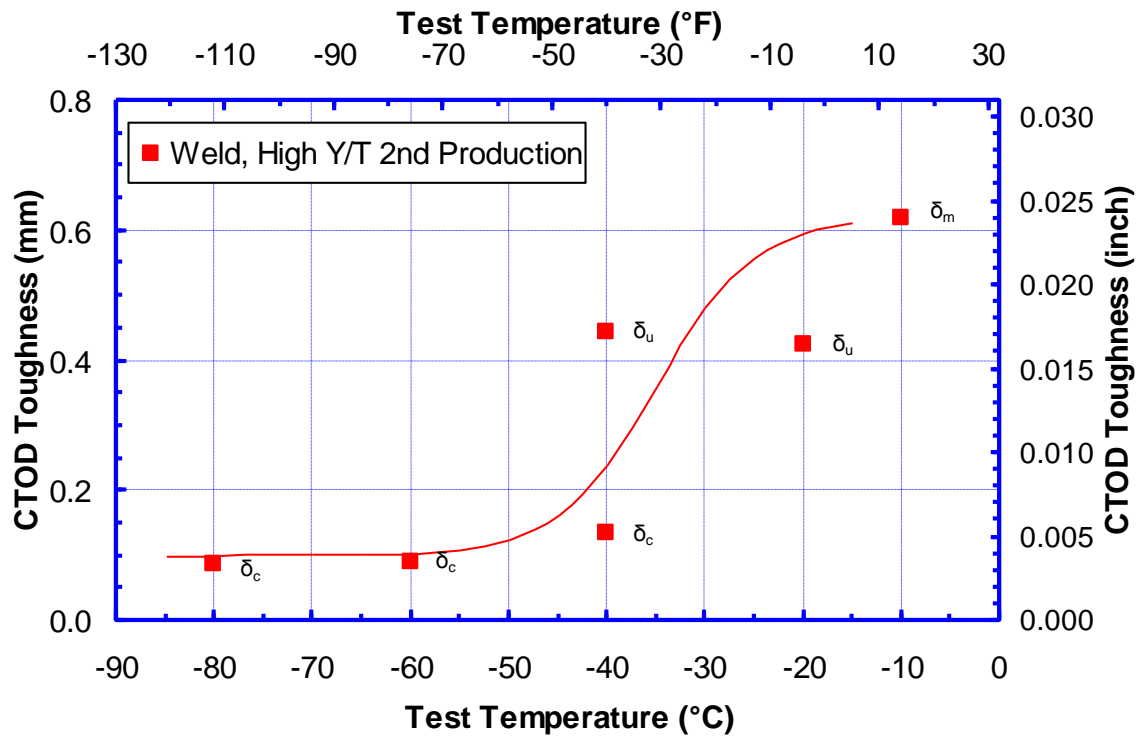


Figure 3.36 Weld metal CTOD transition curve of the overmatched weld of high Y/T X65 pipe

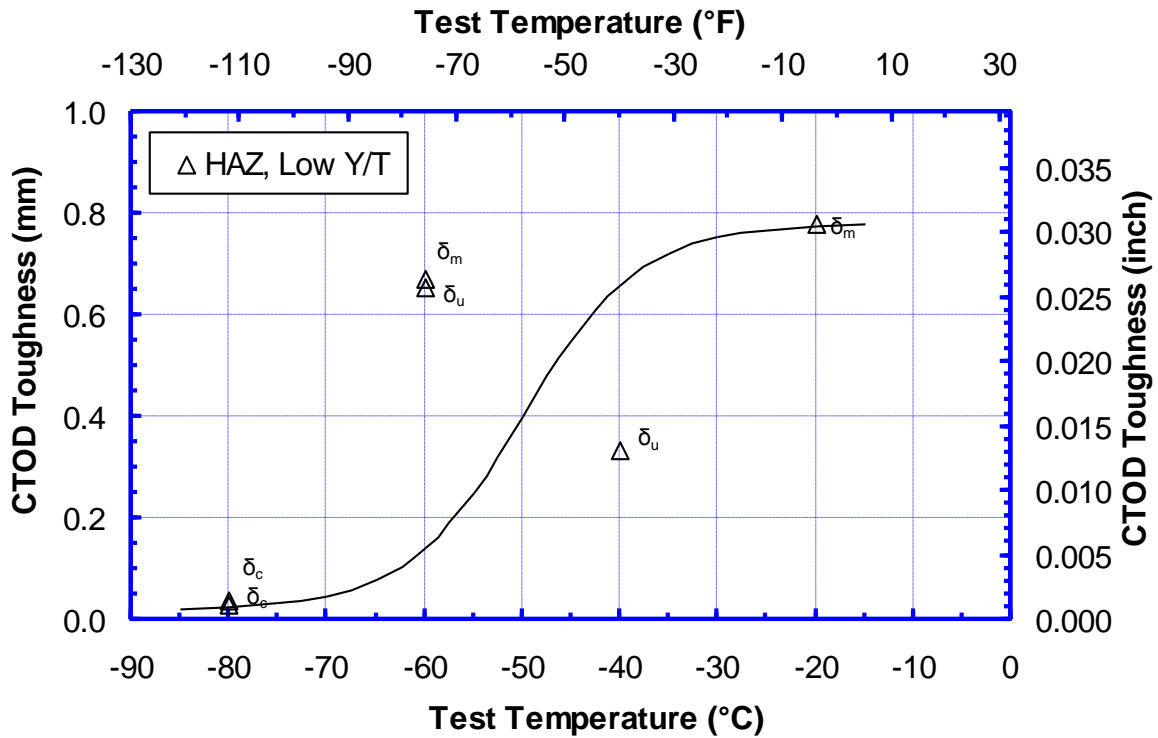


Figure 3.37 HAZ CTOD transition curve of low Y/T X65 pipe

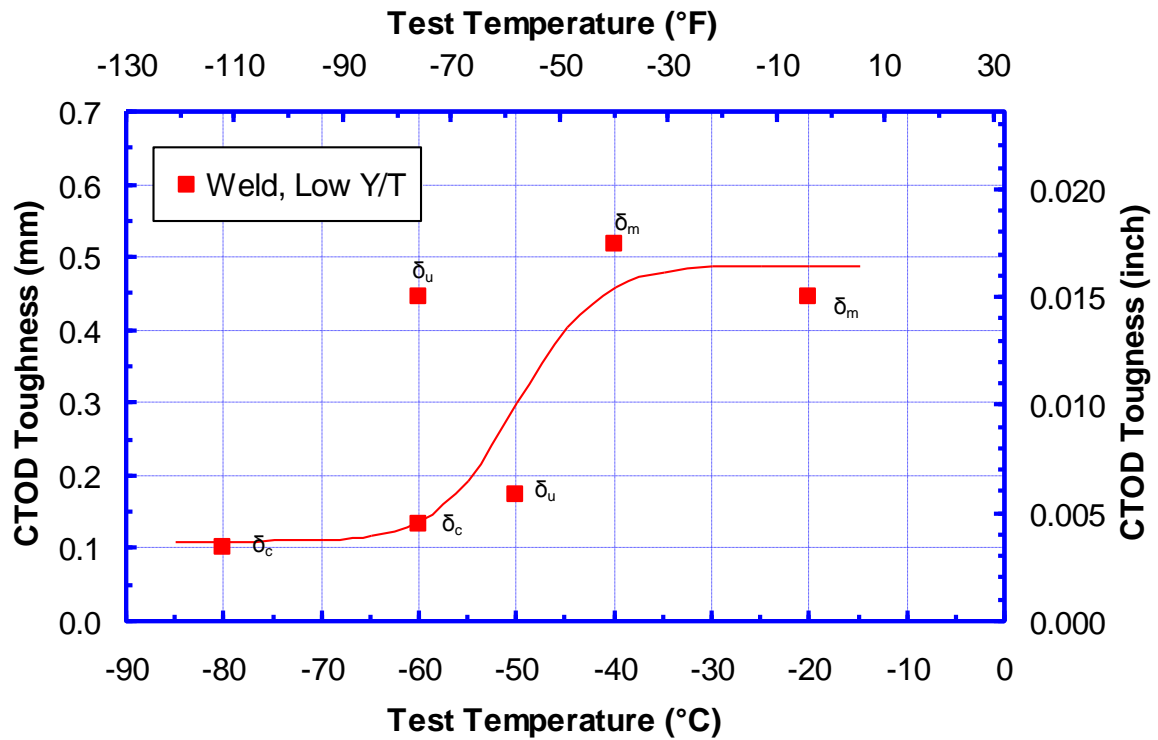


Figure 3.38 Weld metal CTOD transition curve of low Y/T X65 pipe

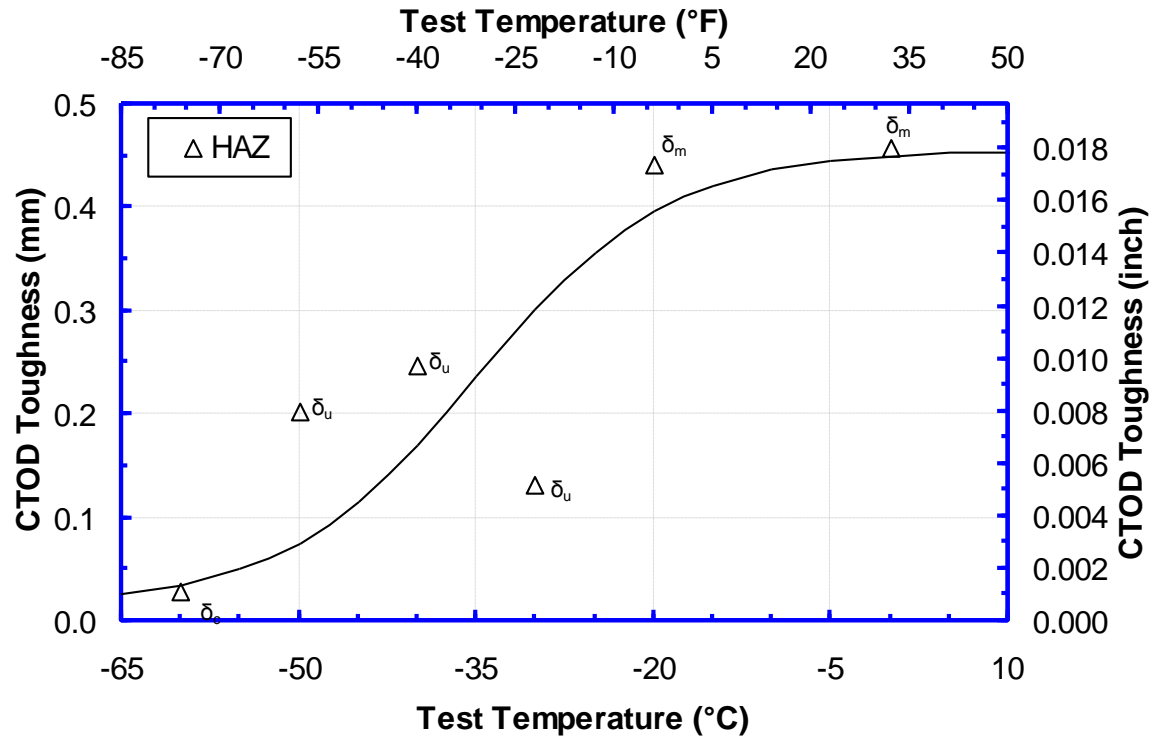


Figure 3.39 HAZ CTOD transition curve of X80 weld

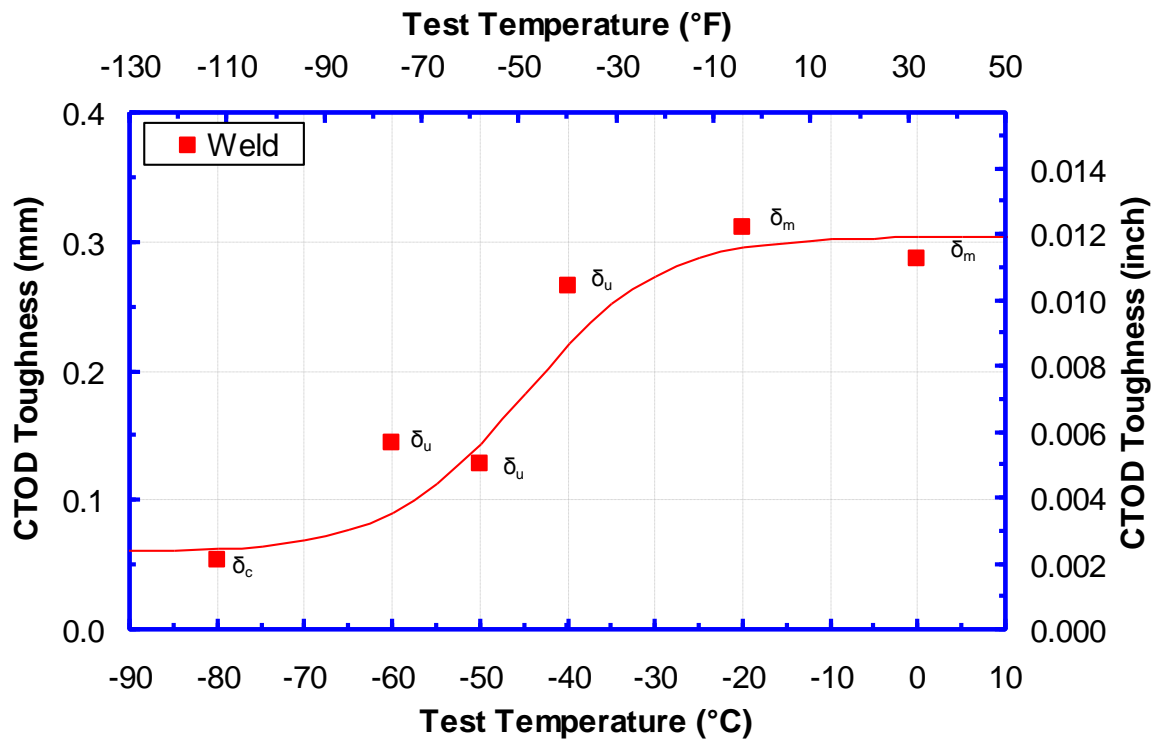


Figure 3.40 Weld metal CTOD transition curve of X80 weld

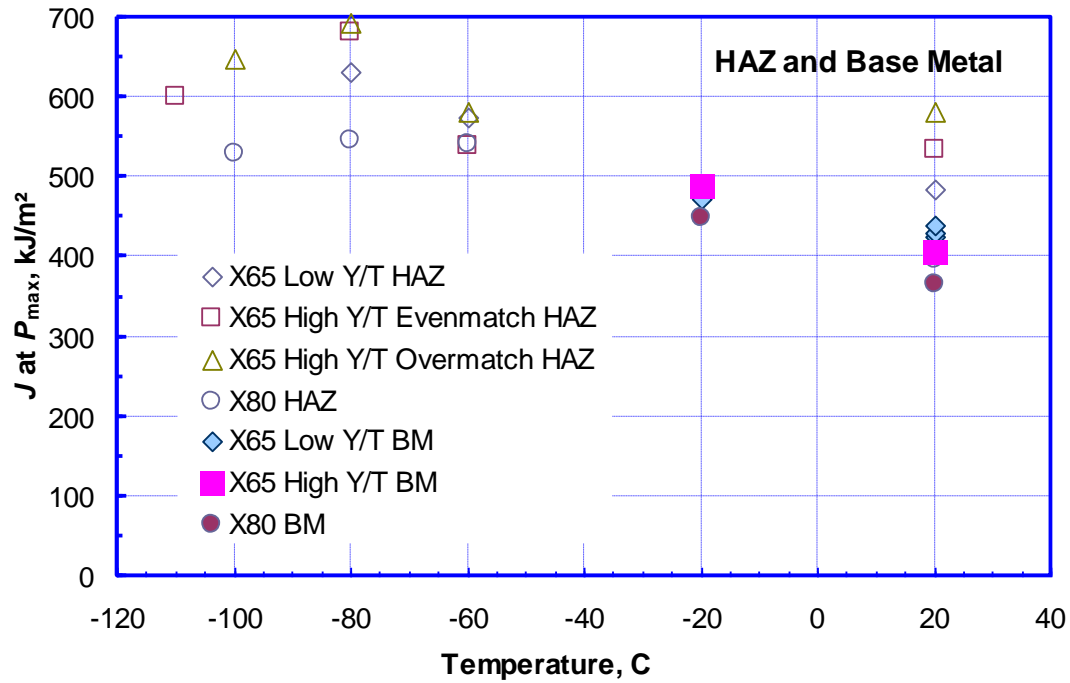


Figure 3.41 Temperature dependence of base metal and HAZ J at P_{max} for X65 and X80 welds

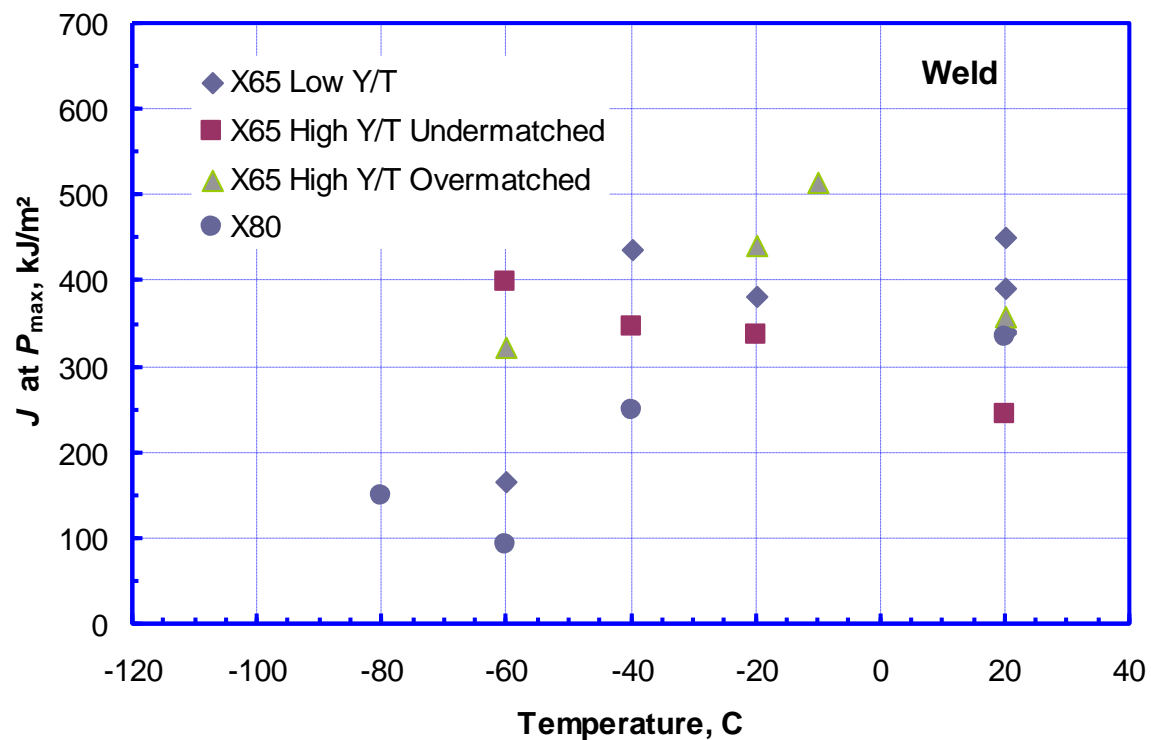


Figure 3.42 Temperature dependence of weld metal J at P_{max} for X65 and X80 welds

4 Pre-Test Analysis

4.1 Objectives and Scope

The pre-test analysis was conducted for the large-scale tests, i.e. CWP and full-scale pipe (FSP) tests. The primary purposes of the pre-test analysis are:

- (1) determine the proper aspect ratio of the CWP specimens,
- (2) determine the proper spacing of the two girth welds of the same FSP specimen,
- (3) determine the proper number of installed flaws in a single girth weld of the FSP specimen,
- (4) recommend the best instrumentation plans for the CWP and FSP tests in order to get the most relevant and high quality data,
- (5) provide input to the initial flaw size for the test specimens,
- (6) recommend the most relevant test pressure to maximize the effects of internal pressure, and
- (7) determine if the customary unloading magnitude for the unloading compliance measurement would alter the material behavior at the flaw tip.

With respect to the girth weld spacing of the FSP specimens and the number of flaws in the single girth weld, the objectives are to have the maximum number of flaws possible in a given specimen, without those flaws interacting. In other words, the welds and flaws should be a sufficient distance away from each other, so the behavior of one flaw does not affect the behavior of the other flaws.

With respect to the flaw sizing, the objective is to have the TSC in the most useful range for model development as well as from the viewpoint of practical application. The target strain range is 2-4%. It is also desirable to have the same flaw size among CWP, non-pressurized FSP, and pressurized FSP tests so that (1) the correlation between the CWP and non-pressurized FSP tests and (2) the effect of the pressure can be examined under as identical conditions as possible. Consequently, it is not always possible to have the target strain in the desirable range. In all cases, efforts were made to minimize the chance of failures at very low strains, as such data would not be useful for model development. This effectively put an upper limit on the flaw size for a given material condition. On the other hand, if the flaw is too small, there would be increased risk of failure in the pipe body away from the flawed plane. Efforts were made to avoid a scenario like this too.

With respect to the instrumentation plan, the objective is to acquire data in the regions which most closely resemble the data requirement of actual long pipelines. The local effects of the test specimens, such as those due to the limited length of the specimens, should be minimized.

The pre-test analysis was conducted using FEA. In most cases, multiple rounds of pre-test analysis were conducted as more specimen-specific data became available.

The ultimate goal is to (1) understand the influence of the test setup and procedures on the measured strains and (2) optimize the test setup and procedures to develop quality test data.

4.2 Curved Wide Plate Tests

In recent years, CWP tests have been increasingly used to determine tensile failure strains [56,57,58] and used in welding procedure qualifications for high strain applications [5]. To ensure consistency and accuracy in failure strain measurement, the test setup and procedures need to be carefully studied.

4.2.1 Specimen Geometry and Strain Measurement Procedure

The schematic drawing of a CWP specimen is shown in Figure 4.1. The specimen is made of two curved plates that were welded together. The middle section of the specimen has a reduced width. The length and width of the reduced section are L and W , respectively. The flaw is in either the weld center or heat-affect zone (HAZ).

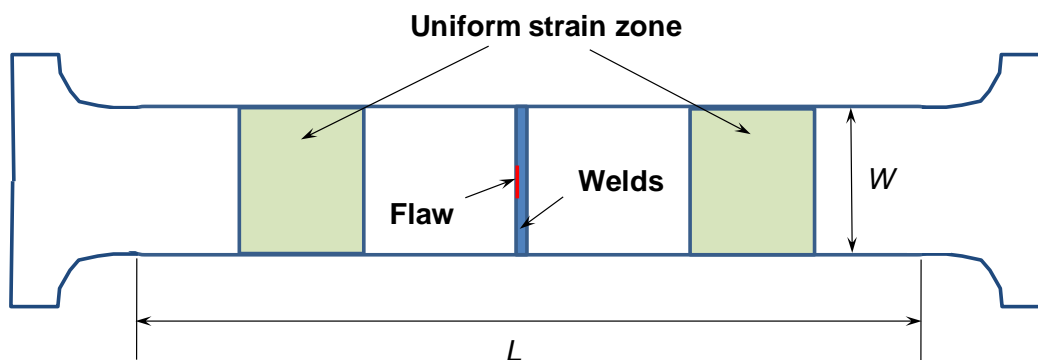


Figure 4.1 Schematic drawing of the curved-wide plate specimen

In published test data, the specimen width generally varied from 200 mm to 450 mm [14]. Meanwhile, the length of CWP specimens also varied from test to test. Therefore, the CWP specimens had different length to width ratios (L/W). The failure strain was usually measured by relative elongation of the reduced section of the specimen. However, the strain in the reduced section is not uniform, due to weld mismatch and strain concentration induced by the flaw and the end section of the specimen. Consequently, the measured strain could change with specimen size and may not represent the actual strain in pipeline. Since the strain concentration is near the weld/flaw and the end section, a uniform strain zone could exist in the specimen if the specimen length to width ratio is large enough (as shown in Figure 4.1). As the strain in the uniform zone is not affected by the weld and the ends of the specimen, its value is a good representation of the nominal strain in a long pipeline.

Based on pipe diameter and equipment capacity, the specimen width was decided to be 229 mm (9 inch). This specimen width forms the baseline geometry. From this baseline, specimens with different length to width ratios (L/W) were analyzed with FEA. A typical longitudinal strain contour of a CWP specimen ($L/W = 4$) is shown in Figure 4.2. Due to symmetry conditions, only a quarter of the specimen was modeled and shown. It can be observed

that both the end section of the specimen and the flaw induce certain strain concentration. A relatively uniform strain zone exists in the middle, between the weld and the end section.

The distribution of the longitudinal strain along the center and edge lines of the specimen (see the definition in Figure 4.2) is shown in Figure 4.3 and Figure 4.4 for different weld mismatch levels. A weld overmatch of 25% was used in Figure 4.4 to demonstrate the extent of the weld mismatch effect. The 25% overmatch was consistent with the overmatch level found in the first weld qualification data. In the uniform strain zone, the strains along the center and edge lines should overlap. It can be observed that the end section effect on strain extends about $0.75W$ independent of applied strain levels. The effect of the flaw/weld on strain could extend $0.5W$ to $1.0W$ depending on the applied strain level and weld mismatch. The size of the uniform strain zone decreases as the applied strain or weld strength mismatch increases. However, if the strain is measured along the center line of the specimen, the effect of the flaw/weld extends about $0.5W$ independent of the applied strain and slightly dependent of the weld mismatch. Therefore, in order to obtain a finite zone of uniform strain ($\sim 0.25W$), the specimen length is at least $3.0W$, i.e. $L/W = 2.0 \times (0.75 + 0.50 + 0.25)$.

The recommendation is therefore, $L \geq 4W$. For $W = 229$ mm, the $L = 916$ mm or greater.

4.2.2 Initial Flaw Size

4.2.2.1 Flaw Size of X65 CWP Specimens

To determine the flaw size of the CWP, specimens of various flaw sizes were analyzed for all three groups of materials with FEA:

- (1) X65 (high Y/T) pipe with an evenmatched weld,
- (2) X65 (high Y/T) pipe with an overmatched weld,
- (3) X65 (low Y/T) pipe with an overmatched weld.

The CTOD driving forces were obtained from those FEA. Flaw failure was assumed to take place as the driving forces reach the toughness, where the CTOD toughness of the three materials was assumed to be between 0.4 mm to 0.6 mm. It was determined that in order to obtain a target failure strain between 2.0% to 4.0%, a 3-mm deep and 50-mm long flaw should be used for the CWP specimen of the X65 (high Y/T) pipe with overmatched weld (as shown in Figure 4.5). Similar flaw size was determined for the X65 (low Y/T) pipe with overmatched weld. For the CWP with the X65 (high Y/T) pipe and evenmatched weld, the flaw was determined to be 3-mm deep and 35-mm long.

4.2.2.2 Flaw Size of X80 CWP Specimens

As shown in Figure 4.6, the stress-strain curves of the X80 pipes show an unexpected small uniform strain ($\sim 4\%$ in the longitudinal direction and $\sim 2\%$ in the transverse direction). At the same time, the weld stress-strain curves show a large uniform strain ($\sim 12\%$) and large strength overmatch. As a result, the design of the flaw size for the X80 CWP specimens becomes a

challenge, since the target failure strain of 2% to 4% is very close to the uniform strain of the pipe material.

Due to the relatively large weld overmatch and small pipe uniform strain, the specimen tends to fail in the pipe body if the target failure strain is greater than 2%. In order to produce flow failure, relatively large flaw size needs to be used and the failure strain is likely to be less than 2%. As shown in Figure 4.7, a 3-mm deep and 50-mm long flaw can either lead to a failure less than 2% strain or end up with pipe body failure. The property variation of the actual materials can make the situation even worse. A flaw deeper than 3 mm will tend to cause a low strain failure and a flaw less shallow than 3 mm will tend to cause pipe body failure. As a result, flaw sizes around 3 mm × 50 mm are recommended for the tests.

4.2.3 Unloading Magnitude

Unloading compliance method was used to measure flaw growth in several CWP tests. To get quality compliance measurement, it is necessary to have enough unloading magnitude. On the other hand, large unloading may change the stress/strain state at the flaw tip. For example, compressive stress/strain may be developed during unloading near the flaw tip. As a result, the material may experience tensile-compressive cyclic loading, which can alter the materials' behavior.

The effect of unloading on the stress state near a flaw tip was analyzed by FEA. In the FEA simulations, the specimen was loaded to the first specified strain and then unloaded by about 20% of the applied load. The specimen was then loaded to the next specified strain and then unloaded. The process was repeated several times and the unloading magnitude was kept to about 20% of the applied load (or about 0.05% strain). The distribution of the normal stress (which opens the flaw) ahead of the flaw tip, was plotted before and after the unloading as shown in Figure 4.8. The results indicate that the first unloading cycle has the most impact on the stress state at the flaw tip. Compressive stress is shown in a 0.05-mm wide area ahead of the flaw tip, which is about 10 times of the grain size. The area affected by the unloading decreases rapidly with the number of unloading cycles. In three cycles, the compressive stress is only shown in a negligible area at the flaw tip. Therefore, it is concluded that a 20% unloading in the load does not have a significant effect on the material's behavior near the flaw tip.

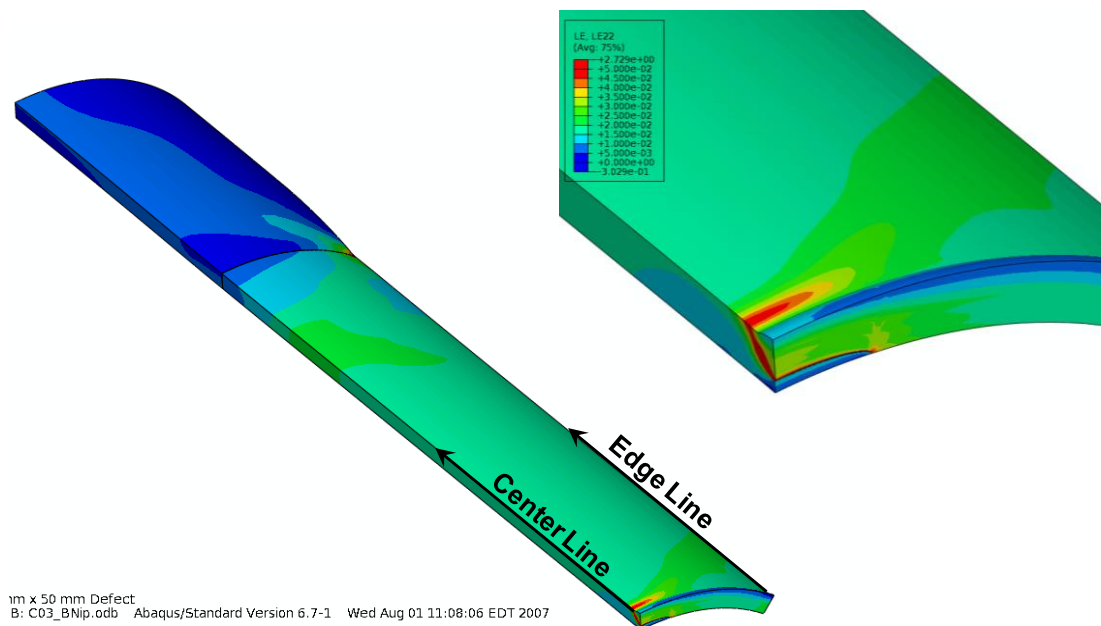
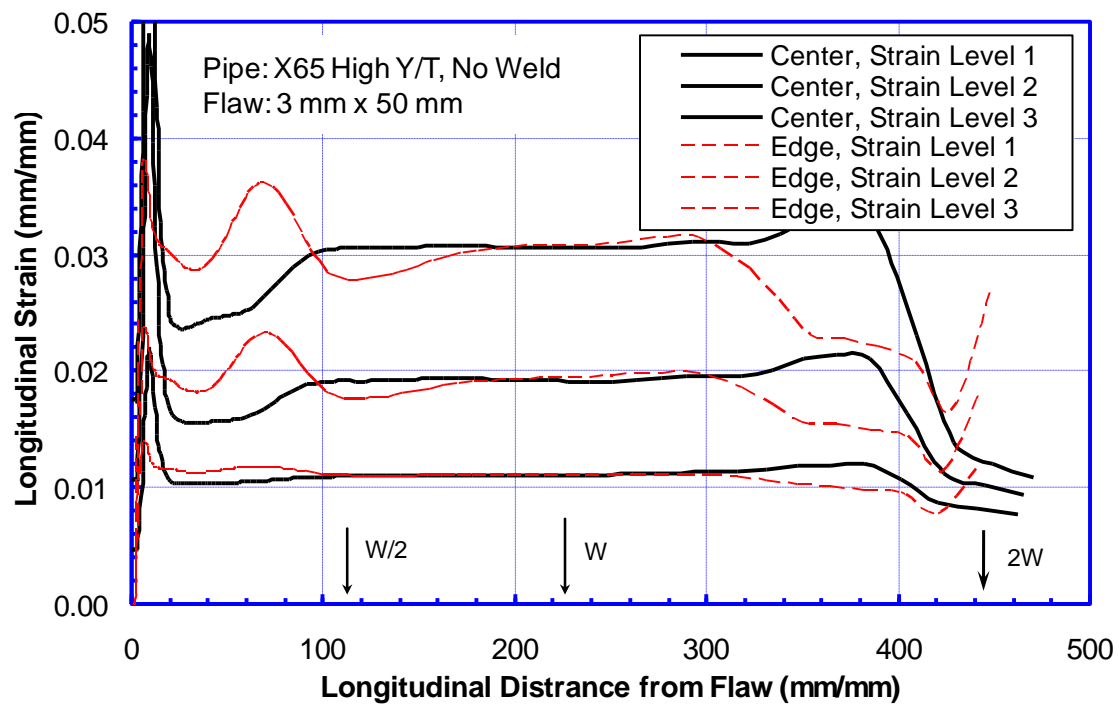
Figure 4.2 Longitudinal strain contour in sample CWP specimen ($L/W = 4$)

Figure 4.3 Longitudinal strain along specimen length (no weld)

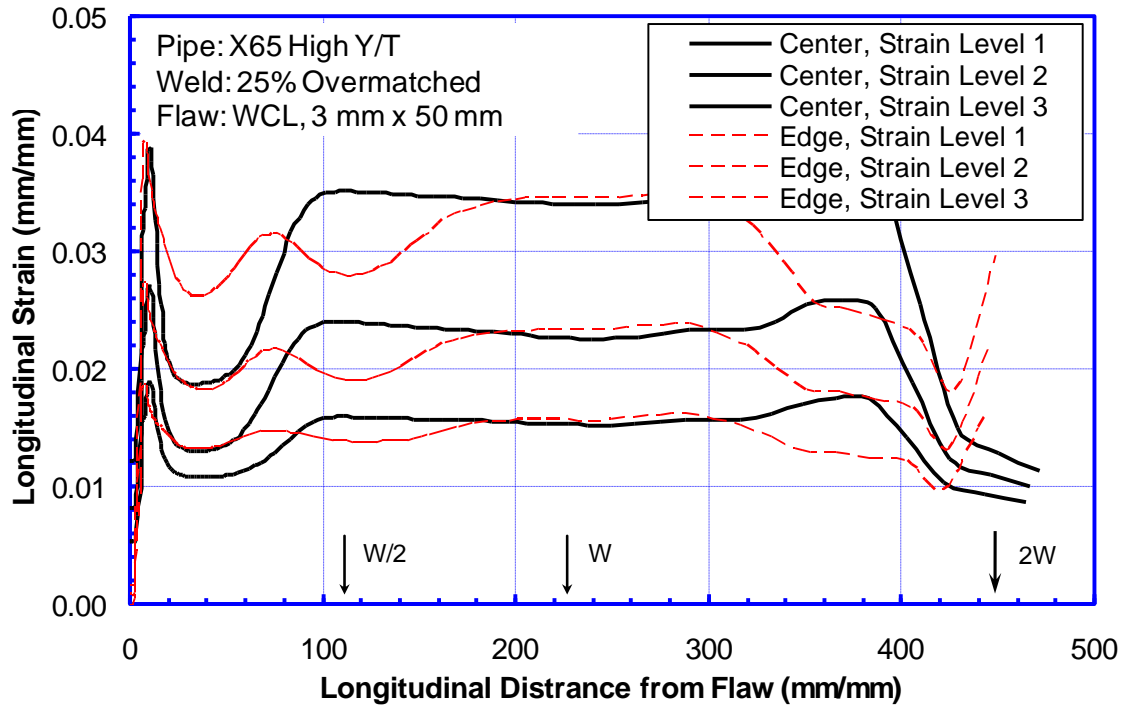


Figure 4.4 Longitudinal strain along specimen length (25%-overmatched weld)

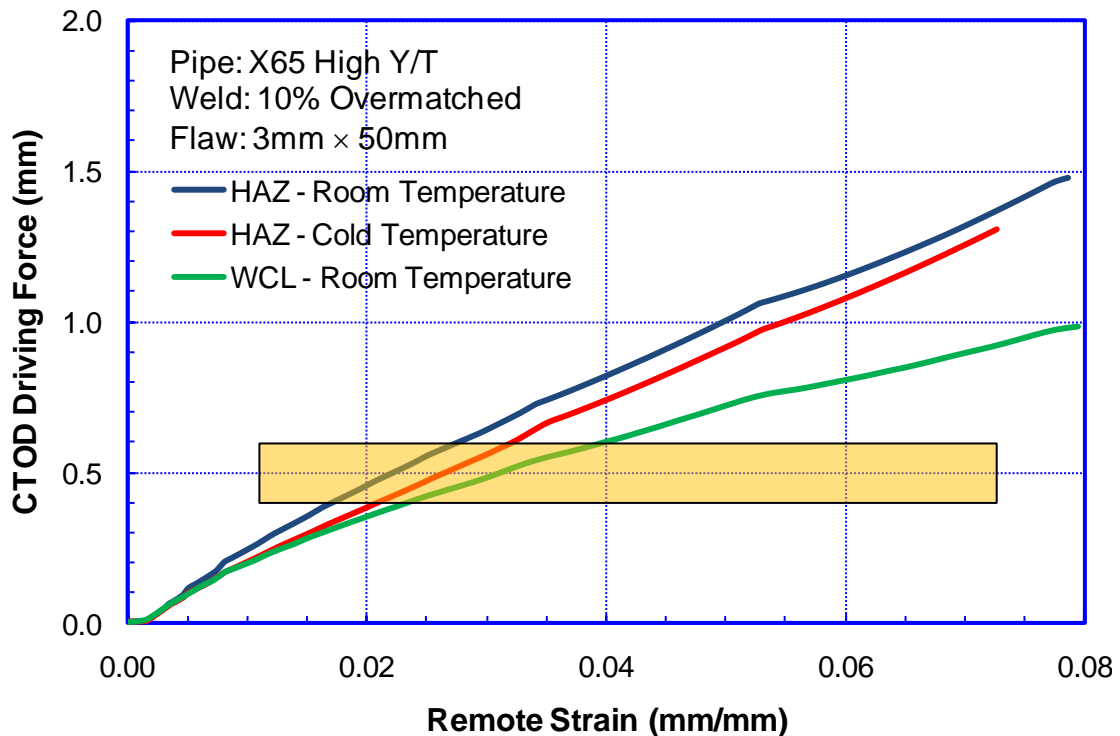


Figure 4.5 CTOD driving force of sample CWP specimen for flaw sizing

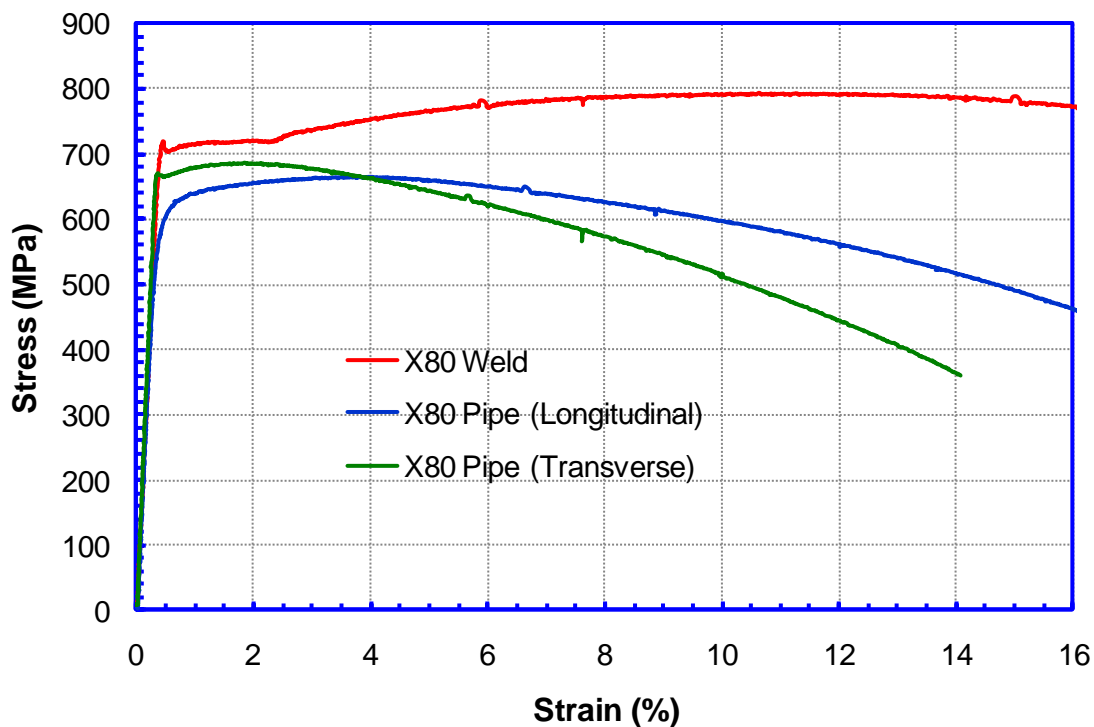


Figure 4.6 Stress-strain curves of X80 pipe and weld

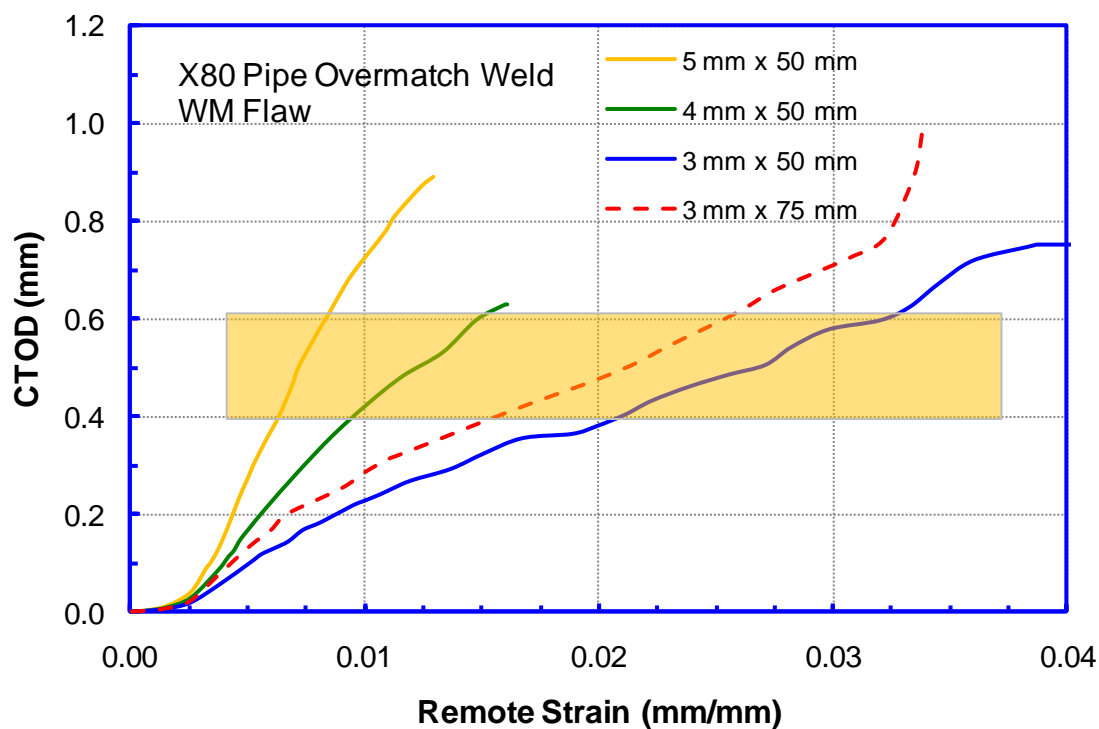


Figure 4.7 CTOD driving force curves of X80 CWP for flaw sizing

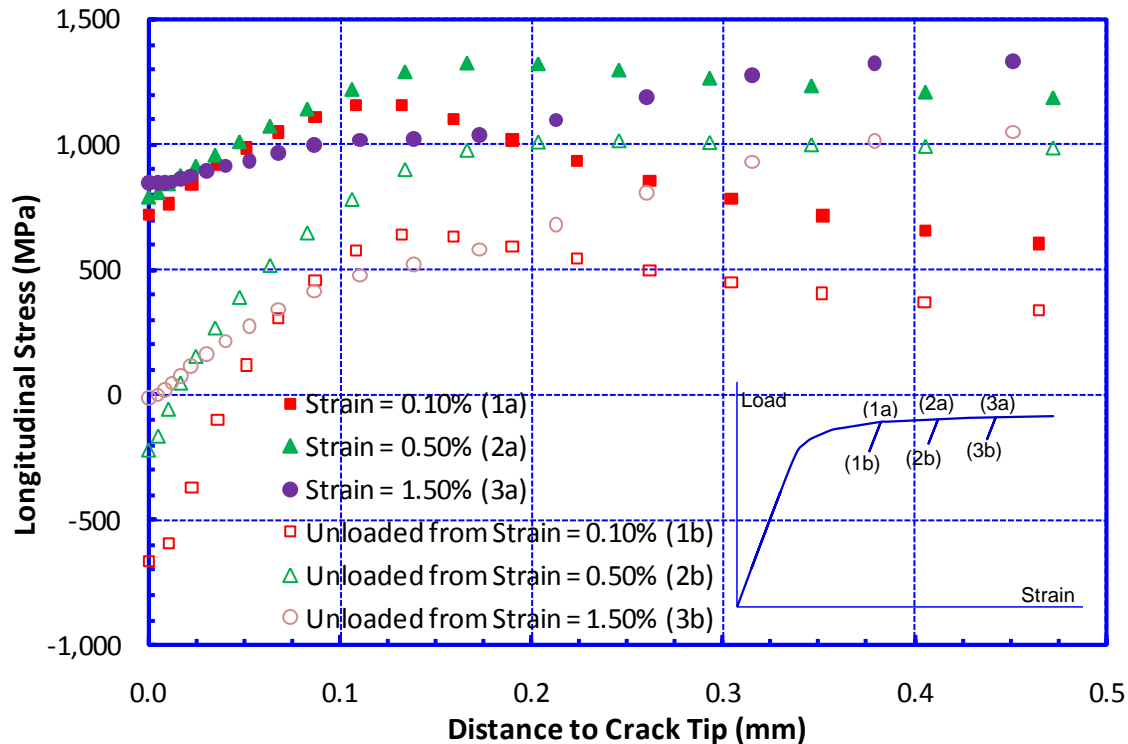


Figure 4.8 Effect of unloading on crack tip stress state

4.3 Full Scale Pipe Tests

4.3.1 Specimen Geometry and Strain Measurement Procedure

The schematic drawing of a FSP specimen is shown in Figure 4.9. The specimen is made of three pipe segments that were jointed by two welds. The length of each pipe segment is L and the outside diameter of the pipe is D . Both ends of the specimen are attached to a plate in order to contain internal pressure and apply load. Multiple flaws are prepared in each weld (either in weld center or HAZ) to obtain more test data in one test. Similar to the CWP, the weld/flaw and end section (plate) may induce strain localization. Uniform strain zones may exist if the length of each pipe segment is greater than a minimum required value (as shown in Figure 4.9). In addition, the flaws in the same weld may interact with each other and affect the crack driving force. Therefore, the maximum number of flaws which can be allowed in each weld without causing flaw interaction needs to be analyzed. In the following analysis, the X65 (high Y/T) pipe is used and no weld is modeled to simplify the model. The conclusions should be applicable to the X65 (low Y/T) pipe as well.

4.3.1.1 Separation of the Girth Welds and Specimen Length

Finite element models with line spring and shell elements were constructed to calculate the minimum length of the pipe segment to allow finite uniform strain zone. The results show that the minimum length is sensitive to flaw depth but not to material properties. The minimum required length as a function of flaw depth for 50-mm long flaws is shown in Figure 4.10, where

the length is normalized by pipe diameter. It is seen that the minimum length increases as the flaw depth increases. The length of $1.5D$ is recommended for flaws of 3-mm deep and 50-mm long (and less) with the consideration of a 1.5-mm flaw growth.

4.3.1.2 Maximum Number of Flaws without Interaction

To investigate the possible interaction of multiple flaws in the same weld, FEA with 3D solid elements were constructed. A typical longitudinal strain contour is shown in Figure 4.11 for a joint with two flaws of 4.5-mm deep and 50-mm long. The strain contour is shown at the CTOD driving force of 1.2 mm. It shows that the internal pressure increases the plastic zone of each flaw and enhances flaw interactions.

The effect of flaw interaction on the crack driving force is shown in Figure 4.12 and Figure 4.13. The hoop stress resulted from internal pressure is 72%SMYS. Figure 4.12 shows the CTOD driving force at the deepest point of the flaw and Figure 4.13 shows the J -integral along the whole flaw front. The results demonstrate that for the 12-inch OD pipe, the crack driving force along the whole flaw front is not affected by the adjacent flaw if the weld contains only two flaws of 3-mm deep and 50-mm long (assuming 1.5-mm flaw growth).

4.3.2 Flaw Size

Similar to the CWP specimens, FEA were performed to determine the flaw size for the FSP. The focus was given to (1) balance the failure strain with and without pressure while keeping the same flaw size and (2) keep similar flaw size with those in the CWP. The results show that the same flaw size recommended for the CWP specimens can be used for the FSP specimens as shown in Figure 4.14.

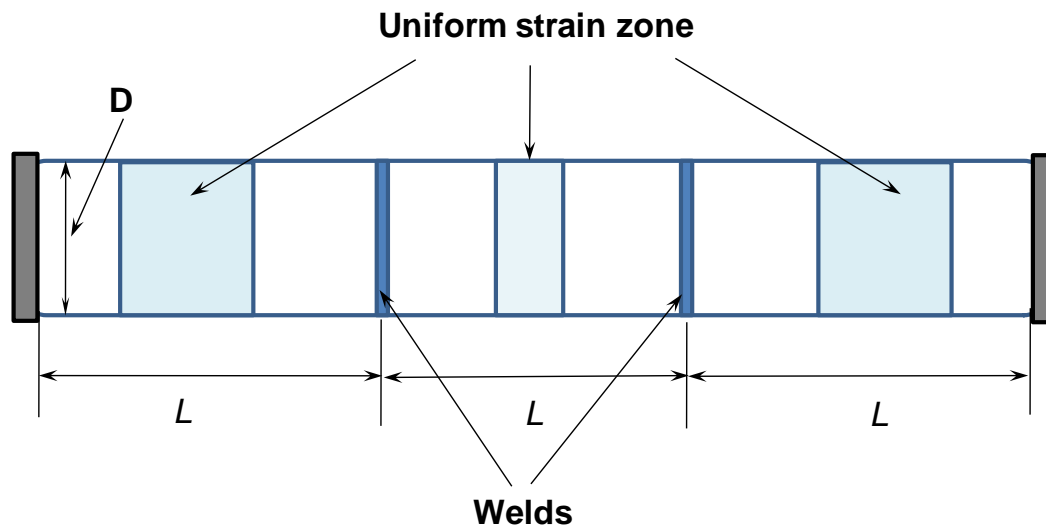


Figure 4.9 Schematic drawing of the full-scale pipe specimen

4.3.3 Pressure

The internal pressure can have great effect on the crack driving force and failure strain. Previous FEA [59] showed that the pressure can greatly increase the crack driving force. As

pressure increases, the CTOD driving force first increases and then decreases. The pressure that can produce the largest driving force depends on the flaw size and material property. In general, the pressure that results in a hoop stress of 60% to 80% of the pipe yield strength maximizes the driving force as shown in Figure 4.15. Furthermore, the CTOD driving force in this pressure range is not very sensitive to the pressure. As the result, the internal pressure which would produce hoop stress in the range of 60-80% of the corresponding yield strength, is recommended to be used in the tests. It should be noted that the yield strengths of the high and low Y/T X65 pipes used in this project are close to X70 and X56, respectively.

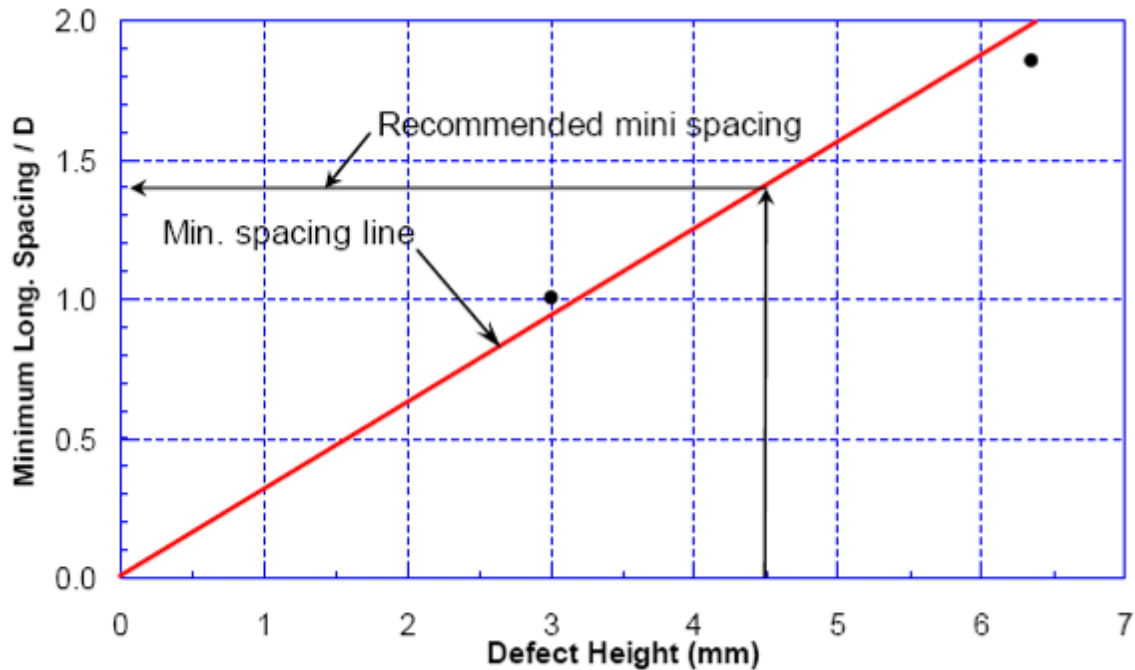


Figure 4.10 Minimum pipe segment length for uniform strain zone

Hoop Stress = 0.0

Hoop Stress / SMYS = 0.72

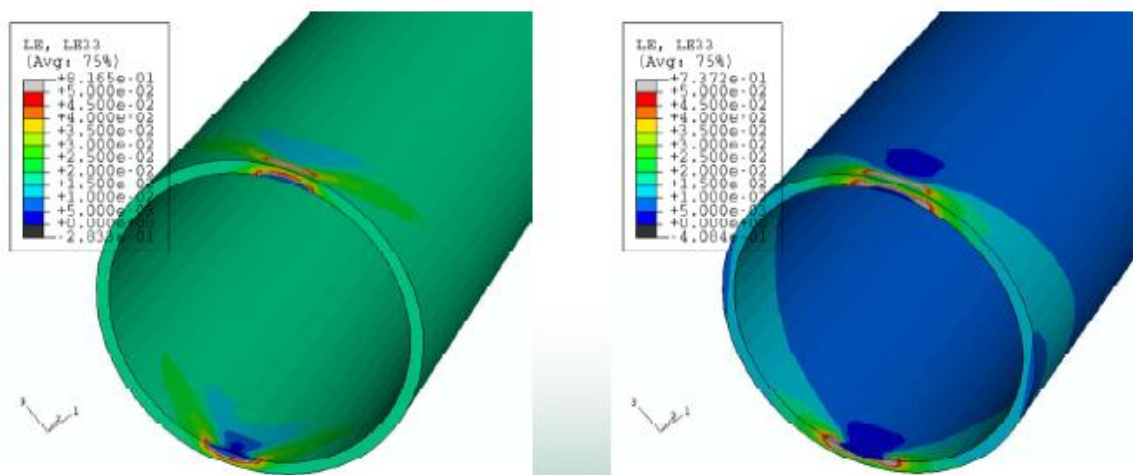


Figure 4.11 Typical strain contours of a pipe joint with multiple flaws

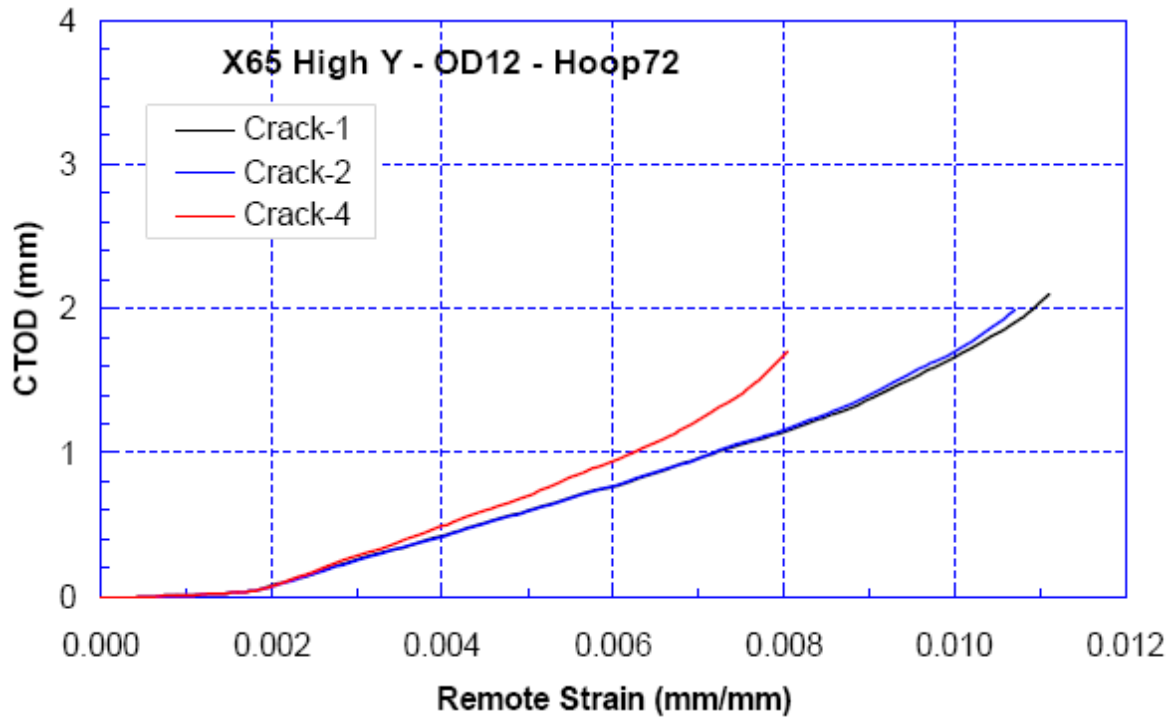


Figure 4.12 Effect of flaw interaction on CTOD driving force at the deepest point

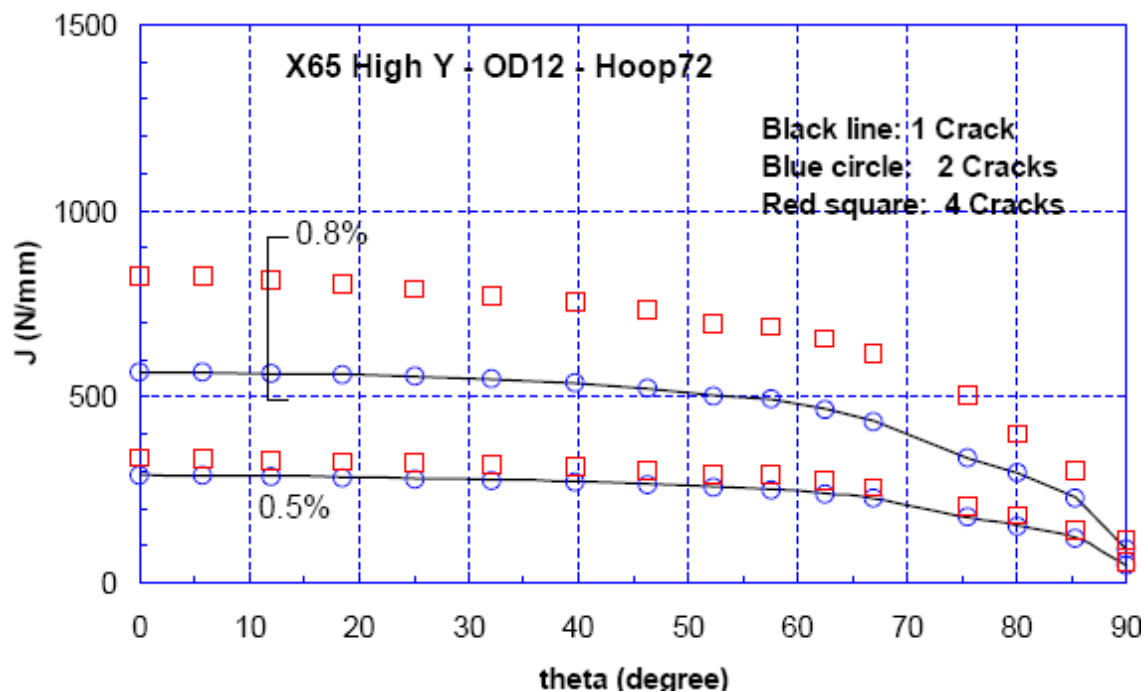


Figure 4.13 Effect of flaw interaction on J -integral along the flaw front

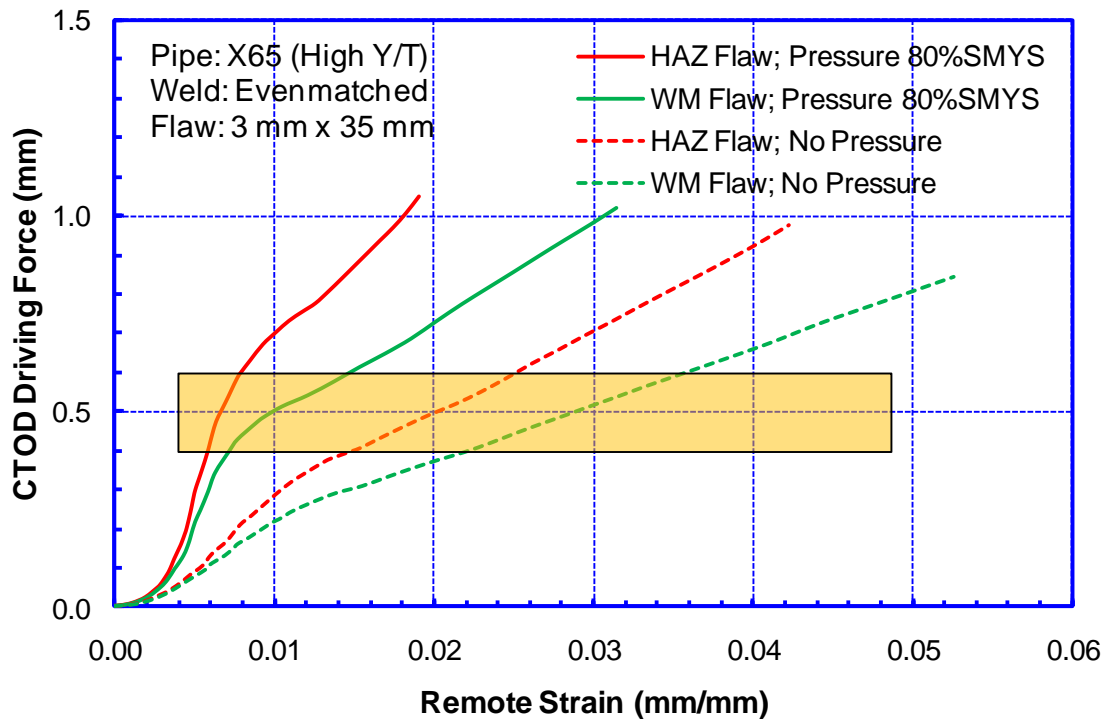


Figure 4.14 CTOD driving force of sample FSP specimen for flaw sizing

4.4 Pre-Test Analysis Summary

For CWP, the following conclusions are drawn from the pre-test analysis:

- (1) The strain should be measured from the uniform strain zone. The uniform strain zone is at least $0.5W$ away from the weld and $0.75W$ away from the end section.
- (2) To maintain a uniform strain zone of finite size, the length to width ratio (L/W) of the CWP specimen should be greater than 3.
- (3) The flaw size is recommended to be 3-mm deep and 35-mm long for the X65 high Y/T pipe material with an evenmatched weld.
- (4) The flaw size is recommended to be 3-mm deep and 50-mm long for both X65 high and low Y/T pipe materials with an overmatched weld.
- (5) The strain unloading of 0.05% (i.e. 20% load) should not change the materials' behavior near the flaw tip.

For FSP, the following conclusions are drawn from the pre-test analysis:

- (1) The strain should be measured in the uniform strain zone. To maintain a finite uniform strain zone, the length to diameter ratio (L/D) of each pipe segment should be greater than 1.5.
- (2) The flaw size is recommended to be 3-mm deep and 35-mm long for the X65 high Y/T pipe material with an evenmatched weld.
- (3) The flaw size is recommended to be 3-mm deep and 50-mm long for both X65 high and low Y/T pipe materials with an overmatched weld.

- (4) To prevent flaw interaction, there should be at most two flaws in each weld.
- (5) The internal pressure which produces hoop stress in the range of 60-80% of the actual yield strength can maximize the internal pressure effects.

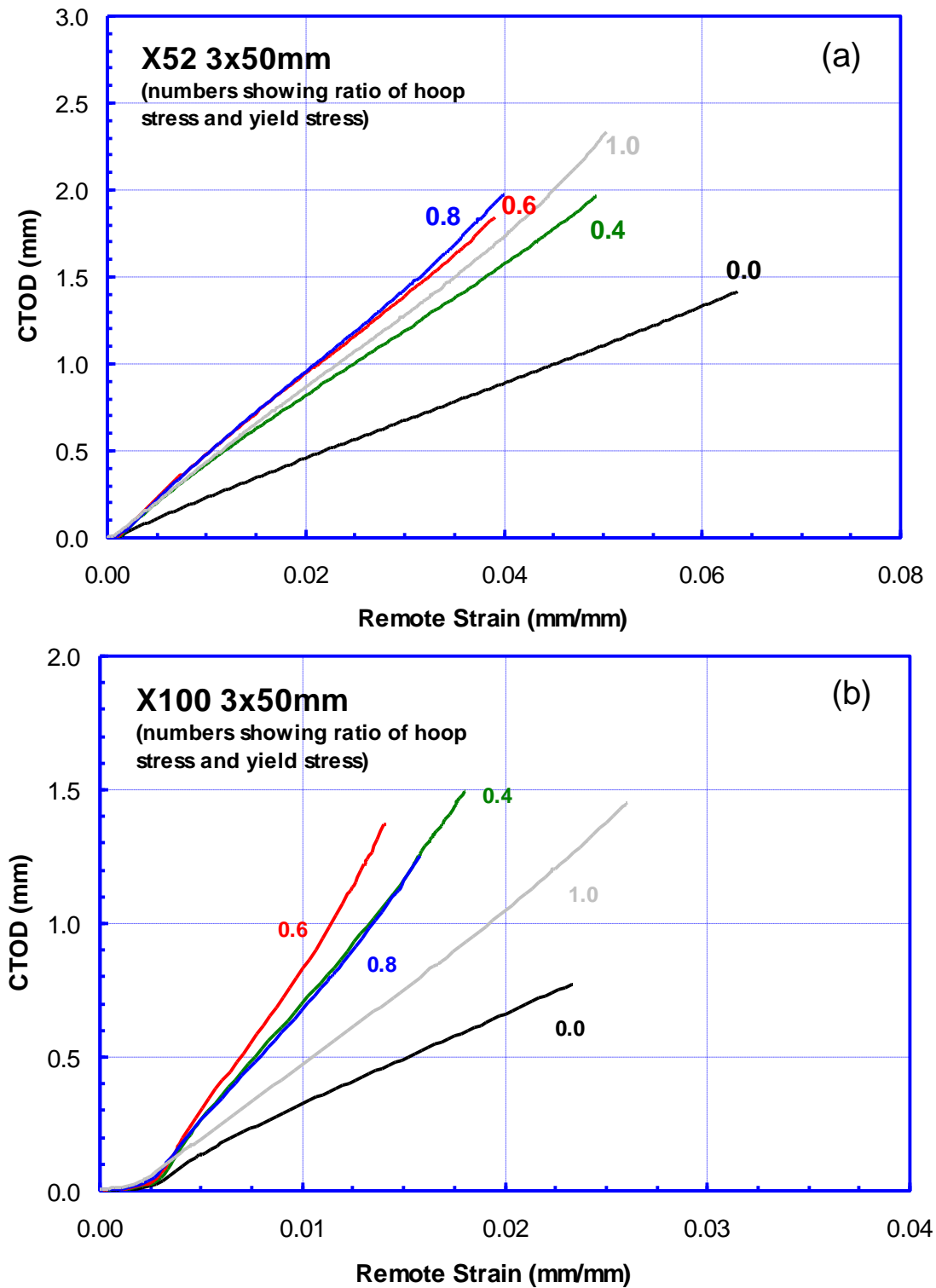


Figure 4.15 Effect of internal pressure on CTOD driving force [59]

5 Large-Scale Tests

5.1 Overview

The large-scale experimental program carried out by C-FER Technologies (1999) Inc. (“C-FER”) consisted of 34 axial tension tests on specimens fabricated from 12.75-inch (324-mm) diameter by 0.5-inch (12.7-mm) wall, Grade X65 (448 MPa) ERW line pipe and 10 axial tension tests on specimens fabricated from 24-inch (610-mm) diameter by 0.5-inch (12.7-mm) wall, Grade X80 (551 MPa) UOE DSAW line pipe. All tests were carried out in C-FER’s 15,000-kN Tubular Testing System located at C-FER’s test facility in Edmonton, Alberta.

The primary focus of the large-scale testing was on the specimens fabricated from the 12.75-inch diameter X65 line pipe, because the axial stress-strain response of the pipe body material associated with the 24-inch diameter X80 line pipe was found to be not well suited to strain-based design applications¹.

For the large-scale tests, the specimen fabrication details and test conditions were chosen to exercise a number of parameters which are known to have a significant impact on the tensile strain capacity of welded line pipe including the internal pressure level, the strain hardening characteristics of the pipe body and weld material, the degree of weld strength mismatch, and the size and location of the weld flaws. The majority of the pipe and plate tests were performed at room temperature to ensure effectively ductile material behavior. Selected tests were performed at a reduced temperature to assess the effects of reduced temperature on strain capacity.

With specific regard to the tests on 12.75-inch diameter pipe material, 24 tests were performed on full pipe specimens and 10 tests were performed on curved wide plate (CWP) panels cut from pipes. All specimens contained circumferentially oriented, surface breaking flaws intended to simulate fabrication-induced girth weld flaws. A majority of the pipe specimens were tested with high internal pressure, but a significant proportion were tested with very low internal pressure (effectively no pressure) to clearly establish the effects of pressure on strain capacity. The test parameters for the CWP panels were chosen to align with the test parameters for the effectively unpressurized pipe specimens to assess the degree to which the strain capacities based on wide plate tests agree with the strain capacities obtained from full-scale pipe tests.

Testing of the 24-inch diameter pipe material was limited to a series of eight tests on CWP panels cut from girth welded pipes. As for the CWP specimens cut from 12.75-inch pipe, all specimens contained circumferentially oriented, surface breaking flaws intended to simulate fabrication induced girth weld flaws.

¹ The problematic axial strain response of the X80 line pipe material which was made available to this project is not considered representative of X80 material in general.

5.2 Test Program Design

5.2.1 Pipe Tests

5.2.1.1 Specimen Design Considerations

The pipe specimens, all involving 12.75-inch diameter line pipe, were designed to incorporate two girth welds with multiple circumferentially oriented flaws in each weld. The overall specimen length, the position of the girth welds and the number of flaws per weld were established through extensive preliminary analysis (see Section 4.3.1). The adopted specimen geometry was intended to ensure that on either side of each girth weld, a so-called uniform strain zone would exist within which the axial strains in the pipe body would be expected to be unaffected by discontinuities associated with flaws and specimen end effects (see Section 4.3.1.1). Similarly, the decision to install only two flaws per girth weld (separated by 180 degrees) was dictated by the distance shown by analysis to be necessary to ensure that there would be no interaction between the flaws (see Section 4.3.1.2).

5.2.1.2 Test Parameters

The primary test parameters for the large-scale pipe tests were internal pressure, pipe body strain hardening characteristics, weld strength mismatch, flaw size and flaw location (i.e. pipe body, weld metal or heat affected zone). While a majority of the tests were performed at room temperature (approximately 20°C) to ensure effectively ductile material behavior, two tests were performed at a reduced temperature of -20°C to assess the effects of reduced temperature on strain capacity.

With regard to pressure, the high pressure pipe tests were performed at pressure levels which were chosen to produce a hoop stress in the range of 70 to 75% of the actual pipe body yield stress. (Prior analysis has shown that the detrimental effects of internal pressure on strain capacity are maximized when the hoop stress is in the range of 60 to 80% of yield strength [60].) The low pressure pipe tests were performed at a pressure that was just sufficient to provide an indication of through-wall flaw extension (i.e. leakage).

To exercise a range of pipe body strain hardening characteristics, as reflected by the material's yield-to-tensile (Y/T) strength ratio, test specimens were fabricated from two different orders of line pipe. The pipe referred to as High Y/T material exhibited an average longitudinal Y/T ratio of 0.92, and the material referred to as Low Y/T exhibited a Y/T ratio of 0.88.

For girth welded test specimens, two levels of weld strength mismatch were considered. The welds referred as over-matched had a yield strength 8 to 9% higher than that of the pipe body and a tensile strength 14 to 19% higher than that of the body. The welds referred to as evenmatched had a strength of 96% of the body material at yield and 104% of the body material at ultimate.

See Section 3 for a detailed discussion of the pipe body and weld metal properties.

5.2.1.3 Specimen Fabrication

The as-received plane pipe and girth welded pipe pieces were trimmed to their final test length and then marked with a reference grid to facilitate the placement of flaws and transducer mounting fixtures and to provide a reference system for detailed specimen geometry measurements (i.e. length, diameter, circumference and wall thickness).

Circular steel plates were then welded to each specimen end, using a full-penetration gas metal arc welding (GMAW) procedure, to enable pressure containment and to provide a means to transfer axial load from the test machine to the test specimen. To ensure concentric loading, the end plates were positioned so that the centroids of the pipe section and end plates were aligned.

Prior to the installation of flaws in specimens containing girth welds, the OD weld cap on each specimen was ground flush with the pipe body over a circumferential extent which coincided with the intended flaw location. (The circumferential extent of the ground region typically extended 10 to 20 mm beyond the length of the flaw.)

Flaws were cut in the outer surface of each specimen using a circular saw blade with a diameter of 57 mm and a thickness of 0.15 mm. This cutting tool produced a flaw with a maximum width of 0.21 mm. The tooling used to install the flaws is capable of depth control to within ± 0.1 mm and surface breaking length control to within ± 1 mm. The depth profile achieved is shown schematically in Figure 5.1. Actual flaw dimensions were measured following flaw installation with the depth being measured at 5-mm intervals along the flaw length using a feeler gauge.

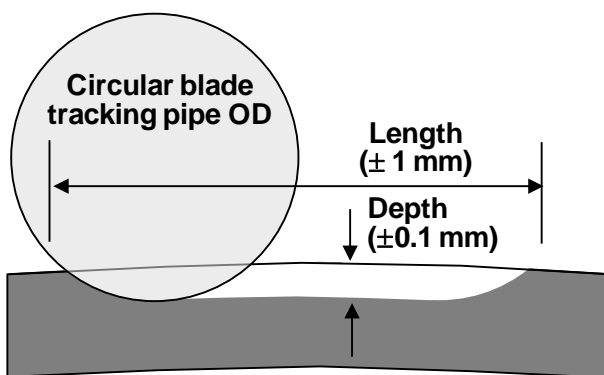


Figure 5.1 Profile of Saw-cut Flaws in Pipes and Plates

In girth welded specimens, the flaws were either placed in the weld metal (WM), at the weld centerline, or in the adjacent heat affected zone (HAZ). HAZ flaw placement was facilitated by pipe body scribe marks placed prior to welding and weld macros, the intent being for the base of the saw cut to intersect the coarse-grained region of the HAZ.

A test specimen summary including key geometric parameters and flaw dimensions is provided in Table 5.1. A comprehensive tabulation of specimen and flaw geometry is given in the test data sheets provided in Appendix 5A.

Table 5.1 Pipe Specimen Geometry and Flaw Details

Specimen Number	Pipe Body Material*	Girth Welds*	Overall Specimen Length (mm)	Individual Weld Can Lengths (mm)	Average Outside Diameter (mm)	Average Wall Thickness (mm)	Flaw Location	Number of Flaws and Nominal Dimensions (mm)
1.1	High Y/T	None	2,138	Single can	324.4	12.70	Pipe body	4 @ 3 × 50
1.2	High Y/T	None	2,140	Single can	324.4	12.77	Pipe body	4 @ 3 × 50
1.3	Low Y/T	None	2,139	Single can	324.0	12.70	Pipe Body	4 @ 3 × 50
1.4	Low Y/T	None	2,134	Single can	323.8	12.68	Pipe Body	4 @ 3 × 50
1.5	High Y/T	Even-match	2,184	689 804 691	324.4	12.81	Weld Metal	4 @ 3 × 35
1.6	High Y/T	Even-match	2,176	691 790 695	324.5	12.82	Weld Metal	4 @ 3 × 35
1.7	High Y/T	Even-match	2,176	686 801 689	324.4	12.74	HAZ	4 @ 3 × 35
1.8	High Y/T	Even-match	2,173	674 825 674	324.4	12.81	HAZ	4 @ 3 × 35
1.9	High Y/T	Over-match	2,179	709 759 712	324.4	12.65	Weld Metal	4 @ 3 × 50
1.10	High Y/T	Over-match	2,199	701 797 703	324.5	12.71	Weld Metal	4 @ 3 × 50
1.11	High Y/T	Over-match	2,207	708 796 702	324.6	12.68	HAZ	4 @ 3 × 50
1.12	High Y/T	Over-match	2,208	707 799 702	324.4	12.64	HAZ	4 @ 3 × 50
1.13	High Y/T	Over-match	2,725	984 785 954	324.5	12.69	HAZ	4 @ 3 × 50
1.14	High Y/T	Over-match	2,761	981 804 975	324.5	12.73	HAZ	4 @ 3 × 50
1.15	Low Y/T	Over-match	2,236	702 824 708	323.8	12.49	HAZ	4 @ 3 × 50
1.16	Low Y/T	Over-match	2,227	706 812 709	323.7	12.55	HAZ	4 @ 3 × 50
1.17	High Y/T	Over-match	2,247	719 815 713	324.3	12.62	Weld Metal	4 @ 3 × 35
1.18	High Y/T	Over-match	2,209	713 782 713	324.3	12.64	HAZ	4 @ 3 × 35
1.19	High Y/T	Over-match	2,205	687 823 692	324.3	12.64	Weld Metal	4 @ 3 × 50
1.20	Low Y/T	Over-match	2,207	703 800 703	323.7	12.51	Weld Metal	4 @ 3 × 50
1.21	High Y/T	Even-match	1,392	700 693	324.3	12.50	Weld Metal	2 @ 3 × 50
1.22	High Y/T	Even-match	1,402	700 702	324.4	12.59	HAZ	2 @ 3 × 50
1.23	High Y/T	Overmatch	1,400	699 703	324.3	12.63	Weld Metal	2 @ 2 × 70
1.24	High Y/T	Overmatch	1,324	696 624	324.4	12.78	HAZ	2 @ 3 × 50

* See Table 3.3 for tensile properties of high and low Y/T pipe body material and even- and over-matched girth welds.

5.2.1.4 Test Configuration and Instrumentation Layout

The as-tested geometric configuration of a typical pipe specimen containing two girth welds is shown schematically in Figure 5.2a². The instrumentation layout for each room temperature test is shown in Figure 5.2b.

² Four tests were also conducted on plane pipe specimens without girth welds having similar overall geometries and due to a limited pipe material supply, some of the later pipe tests were performed on shorter specimens containing only a single girth weld.

Linear variable differential transformers (LVDTs) were employed to measure average axial strains over half-diameter gauge lengths consistent with the estimated length of the uniform strain zones and over longer two-diameter gauge lengths bridging the flaw locations. Multiple LVDTs were installed at each cross-section to provide a degree of measurement redundancy and to facilitate strain averaging so that bending deformations, due to specimen out-of-straightness, would not factor into the axial strain estimates obtained for a given cross-section. Individual LVDTs were attached to mounting posts which were spot welded to the outer surface of the specimen. Figure 5.3a shows the LVDT mounting posts prior to the transducer installation.

Clip gauges bridging each flaw were attached to the pipe surface to measure flaw mouth opening, referred to herein as crack mouth opening displacement (CMOD). The mounting blocks and knife edge supports for the clip gauges are shown prior to gauge installation in Figure 5.3b (see also detail in Figure 5.2 for clip gauge mounting geometry).

A limited number of strain gauges were used to determine hoop strain and to provide redundant spot checks on axial strains determined using LVDTs.

Internal pressure, axial tensile load and overall specimen elongation were also measured during each test.

For the low temperature tests, the instrumentation described above was supplemented by a number of thermocouples, which were employed to monitor the temperature of the outer surface of the test specimen at selected locations. Temperature measurements were recorded at the flaw locations, at multiple locations within the uniform strain zones and at the specimen ends.

The exact placement of thermocouples in the low temperature tests and the test-specific variations in the general instrumentation layout described above are documented in the test data sheets provided in Appendix 5A.

A photograph of a typical pipe specimen immediately prior to room temperature testing is shown in Figure 5.4.

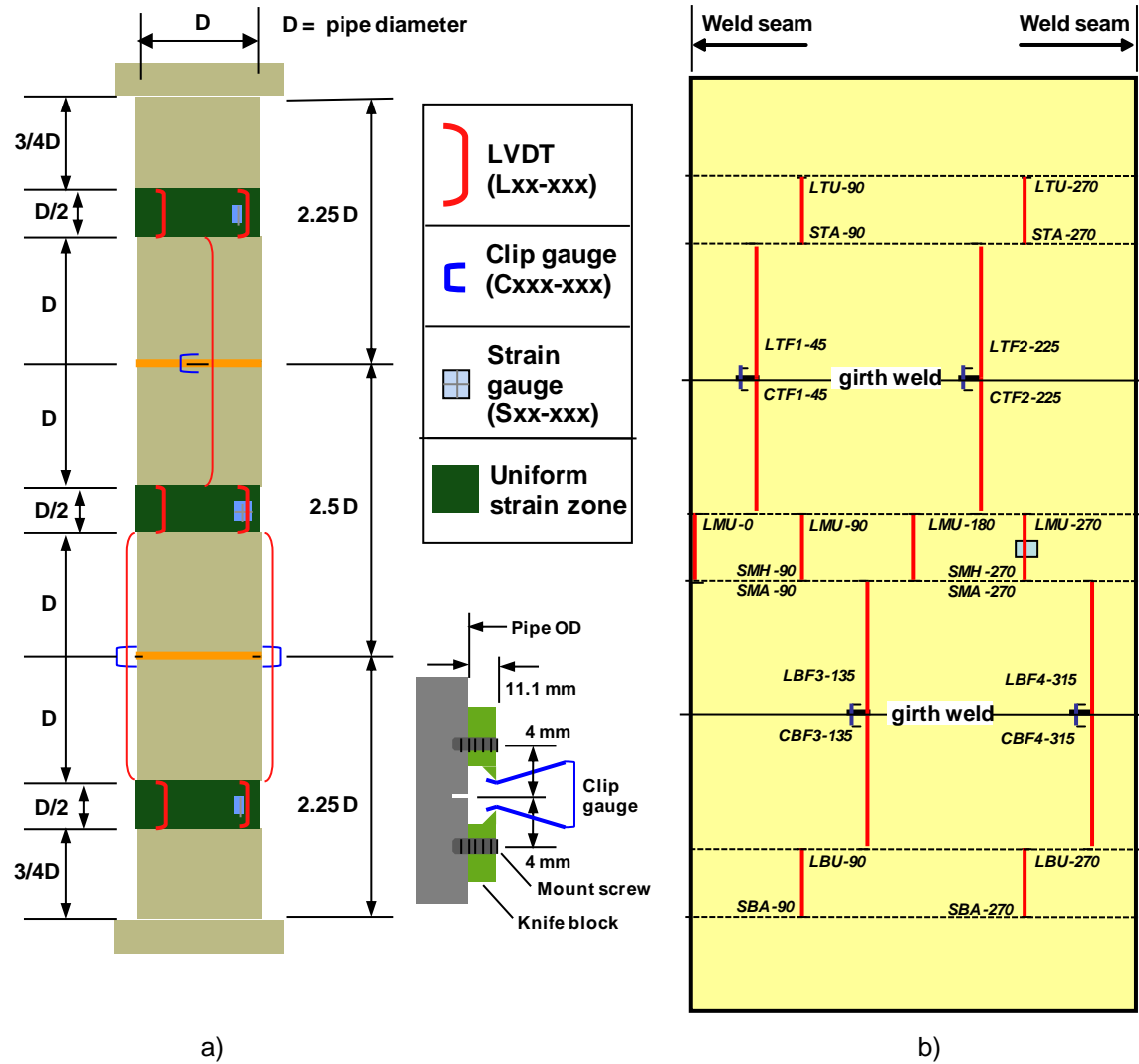
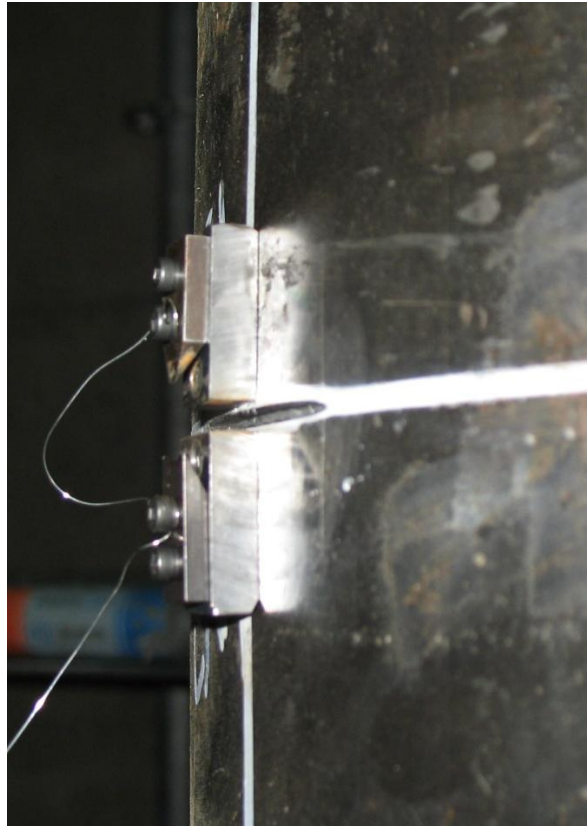


Figure 5.2 Typical Pipe Specimen Geometry and Instrumentation Layout



a) LVDT Mounting Posts



b) Clip Gauge Attachments Fixtures

Figure 5.3 Pipe Specimen Transducer Mounting Details

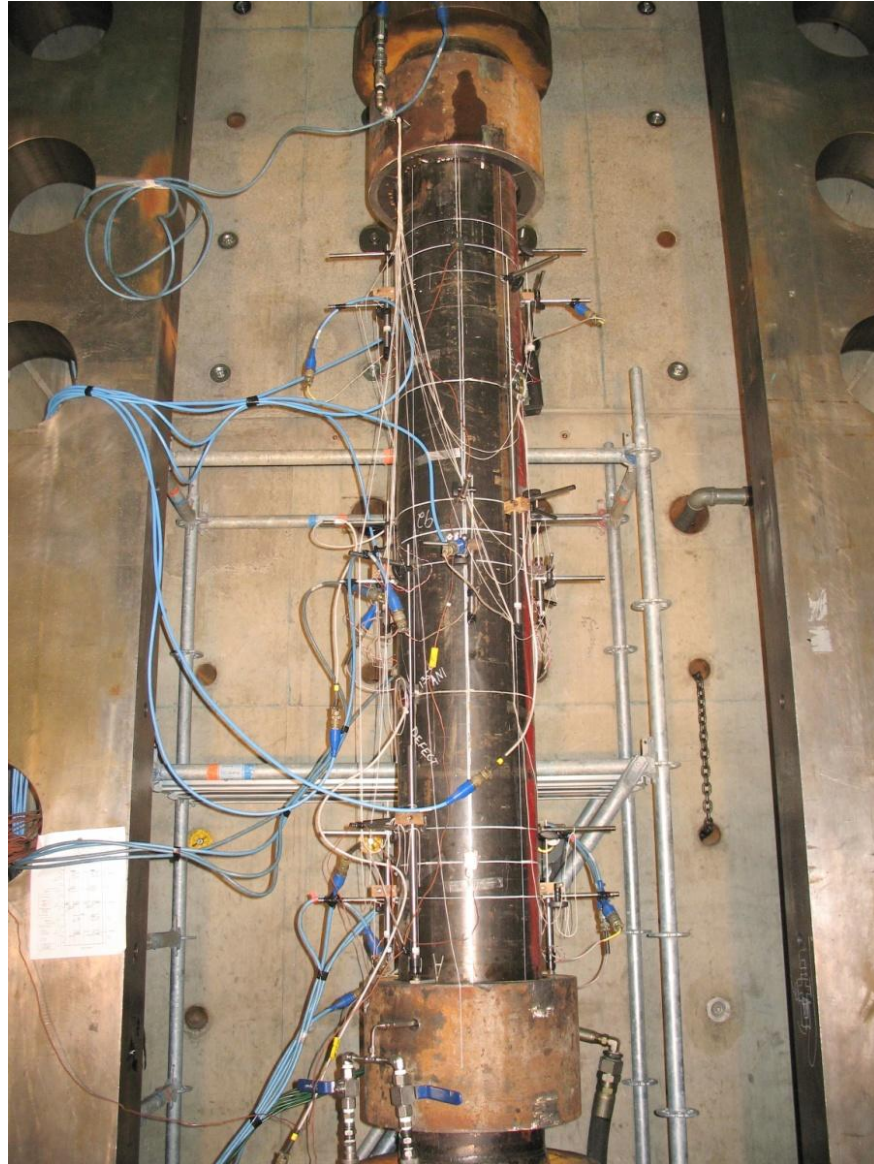


Figure 5.4 Typical Pipe Specimen Ready for Testing

5.2.1.5 Test Procedure

Pipe specimens subject to testing at room temperature were initially restrained in the axial direction and then pressurized with water to the prescribed internal pressure level. Specimens were subsequently loaded to failure under direct axial tension. Axial loading was carried out in a displacement-controlled mode with a prescribed test machine crosshead separation rate, which produced a nominal axial strain rate in each test specimen of about 1×10^{-5} per second. Testing was terminated when loss of pressure containment occurred (i.e. through-wall flaw extension) or when pipe body failure was imminent (i.e. in the event of axial strain localization in the pipe body away from flaw locations).

Pipe specimens subjected to low temperature testing were filled with a glycol solution which was chilled using liquid-nitrogen-fed cooling coils contained within each specimen. Specimens were first brought to the target temperature, then restrained in the axial direction, then pressurized to the prescribed level and finally loaded to failure under direct axial tension. A temperature controller feeding back on the thermocouples was employed to manage the passage of liquid nitrogen through the cooling coils and thereby to maintain the specimen temperature to within $\pm 2^{\circ}\text{C}$ of the target temperature over the entire gauged length of the specimen for the duration of each test.

All instrument readings were automatically recorded during each test using a computer-based data acquisition system and the resulting data files were stored in a spreadsheet compatible format to facilitate post-processing and interpretation.

5.2.2 Curved Wide Plate Tests

5.2.2.1 Specimen Design Considerations

The CWP specimens were designed to incorporate a single girth weld with a single circumferentially oriented flaw in each weld. The overall specimen length was established on the basis of preliminary analysis (see Section 4.2.1) to ensure that on either side of the girth weld a uniform strain zone would exist, within which the axial strains in the plate body would be expected to be unaffected by the discontinuities associated with the flaw and specimen end effects.

5.2.2.2 Test Parameters

For the CWP tests performed on panels cut from the 12.75-inch diameter pipe, the primary test parameters were pipe body strain hardening characteristics, weld strength mismatch, flaw size and flaw location (i.e. weld metal or heat affected zone). The parameter values and ranges were aligned with those of the corresponding 12.75-inch diameter pipe tests (see Section 5.2.1.1). As with the pipe tests, a majority of the CWP tests were performed at room temperature (approximately 20°C) to ensure effectively ductile material behavior; however, two identical tests were performed at a reduced temperature of approximately -20°C to assess the effects of reduced temperature on strain capacity.

For the CWP tests performed on panels cut from the 24-inch diameter pipe, the primary test parameters were flaw size and flaw location. A single order of line pipe material was used in specimen fabrication (with an average longitudinal Y/T ratio of 0.92) and all specimens were girth welded using a single weld procedure (which had a yield strength 15% higher than that of the pipe body and a tensile strength 19% higher than that of the body material).

See Section 3 for a detailed discussion of the pipe body and weld metal properties.

5.2.2.3 Specimen Fabrication

Upon receipt, the girth welded pipe pieces were rough cut length-wise into panels. These panels were then trimmed to their final as-tested length and machined to the prescribed width

over the intended reduced section length. The specimens were then marked with a reference grid to facilitate the placement of flaws and transducer mounting fixtures, as well as to provide a reference system for detailed specimen geometry measurements (i.e. length, width, and wall thickness).

Circular steel plates were then welded to each specimen end using a full-penetration gas metal arc welding (GMAW) procedure, to provide a means to transfer axial load from the test machine to the test specimen. To ensure concentric loading, the end plates were positioned such that the centroid of the wide plate gauge section coincided with that of the end plates.

Prior to the installation of the flaw in each specimens, the OD weld cap was ground flush with the pipe body over a circumferential extent which coincided with the intended flaw location. (The circumferential extent of the ground region typically extended 10 to 20 mm beyond the length of the flaw.)

The flaw locating and cutting procedure was identical to that used for the pipe specimens (see Section 5.2.2.2).

A CWP test specimen summary including key geometric parameters and flaw dimensions is provided in Table 5.2, for specimens cut from 12.75-inch diameter pipe material, and in Table 5.3, for specimens cut from 24-inch diameter pipe. A comprehensive tabulation of CWP specimen and flaw geometry is given in the test data sheets provided in Appendices 5B and 5C for the 12.75-inch and 24-inch diameter pipe material, respectively.

Note that to the extent possible, given the available sample material, CWP tests were performed on matching pairs of test specimens. (Nominally identical specimens are delineated in Tables 5.2 and 5.3 by the letters 'a' and 'b' appended to the specimen number (e.g. Specimens 3.1a and 3.1b).

Table 5.2 CWP Specimen Geometry and Flaw Details – 12.75-inch Diameter Pipe

Specimen Number	Pipe Body Material*	Girth Welds*	Reduced Section Length (mm)	Reduced Section Width (mm)	Average Wall Thickness (mm)	Flaw Location	Nominal Flaw Dimensions (mm)
3.1a	High Y/T	Even-match	1,028	224	12.73	Weld metal	3 × 35
3.1b	High Y/T	Even-match	1,034	224	12.77	Weld metal	3 × 35
3.2a	High Y/T	Even-match	1,027	224	12.72	HAZ	3 × 35
3.2b	High Y/T	Even-match	1,032	224	12.71	HAZ	3 × 35
3.3a	High Y/T	Over-match	1,041	225	13.00	Weld metal	3 × 50
3.3b	High Y/T	Over-match	1,044	225	12.95	Weld metal	3 × 50
3.4a	High Y/T	Over-match	1,042	225	12.98	HAZ	3 × 50
3.4b	High Y/T	Over-match	1,038	225	12.96	HAZ	3 × 50
3.5a	High Y/T	Over-match	1,039	225	12.99	HAZ	3 × 50
3.5b	High Y/T	Over-match	1,042	225	13.03	HAZ	3 × 50

* See Table 3.3 for tensile properties of high and low Y/T pipe body material and even- and over-matched girth welds.

Table 5.3 CWP Specimen Geometry and Flaw Details – 24-inch Diameter Pipe

Specimen Number	Pipe Body Material*	Girth Welds*	Reduced Section Length (mm)	Reduced Section Width (mm)	Average Wall Thickness (mm)	Flaw Location	Nominal Flaw Dimensions (mm)
4.1	High Y/T	Over-match	1,383	304	12.84	Weld metal	4 × 50
4.2	High Y/T	Over-match	1,384	305	12.84	Weld metal	3.5 × 50
4.3a	High Y/T	Over-match	1,390	305	12.86	Weld metal	3 × 50
4.3b	High Y/T	Over-match	1,383	305	12.83	Weld metal	3 × 50
4.4	High Y/T	Over-match	1,386	305	12.90	HAZ	4 × 50
4.5	High Y/T	Over-match	1,389	304	12.83	HAZ	3.5 × 50
4.6a	High Y/T	Over-match	1,383	305	13.00	HAZ	3 × 50
4.6b	High Y/T	Over-match	1,390	304	12.81	HAZ	3 × 50

* See Table 3.3 for tensile properties of high and low Y/T pipe body material and even- and over-matched girth welds.

5.2.2.4 Test Configuration and Instrumentation Layout

The as-tested geometric configuration of a typical CWP specimen from the 12.75-inch diameter pipe series is shown schematically in Figure 5.5a. The instrumentation layout for each CWP test is shown in Figure 5.5b.

LVDTs were employed to measure average axial strains over gauge lengths consistent with the length of the uniform strain zones and over a longer gauge length bridging the girth weld and contained flaw. Two LVDTs were installed at each cross section to provide a degree of measurement redundancy and to facilitate strain averaging so that bending deformations, due to lack of specimen straightness and load eccentricity, would not factor into the average axial strain estimates obtained for a given cross-section location. As in the pipe tests, clip gauges bridging each flaw were installed to measure CMOD (see detail in Figure 5.5 for clip gauge mounting geometry), and strain gauges were used on some tests to provide redundant spot checks on axial strains determined using LVDTs. Axial tensile load and overall specimen elongation were also recorded during each test.

For the low temperature tests, the instrumentation described above was supplemented by a number of thermocouples which were employed to monitor the temperature of the inner and outer surface of the CWP specimen at selected locations. Temperature measurements were recorded at the flaw locations, and over a grid pattern which extended the full length of the reduced section.

The exact placement of thermocouples in the low temperature tests and the test-specific variations in the general instrumentation layout described above are documented in the test data sheets provided in Appendix 5B and 5C, for CWP specimens cut from 12.75-inch diameter pipe and 24-inch diameter pipe, respectively.

A photograph of a typical CWP specimen prior to testing at room temperature is shown in Figure 5.6.

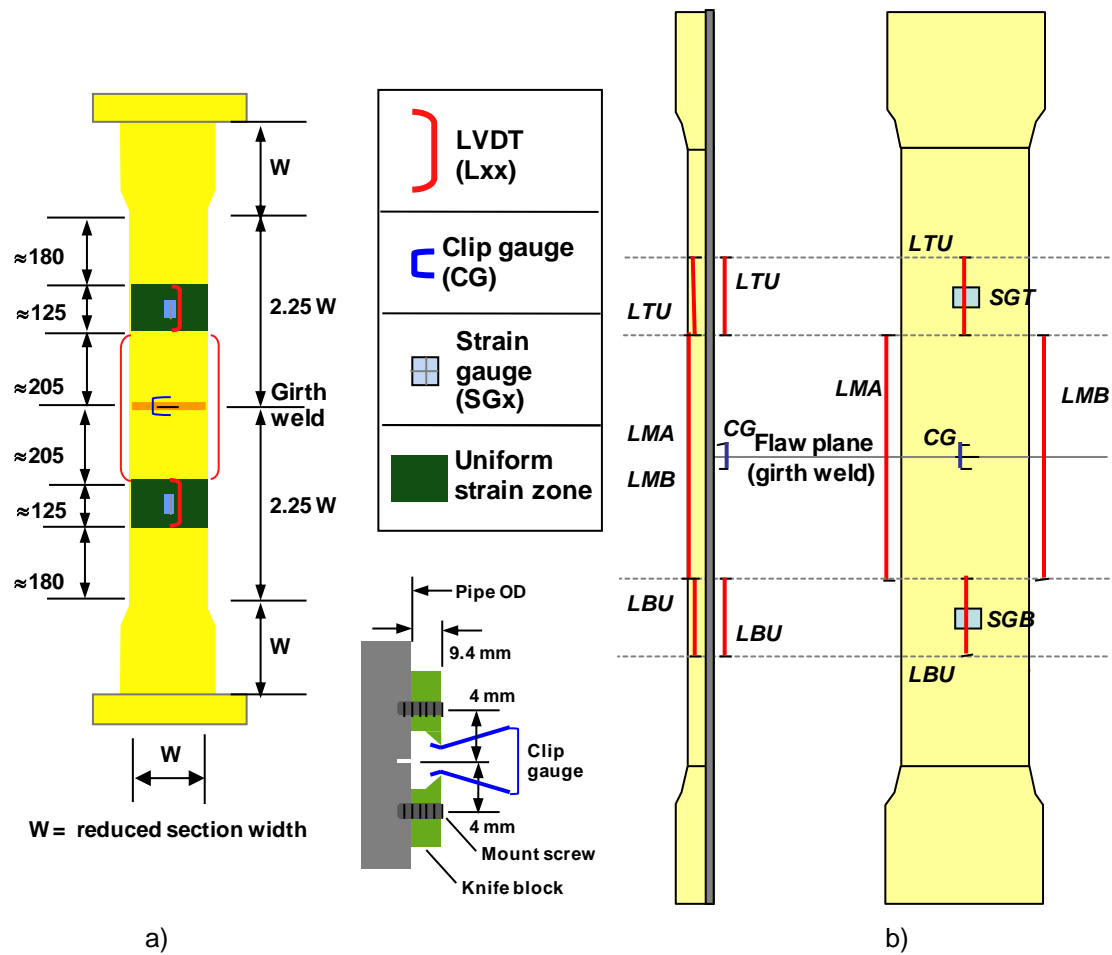


Figure 5.5 CWP Specimen Geometry and Instrumentation Layout – 12.75-inch Diameter Pipe

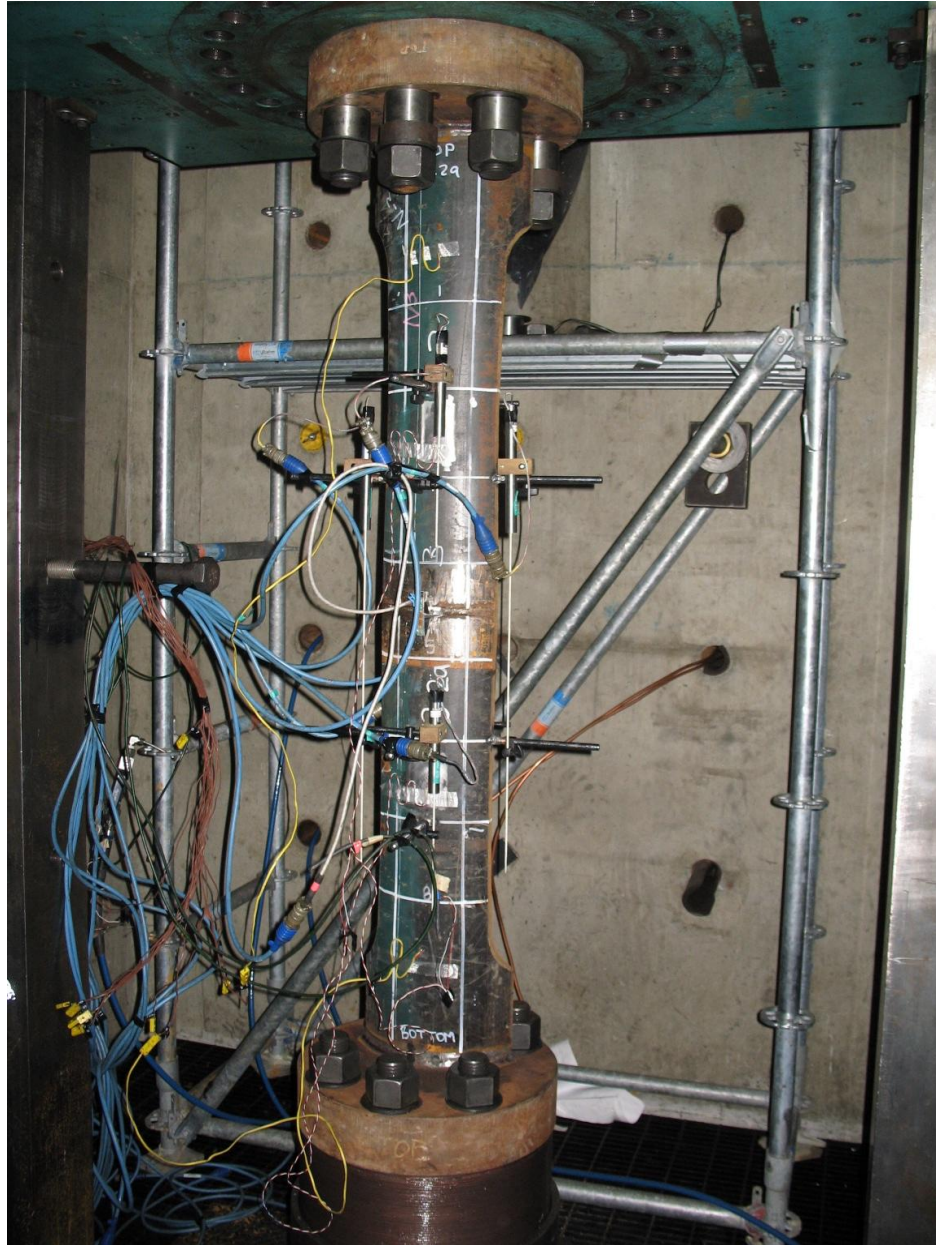


Figure 5.6 Typical CWP Specimen Ready for Testing

5.2.2.5 Test Procedure

Specimen loading was carried out in a displacement controlled mode, with a prescribed test machine crosshead separation rate, which produced a nominal axial strain rate similar to that used in the pipe tests (i.e. 1×10^{-5} per second). Testing was terminated when the drop in axial load exceeded 2 to 3% of the peak load value, or when axial strain reversal in the remote uniform strain regions of the plate specimen was observed, the latter being indicative of post-peak strain localization in the region of the plate containing the flaw.

CWP specimens subject to low temperature testing were cooled to the required test temperature using a liquid-nitrogen-fed surface refrigeration system, which was attached to the ID surface of the specimen over the length and width of the reduced section. The cold specimens were first brought to the target temperature and then loaded to failure under direct axial tension. A temperature controller feeding back on the thermocouples was employed to manage the liquid nitrogen flow into the cooling panel and to thereby maintain the specimen temperature to within $\pm 2^{\circ}\text{C}$ of the target temperature over the entire gauged length of the specimen for the duration of each test.

Photographs of a CWP specimen immediately prior to testing, showing the refrigeration system and thermocouples employed for specimen cooling and temperature monitoring, are shown in Figure 5.7.

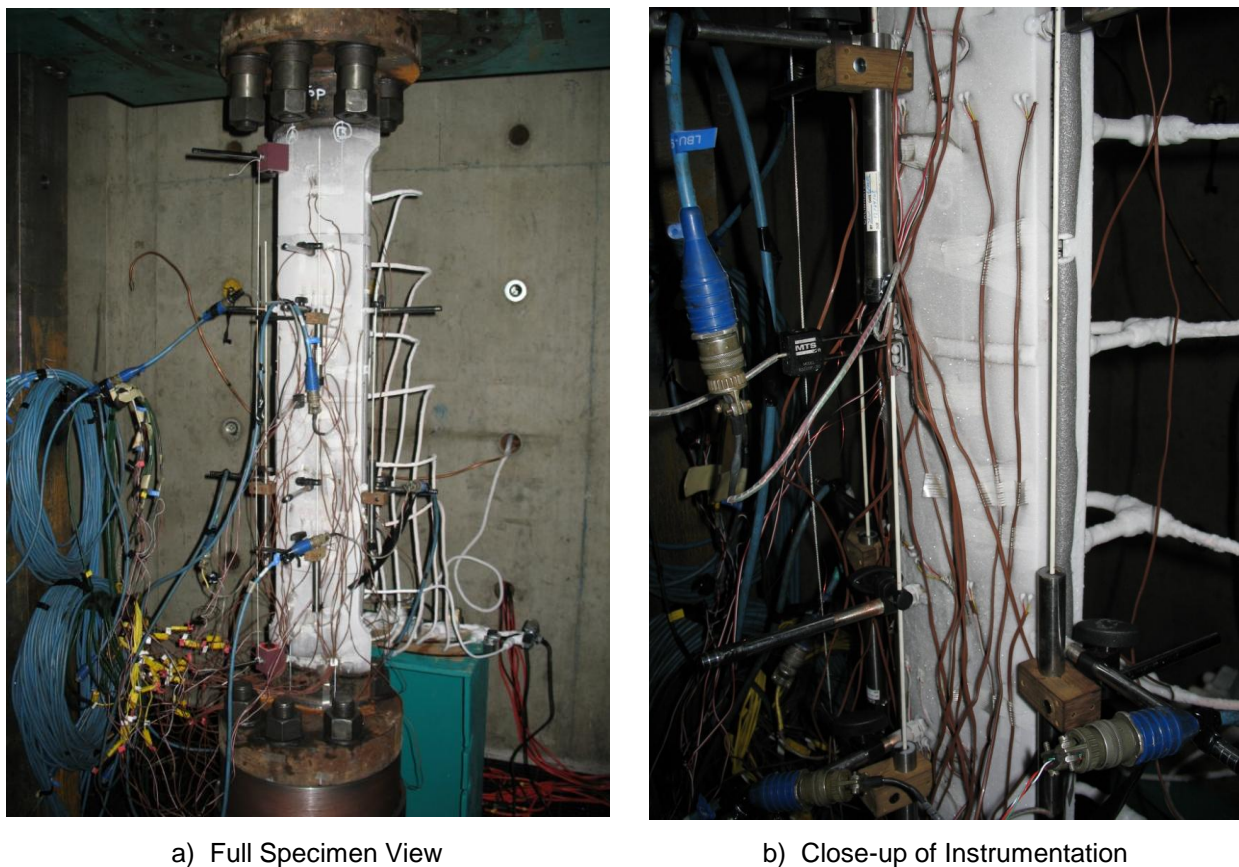


Figure 5.7 CWP Specimen Prior to Testing at Low Temperature

To facilitate the post-test analysis of flaw growth using the unloading compliance method, selected CWP tests on specimens taken from 12.75-inch pipe, and all of the CWP tests on specimens taken from 24-inch pipe, were subjected to repeated unload and reload steps³. The unload/reload steps were typically initiated at remote axial strain levels of 0.1%, 0.15% and 0.5%, and then at 0.2% strain increments beyond that point until the test was terminated. At each prescribed unload point, the loading was stopped and the test machine actuator was held fixed for 30 seconds prior to the initiation of each unload and reload cycle. The magnitude of each unloading step was approximately 20% of the applied load at the hold point.

All instrument readings were automatically recorded during each test using a computer-based data acquisition system and the resulting data files were stored in a spreadsheet compatible format to facilitate post-processing and interpretation.

5.3 Test Results

5.3.1 Pipe Tests

The axial load and key displacement and strain values for each test specimen, at the attainment of peak axial load and at the test end point, are summarized in Table 5.4. Also tabulated are the associated test pressures and temperatures, and an indication of the mode and location of the specimen failure.

The determination of the axial deformation and remote strain at peak load was facilitated by smoothing the axial load data (and gross axial stress data) to filter out localized peaks and valleys in the load versus displacement curves which are generally attributable to low-level transducer and signal conditioning noise. Load (and stress) smoothing was achieved by replacing the individual point-in-time data readings with a moving average, calculated from multiple point-in-time data points on either side of the target read point.

While each pipe specimen contained multiple nominally identical flaws (in terms of size and placement location relative to the welds), in the latter stages of each test, the CMOD associated with one flaw would exceed that of all others and through-wall extension and ultimately loss of pressure containment at that flaw location would typically define the test end point. The tabulated CMOD values pertain to the flaw with the dominant load-deformation response.

The typical axial load versus deformation response of a representative pair of test specimens (one pressurized and one effectively unpressurized) is shown in Figure 5.8. As noted above, the divergent CMOD versus strain curve is associated with the flaw which ultimately precipitated specimen failure.

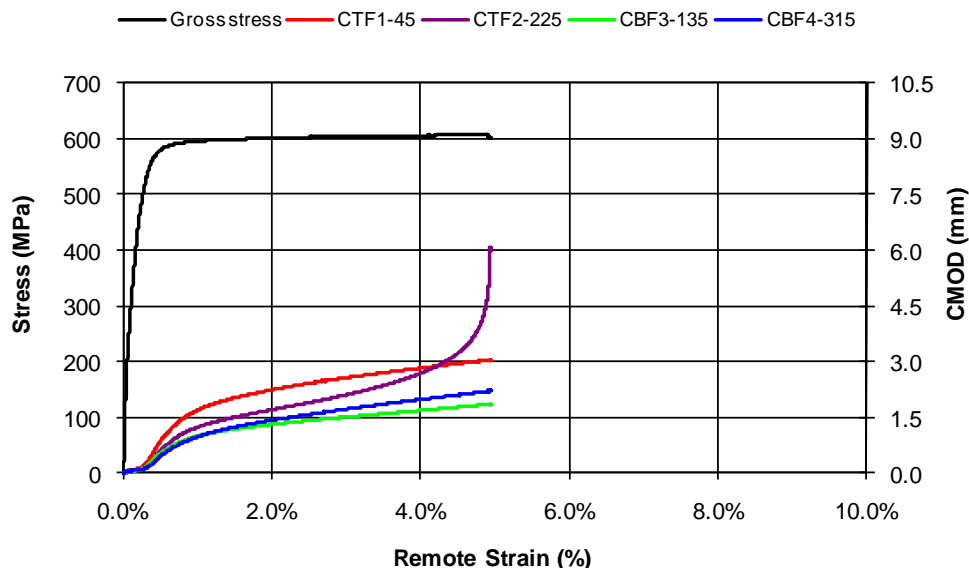
³ The collection and interpretation of the additional unloading compliance data was outside the original work scope and was added part way through the large-scale experimental program at the request of the program funding participants to facilitate further analysis by others following completion of this research program.

Table 5.4 Summary of 12-inch Diameter Pipe Test Results

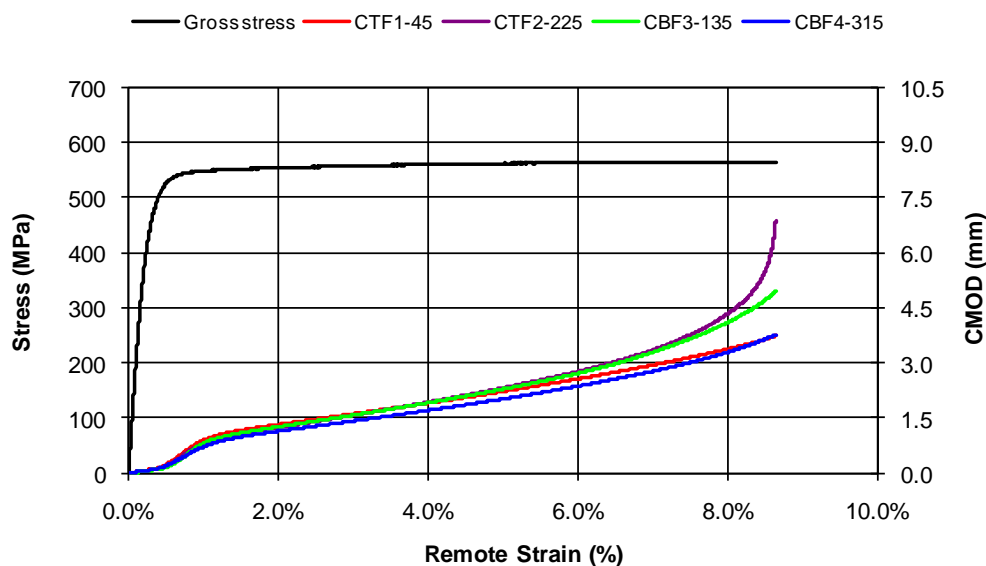
Specimen Number	Test Temp. (°C)	Test Pressure (MPa)	At Maximum Load				At Test End				Failure Location and Mode
			Applied Load (kN)	Gross Stress (MPa)	CMOD (mm)	Remote Strain ¹ (%)	Applied Load (kN)	Gross Stress (MPa)	CMOD (mm)	Remote Strain ¹ (%)	
1.1	21	30.20	7,338	590	2.81	0.83	7196	579	6.16	0.90	Flaw leak
1.2	22	0.50	6,934	555	3.38	1.88	6,847	548	6.06	2.02	Flaw leak
1.3	22	24.20	6,050	487	3.85	1.51	5,971	481	5.98	1.56	Flaw leak
1.4	22	0.38	5,694	460	4.61	2.77	5,658	457	6.17	2.84	Flaw leak
1.5	21	30.25	7,422	592	3.49	1.58	7,355	587	5.57	1.66	Flaw leak
1.6	22	0.33	7,032	560	3.73	4.64	7,008	558	No data	4.78	Flaw leak
1.7	22	30.20	7,563	606	3.75	4.74	7,499	601	6.06	4.94	Flaw leak
1.8	25	0.34	7,083	565	4.44	8.07	7,063	563	6.86	8.64	Flaw leak
1.9	20	30.28	7,244	585	2.93	0.64	7,156	578	4.99	0.67	Flaw leak
1.10	20	0.34	6,946	558	4.18	3.10	6,876	553	6.29	3.20	Flaw leak
1.11	21	30.20	7,445	599	4.50	1.24	7,362	592	6.44	6.44	Flaw leak
1.12	22	0.34	7,031	568	4.33	2.69	6,975	563	6.30	2.80	Flaw leak
1.13	-20	30.20	7,637	614	4.77	1.59	7,570	609	6.17	1.62	Flaw leak
1.14	-20	0.30	7,220	579	2.97	3.12	7,208	578	3.59	3.18	Flaw plane rupture
1.15	19	24.20	Maximum load not achieved (load peak and flaw failure imminent ²)				6,286	515	4.05	4.20	End cap failure
1.16	25	0.34	5,819	474	5.85	6.81	5,795	473	> 7.13	6.92	Flaw leak
1.17	22	30.20	7,479	605	3.80	2.13	7,434	602	5.93	2.24	Flaw leak
1.18	22	30.20	7,497	606	2.10	7.73	7,443	601	2.32	9.87	Pipe body necking
1.19	22	30.20	7,323	592	3.13	1.39	7,236	585	5.74	1.48	Flaw leak
1.20	22	24.20	6,294	515	3.52	3.97	6,249	511	5.65	4.10	Flaw leak
1.21	29	30.20	7,295	596	3.14	0.72	7,199	588	5.45	0.77	Flaw leak
1.22	21	30.20	7,514	609	3.75	2.01	7,397	600	6.51	2.12	Flaw leak
1.23	21	30.20	7,271	588	2.50	0.69	7,117	575	5.33	0.73	Flaw leak
1.24	17	30.20	7,530	602	3.05	2.28	7,418	593	5.94	2.45	Flaw leak ²

1. Average axial strain determined from all LVDTs contained within the uniform strain zones remote from girth welds and flaws.

2. Flaw location for governing flaw failed to intercept the targeted HAZ – actual location in base metal beyond.



a) Specimen 1.7 – High Y/T Pipe, Even-matched Welds, 3 × 35 mm HAZ flaws, High Pressure



b) Specimen 1.8 – High Y/T Pipe, Even-matched Welds, 3 × 35 mm HAZ flaws, No Pressure

Figure 5.8 Typical Load Deformation Response of 12.75-inch Diameter Pipe Specimens

5.3.2 Curved Wide Plate Tests

5.3.2.1 Overall Load Deformation Response and Axial Strain Capacity

The axial load and key displacement and strain values for each test specimen, at the attainment of peak axial load and at the test end point, are summarized in Tables 5.5 and 5.6, for CWP tests on panels cut from 12.75-inch and 24-inch diameter pipes, respectively. Also tabulated are the associated test temperatures and an indication of the mode and location of specimen failure.

Table 5.5 Summary of CWP Test Results – 12.75-inch Diameter Pipe

Specimen Number	Test Temp. (°C)	At Maximum Load				At Test End				Failure Mode and Location
		Applied Load (kN)	Gross Stress (MPa)	CMOD (mm)	Remote Strain ¹ (%)	Applied Load (kN)	Gross Stress (MPa)	CMOD (mm)	Remote Strain ¹ (%)	
3.1a	21	1,623	569	2.80	6.81	1,598	560	4.42	7.10	Strain localization in flaw region
3.1b	21	1,623	568	2.84	4.50	1,591	557	4.57	4.68	See 3.1a
3.2a	21	1,650	580	2.91	11.62	1,635	575	3.17	15.44	Strain localization in body region
3.2b	22	1,651	579	3.80	8.46	16,36	574	5.57	9.08	See 3.1a
3.3a	23	1,613	551	2.74	1.81	1,579	540	4.00	1.87	See 3.1a
3.3b	22	1,613	554	2.71	2.80	1,572	540	4.33	2.94	See 3.1a
3.4a	21	1,600	548	3.23	1.94	1,536	526	4.76	2.02	See 3.1a
3.4b	21	1,616	527	2.80	1.57	1,565	537	4.86	1.76	See 3.1a
3.5a	-20	1,698	581	2.84	4.18	1,677	574	4.45	4.54	See 3.1a
3.5b	-20	1,701	581	2.86	3.81	1,682	575	4.05	3.99	See 3.1a

1. Average axial strain determined from all LVDTs contained within the uniform strain zones remote from girth welds and flaws.

Table 5.6 Summary of CWP Test Results – 24-inch Diameter Pipe

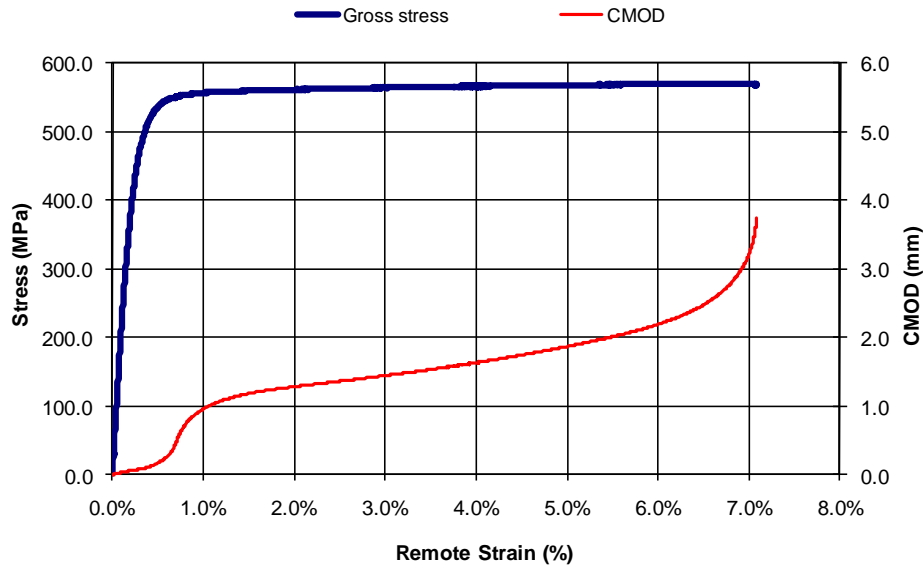
Specimen Number	Test Temp. (°C)	At Maximum Load				At Test End				Failure Mode and Location
		Applied Load (kN)	Gross Stress (MPa)	CMOD (mm)	Remote Strain ¹ (%)	Applied Load (kN)	Gross Stress (MPa)	CMOD (mm)	Remote Strain ¹ (%)	
4.1	20	2,674	685	1.43	1.17	2,639	676	3.15	1.31	Strain localization in flaw region
4.2	20	2,681	686	1.60	0.99	2,644	676	3.46	1.05	See 4.1
4.3a	20	2,652	676	1.82	1.19	2,621	668	3.38	1.27	See 4.1
4.3b	21	2,652	678	1.78	2.17	2,617	669	3.01	2.34	See 4.1
4.4	20	2,761	702	1.69	1.17	2,732	695	2.84	1.24	See 4.1
4.5	20	2,666	683	2.89	1.58	2,631	674	3.49	1.76	See 4.1 ²
4.6a	20	2,715	686	2.25	0.93	2,688	679	3.66	0.97	See 4.1
4.6b	21	2,669	685	1.61	2.81	2,563	658	1.79	3.94	See 4.1 ³

1. Average axial strain determined from all LVDTs contained within the uniform strain zones remote from girth welds and flaws.

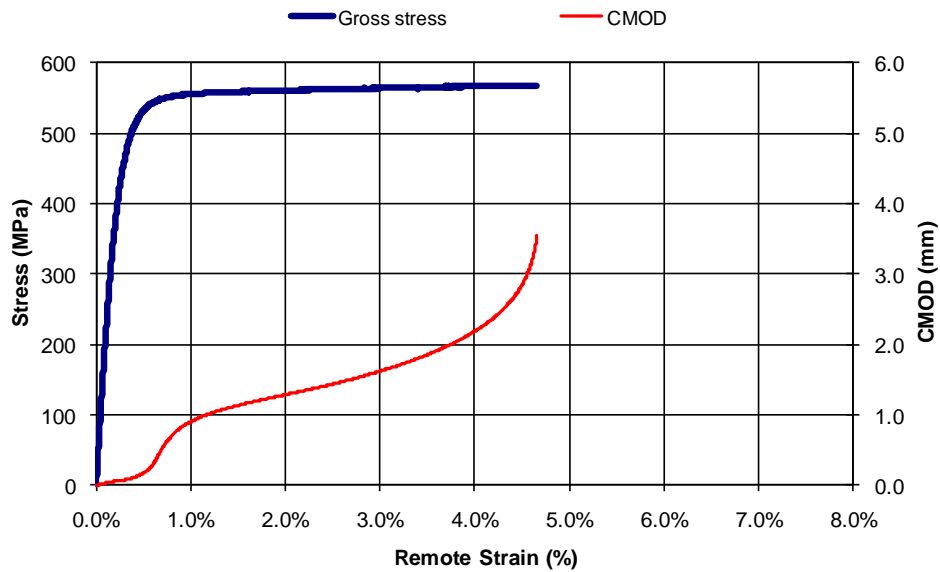
2. Flaw location failed to intercept targeted HAZ – actual location intercepted outer edge of weld metal.

3. Flaw location failed to intercept targeted HAZ – actual location in base metal beyond.

The typical axial load versus deformation response of a representative pair of CWP test specimens is shown in Figure 5.9.



a) Specimen 3.1a – High Y/T Pipe, Even-matched Weld, 3 × 35 mm Weld Metal Flaw



b) Specimen 3.1b – High Y/T Pipe, Even-matched Weld, 3 × 35 mm Weld Metal

Figure 5.9 Typical Load Deformation Response of CWP Specimens from 12.75-inch Diameter Pipe

The results shown in Figure 5.9 are for a pair of CWP specimens (3.3a and 3.3b) which were nominally identical in terms of pipe body and weld properties, and in terms of nominal flaw size and placement location. The differing results with respect to axial strain capacity highlight the variability inherent in the stress-strain response of girth welded line pipe containing flaws in the

vicinity of welds. This inherent variability reinforces the value of performing multiple identical CWP tests⁴.

5.3.2.2 Supplementary Test Data – Unloading Compliance Measurements

As discussed in Section 5.2.2.5, selected CWP specimens were subjected to partial unload and reload steps to facilitate the determination of the axial compliance (i.e. flexibility) of the test specimens in the immediate vicinity of the flaws. This information can be used in combination with finite element analysis to estimate flaw growth as a function of axial strain level.

To illustrate the process of determining the required compliance data, reference is made to Figure 5.10, which is a plot of the overall load deformation response of a selected CWP specimen, which was subjected to repeated unload/reload steps. The three unloading steps highlighted in the figure are reproduced in Figure 5.11 at a magnified scale which shows the individual load versus CMOD data points associated with each of the highlighted unloading steps. The slopes of the best fit lines through each set of data points are a measure of the axial stiffness of the specimen at the flaw location⁵. The reduced stiffness associated with progressively higher axial strain levels is indicative of flaw growth. The compliance value to be associated with each axial strain level is the inverse of the stiffness that is calculated for the associated unload/reload step.

Figure 5.12 is an example of the CWP specimen compliance values, as determined from the calculated stiffness of each unload/reload step, as a function of the remote axial strain level. Three compliance values are shown in the figure for each strain level, one based on a best fit to the unloading data only, one based on a best fit to the reloading data only, and one based on a best fit to the unloading and reloading data combined. For the CWP Specimen shown in Figure 5.12, the compliance data suggests that significant flaw growth began at a remote axial strain level of approximately 0.9% (the strain level at which the compliance values clearly start to increase).

Similar results, in both graphical and tabular format, are provided in Appendix 5D for each of the CWP specimens which were subjected to compliance measurements (i.e. Specimens 3.3a, 3.3b, 3.4a, 3.4b, 3.5a, 3.5b, 4.1, 4.2, 4.3a, 4.3b, 4.4, 4.5, 4.6a and 4.6b).

⁴ It is noted that in order to achieve comparable estimates of strain capacity between pipe specimens and corresponding CWP specimens, multiple CWP specimens (the number being equal to the number of flaws in the corresponding pipe specimen) should be tested with the minimum strain capacity being compared with that of the corresponding pipe. It is acknowledged that testing matched pairs of CWP specimens does not exercise the same number of nominally identical flaws as a pipe test on a specimen with up to four flaws and this factor should be kept in mind when comparing and interpreting the results obtained from CWP and pipe specimens.

⁵ Prior to the calculation of stiffness, the unload/reload data sets were filtered to eliminate the initial and final non-linear stages of each unload/reload step.

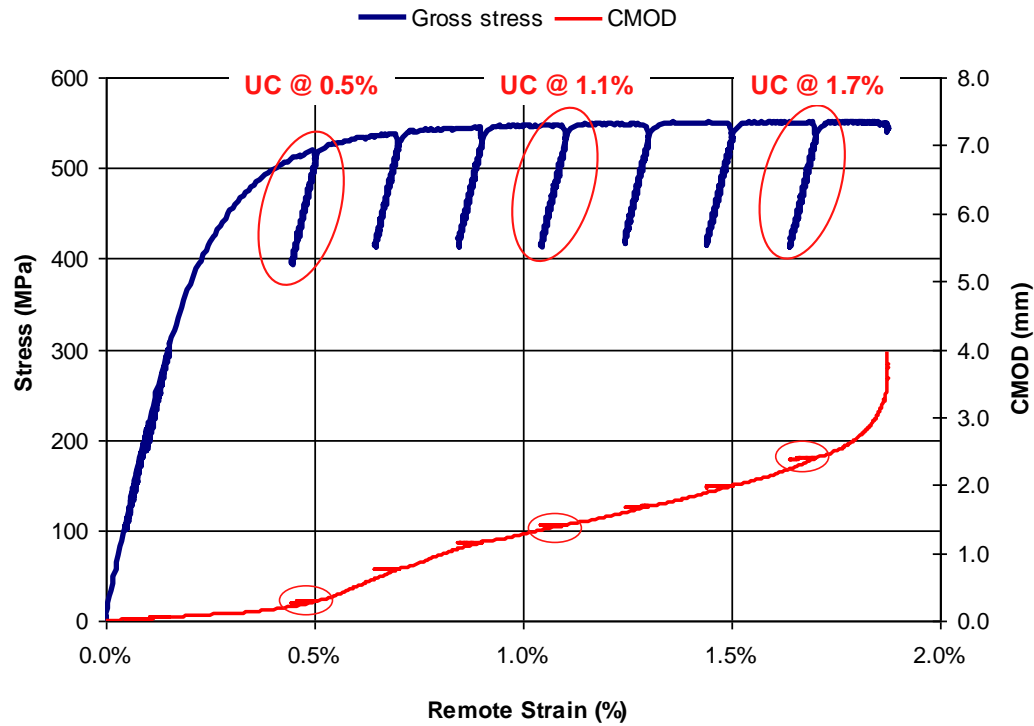


Figure 5.10 Load versus Deformation Response of CWP Specimen 3.3a with Selected Unload Steps Highlighted

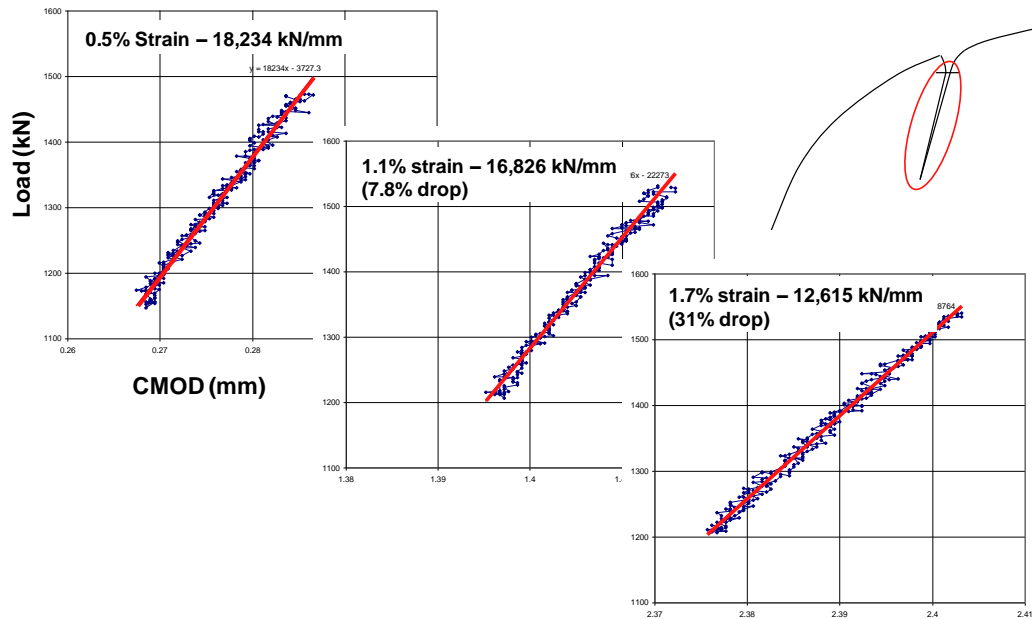


Figure 5.11 Magnified View of the Axial Load versus CMOD Data Points for Selected Unload Steps on CWP Specimen 3.3a together with Best Fit Stiffness Curves

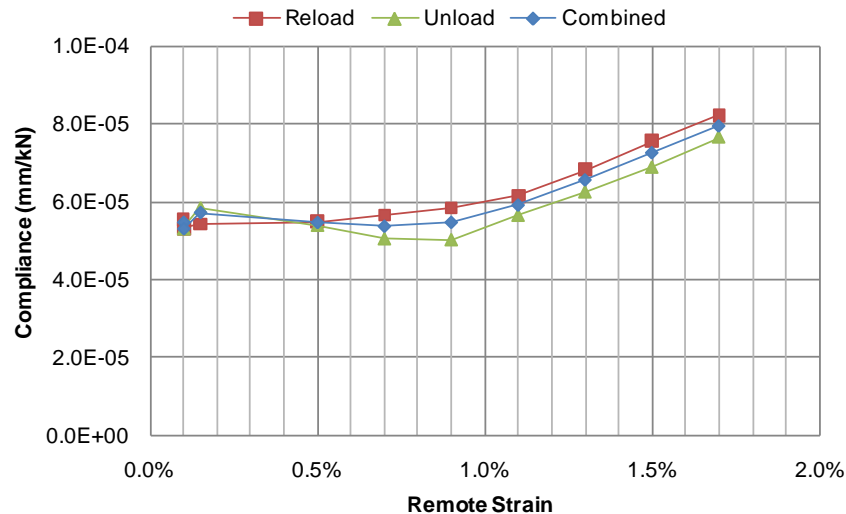


Figure 5.12 Compliance Curve for CWP Specimen 3.3a

5.4 Results Summary and Discussion

5.4.1 Specimens Fabricated from 12.75-inch Diameter Pipe

5.4.1.1 Strain Capacity Summary

The axial tensile strain capacities associated with the 34 tests (24 pipe and 10 CWP) performed on specimens fabricated from the 12.75-inch diameter pipe material are summarized in Table 5.7. The tabulated strain capacities are the remote axial strains⁶ associated with the attainment of peak specimen load. The tabulation focuses on strain at peak load because this constitutes the most conservative estimate of strain capacity and for a pipeline subjected to active loads, the attainment of peak load would constitute the strain level beyond which failure would be imminent. (Note that strain levels beyond the strain at peak load can only be sustained under true deformation-controlled loading conditions.)

In general, pipe specimens which were effectively unpressurized exhibited axial tensile strain capacities in the range of 2 to 8%, whereas the matching highly pressurized pipe specimens exhibited systematically lower strain capacities in the range of 1 to 5%. The limited number of tests on pipe specimens at reduced temperature (i.e. -20°C) exhibited axial strain capacities either greater than or comparable to the strain capacities of the corresponding room temperature test specimens.

With regard to the CWP specimens, the lower of the two axial strain capacities obtained from each pair of matching panel tests are broadly comparable to the strain capacities associated with the corresponding unpressurized pipe specimens.

⁶ Recall that the remote strain is the average of strain measurements obtained from the displacement transducers bridging the uniform strain zones, which are remote (i.e. well separated) from the girth welds and flaw locations.

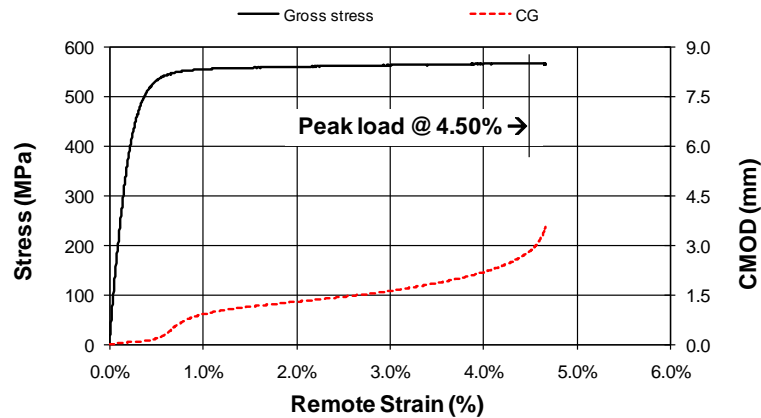
A representative comparison of the load deformation response and the strain capacities of selected pipe specimens (both pressurized and unpressurized) and a corresponding CWP specimen is provided in Figure 5.13.

Table 5.7 Summary of Axial Strain Capacities for Pipe and CWP Specimens from 12.75-inch Diameter Pipe

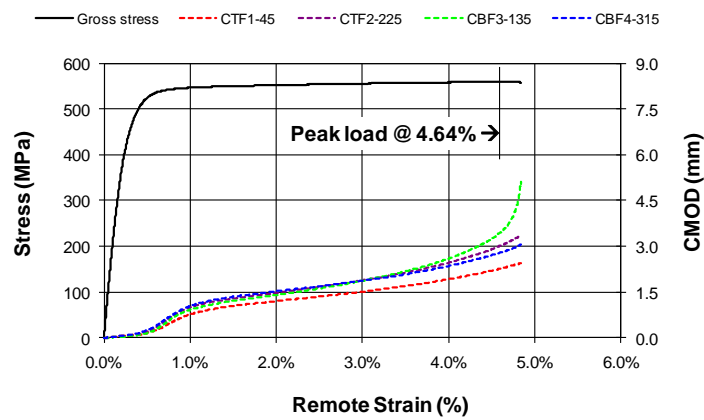
Pipe Body Y/T Ratio	Flaw Size (mm)	Flaw Location	Relative Weld Strength	Temp. (°C)	Axial Strain Capacity ¹ (%)		
					Curved Wide Plate ²	Pipe at Low Pressure ³	Pipe at High Pressure ^{2,4}
High	3 × 50	Body	---	≈20	---	1.9	0.8
“	3 × 35	Weld metal	Even-match	≈20	4.5 6.8	4.6	1.6
	3 × 35	HAZ	Even-match	≈20	8.5 11.6	8.1	4.7
“	3 × 50	Weld metal	Even-match	≈20	---	---	0.7
	3 × 50	HAZ	Even-match	≈20	---	---	2.0
“	3 × 35	Weld metal	Over-match	≈20	---	---	2.1
	3 × 35	HAZ	Over-match	≈20	---	---	7.7 ⁵
“	3 × 50	Weld metal	Over-match	≈20	1.8 2.8	3.1	0.6 1.4
	3 × 50	HAZ	Over-match	≈20	1.6 1.9	2.7	1.2 2.3
“	3 × 50	HAZ	Over-match	-20	3.8 4.2	3.1	1.6
	2 × 70	Weld metal	Over-match	≈20	---	---	0.7
Low	3 × 50	Body	---	≈20	---	2.8	1.5
“	3 × 50	Weld metal	Over-match	≈20	---	---	4.0
		HAZ	Over-match	≈20	---	6.8	4.2 ⁶

Note:

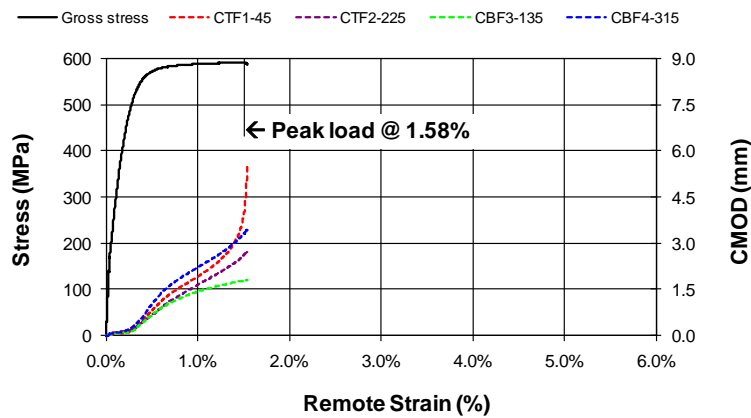
- 1) Strain at peak load.
- 2) Two strain values reported, one for each of the two identical tests.
- 3) Pressure level approximately 300 kPa - sufficient to indicate leakage.
- 4) Pressure level = 30.2 MPa for high Y/T pipes and 24.2 MPa for low Y/T pipes.
- 5) Specimen failure in pipe body.
- 6) Premature failure at end cap (peak load imminent).



a) Curved Wide Plate (Specimen 3.1b)



b) Pipe – Effectively No Pressure (Specimen 1.6)



c) Pipe – High Pressure (Specimen 1.5)

Figure 5.13 Representative Plate and Pipe Test Specimen Load Deformation Response – High Y/T Pipe, Even matched Welds, 3 × 35 mm Weld Flaws

5.4.1.2 Discussion of Results

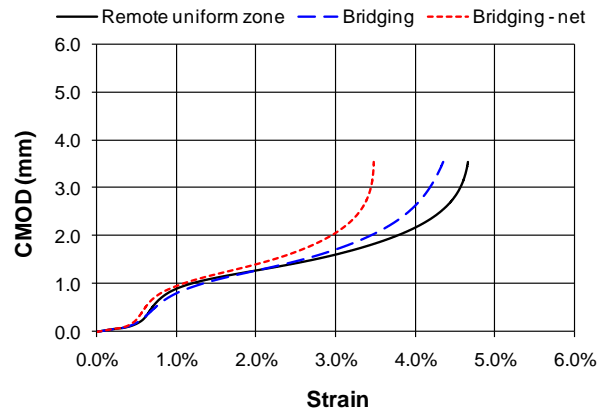
5.4.1.2.1 *Sensitivity of Reported Strain Capacity to Method of Measurement*

In this work, the remote axial strain, as obtained from the measurement of pipe body deformations in the uniform strain regions removed from the flaw locations, has been adopted as the preferred strain measure. This is because these strain values are expected to be more representative of overall pipe body strain levels away from strain field disruptions associated with the flaw locations. In addition, averaging axial strain measurements from multiple pipe body regions serves to smooth out the variability in both load-deformation response and strain capacity, which is attributable to the inherent lack of uniformity in line pipe material stress-strain response.

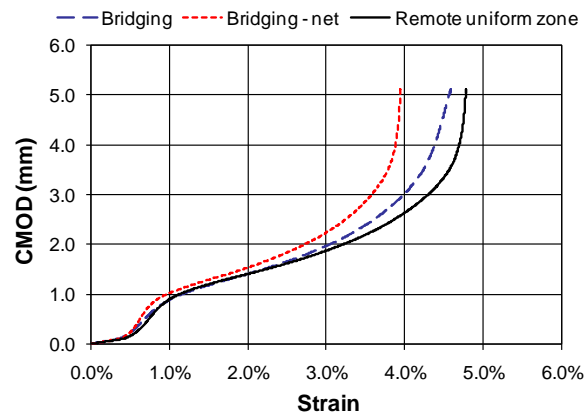
The sensitivity of reported axial strains to the location where the strain is measured, is illustrated in Figure 5.14. Each of the plots in Figure 5.14 (one for a CWP, one for an effectively unpressurized pipe and one for a highly pressurized pipe) shows the calculated relationship between crack mouth opening displacement (CMOD) and axial strain for a single flaw, where in each case the axial strain is calculated three different ways. The “bridging” strain curve in each plot pertains to the case where strain is estimated by dividing the specimen elongation, as recorded by the LVDTs bridging the girth welds and flaws, by the initial LVDT gauge length. The “bridging – net” strain pertains to the case where strain is again estimated from the LVDTs bridging the flaws, but with the CMOD subtracted from the total elongation to provide a more conservative (i.e. lower) estimate of the effective average axial strain. Lastly, the “remote uniform zone” strain pertains to the case where strain is estimated by averaging the specimen elongation recorded by the LVDTs bridging the uniform strain zones and dividing the result by the initial LVDT gauge length.

Figure 5.14 shows that axial strain estimates can differ by more than 30%, depending on where deformations are measured and how the strain is calculated from those deformations. Taking the strain capacity obtained from measurements in the uniform strain zones as the reference strain, the plotted results show that it is generally conservative to estimate strain capacity using a gauge length that bridges the girth weld and flaw location, provided that the CMOD is subtracted from the total elongation. The degree of conservatism associated with this approach will be dependent on the chosen gauge length. In addition, while strain estimates based on a gauge length that bridges the girth weld and flaw, without CMOD adjustment, will be less conservative, the potential exists for this method to non-conservatively overestimate strain capacity (see Figure 5.14c).

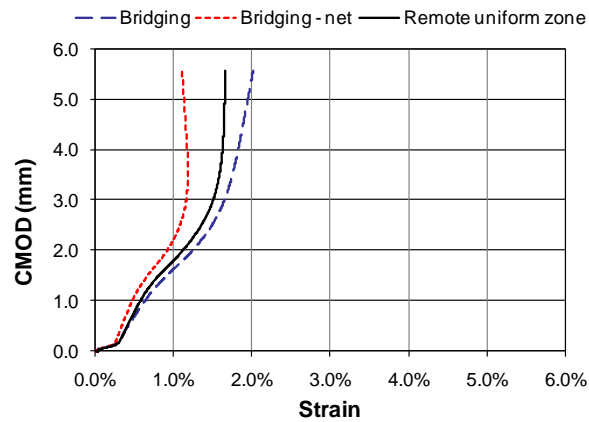
These findings support the position that the strain capacity estimates, obtained from far field measurements, are preferred because they are relatively insensitive to the chosen gauge length (provided they are contained within the uniform strain zone) and not influenced by flaw-induced discontinuities and the relative strain hardening characteristics of the pipe body and weld metal. More detailed discussion of uniform strain zones can be found in reference [61].



a) Curved wide plate



b) Pipe - low pressure



c) Pipe - high pressure

Figure 5.14 Comparison of Methods Used to Obtain Axial Strain Measurements – High Y/T Pipe, Even-matched Welds, 3 × 35 mm weld Metal Flaws

5.4.1.2.2 Observed Trends Based on Test Results

5.4.1.2.2.1 Effect of Internal Pressure

The reduction in axial strain capacity due to high internal pressure is illustrated in Figure 5.15 for a specific subset of the test data. This data set pertains to specimens containing 3×50 mm flaws located in either the pipe body or the HAZ, with the HAZ flaws being associated with over-matched welds. The figure plots the ratios between the strain capacities obtained from matching pipe tests, one with very low pressure (effectively unpressurized) and the other with high internal pressure. For the two cases involving the high Y/T pipe, the reduction in strain capacity is shown to slightly exceed 50%, whereas for the low Y/T pipe, which by definition possesses more beneficial strain hardening characteristics, the reduction is slightly less than 50%.

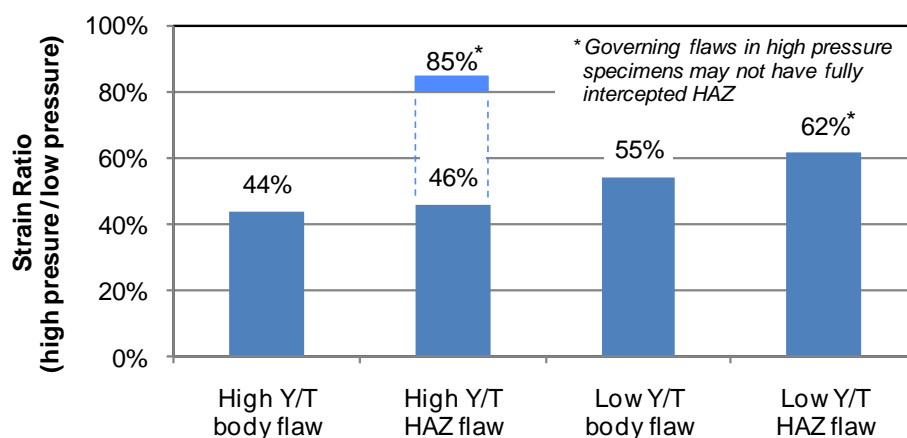


Figure 5.15 Effect of Pressure on Strain Capacity
(All Flaws 3×50 mm with HAZ Flaws Adjacent to Over-matched Welds)

Note that two strain ratios are reported for the parameter combination involving high Y/T pipe with HAZ flaws. This reflects the fact that the high pressure test was repeated and the differing strain ratios reflect the differing strain capacities obtained for the matching pair of high pressure tests. As noted in the figure, the higher strain ratio (indicating a reduced impact of pressure on strain capacity) is associated with the high pressure specimen in which the flaw placement location was problematic. On this basis the lower strain ratio is considered a more valid reflection of the pressure effect. That said, the reported strain ratio variation for a particular parameter combination is, at least in part, indicative of the inherent variability in axial strain capacity of welded line pipe.

Another comparison of the effect of internal pressure is provided in Figure 5.16. This data set pertains to the high Y/T pipe body material only with specimens containing, in one case 3×50 mm flaws located at the centerline of over-matched welds, and in the other case 3×35 mm flaws located in the HAZ of even-matched welds. The reduction in strain capacity due to pressure is seen to be more pronounced for flaws contained within the weld metal as

compared to the HAZ, with a maximum strain capacity reduction in the range of 80% being indicated for the 3×50 mm flaws contained within the over-matched weld metal.

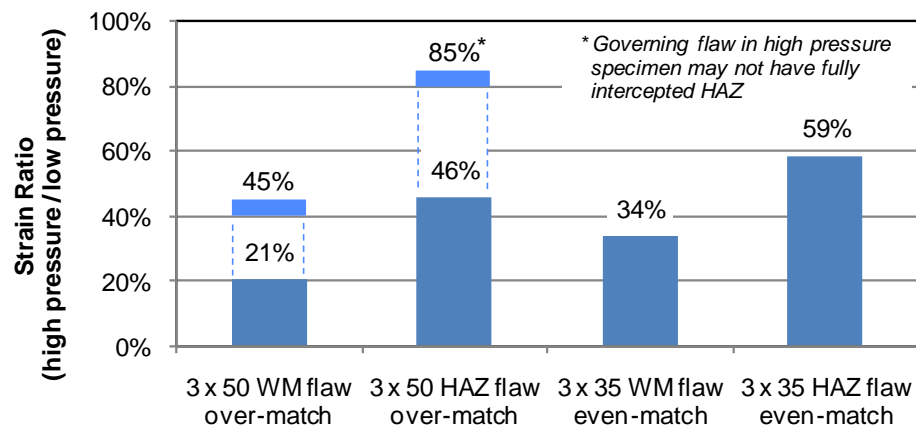


Figure 5.16 Effect of Pressure on Strain Capacity
(All Flaws in Weld Region of High Y/T Pipe)

Taken together, the results shown in Figures 5.15 and 5.16 suggest that the strain capacity reduction due to pressure is slightly less for flaws located in the HAZ when compared to identical flaws in the pipe body and similarly less for flaws located in the HAZ when compared to identical flaws in the weld metal. This finding is consistent with the assumption that the additional reinforcement provided by the weld cap (and the weld strength mismatch where applicable) will, to some extent, serve to shield HAZ flaws from the detrimental effects of biaxial loading. However, given the limited amount of test data involved in the comparison, and the scatter inherent in strain capacities associated with flaws in the vicinity of welds, this finding should be viewed with caution.

It is noted that the more general finding, that internal pressure is associated with a significant reduction in axial strain capacity, is not unique to this testing program. Similar test behavior has been reported by others (e.g. [62] and [63]). The results presented herein do, however, provide much needed additional information on the magnitude of the effect as a function of various test parameters.

5.4.1.2.2.2 Effect of Y/T Ratio

The effect of Y/T on strain capacity is shown in Figure 5.17. This figure plots the ratios between the strain capacities obtained from matching pipe tests, one made from high Y/T material and the other from the lower Y/T material. As in Figure 5.15, all cases compared in Figure 5.17 involved 3×50 mm flaws located in either the pipe body or the HAZ, with the HAZ flaws being associated with over-matched welds. The strain capacity reduction is shown to vary from about 30% to 70% with a higher capacity reduction being associated with specimens having flaws in the HAZ. For a given flaw location (i.e. body or HAZ), the reduction is shown to be more pronounced for the pressurized specimens. (As noted in the figure, the plotted strain ratios

for the high pressure specimens containing HAZ flaws are influenced by the fact that the strain capacity of the low Y/T specimen is somewhat overestimated because while flaw failure was imminent, failure actually occurred due to end cap rupture. Had premature end cap failure not occurred, the strain capacity estimate would have potentially been slightly higher and the plotted strain ratios slightly lower for this pressure and flaw location combination.)

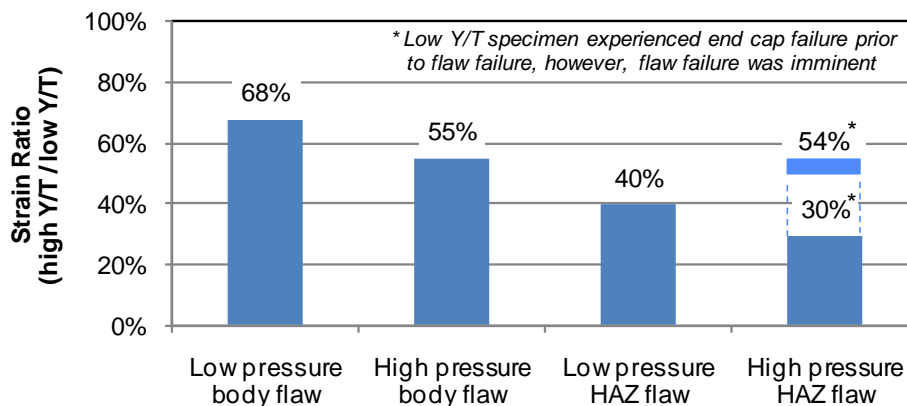


Figure 5.17 Effect of Y/T Ratio on Strain Capacity
(All Flaws 3 × 50 mm with HAZ Flaws Adjacent to Over-matched Welds)

The general reduction in strain capacity with increased Y/T is consistent with the assumption that material having a lower strain hardening potential (i.e. a higher Y/T ratio) will sustain lower axial strains. The more pronounced reduction in strain capacity for the specimens with HAZ flaws is attributed, at least in part, to HAZ softening, the presence of which has been confirmed through micro-hardness measurements of the welds (see Section 3.3).

It is noted that the above discussion suggests that the strain capacity difference is largely attributable to differences in pipe body Y/T. In fact, the difference in the average axial Y/T ratio between the so-called high Y/T and low Y/T pipe material was not that large (see

Table 3.3). In addition, other pipe body and weld metal properties were different between the two sets of specimens. So while differences in pipe body Y/T no doubt impact strain capacity, other factors may have also contributed to the magnitude of the reported differences.

5.4.1.2.2.3 Effect of Temperature

The effect of test temperature on strain capacity is illustrated in Figure 5.18. The plotted data set pertains to specimens fabricated from high Y/T pipe material with over-matched welds containing 3 × 50 mm flaws located in the HAZ. The figure plots the ratios between the strain capacities obtained from matching pairs of either CWP or pipe tests, with one specimen from each pair being tested at a reduced temperature of -20°C and the other being tested at room temperature (approximately 20°C). The figure shows that for the CWP and effectively unpressurized pipe specimens, the reduced temperature results in an increase in axial strain capacity. For the highly pressurized pipes, the strain capacity increase with reduced temperature, which is indicated for the uni-axially loaded specimens, is indicated for only one of the two test

pairs. However, as noted in the figure, the placement of the capacity-controlling HAZ flaw in one of the two pressurized pipe specimens tested at room temperature was problematic. If the strain capacity ratio associated with the problematic pipe test is set aside, the remaining results indicate that the axial strain capacity is consistently higher in the specimens tested at low temperature.

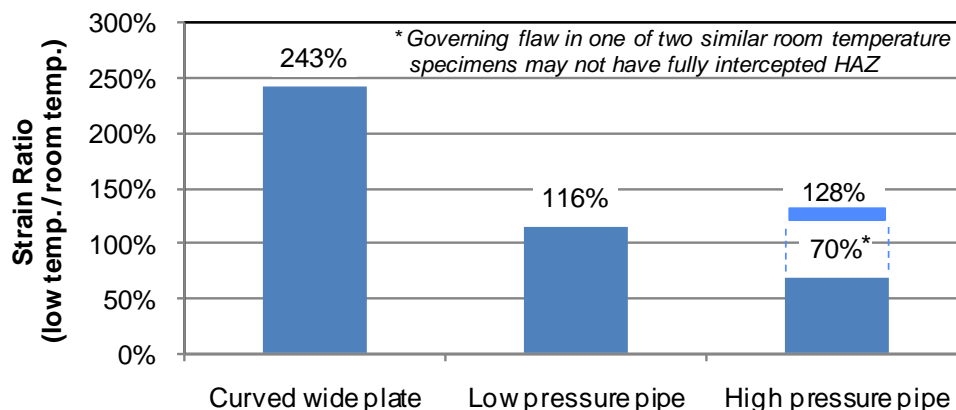


Figure 5.18 Effect of Temperature on Strain Capacity
(All Flaws 3 × 50 mm in HAZ of Over-matched Welds)

The finding that a reduced temperature does not result in a detrimental effect on strain capacity is consistent with the small-scale material test results (see Section 3.7), which indicate that the ductile-to-brittle transition temperature for fracture initiation of both the pipe body material and the weld metal are well below the chosen reduced test temperature of -20°C. For pipe material operating at a reduced temperature, provided that it is above the transition temperature, a reduction in strain capacity would not normally be expected.

The observed increase in strain capacity associated with the low temperature tests is primarily attributed to the impact of reduced temperature on the strain hardening characteristics of the pipe body and weld metal. The yield and tensile strength of steel tends to progressively increase with falling temperature and, for the materials tested herein, the increase in tensile strength at -20°C was found to be proportionally more than the increase in yield strength (see Section 3.4.1.2). This disproportionate temperature effect on material strength results in a lower effective Y/T ratio for the material tested at low temperature and, as noted above, a lower Y/T ratio is typically associated with more favorable strain hardening characteristics and, by implication, higher axial strain capacity.

5.4.1.2.2.4 *Effect of Specimen Geometry*

The influence of specimen type on strain capacity is illustrated in Figure 5.19. This figure plots the ratios between the strain capacities obtained from matching CWP and effectively unpressurized pipe tests. (Note that for this comparison, the lower of the strain capacities obtained from two otherwise identical CWP tests are compared to the results obtained from the single corresponding pipe, which contained multiple flaws.) The strain capacities for CWP

specimens with 3×35 mm flaws in either the weld metal or the HAZ are shown to be very similar to the strain capacities obtained from the corresponding pipe specimens (i.e. within about 5%). However, the strain capacity estimates obtained from CWP tests on specimens with 3×50 mm flaws in similar locations are shown to be significantly lower (i.e. about 40% lower) than the capacities obtained from the pipe tests.

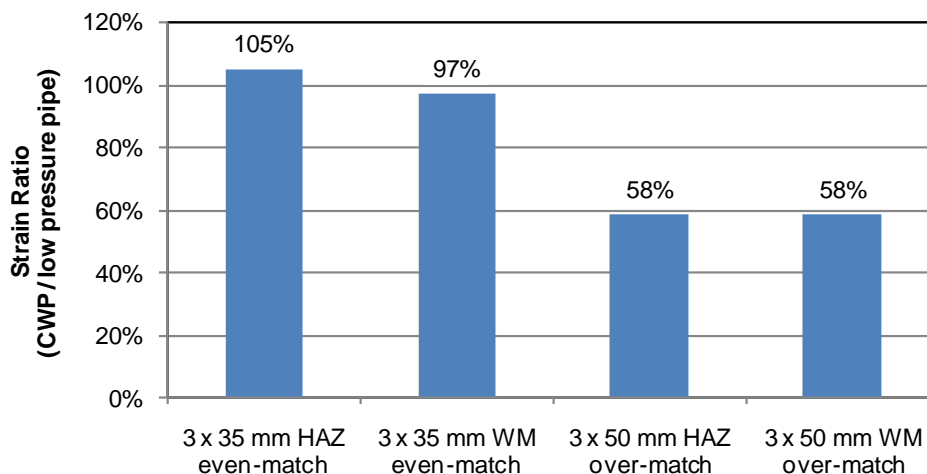


Figure 5.19 Effect of Specimen Geometry on Strain Capacity

These findings emphasize the importance of careful consideration in the sizing of CWP panel specimens and the selection of flaw sizes. If the cross-sectional area (and total width) of the flaw is small relative to that of the CWP panel, the lateral extent of the non-uniform strain field surrounding the flaw will be effectively contained by the width of the CWP panel and the axial strain behavior of the CWP specimen would be expected to be much like that of an unpressurized pipe specimen containing a similar flaw. As the flaw size is increased, the degree to which the non-uniform strain field surrounding the flaw is influenced by the finite width of the CWP panel will also increase and the potential for divergent behavior between otherwise similar CWP and pipe specimens will also increase.

While it is difficult to draw conclusions based on a limited number of CWP tests, due to the scatter inherent in strain capacity estimates associated with flaws in the vicinity of welds, for the materials tested in this program, the results shown in Figure 5.19 suggest that for the chosen CWP panel width (i.e. nominally 225 mm), the 3×50 mm flaws may have been too large to behave as if they were effectively contained within a full pipe section. It is noted that while direct comparisons between CWP tests and pipe tests are meaningful only when flaw size is carefully chosen to ensure comparable behavior, in other cases numerical analysis methods can be employed to establish the correlation between the results obtained from CWP panel and full-scale pipe tests.

5.4.1.2.2.5 *Summary*

Consistent with the findings of other contemporary large-scale testing programs, the pipe tests reported herein demonstrate the significant detrimental impact on axial strain capacity of

biaxial loading due to internal pressure, an effect which is not captured by CWP tests. A comparable degree of sensitivity in strain capacity is also shown to be attributable to the strain hardening characteristics of both the pipe body and weld material. The tests also demonstrate that while the axial strain capacity of circumferential flaws in the weld metal or HAZ could be enhanced due to weld strength over-match and the geometric reinforcement provided by the weld cap, other factors can undermine the effective strain capacity associated with flaws in this region. The limited testing performed at low temperature (i.e. -20°C) supports the position that girth welded line pipe, which is operating above the transition temperature of both the body material and the weld metal, does not experience a reduction in axial strain capacity with reduced temperature. Lastly, the tests highlight the importance of specimen design and instrumentation layout in ensuring that the strain measurements obtained are representative of full-scale pipe behavior.

5.4.2 Specimens Fabricated from 24-inch Diameter Pipe

5.4.2.1 Strain Capacity Summary

The axial tensile strain capacities associated with the eight tests performed on CWP specimens fabricated from the 24-inch diameter pipe material are summarized in Table 5.8. The tabulated strain capacities are the remote axial strains associated with the attainment of peak specimen load.

Table 5.8 Summary of Axial Strain Capacities for CWP Specimens
from 24-inch Diameter Pipe

Pipe Body Y/T Ratio	Flaw Size (mm)	Flaw Location	Relative Weld Strength	Temp. ($^{\circ}\text{C}$)	Axial Strain Capacity ¹ (%)		
					Curved Wide Plate ²	Pipe at Low Pressure	Pipe at High Pressure
High	4 × 50	Weld metal	Over-match	≈20	1.2	---	---
"	3.5 × 50	Weld metal	Over-match	≈20	1.0	---	---
"	3 × 50	Weld metal	Over-match	≈20	1.2 2.2	---	---
"	4 × 50	HAZ	Over-match	≈20	1.2	---	---
	3.5 × 50	HAZ	Over-match	≈20	1.6	---	---
	3 × 50	HAZ	Over-match	≈20	0.9 2.8	---	---
Note: 1) Strain at peak load. 2) Two strain values reported, one for each of the two identical tests.							

In general, the CWP specimens, regardless of flaw size or placement location, exhibited excessively low axial strain capacities with the pipe body material exhibiting strain hardening characteristics that are not well suited to applications where high axial strain capacity is desired.

On this basis, the testing program was re-focused on the testing of specimens fabricated from the 12.75-inch diameter pipe material, which possessed more desirable and appropriate axial strain hardening characteristics.

5.5 Appendix 5A - 5D

Appendix 5A to Appendix 5D are given in separate electronic files for easy file management. The contents and name of the files are listed below.

Appendix 5A – 12-inch diameter pipe test results,

File name: “FinalReport_ABD1_Project1_Appendix5A.pdf”;

Appendix 5B – 12-inch diameter curved wide plate test results,

File name: “FinalReport_ABD1_Project1_Appendix5B.pdf”;

Appendix 5C – 24-inch diameter curved wide plate test results,

File name: “FinalReport_ABD1_Project1_Appendix5C.pdf”;

Appendix 5D – Curved wide plate unloading compliance data,

File name: “FinalReport_ABD1_Project1_Appendix5D.pdf”.

6 Post-Test Physical Examination

6.1 Background and Objectives

The primary objective of the post-test physical examination process is to determine the condition of the material in the vicinity of each full-scale pipe specimen flaw at the point of test termination. The features examined included the overall deformation of the pipe, the residual crack mouth opening displacement (CMOD), the appearance of fracture surface, the amount of flaw growth and the flaw growth path. It is noted that the deformation state at the point of test termination does not typically correspond to the deformation state associated with the attainment of the tensile strain capacity. While the tensile strain capacity is typically associated with the point of maximum axial load, all except one of the pipe specimens sustained additional axial deformation, with an accompanying load drop, prior to test termination.

The 24 full-scale 12-inch OD pipe specimens contained multiple flaws placed nominally into the same region of each specimen (i.e. pipe body, weld centerline, or HAZ). The standard specimen configuration involved two well-separated pairs of diametrically opposed flaws (i.e. 4 flaws per specimen). However, four shorter specimens contained only one diametrically opposed pair of flaws (i.e. 2 flaws per specimen). For all but two specimens, test termination was defined as the point at which loss of containment occurred due to through-wall extension of one flaw. The wall-breaching flaw from each specimen was retained by C-FER for post-test examination, and all of the non-breaching flaws were forwarded to a metallurgical lab for post-test examination under CRES supervision.

6.2 Flaws Subjected to Detailed Examination

The pipe test specimens with flaws subjected to detailed post-test analysis are listed in Table 6.1. The specimens are grouped by pipe type and weld production.

6.3 Flaw Examination Results

6.3.1 Non-Breaching Flaws

6.3.1.1 Procedure for Post-Test Flaw Examination

An example of the pipe sections containing the non-breaching flaws from a typical pipe specimen, as received from C-FER, is shown in Figure 6.1.

The preparation of the metallographic samples involved the following steps as shown in Figure 6.2.

1. Extract a small section of the material around the flaw, with the perimeter located approximately 2 inches from the flaw in all directions.
2. Cut the piece at mid-flaw-width into two halves.
3. Immerse one of the halves in liquid nitrogen and break it along the flaw plane by applying an impact load.

4. Cut the other half on multiple planes to expose the cross sections at three locations along the flaw length.

Table 6.1 Pipe specimens subjected to detailed post-test analysis

Case No.	Pipe Material	Weld	Test No.	Pressure (%SMYS)	Test Temp.	Number of Flaw	Flaw Size (mm x mm)	Flaw Location
1	High Y/T	N/A	1.1	80	Room	4	3 x 50	Pipe
2			1.2	0	Room	4	3 x 50	Pipe
3	Low Y/T	N/A	1.3	80	Room	4	3 x 50	Pipe
4			1.4	0	Room	4	3 x 50	Pipe
5	High Y/T	First Production	1.5	80	Room	4	3 x 35	WM
6			1.6	0	Room	4	3 x 35	WM
7			1.7	80	Room	4	3 x 35	HAZ
8			1.8	0	Room	4	3 x 35	HAZ
9			1.21	80	Room	2	3 x 50	WM
10			1.22	80	Room	2	3 x 50	HAZ
11	High Y/T	Second Production	1.11	80	Room	4	3 x 50	HAZ
12			1.12	0	Room	4	3 x 50	HAZ
13			1.9	80	Room	4	3 x 50	WM
14			1.10	0	Room	4	3 x 50	WM
15			1.13	80	Low	4	3 x 50	HAZ
16			1.14	0	Low	4	3 x 50	HAZ
17			1.17	80	Room	4	3 x 35	WM
18			1.18	80	Room	4	3 x 35	HAZ
19			1.19	80	Room	4	3 x 50	WM
20			1.23	80	Room	2	2 x 70	WM
21			1.24	80	Room	2	3 x 50	HAZ
22	Low Y/T		1.15	80	Room	4	3 x 50	HAZ
23			1.16	0	Room	4	3 x 50	HAZ
24			1.20	80	Room	4	3 x 50	WM

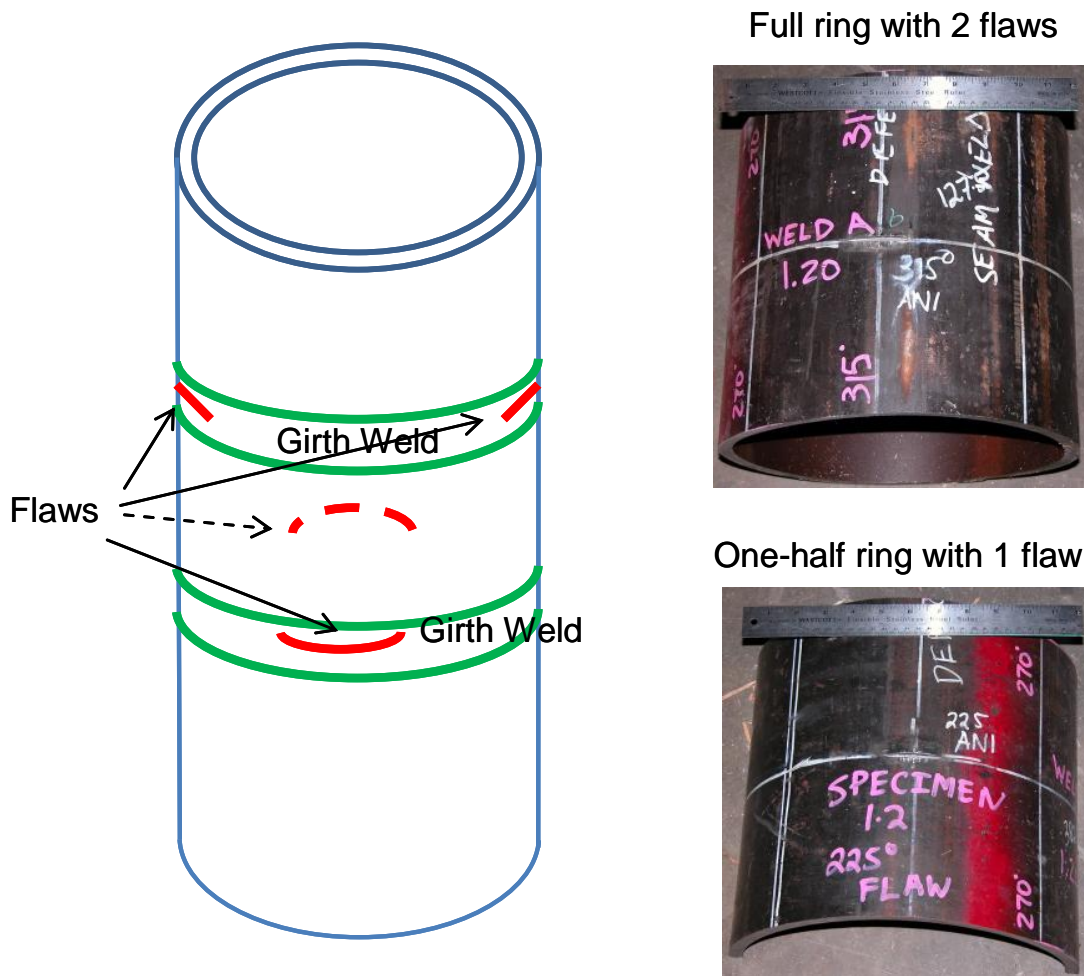


Figure 6.1 Illustration of the pipe pieces as-received from C-FER

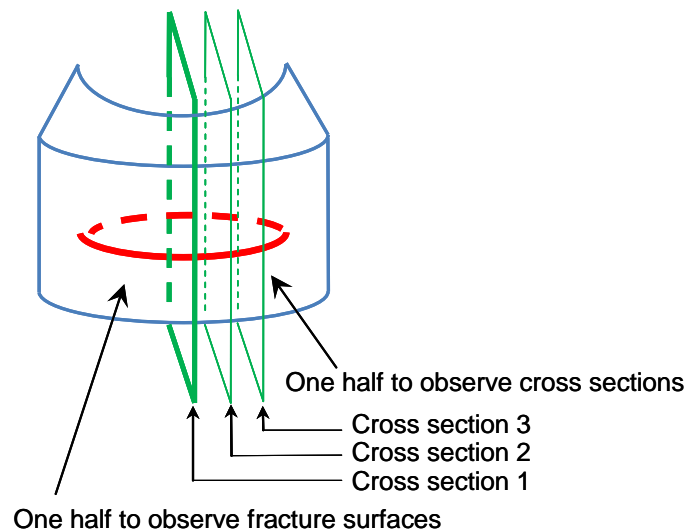


Figure 6.2 Illustration of cutting planes for preparation of metallographic samples

6.3.1.2 Results of Post-Test Analysis

A sample of the results obtained from the post-test analysis is described in this section. The detailed results of all non-breaching flaws are given in Appendix 6A.

Plastic Deformation

Depending on the amount of longitudinal straining occurred in the pipe at the point of test termination, the amount of pipe diameter reduction can be substantial. Figure 6.3 shows the diameter difference between two pipes. Sample 1.1 had a small amount of longitudinal straining ($< 1\%$) at the termination of test. Sample 1.16 had a large amount of longitudinal straining ($> 6\%$). The pipe diameter reduction in Sample 1.16 is much greater than that in Sample 1.1.

Residual Flaw Opening

The residual flaw opening in the received samples were photographed against a dimensional maker (a ruler), see Figure 6.4. To preserve the full 3-D features of the flaws, silicone replicas were made for all flaws. A sample silicone replica is shown in Figure 6.4. Other than the fine opening at the flaw tip, the silicone replica is able to provide a faithful 3-D representation of the flaw.

Flaw Growth Profile Viewed from Fracture Surface

A few samples of the fracture surfaces are shown in Figure 6.5, Figure 6.6, and Figure 6.7. The flaw growth pattern among flaws located in the pipe body, weld centerline and HAZ is generally similar. The amount of flaw growth varies among the specimens at the termination of the test. The final surface of the weld centerline sample exposed at low temperature shows large shinning features typical of deposited weld metal (Figure 6.6).

Flaw Growth Profile Viewed by Cross Sections

The flaw growth profile of a weld centerline flaw of Sample 1.8 is shown in Figure 6.8. The initial flaw size was 3 x 35 mm. The blunting at the initial flaw tip is visible. The flaw grew for approximately 2.5 mm with a sharp tip. In contrast, Sample 1.16 shown in Figure 6.9 had an HAZ flaw of 3 x 50 mm. The amount of flaw growth is quite small. However, the flaw experienced a large amount of blunting, to a degree of 1.5 to 2.0 mm.

The multi-cross-sectional view of the flaws is given in Figure 6.10 and Figure 6.11. It is interesting to note that cross sections of Figure 6.9 and Figure 6.11 are from the same test specimen, Sample 1.16. However, they are from two individual flaws located at 45-deg and 315-deg, respectively. The flaw in Figure 6.9 is very close to the fusion boundary and had a large blunted flaw tip. The flaw in Figure 6.11 was notched at least 2 mm from the fusion boundary. This flaw experienced a large amount of flaw growth and the associated ligament thinning is very pronounced. This illustrates some of challenges associated with locating HAZ flaws and the subsequent effects on the flaw behavior.

The flaw tips and associated microstructure, at different magnifications, are shown in Figure 6.12 and Figure 6.13. In the case of Sample 1.5 (Figure 6.12) the flaw grew largely

straight ahead and stayed in the weld metal. In the case of Sample 1.7 (Figure 6.13), the initial flaw tip was in the deposited weld metal, although it was meant to be an HAZ notched flaw. The flaw subsequently grew into the HAZ.

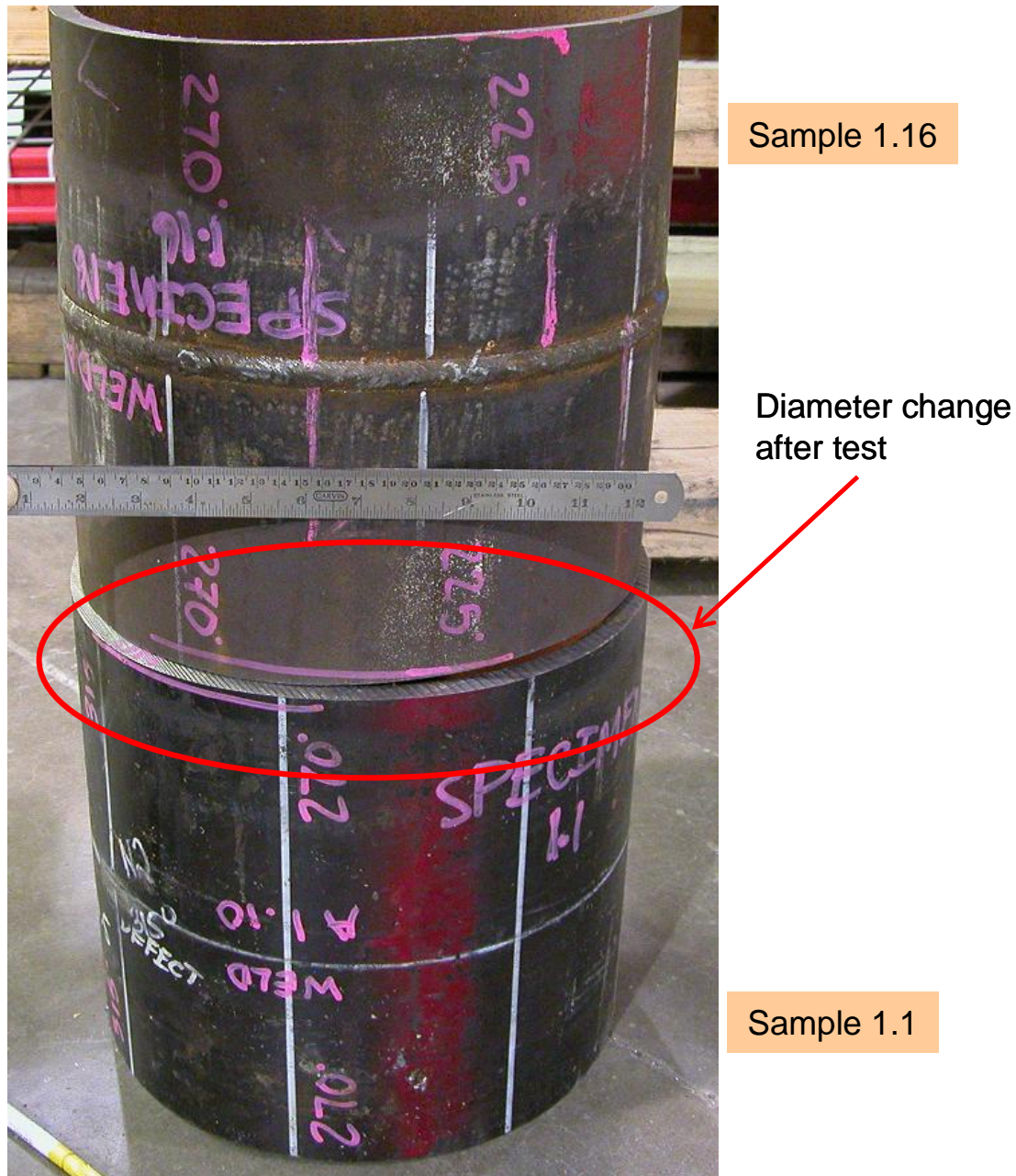


Figure 6.3 Illustration of diameter reduction from longitudinal straining

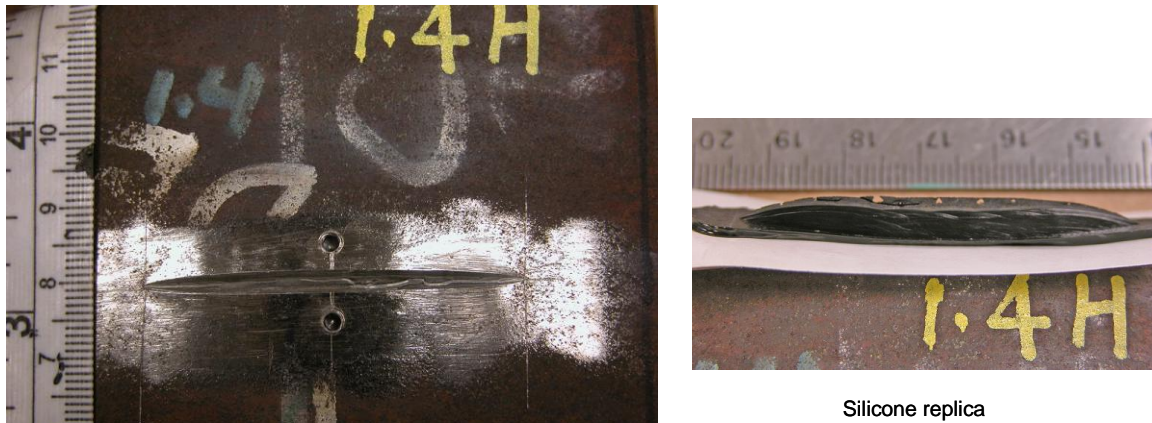


Figure 6.4 Illustration of residual CMOD (left) and the silicone replica made of the flaw (right)

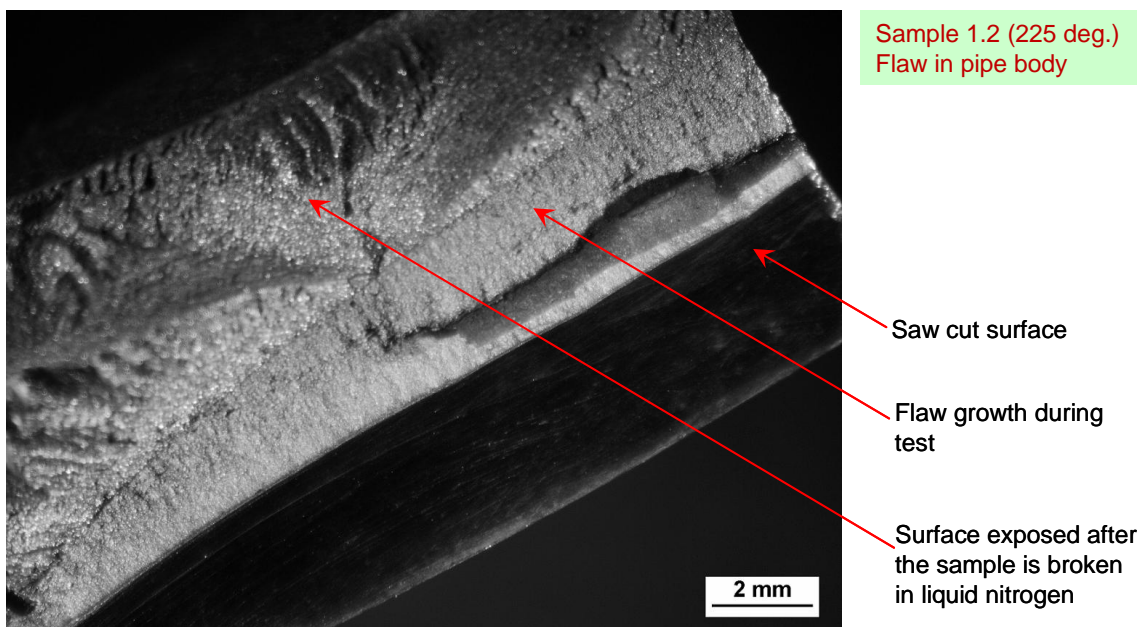


Figure 6.5 Fracture surface of a flaw located in the pipe material

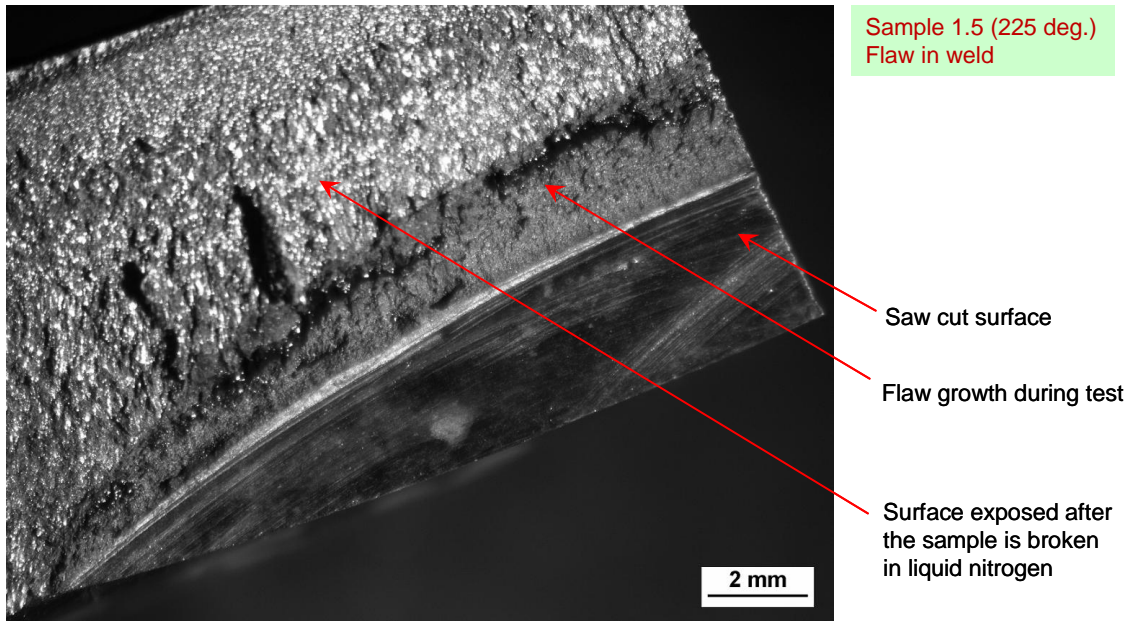


Figure 6.6 Fracture surface of a flaw located in the weld centerline

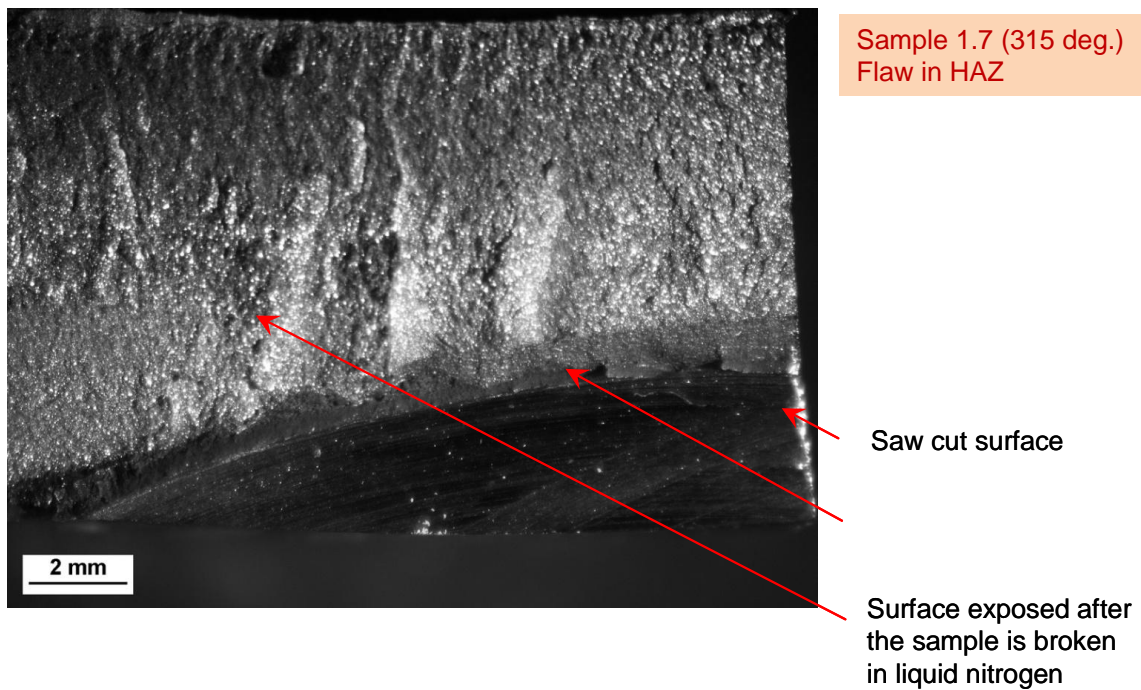


Figure 6.7 Fracture surface of a flaw located in HAZ

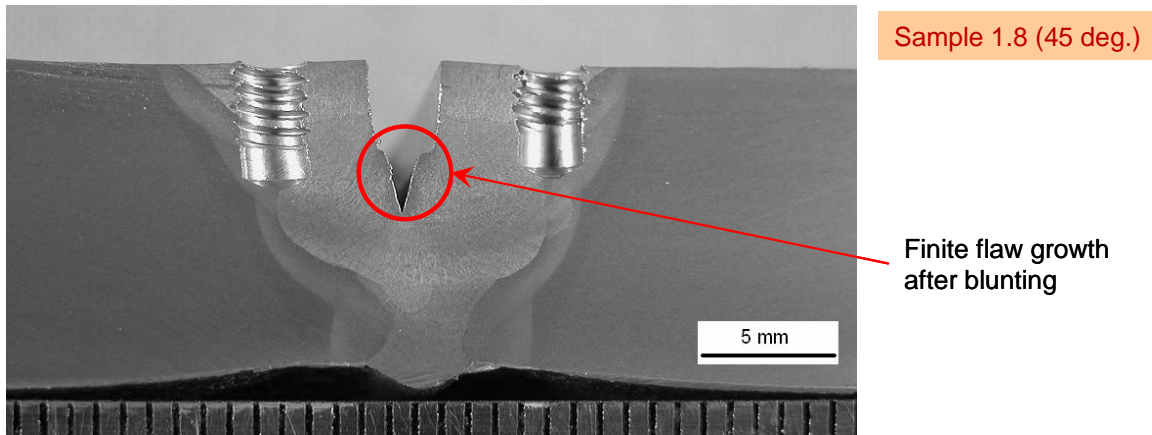


Figure 6.8 Flaw growth path of a flaw located in weld centerline

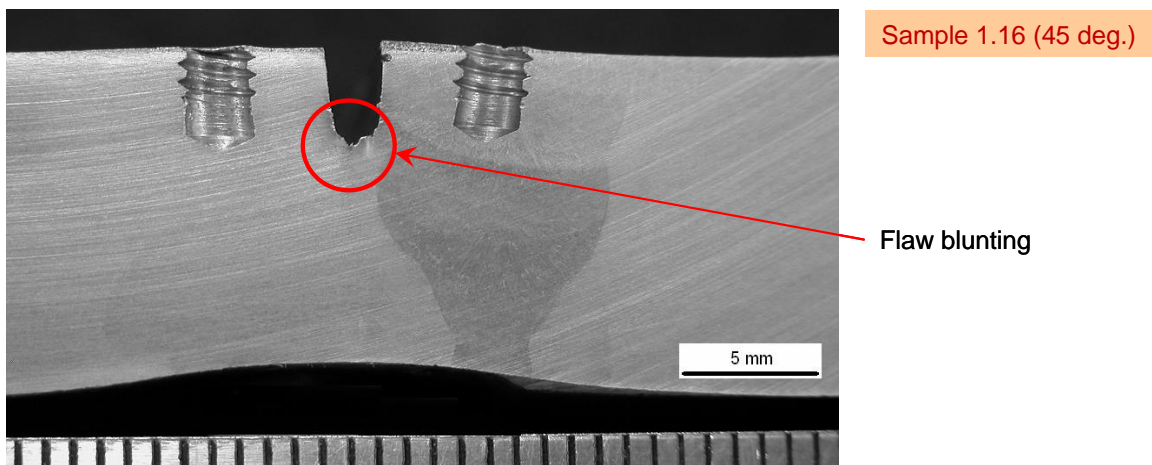


Figure 6.9 Flaw growth path of a flaw located in HAZ

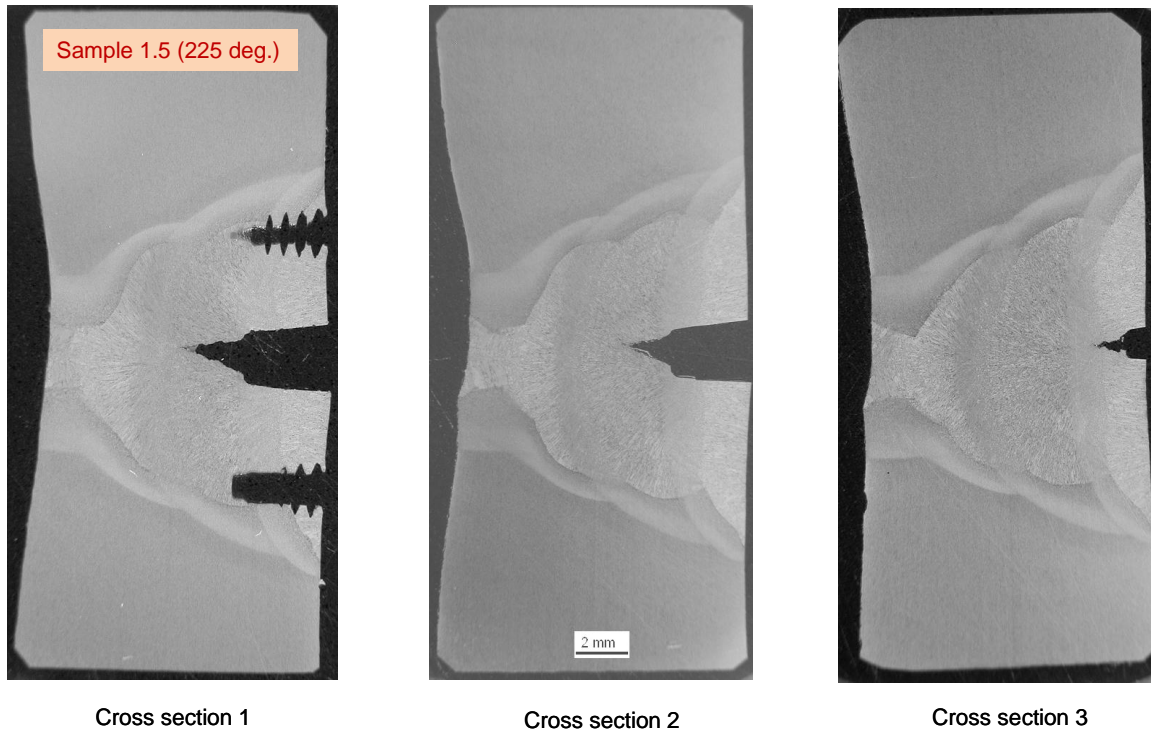


Figure 6.10 Multi-cross-sectional view of a flaw located in the weld

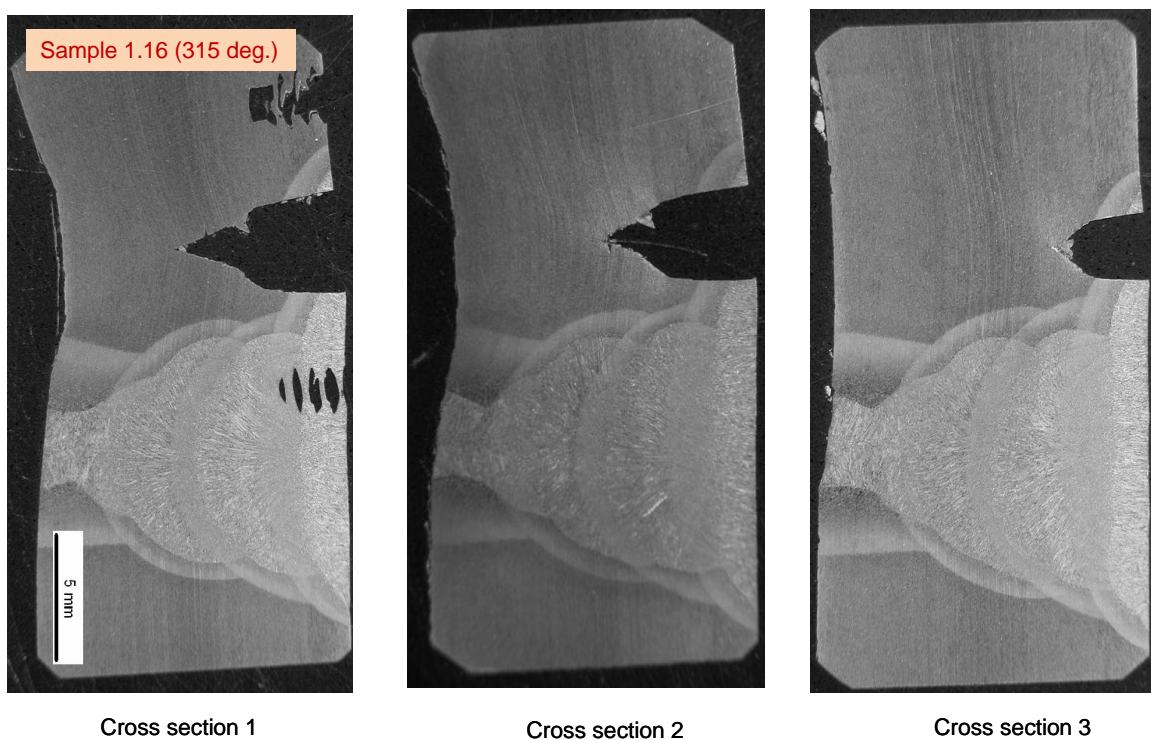


Figure 6.11 Multi-cross-sectional view of a flaw in HAZ

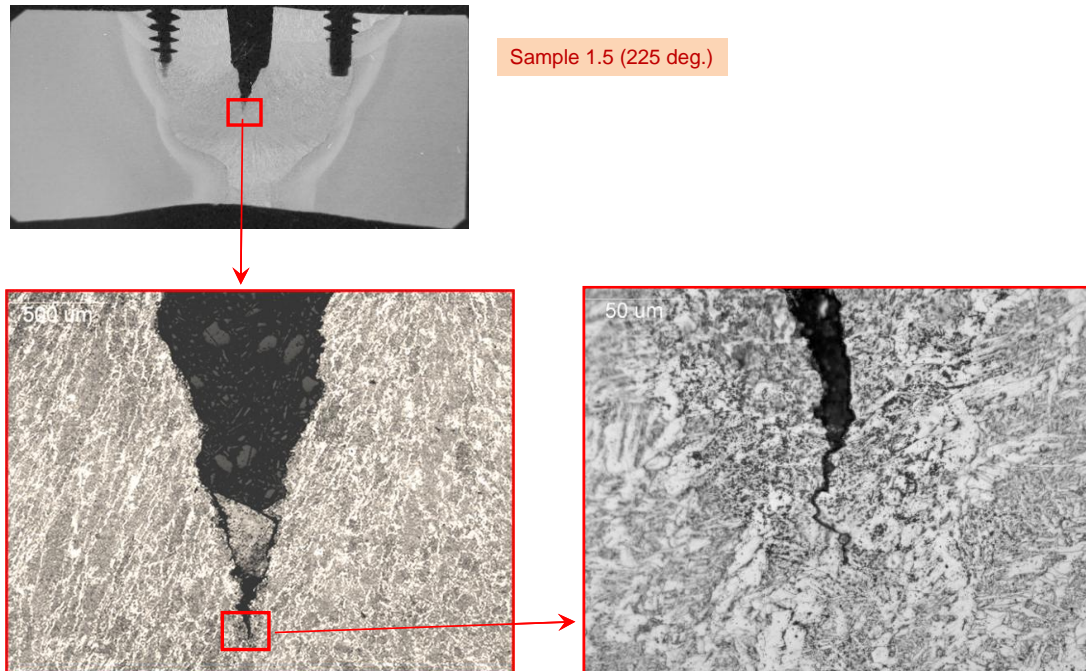


Figure 6.12 A cross-section of a weld flaw at different magnifications

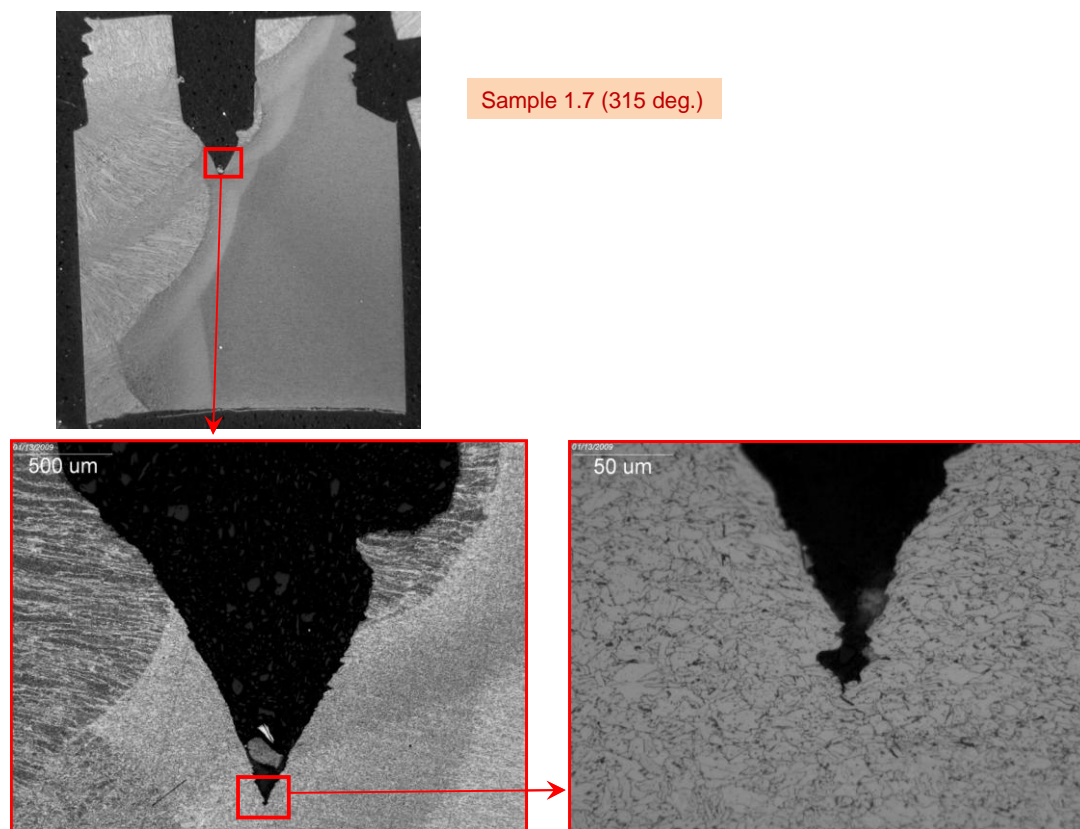


Figure 6.13 A cross-section of an HAZ flaw at different magnifications

Residual CMOD Profile

The residual CMOD (i.e., plastic CMOD) was measured along the length of flaw for all flaws as shown in Figure 6.14 to Figure 6.27.

The multiple flaws in a single test sample were meant to be “identical” under “controllable” conditions, including flaw location, flaw size, and flaw tip acuity. The residual CMOD of the same test sample reflects the variation of flaw behavior under those controllable conditions. In some minority cases, the residual CMOD profiles of the same sample are very close, such as Sample 1.19 and 1.20, both with weld flaws. In many other cases, the residual CMOD profiles are quite different. In many cases, the maximum CMOD among the different flaws can differ by a factor of almost 2. There is no obvious trend in the consistency of residual CMOD profiles between weld and HAZ flaws. In fact, two test specimens with flaws in the pipe body, Samples 1.1 and 1.2, also exhibit fairly large differences in the residual CMOD profile. For paired test specimens, one with internal pressure and the other without internal pressure, the sample without internal pressure typically has large residual CMOD, corresponding to the larger strain achieved for the samples without pressure.

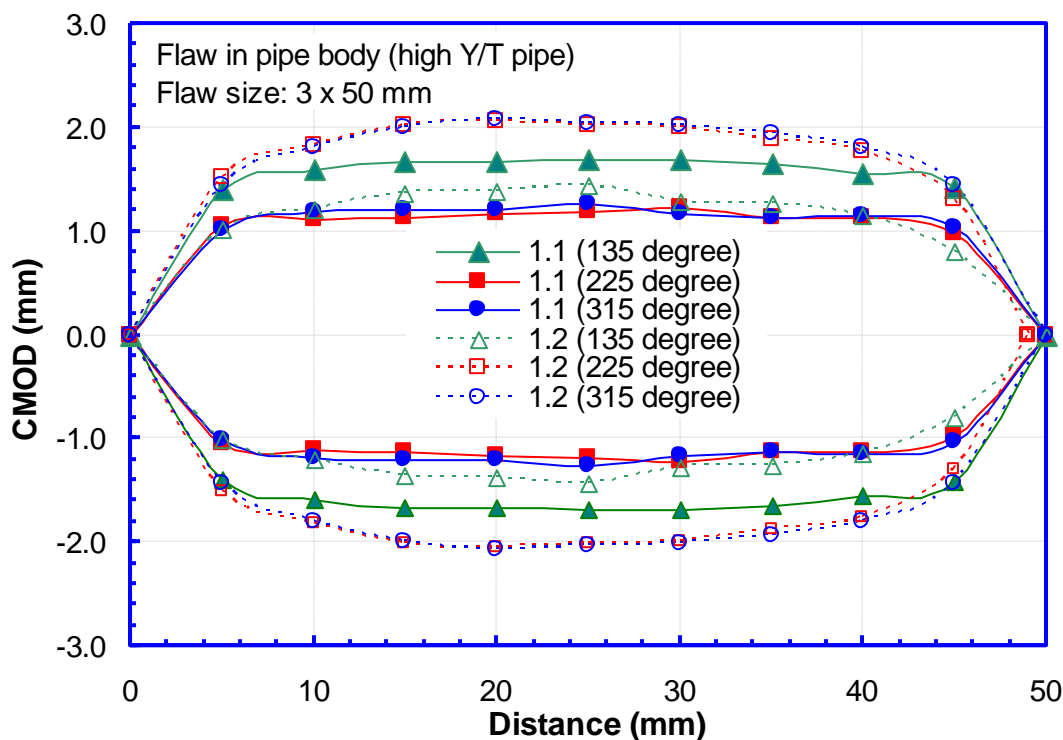


Figure 6.14 Residual CMOD profile of 12" high Y/T pipe with flaws in pipe body

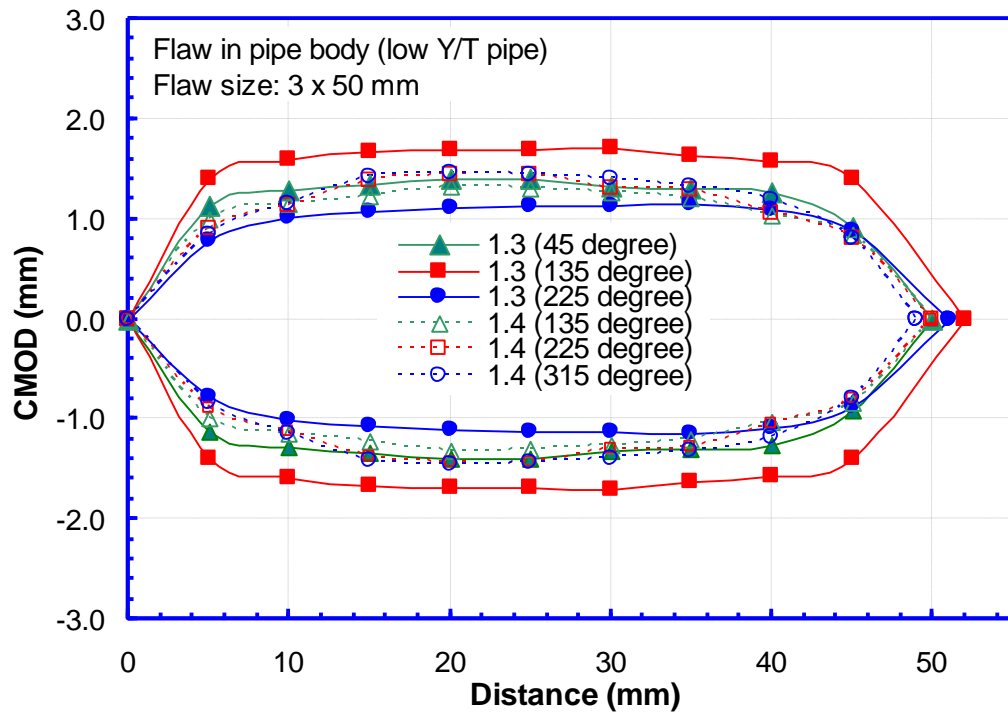
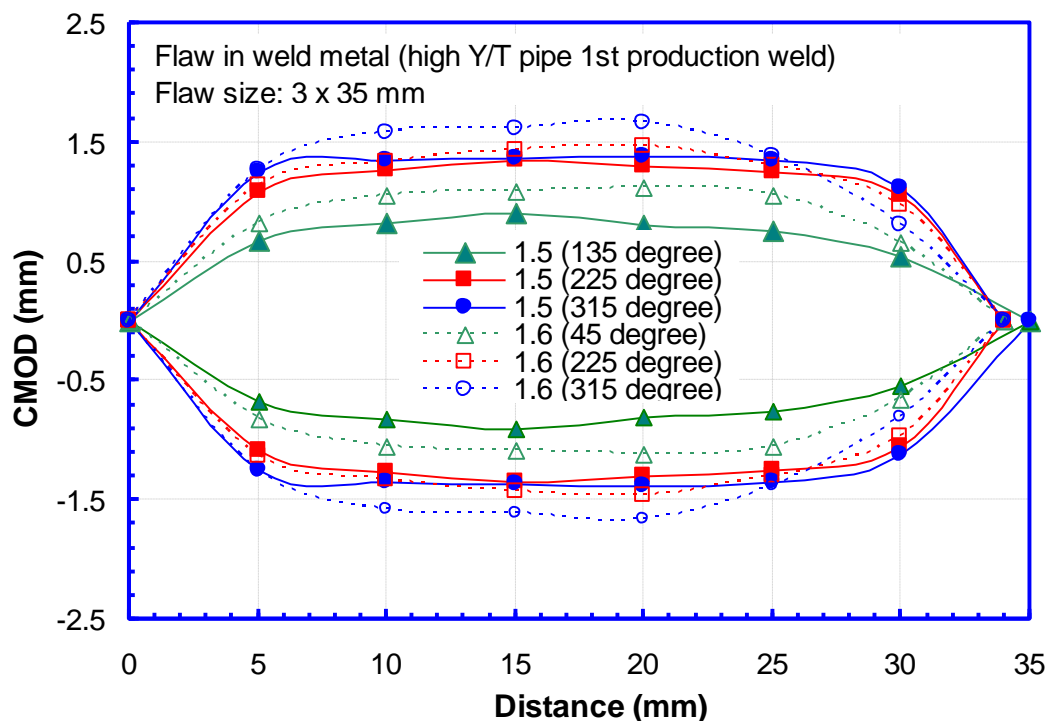
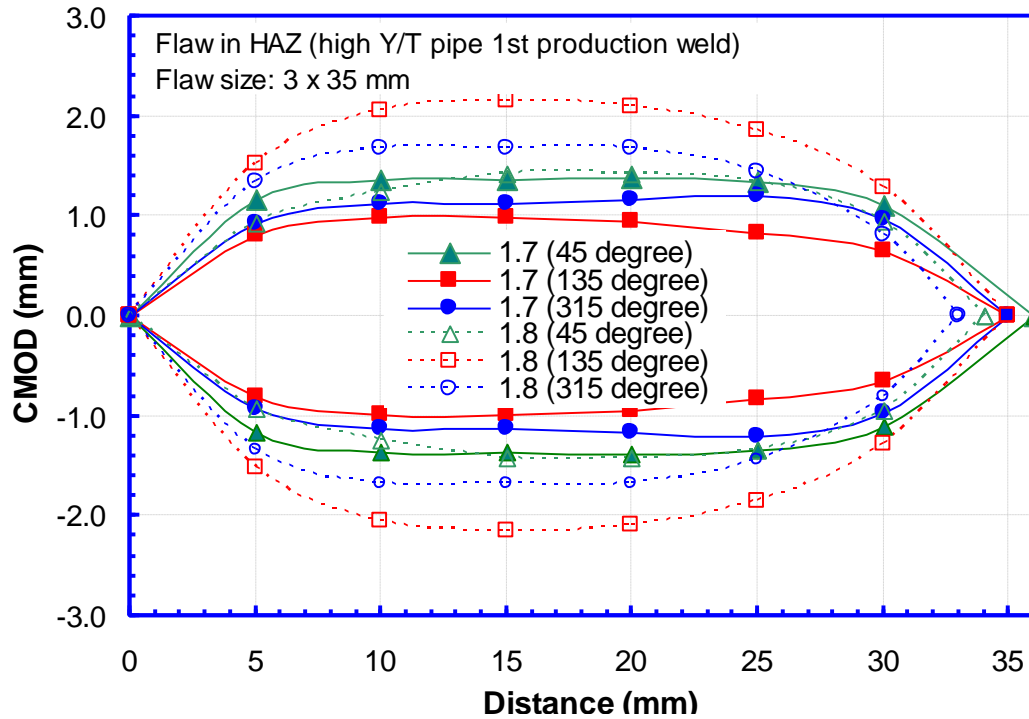
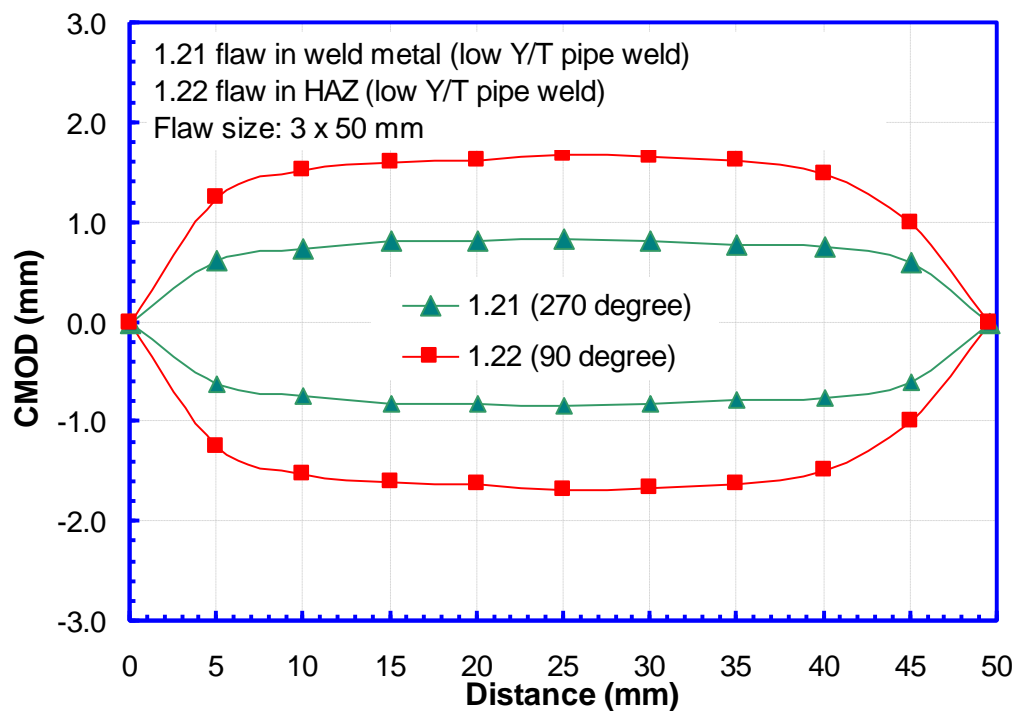


Figure 6.15 Residual CMOD profile of 12" low Y/T pipe with flaws in pipe body

Figure 6.16 Residual CMOD profile of 12" high Y/T pipe with flaws in the 1st production weld metal

Figure 6.17 Residual CMOD profile of 12" high Y/T pipe with flaws in the 1st production HAZFigure 6.18 Residual CMOD profile of 12" high Y/T pipe with flaws in the 1st production weld metal and HAZ

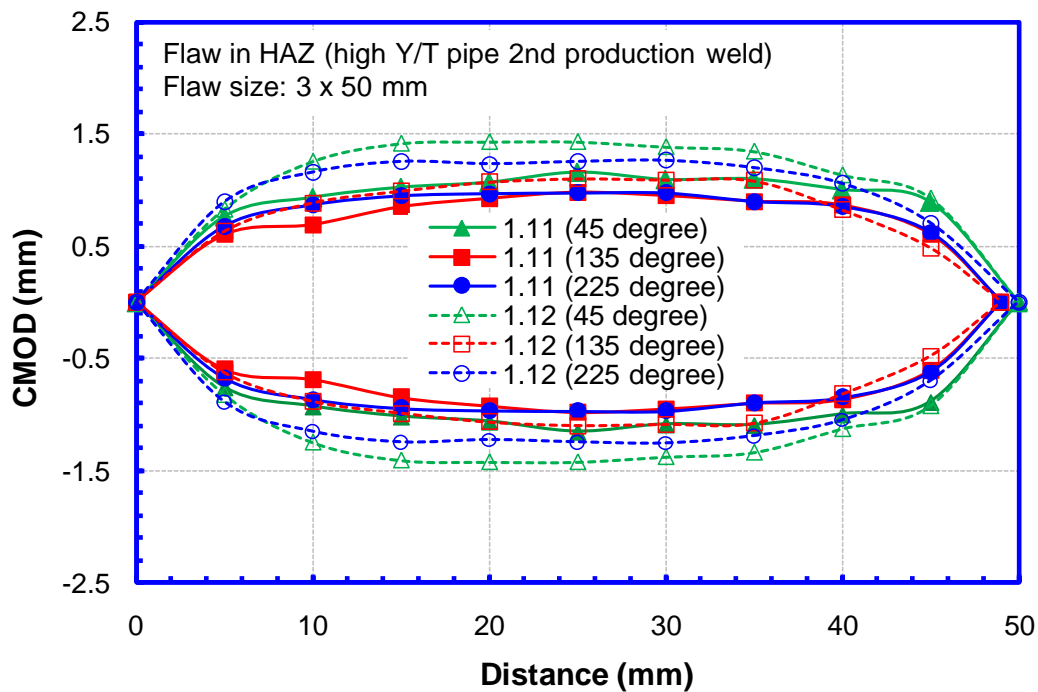


Figure 6.19 Residual CMOD profile of 12" high Y/T pipe with flaws in the 2nd production HAZ

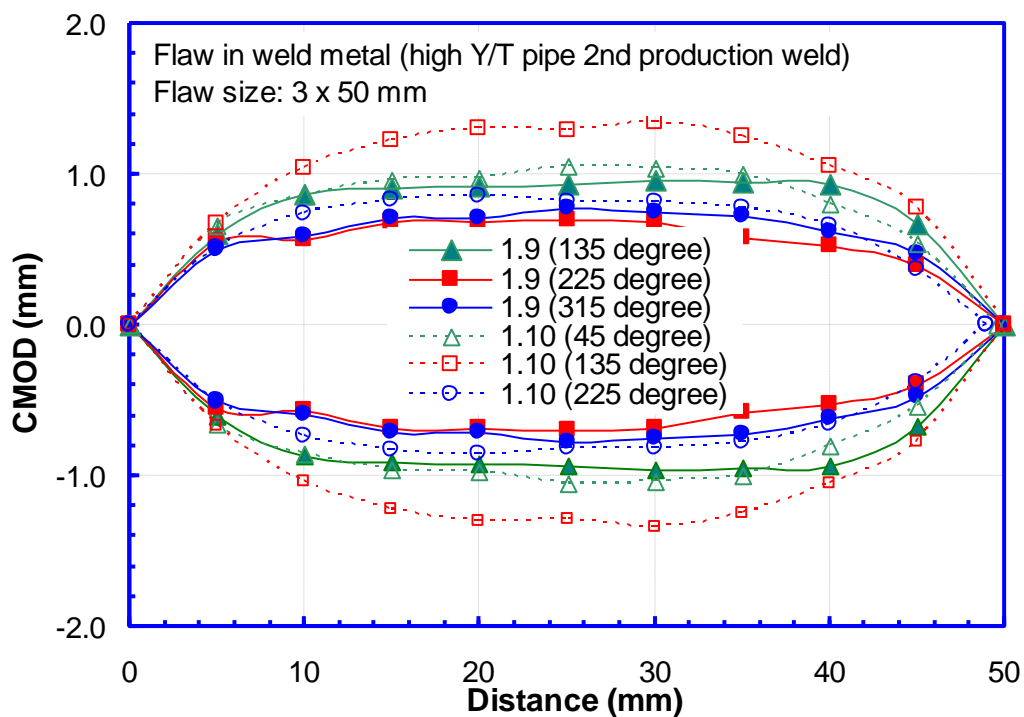


Figure 6.20 Residual CMOD profile of 12" high Y/T pipe with flaws in the 2nd production weld metal

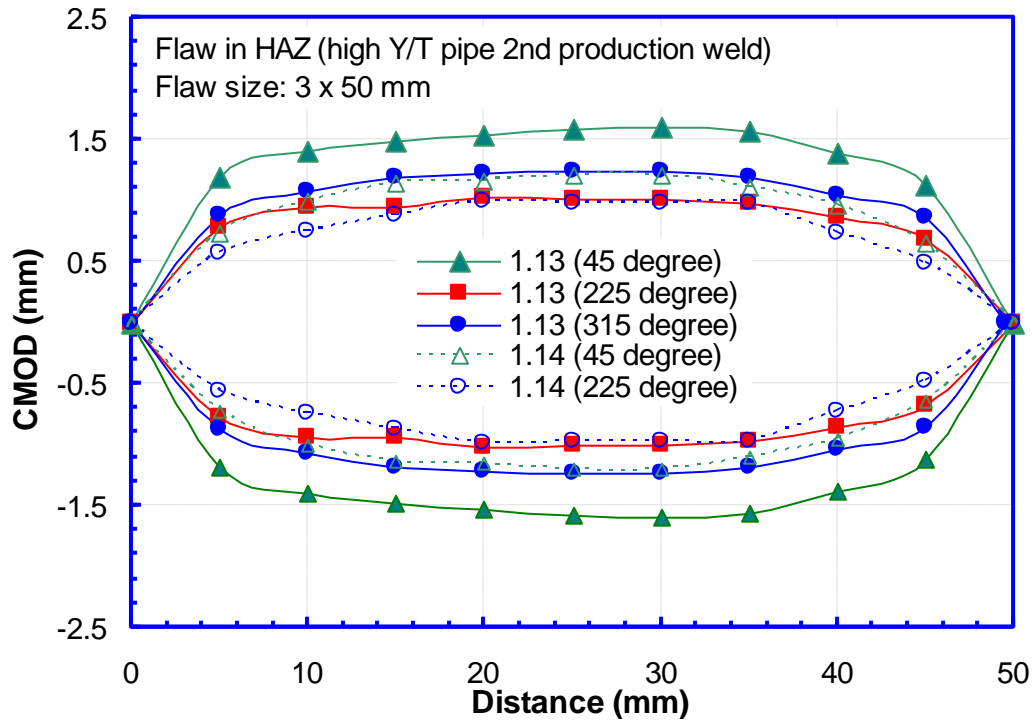


Figure 6.21 Residual CMOD profile of 12" high Y/T pipe with flaws in the 2nd production HAZ

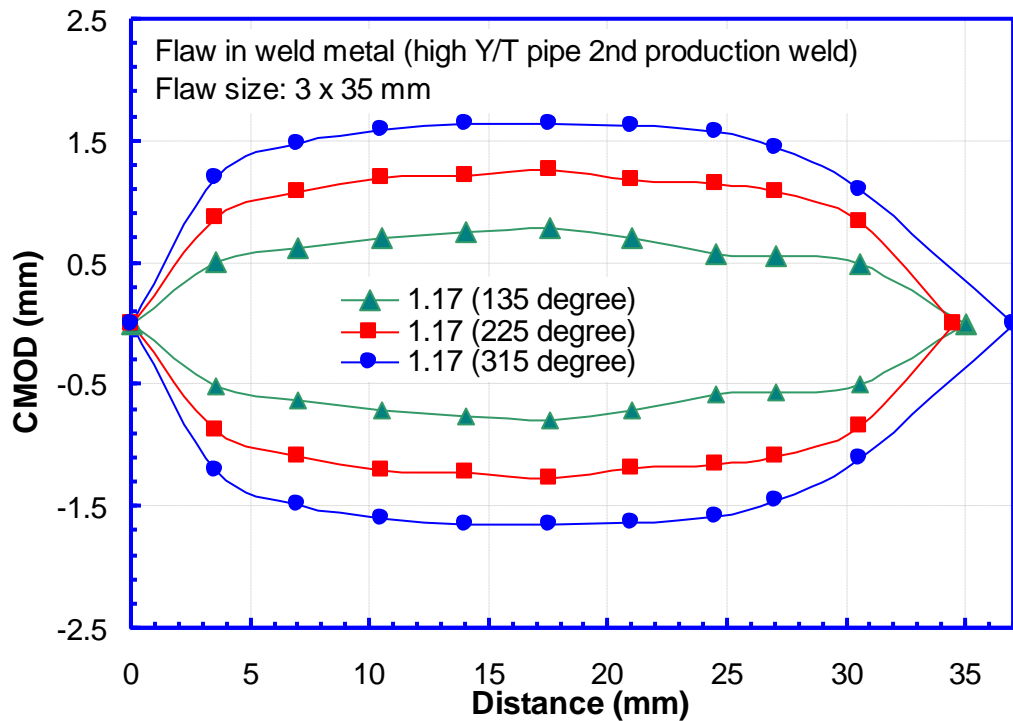


Figure 6.22 Residual CMOD profile of 12" high Y/T pipe with flaws in the 2nd production weld metal

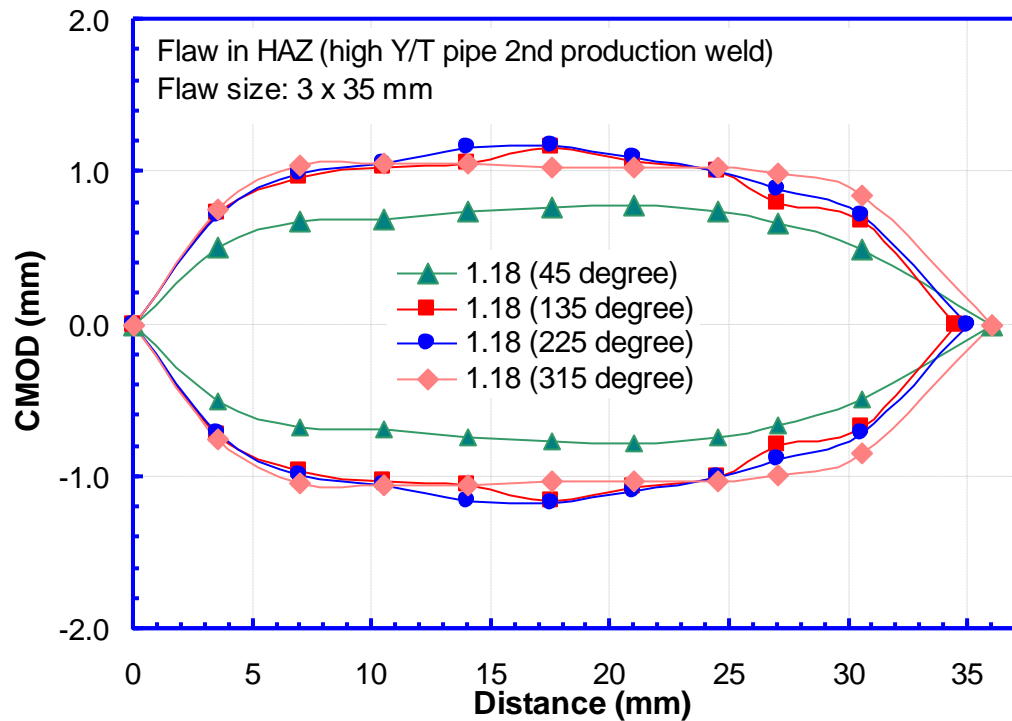


Figure 6.23 Residual CMOD profile of 12" high Y/T pipe with flaws in the 2nd production HAZ

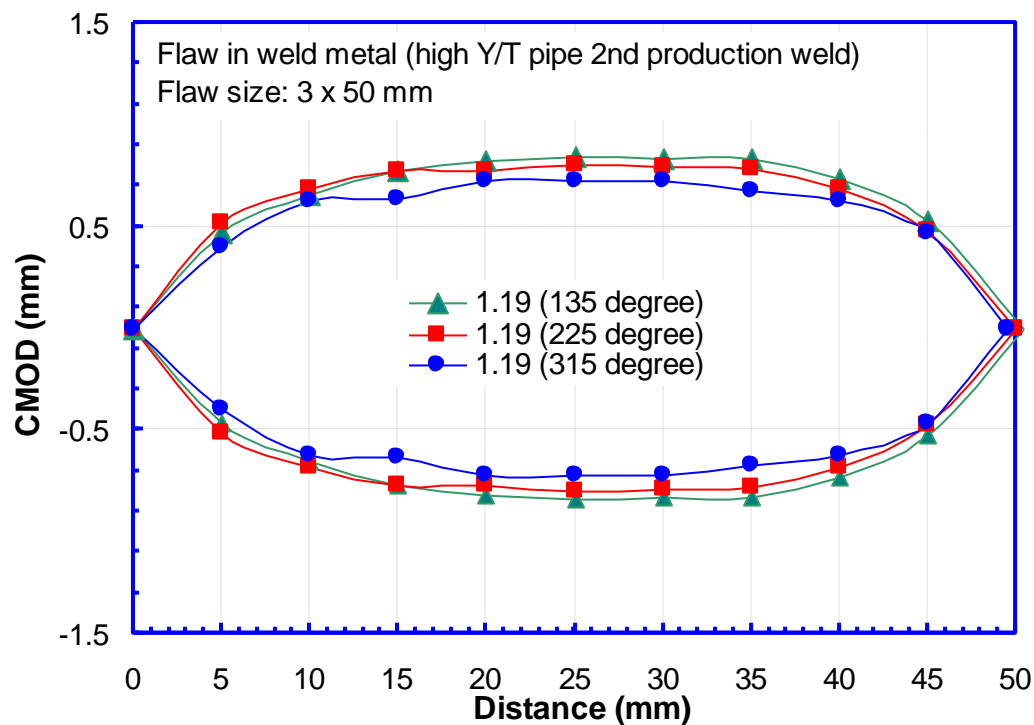


Figure 6.24 Residual CMOD profile of 12" high Y/T pipe with flaws in the 2nd production weld metal

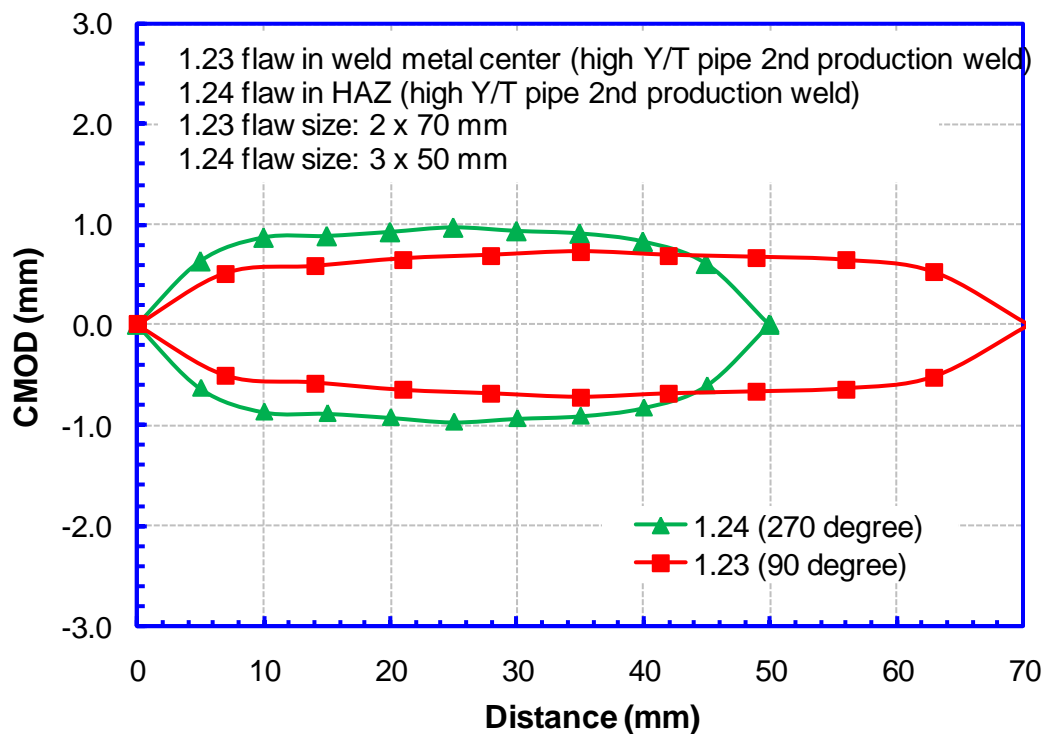


Figure 6.25 Residual CMOD profile of 12" high Y/T pipe with flaws in the 2nd production weld metal and HAZ

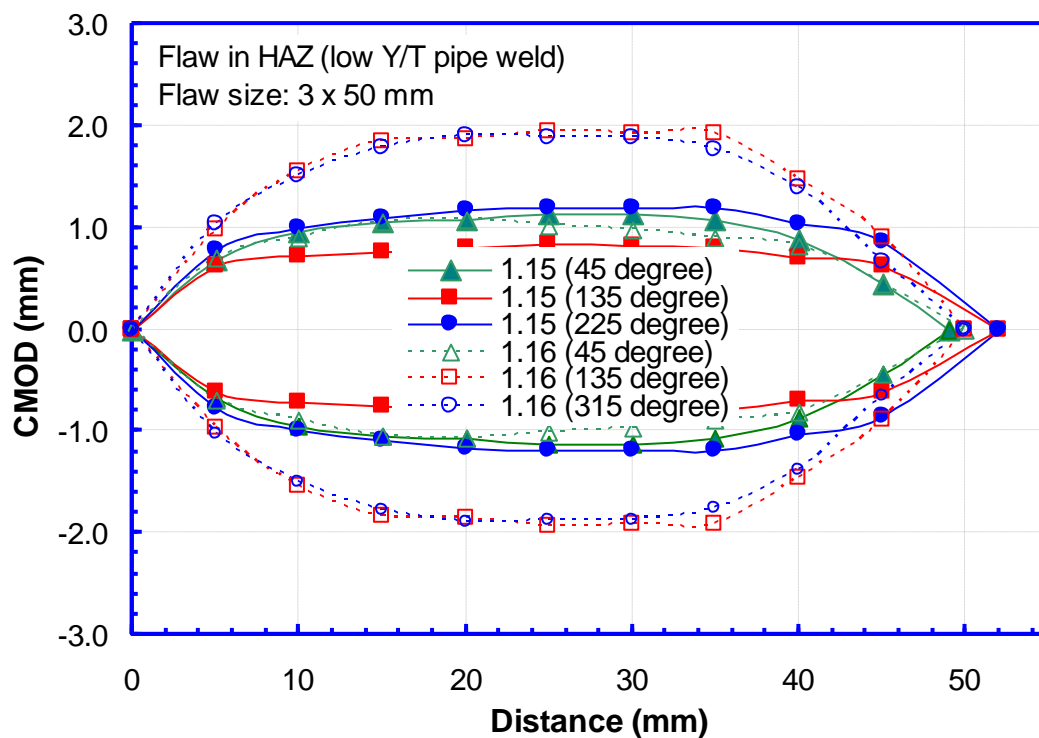


Figure 6.26 Residual CMOD profile of 12" low Y/T pipe with flaws in HAZ

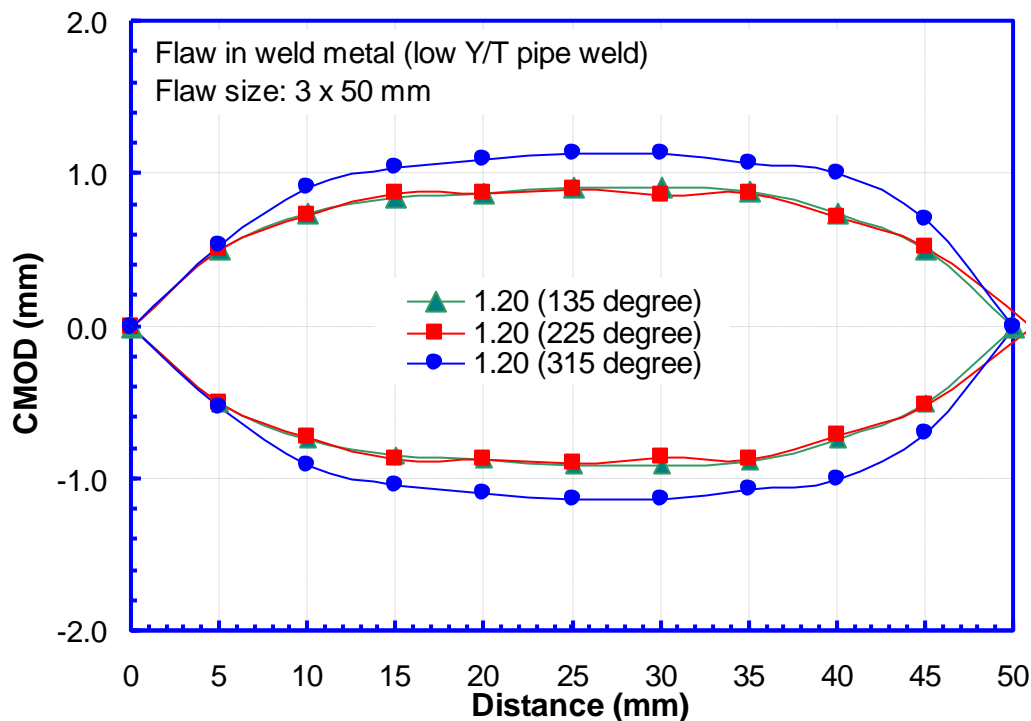


Figure 6.27 Residual CMOD profile of 12" low Y/T pipe with flaws in weld metal

6.3.2 Wall-Breaching Flaws

6.3.2.1 Procedure for Post-Test Flaw Examination

The preparation by C-FER of samples from the as-tested pipes involved the following steps:

1. Extract a small section of the material containing the wall-breaching flaw, with the perimeter being at least 1 inch from the flaw in all directions.
2. Immerse the section in liquid nitrogen and apply an impact force to break the section along the flaw plane to expose the fracture surface.
3. Following photography of the full-length fracture surface, reposition the two pieces and cut cross-wise to expose the weld and flaw cross section at mid length of the flaw.

6.3.2.2 Results of Post-Test Examination

The residual flaw opening profile of each wall-breaching flaw was photographed and measured. The associated residual CMOD profiles are shown in Figure 6.28 through Figure 6.40. Photographs of the opening profile, fracture surface, and mid-length flaw cross section of each wall-breaching flaw form part of the test data sheets provided in Appendix 5A.

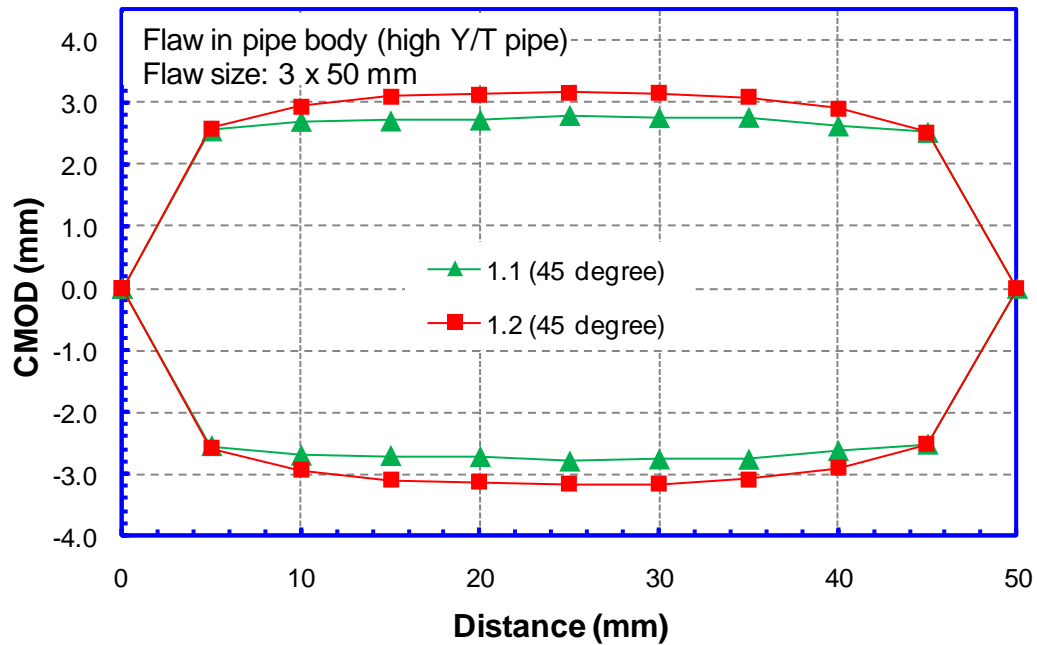


Figure 6.28 Residual CMOD profile of 12" high Y/T pipe with flaws in pipe body

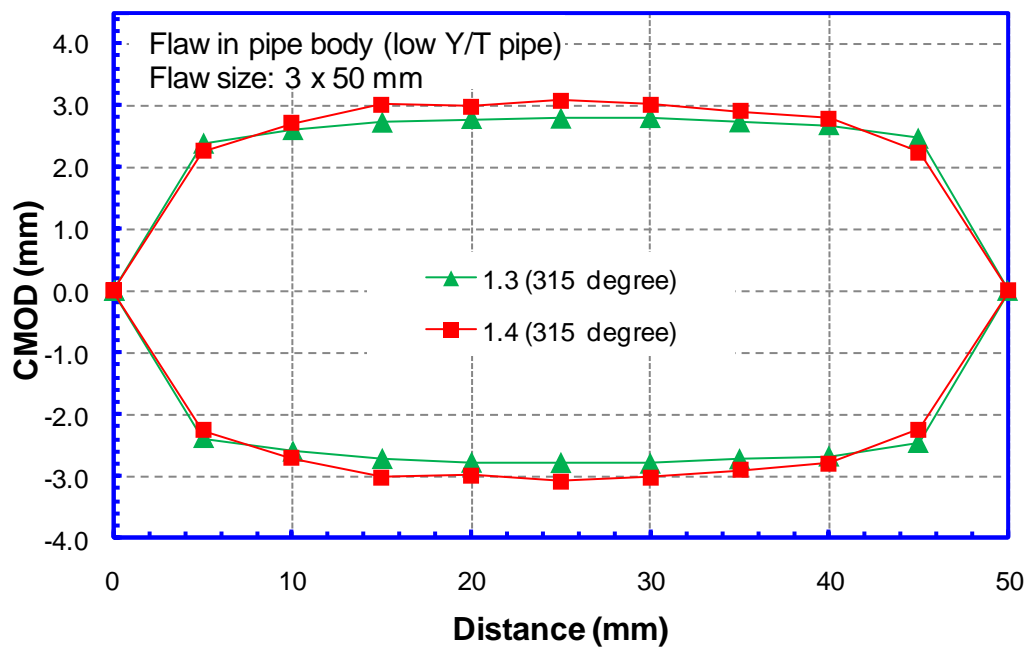


Figure 6.29 Residual CMOD profile of 12" low Y/T pipe with flaws in pipe body

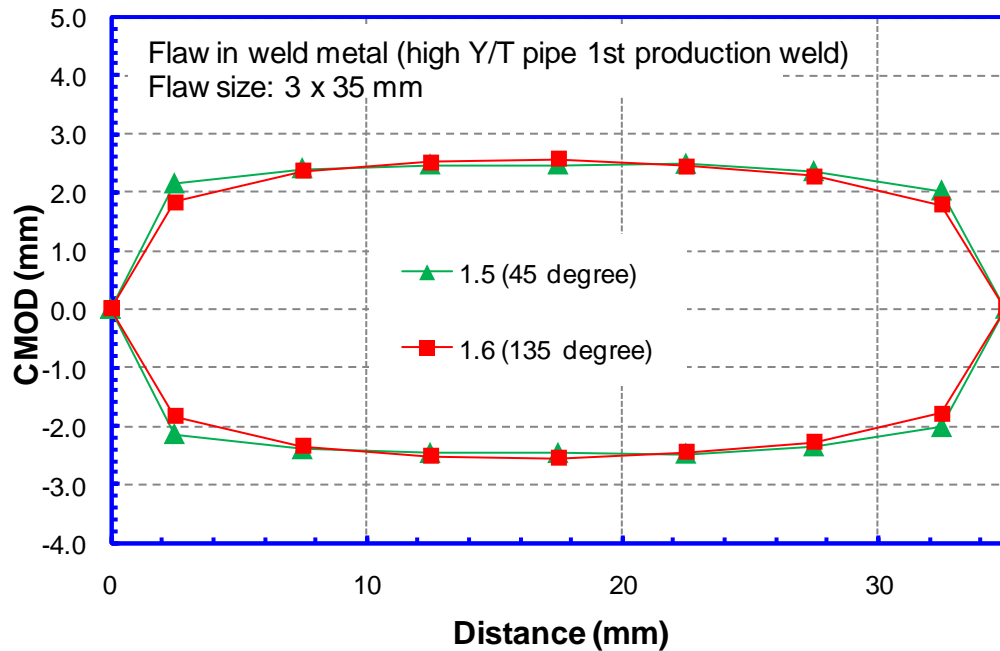


Figure 6.30 Residual CMOD profile of 12" high Y/T pipe with flaws in the 1st production weld metal

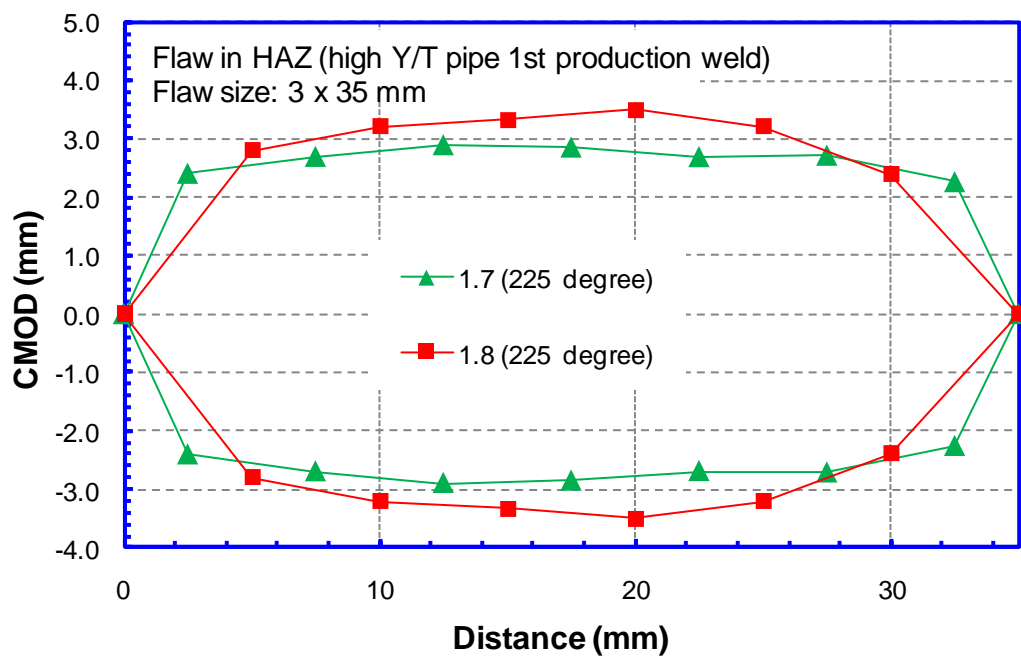


Figure 6.31 Residual CMOD profile of 12" high Y/T pipe with flaws in the 1st production HAZ

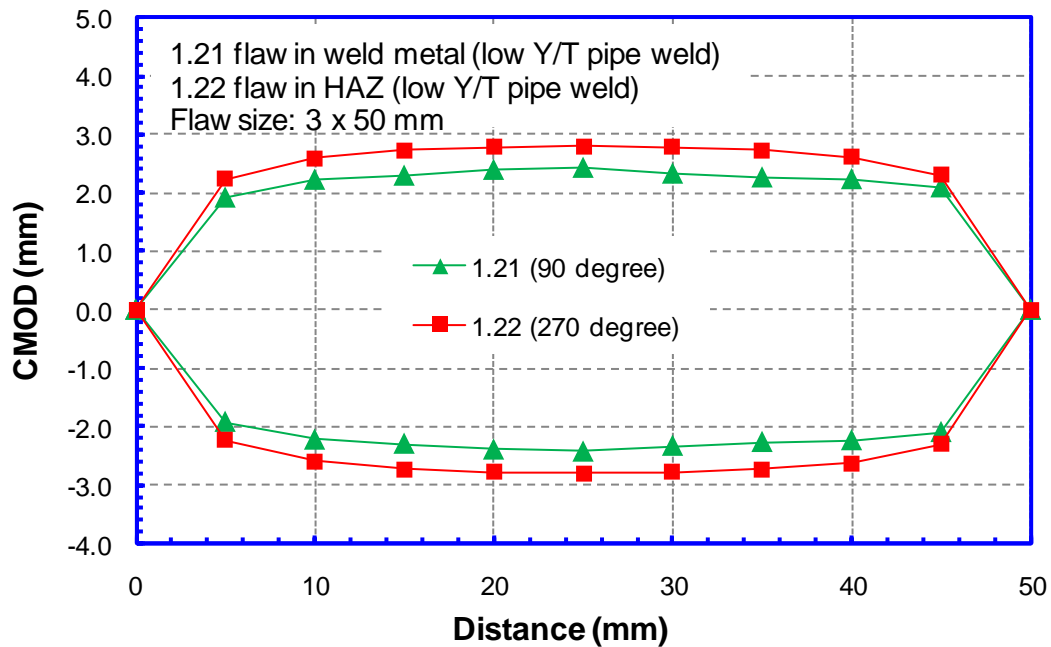


Figure 6.32 Residual CMOD profile of 12" high Y/T pipe with flaws in the 1st production weld metal and HAZ

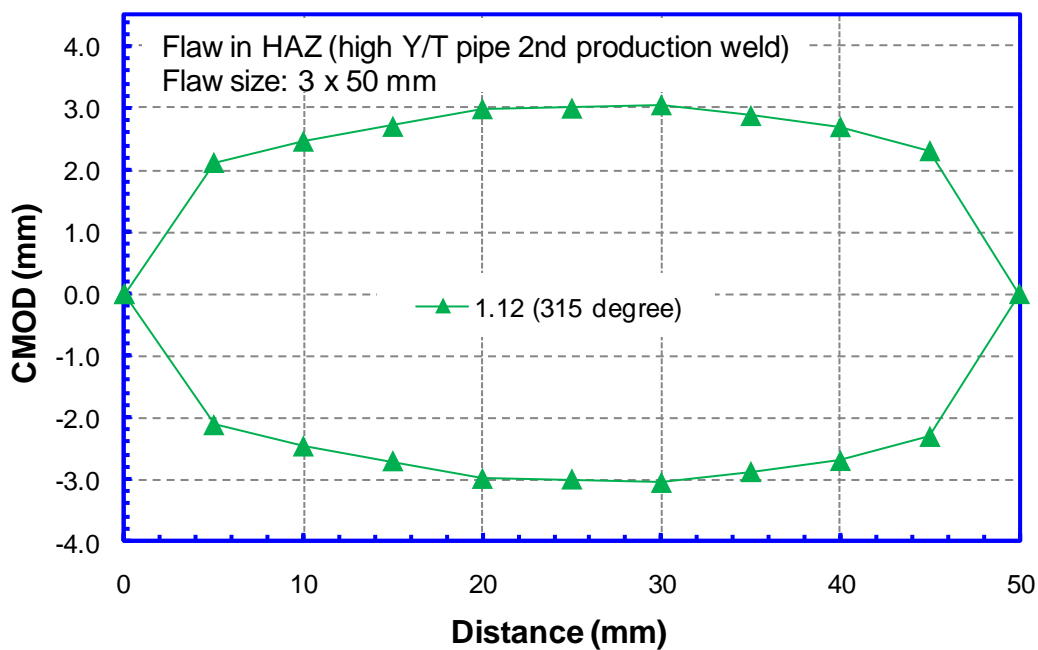


Figure 6.33 Residual CMOD profile of 12" high Y/T pipe with flaws in the 2nd production HAZ

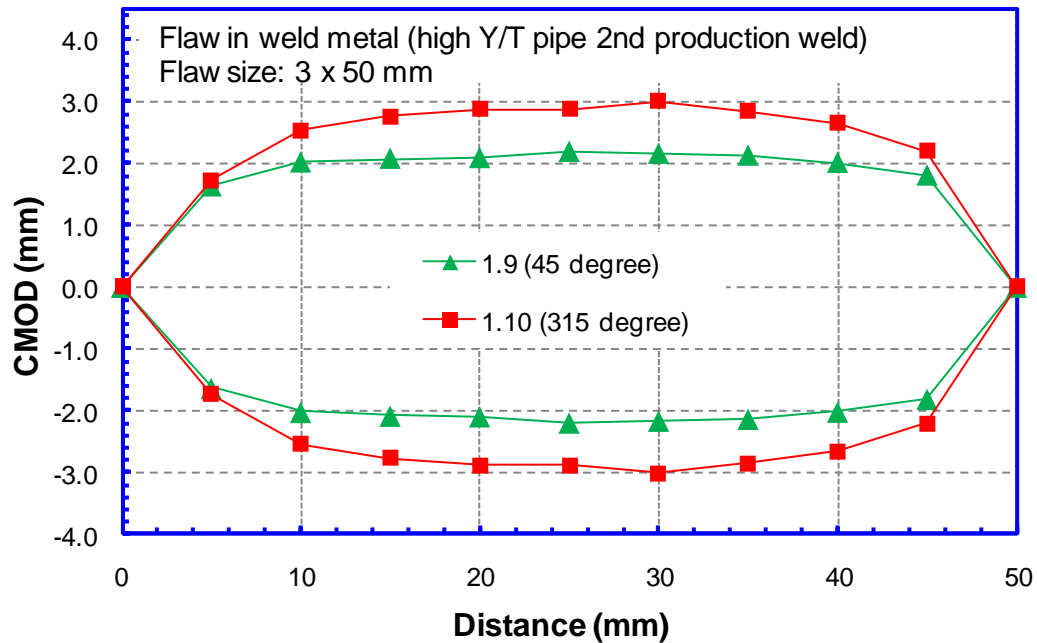


Figure 6.34 Residual CMOD profile of 12" high Y/T pipe with flaws in the 2nd production weld metal

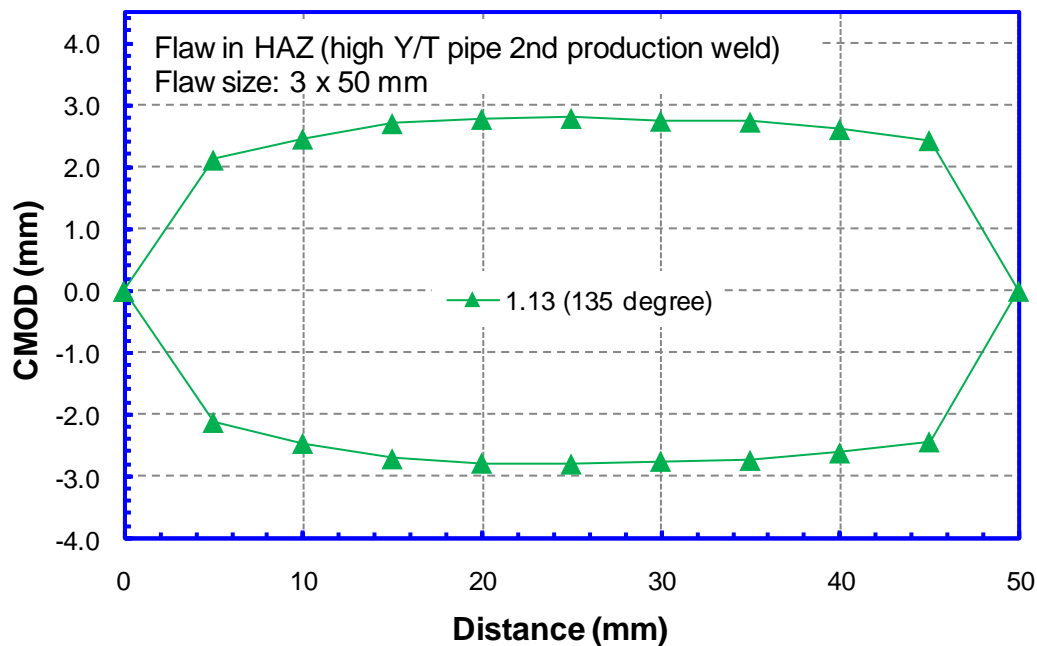


Figure 6.35 Residual CMOD profile of 12" high Y/T pipe with flaws in the 2nd production HAZ

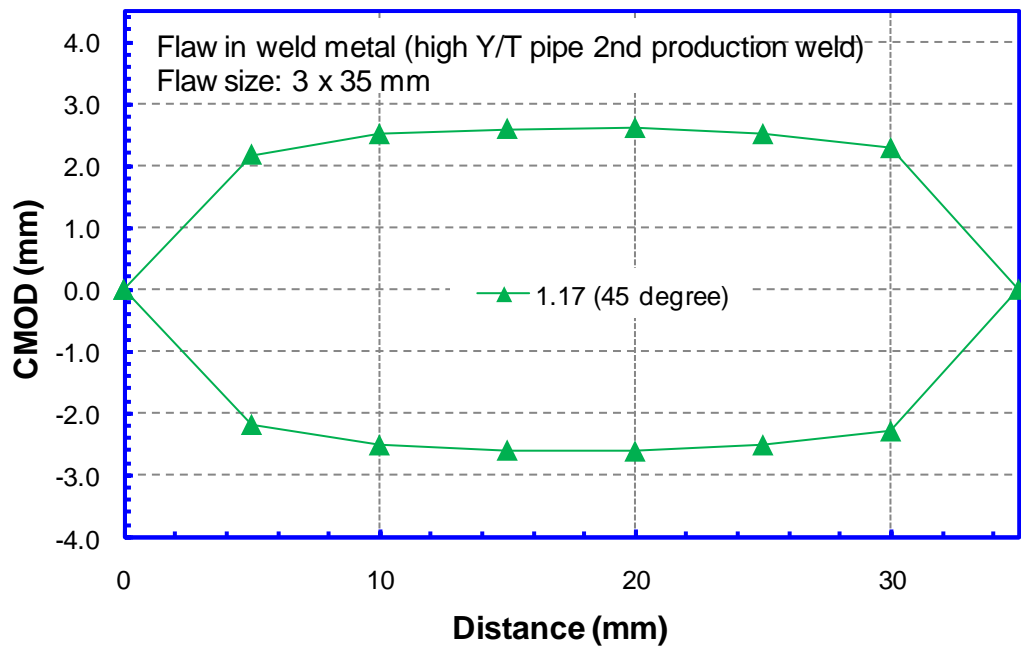


Figure 6.36 Residual CMOD profile of 12" high Y/T pipe with flaws in the 2nd production weld metal

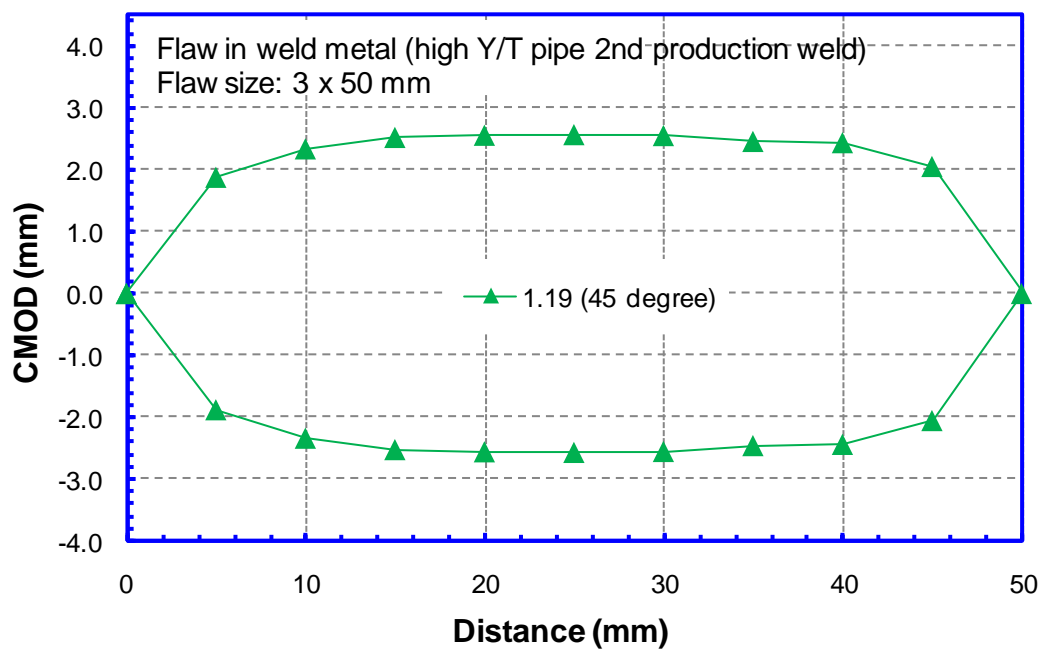


Figure 6.37 Residual CMOD profile of 12" high Y/T pipe with flaws in the 2nd production weld metal

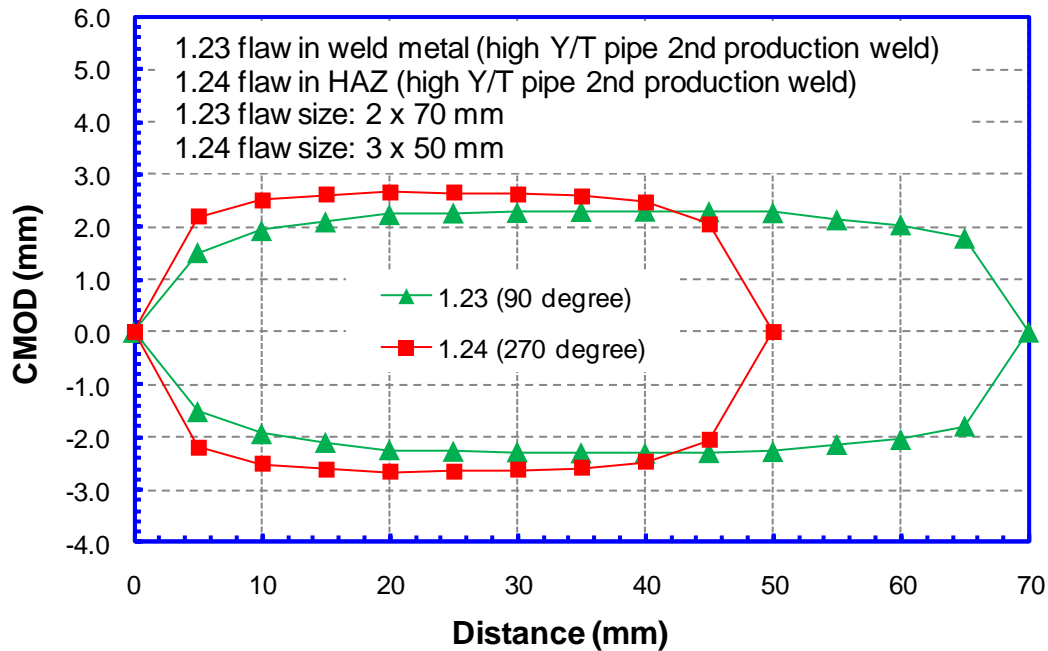


Figure 6.38 Residual CMOD profile of 12" high Y/T pipe with flaws in the 2nd production weld metal and HAZ

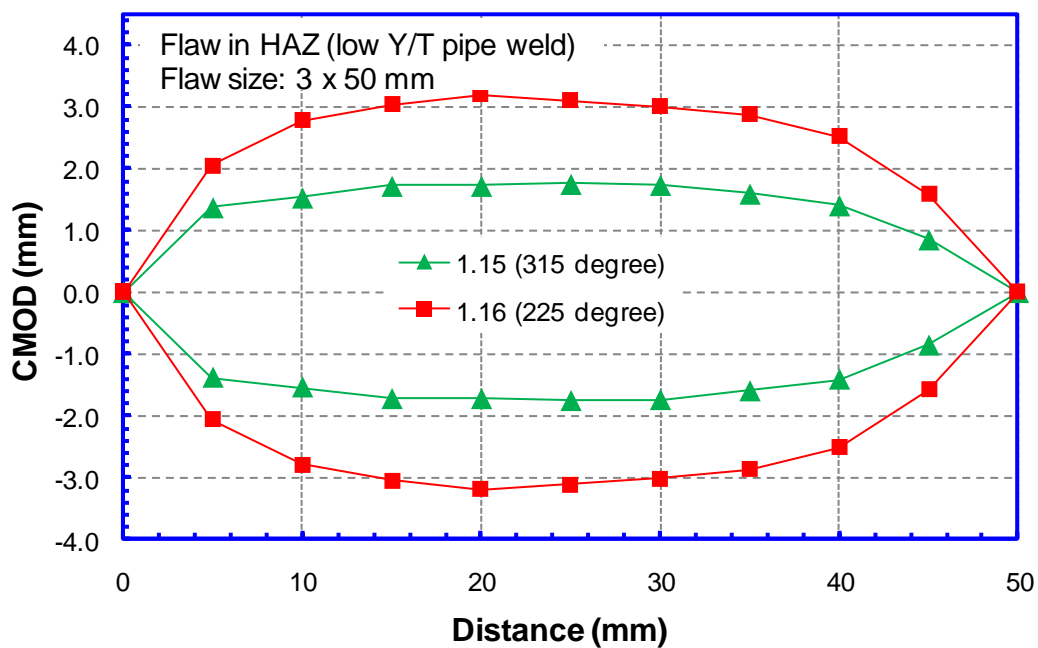


Figure 6.39 Residual CMOD profile of 12" low Y/T pipe with flaws in HAZ

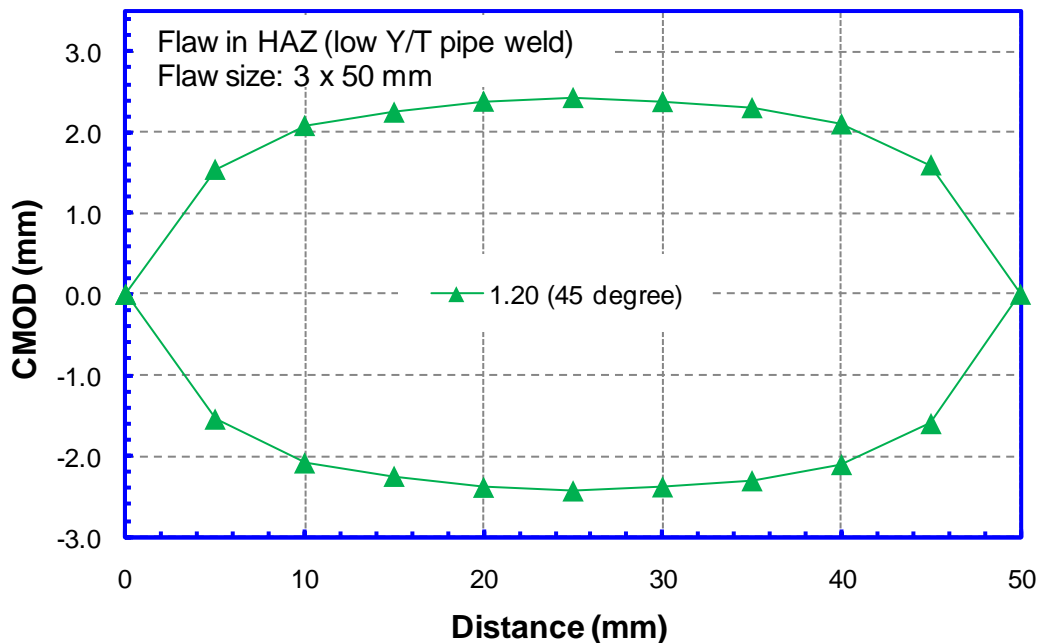


Figure 6.40 Residual CMOD profile of 12" low Y/T pipe with flaws in weld metal

6.4 Summary of Post-Test Examination Results and Observations

The maximum residual CMOD and flaw growth for all flaws examined by CRES are given in Table 6.2. Some general observations are given below.

- (1) For a majority of the test specimens, there are significant variations in the behavior of nominally "identical" flaws subjected to identical loading conditions. These variations are clearly demonstrated by the differences in the residual CMOD, the amount of flaw growth at test termination, and the cross-sectional views of the flaws. Only in isolated cases did "identical" flaws exhibit similar behavior.
- (2) Due to the unsymmetrical and variable nature of the weld profile and variations in weld cap width, the placement of notches in the HAZ can pose considerable challenges if the frame of reference is a single weld profile in combination with the outer extent of the weld cap. The cross-sectional views of the flaws showed that the HAZ notches landed in their intended zone in some cases, but they landed in either the edge of the weld metal or outside the fusion boundary in other cases.
- (3) All other conditions being nominally the same, specimens subjected to internal pressure have smaller residual CMOD values than specimens not subjected to internal pressure. The specimens with internal pressure failed at a lower remote strain, and thus imposed less deformation in the flawed area than specimens without pressure.

Table 6.2 Summary of maximum residual CMOD and flaw growth

Case No.	Pipe Material	Weld	Test No.	Pressure (%SMYS)	Flaw Size (mm x mm)	Flaw Location	Maximum Residual CMOD (mm)						Maximum Flaw Growth (mm)					
							45 deg.	90 deg.	135 deg.	225 deg.	270 deg.	315 deg.	45 deg.	90 deg.	135 deg.	225 deg.	270 deg.	315 deg.
1	High Y/T	N/A	1.1	80	3 x 50	Pipe	5.6	N/A	3.4	2.4	N/A	2.5	Fail	N/A	2.5	1.0	N/A	1.3
2			1.2	0	3 x 50	Pipe	6.4	N/A	2.9	4.1	N/A	4.1	Fail	N/A	1.4	2.6	N/A	2.6
3	Low Y/T	N/A	1.3	80	3 x 50	Pipe	2.8	N/A	3.4	2.3	N/A	5.6	1.6	N/A	2.8	1.3	N/A	Fail
4			1.4	0	3 x 50	Pipe	6.2	N/A	2.6	2.9	N/A	2.9	Fail	N/A	1.5	1.1	N/A	1.7
5	High Y/T	First Production	1.5	80	3 x 35	WM	5.0	N/A	1.8	2.7	N/A	2.8	Fail	N/A	0.9	2.1	N/A	2.0
6			1.6	0	3 x 35	WM	2.2	N/A	5.1	2.9	N/A	3.3	1.5	N/A	Fail	1.4	N/A	1.1
7			1.7	80	3 x 35	HAZ	2.8	N/A	2.0	5.8	N/A	2.4	1.0	N/A	0.7	Fail	N/A	1.5
8			1.8	0	3 x 35	HAZ	2.9	N/A	4.3	7.0	N/A	3.4	2.2	N/A	2.6	Fail	N/A	1.8
9			1.21	80	3 x 50	WM	N/A	4.9	N/A	N/A	1.7	N/A	N/A	Fail	N/A	N/A	0.9	N/A
10			1.22	80	3 x 50	HAZ	N/A	3.4	N/A	N/A	5.6	N/A	N/A	2.0	N/A	N/A	Fail	N/A
11	High Y/T	Second Production	1.11	80	3 x 50	HAZ	2.3	N/A	2.0	1.9	N/A	Fail ¹	1.0	N/A	0.6	0.9	N/A	Fail
12			1.12	0	3 x 50	HAZ	2.9	N/A	2.2	2.5	N/A	6.1	1.7	N/A	0.7	1.2	N/A	Fail
13			1.9	80	3 x 50	WM	4.4	N/A	1.9	1.4	N/A	1.5	Fail	N/A	2.0	0.8	N/A	0.7
14			1.10	0	3 x 50	WM	2.1	N/A	2.7	1.7	N/A	6.0	1.7	N/A	2.1	0.8	N/A	Fail
15			1.13	80	3 x 50	HAZ	3.2	N/A	5.6	2.1	N/A	2.5	2.3	N/A	Fail	1.0	N/A	1.3
16			1.14	0	3 x 50	HAZ	2.4	N/A	Fail ²	2.0	N/A	Fail ²	1.2	N/A	Fail	0.9	N/A	Fail
17			1.17	80	3 x 35	WM	5.2	N/A	1.6	2.5	N/A	3.3	Fail	N/A	0.6	2.1	N/A	3.5
18			1.18	80	3 x 35	HAZ	1.6	N/A	2.3	2.4	N/A	2.1	0.5	N/A	1.0	1.1	N/A	1.1
19			1.19	80	3 x 50	WM	4.6	N/A	1.7	1.6	N/A	1.5	Fail	N/A	0.8	0.9	N/A	0.4
20			1.23	80	2 x 70	WM	N/A	4.6	N/A	N/A	1.5	N/A	N/A	Fail	N/A	N/A	0.5	N/A
21			1.24	80	3 x 50	HAZ	N/A	1.9	N/A	N/A	5.3	N/A	N/A	0.5	N/A	N/A	Fail	N/A
22	Low Y/T		1.15	80	3 x 50	HAZ	2.3	N/A	1.7	2.4	N/A	3.5	0.9	N/A	0.9	0.7	N/A	Fail
23			1.16	0	3 x 50	HAZ	2.1	N/A	3.9	6.4	N/A	3.8	0.5	N/A	2.7	Fail	N/A	2.2
24			1.20	80	3 x 50	WM	4.9	N/A	1.8	1.8	N/A	2.3	Fail	N/A	1.1	1.3	N/A	1.8

1. Failed flaw re-welded in anticipation of re-test. Re-test not carried out.

2. Test ended with full circumferential failure of weld containing failed flaw.

6.5 Appendix 6A

Appendix 6A is given in separate electronic files in a self-contained folder named “Appendix_6A”. The appendix contains detailed post-test analysis data of all flaws that did not breach the pipe wall during tests. All individual data files are located in the subfolder named “Data”. The structure and access of the data files are described in the file named

“FinalReport_ABD1_Project1_Appendix6A.doc” in the “Appendix_6A” folder. All data files must reside in the “Data” subfolder.



7 Post-Test Data Summary and Correlation

7.1 Objectives and Work Scope

FEA were conducted for all CWP and FSP tests using the test parameters to examine the test results. The main objectives of the post-test analysis are to understand the general trend of the material response, provide necessary inputs, and give directions for the development of the 2nd generation model.

The features of the experiment data, including the variations in small-scale and large-scale tests, were reviewed first. The basic inputs to the FEA and the general results of the FEA were then summarized. The main test parameters which can affect the test and simulation results were discussed. Finally, the causes for the difference between the FEA and test results were examined.

7.2 Variation of Test Results under “Identical” Conditions

7.2.1 Load vs. Remote Strain

The relationship between the nominal stress and remote strain obtained from two identical CWP tests are shown in Figure 7.1. The nominal stress-remote strain curves of the two specimens are almost identical prior to the peak stress. The variation of those two curves is much less than the general variation of the stress-strain curves observed from the small-scale testing. However, the strain limits, as defined by the strain values at the peak stresses, differed by as much as 50% (4.36% and 6.6%, respectively). These test results highlighted the possibility of large variations in the strain limits for materials with essentially very flat stress-strain curves, even when the materials behave almost identically.

7.2.2 CMOD versus Remote Strain

Figure 7.2 shows the measured CMOD vs. remote strain relations from two pressurized FSP tests of the X65 high Y/T pipe with overmatched weld. The flaw sizes are 3 mm × 50 mm (depth × length) and located in HAZ. In Figure 7.2(a), the pipe was tested under room temperature. In Figure 7.2(b), the pipe was tested at -20°C. In each pipe, four identical defects were made and the CMOD of each of the four defects were recorded. It can be seen in Figure 7.2(a) that the CMOD curves of the four identical defects differ significantly. The four CMOD curves in Figure 7.2(b) have much less scatter. The comparison of those two tests demonstrates that a high variability in flaw response is possible even when the welding condition and testing procedures are highly controlled in an attempt to produce “identical” properties.

7.3 Stress-Strain Curves Used in FEA

As discussed in the previous sections, the stress-strain curves measured from small-scale tests all showed certain degrees of variation. As an example, Figure 7.3 shows the upper and lower bound of the measured stress-strain curves for the X65 high Y/T pipe material and its welds. The pipe and weld stress-strain curves are paired to demonstrate the highest and lowest weld strength

mismatch. The weld strength mismatch levels are summarized in Table 7.1. The degree of variations depends on the number of tests and the variation increases as the number of tests increases. For instance, only two tests were conducted for the overmatched weld of the X65 high Y/T material and the two tests showed almost identical results. Therefore, the upper and lower bound of the overmatched weld was shown as the same curve (see Figure 7.3(b)). The stress-strain curve is expected to have a greater degree of variations if more tests are done.

The median stress-strain curves of all pipe and weld materials are also determined. The paired median stress-strain curves of pipe and weld are used in the FEA to simulate all test data. Some selected tests were analyzed with the paired stress-strain curves, which give the highest and lowest overmatch, to study the effect of material property variation.

Table 7.1 Weld overmatch variations of X65 high Y/T pipe

X65 (High Y/T)	WM Overmatch by $YS_{0.5\%}$			WM Overmatch by UTS		
	Min	Median	Max	Min	Median	Max
WM Evenmatch	-10%	-2%	6%	-2%	5%	9%
WM Overmatch 10%	5%	9%	16%	12%	15%	18%

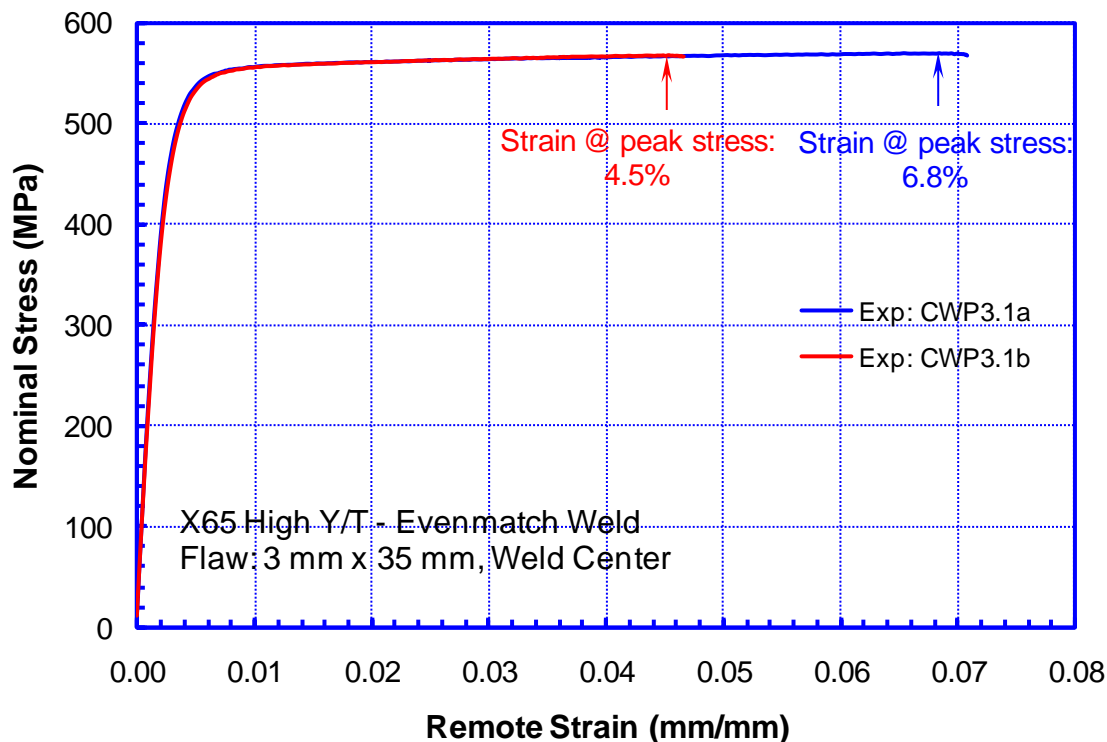


Figure 7.1 Stress-remote strain relations of two identical CWP tests

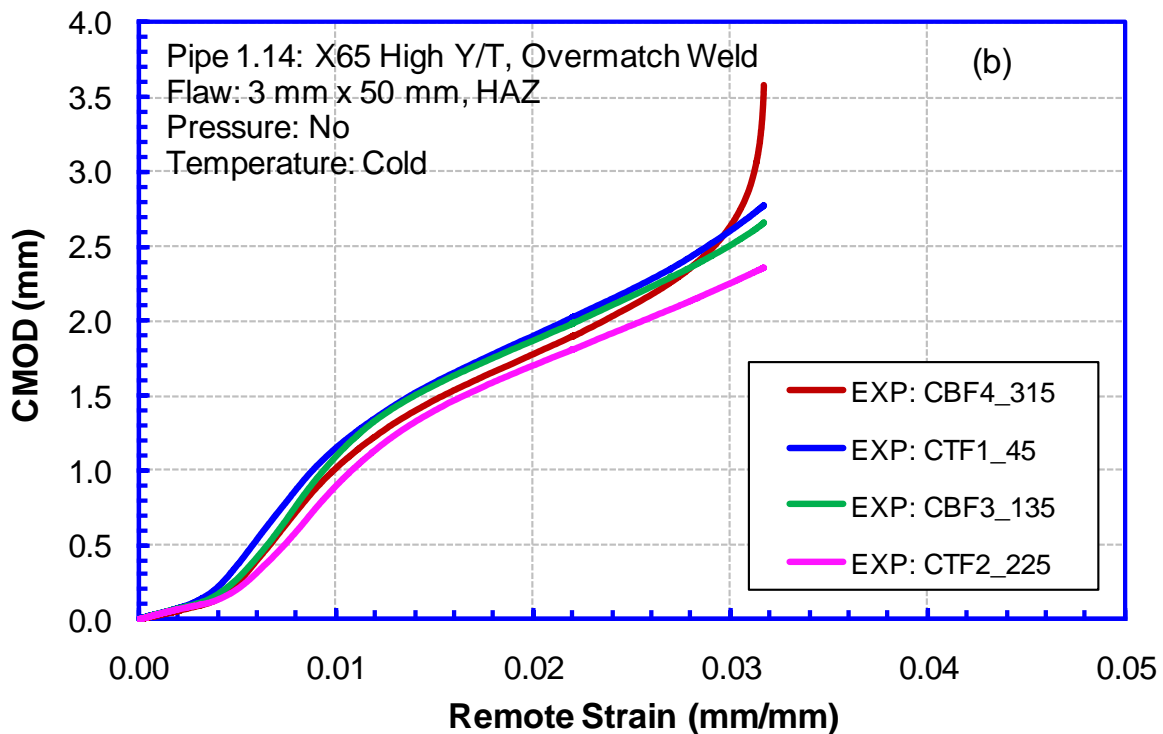
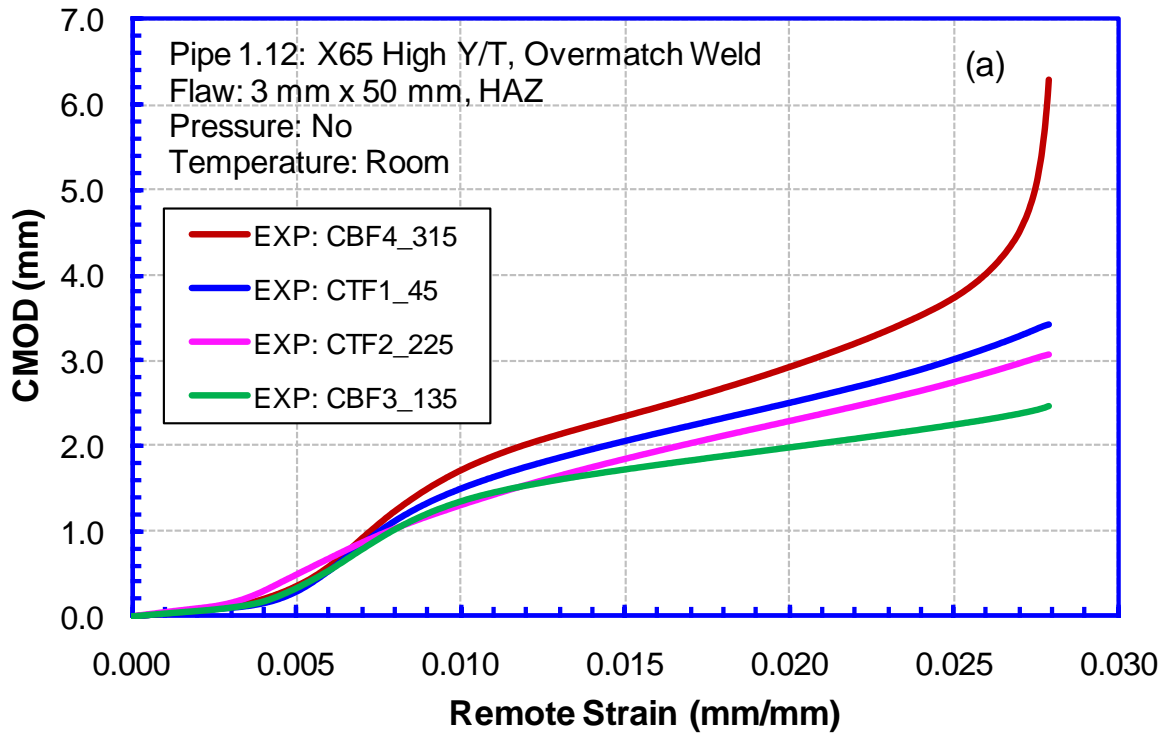


Figure 7.2 CMOD response of identical flaws in two pipe tests

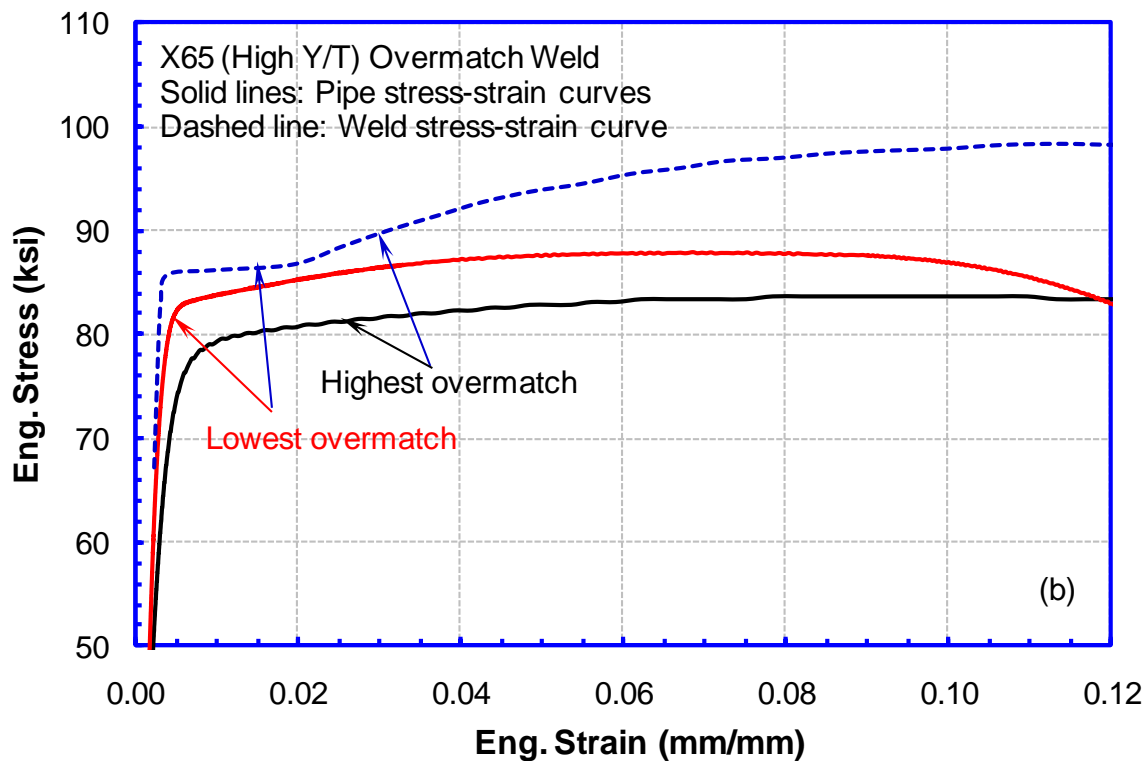
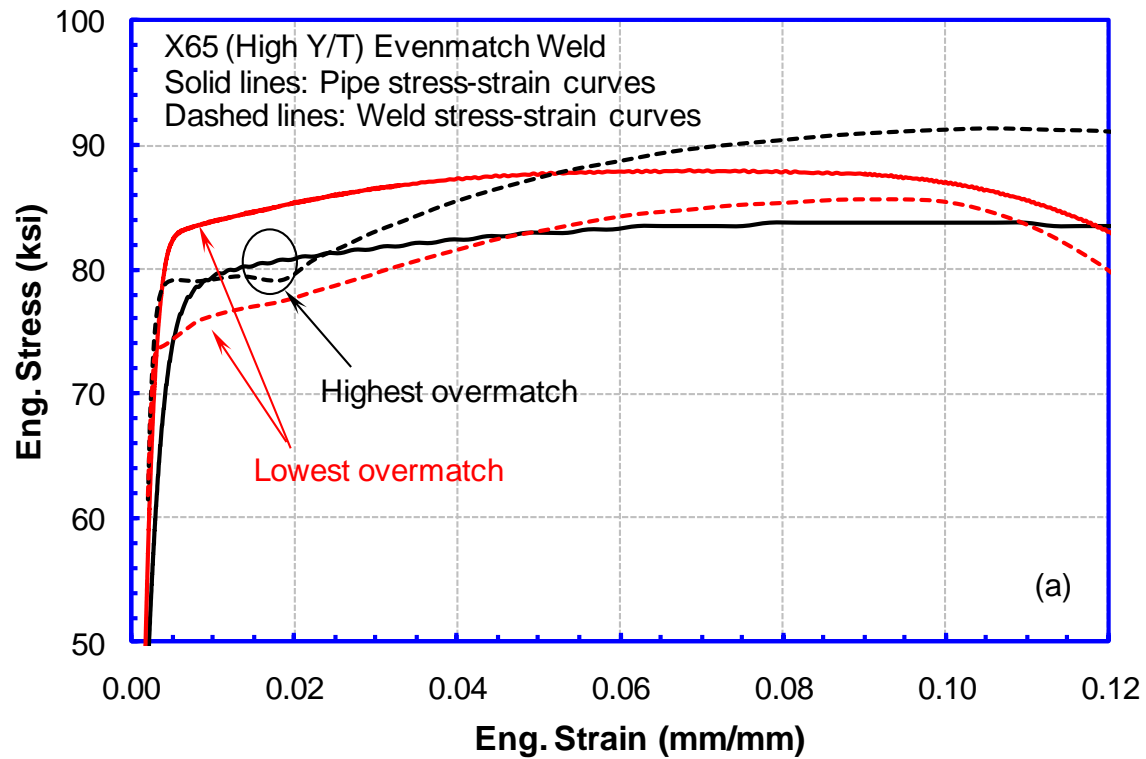


Figure 7.3 Bounding stress-strain curves of X65 high Y/T pipe and welds
(a) evenmatched weld and (b) overmatched weld

7.4 Introduction to FEA Model

Typical finite element models used in the post-test analysis are shown in Figure 7.4 and Figure 7.5 for CWP and FSP, respectively. For the CWP model, half of the specimen is modeled due to symmetry boundary conditions. The dimension of the FEA model matches the actual specimen size precisely. During the simulation, one end of the specimen is fixed and the other end is pulled with pre-defined displacement.

For the FSP model, only one weld is modeled for simplicity. It is believed that this simplification will not affect the analysis results since the pre-test analysis has shown the existence of a uniform zone between the two welds; therefore, the flaws in different welds will not interact. In the model, the length of the pipes on both sides of the weld is the same and equals to the actual length of pipe between the weld and the end plate. Both pipe ends are modeled with a rigid surface to simulate the effect of the end plates. Due to symmetry conditions, only a quarter of the pipe joint is modeled. In the simulation, one pipe end is fixed and the other end is pulled with pre-defined displacement. For pressurized cases, the internal pressure is applied to the inside surface of the pipe at first. The pressure is not applied to the end plate and the pipe is not restrained in the longitudinal direction.

In both CWP and FSP models, the weld geometry is determined from weld macros. Both HAZ and weld metal are modeled. A maximum of 10% HAZ softening is assumed based on the hardness profile. The material strength within the HAZ follows a 2nd order distribution where the maximum softening is reached at the center and the material strength matches the pipe and weld strength at the corresponding interfaces. The HAZ stress-strain curve is created by scaling the pipe stress-strain curve proportionally.

A surface breaking flaw is created on the outside surface of the specimen. The flaw is modeled with fixed depth and length. The weld cap at the flaw area is removed.

Three dimensional (3-D) linear brick finite elements in the commercial finite element software ABAQUS® are used for the FEA. The smallest element size near the flaw tip is about 0.02 mm to 0.05 mm. A similar size of key hole is used at the flaw tip to improve convergence. A mesh sensitivity study is performed to verify the quality of the mesh.

The remote strain is calculated with the relative displacement of the two points on the specimen corresponding to the location of the LVDT mounting point. The CMOD is calculated according to the same setup used in the experiment and both translational and rotational displacements are included.

7.5 Overall Trend in the Comparison of Test and FEA Results

Based on materials, the tests can be divided into five groups: (1) X65 pipe body (low and high Y/T, no welds); (2) X65 low Y/T pipe with overmatched weld; (3) X65 high Y/T pipe with evenmatched weld; (4) X65 high Y/T pipe with overmatched weld; and (5) X80 pipe with overmatched weld. The paired stress-strain curves with median strength overmatch of each

group were used to analyze all CWP and FSP tests. The simulation results were then compared with the test data.

It is found that the consistency between the FEA and test results highly depends on the material group. The simulated CMOD curves match the measured ones fairly well for material groups (2) - X65 low Y/T pipe with overmatched weld, (3) - X65 high Y/T pipe with evenmatched weld, and (5) - X80 pipe with overmatched weld as shown in Figure 7.6 to Figure 7.8. The majority of the simulated results are lower than the measured CMOD curves for material group (1) - X65 pipe body (low and high Y/T, no welds) and (4) - X65 high Y/T pipe with overmatched weld as shown in Figure 7.9 and Figure 7.10(a). However, the simulated curves of some tests in group (4) match the tests very well, as shown in Figure 7.10(b). It should be noted that the two tests shown in Figure 7.10(a) and (b) are duplicate tests with identical test parameters.

It should also be noted that each FSP test usually contains two weld joints and four flaws; therefore, four CMOD curves can be produced in each test. The CWP test can produce only one CMOD curve. However, some FSP specimens only contain one weld therefore, each test can produce only two CMOD curves.

7.6 Effect of Test Parameters

7.6.1 Internal Pressure

The effect of pressure on CMOD vs. remote strain relations is shown in Figure 7.11 and Figure 7.12. The increase of CMOD due to the internal pressure is evident. Among the four tests shown, the behavior of the “identical” flaws can be quite different. Only in the Pipe 1.6 all four flaws behave similarly. In the other three cases, there are considerable differences in the flaw behavior. The FE results generally followed the one with the least amount of CMOD.

7.6.2 Specimen Type – Full-Scale Pipe vs. CWP

A comparison of the full-scale test (Pipe 1.6) and two CWP specimens is shown in Figure 7.13. All specimens had flaws of 3 mm × 35 mm size. The behavior of the full-scale pipe and the CWP specimens is very similar. There is a good agreement between the simulated CMOD vs. strain response and the experimentally measured response.

7.6.3 Flaw Size

The effect of flaw size on the CMOD vs. the remote strain response is shown in Figure 7.14. As expected, larger flaws lead to greater CMOD at the same value of the remote strain. The simulated response follows the lower bound response of the CMOD vs. the remote strain relations among all flaws.

7.6.4 Temperature

The effect of temperature on the CMOD is shown in Figure 7.15 (pressure 80% SMYS) and Figure 7.16 (no pressure), respectively. For simplicity, only the largest CMOD curve from each test is shown. In both tests, it is seen that the decrease in testing temperature (from room

temperature to -20°C) greatly reduces the CMOD. The small-scale tests showed that both strain hardening capacity and yield and tensile strength of the weld metal increase at cold temperature. Those changes in the material stress-strain curves are consistent with the changes observed for CMOD curves in the cold temperature tests.

The FEA results underestimate the effect of the temperature on the CMOD curves. In those FEA simulations, the low temperature pipe stress-strain curves were created by scaling the room temperature stress-strain curves using the ratio calculated from the low and room temperature weld metal stress-strain curves. As the result, the relative weld strength mismatch, either at room temperature or at a low temperature, is the same.

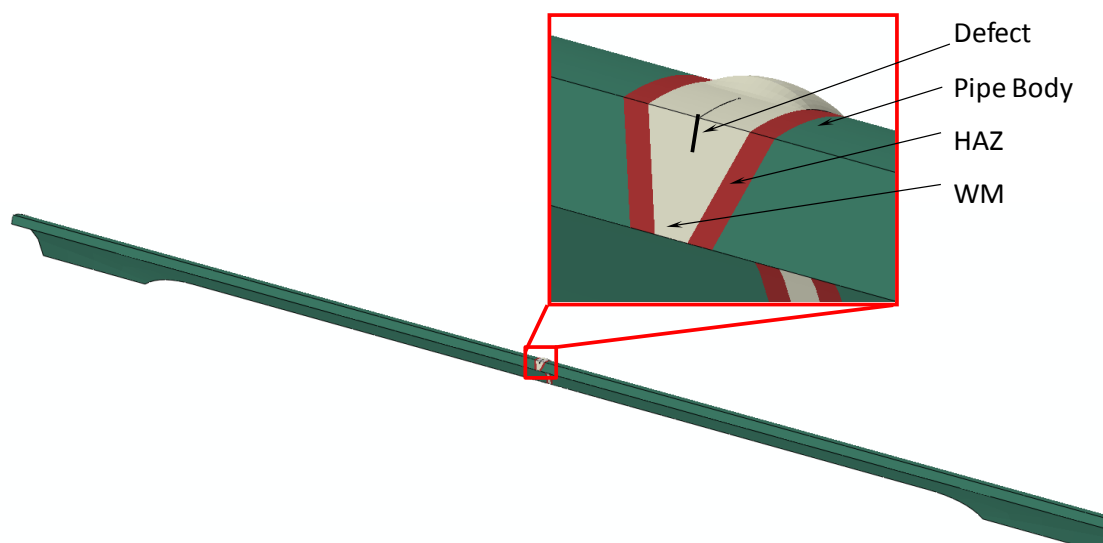


Figure 7.4 Representative finite element model for CWP specimen

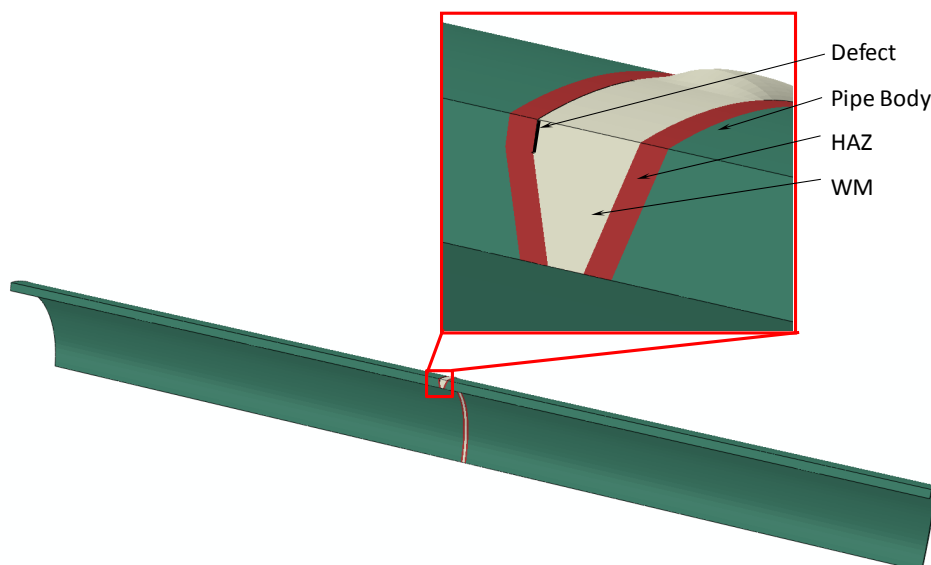


Figure 7.5 Representative finite element model for FSP specimen

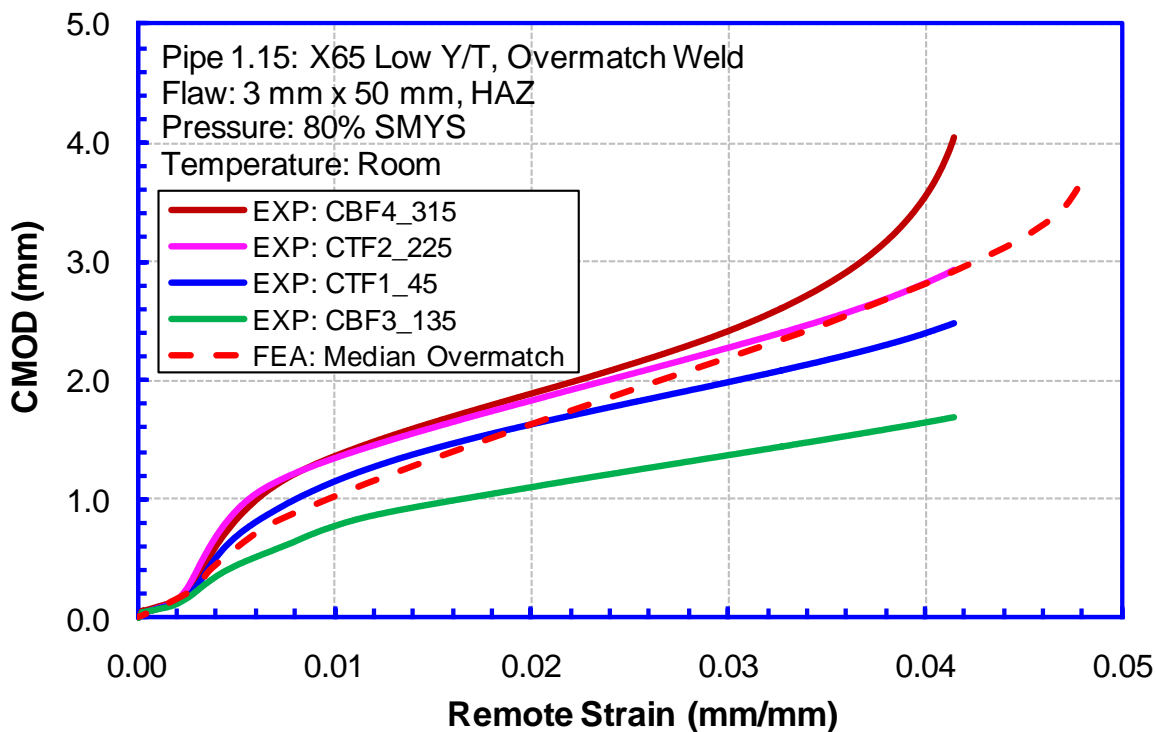


Figure 7.6 Measured and simulated CMOD vs. remote strain relations
 (Pipe: X65 low Y/T; Weld: overmatch)

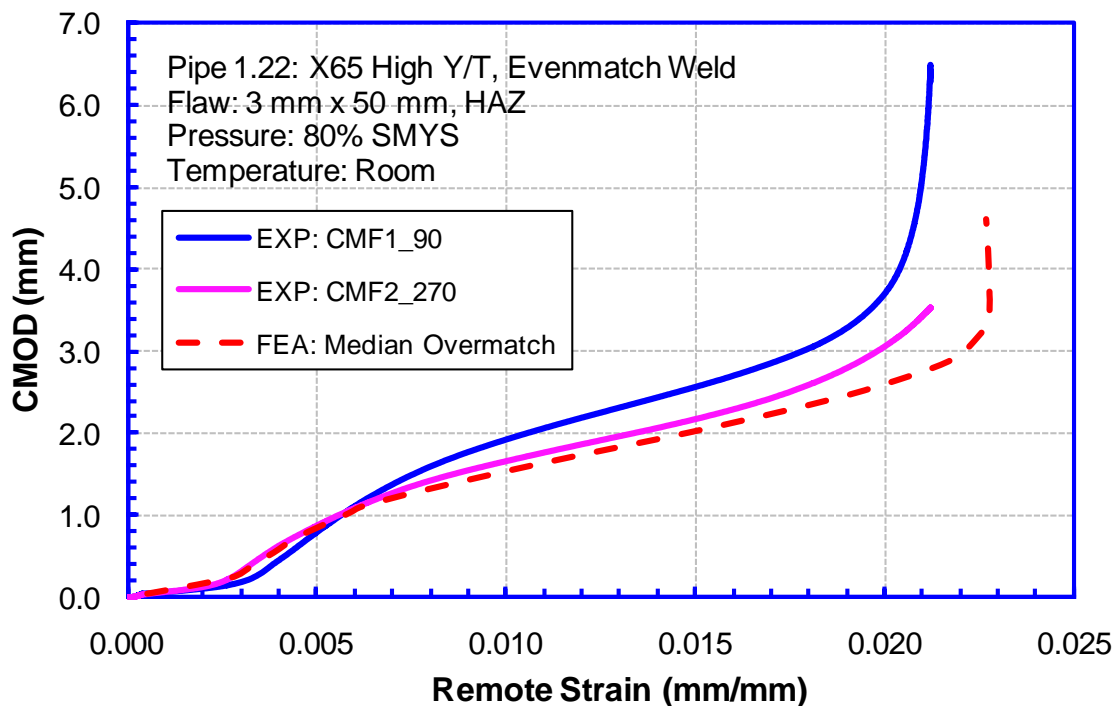


Figure 7.7 Measured and simulated CMOD vs. remote strain relations
 (Pipe: X65 high Y/T; Weld: evenmatch)

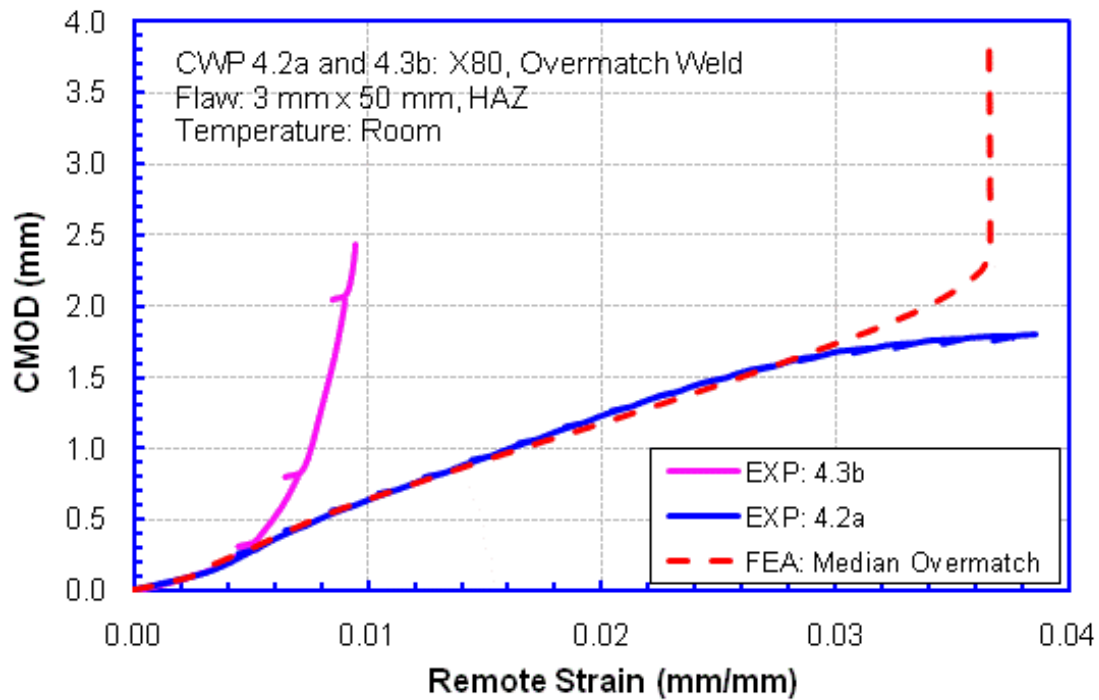


Figure 7.8 Measured and simulated CMOD vs. remote strain relations
(Pipe: X80; Weld: overmatch)

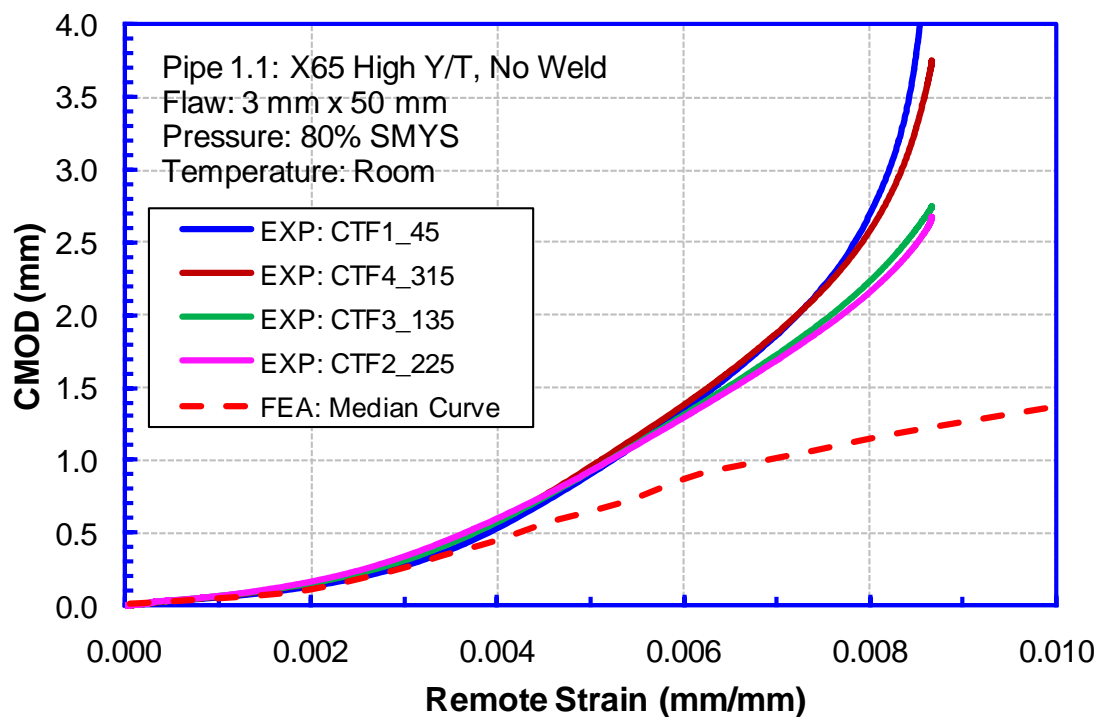


Figure 7.9 Measured and simulated CMOD vs. remote strain relations
(Pipe: X65 high Y/T; Weld: no)

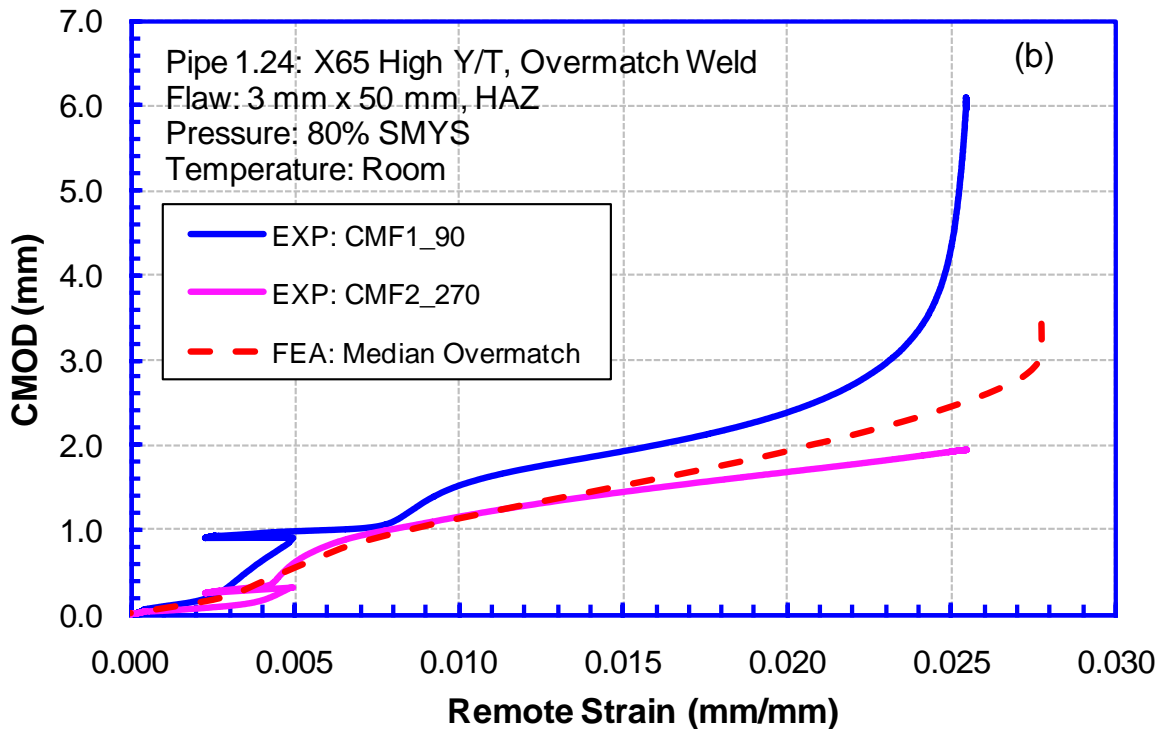
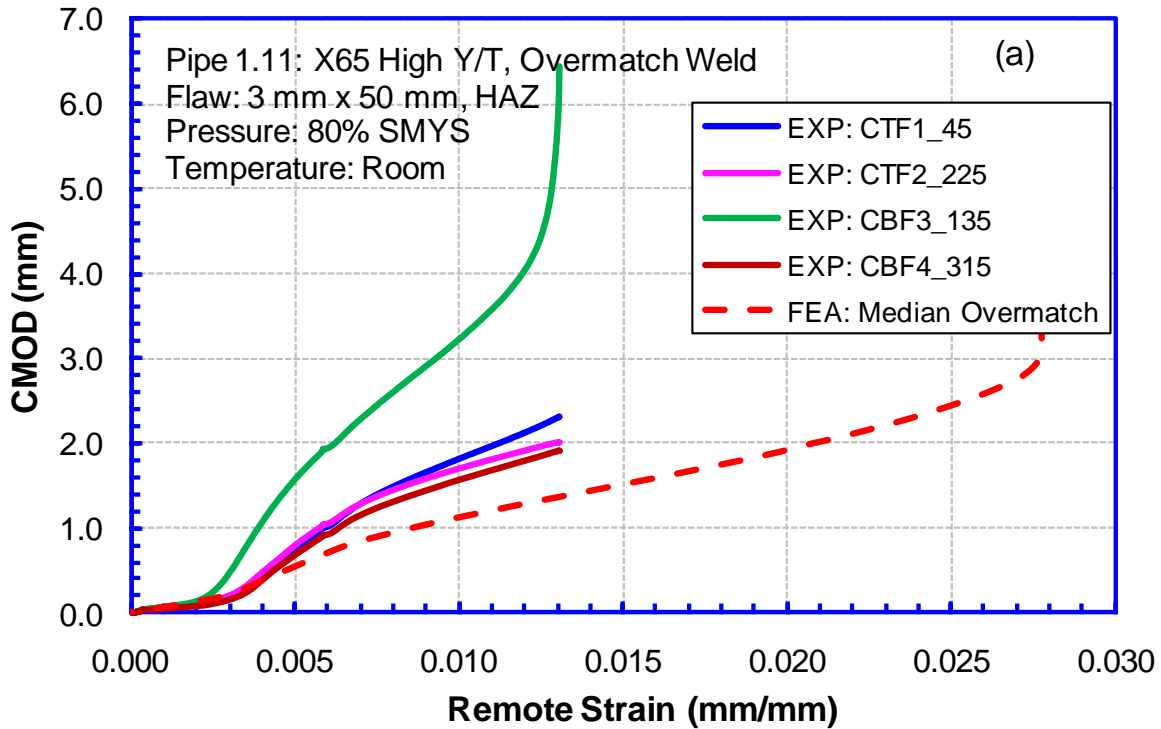


Figure 7.10 Measured and simulated CMOD vs. remote strain relations
(Pipe: X65 high Y/T; Weld: overmatch)

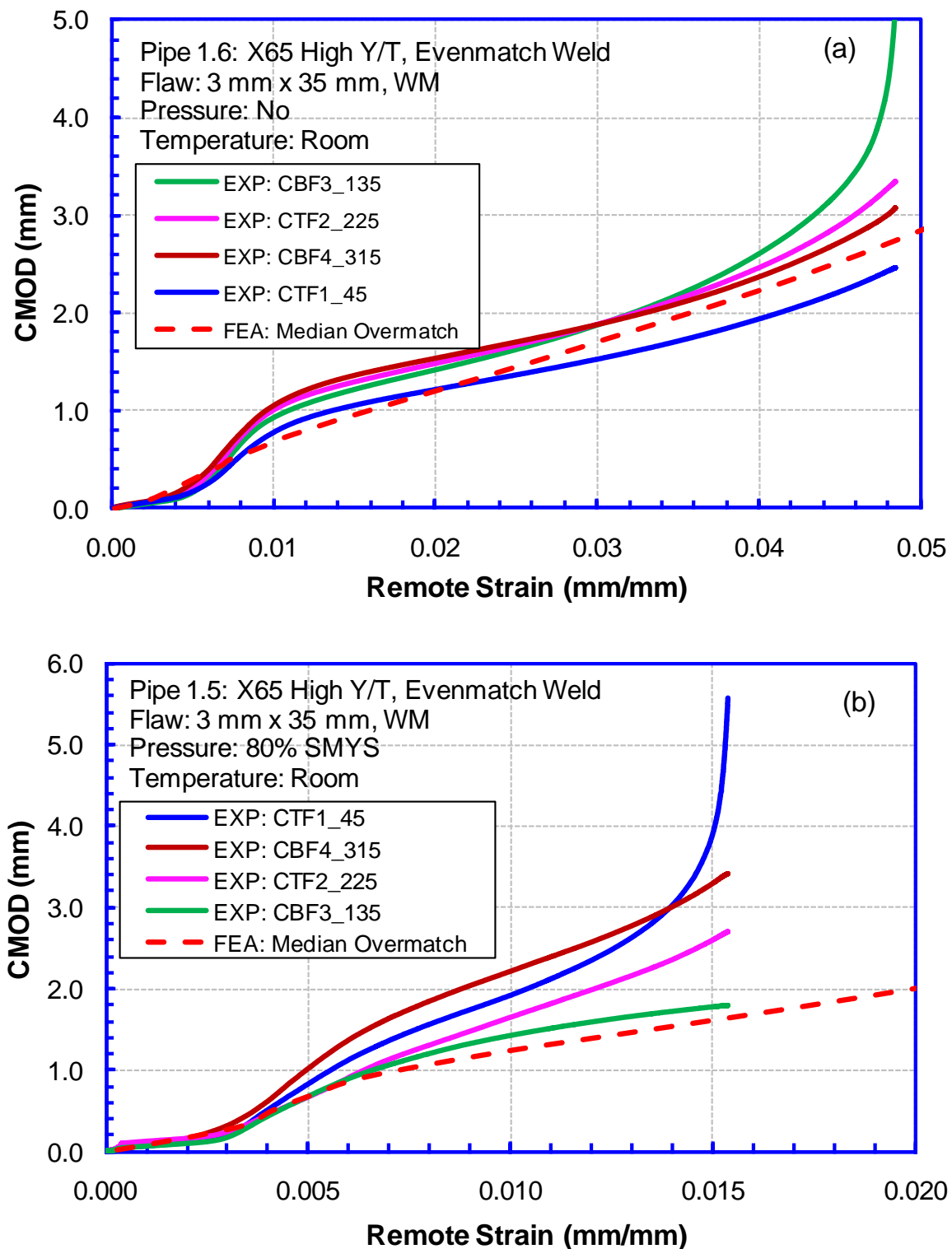


Figure 7.11 Effect of pressure on measured and simulated CMOD (Pipe: X65 High Y/T; Weld: evenmatch; Flaw: 3 mm x 35 mm, WM)

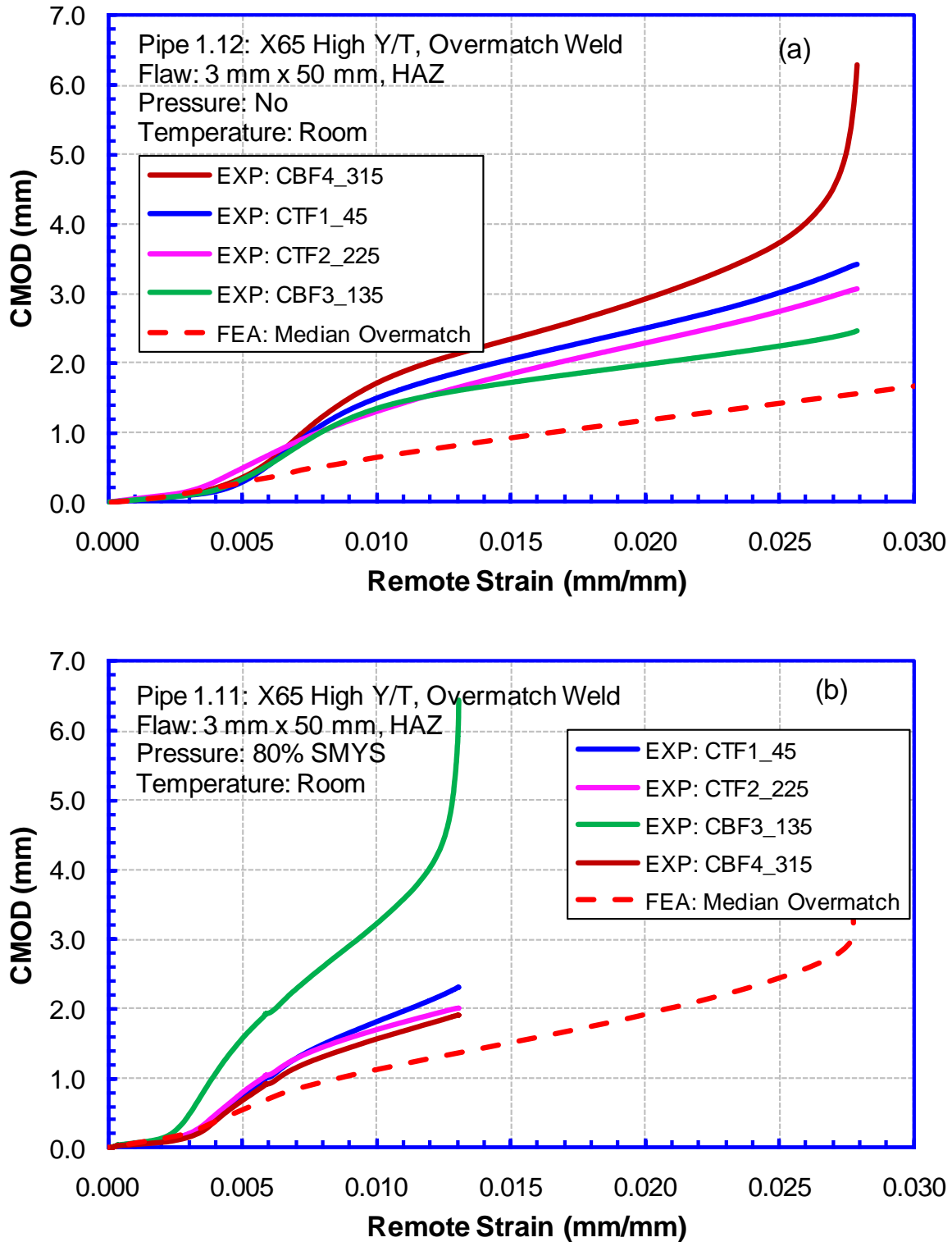


Figure 7.12 Effect of pressure on measured and simulated CMOD (Pipe: X65 High Y/T; Weld: overmatch; Flaw: 3 mm x 50 mm, HAZ)

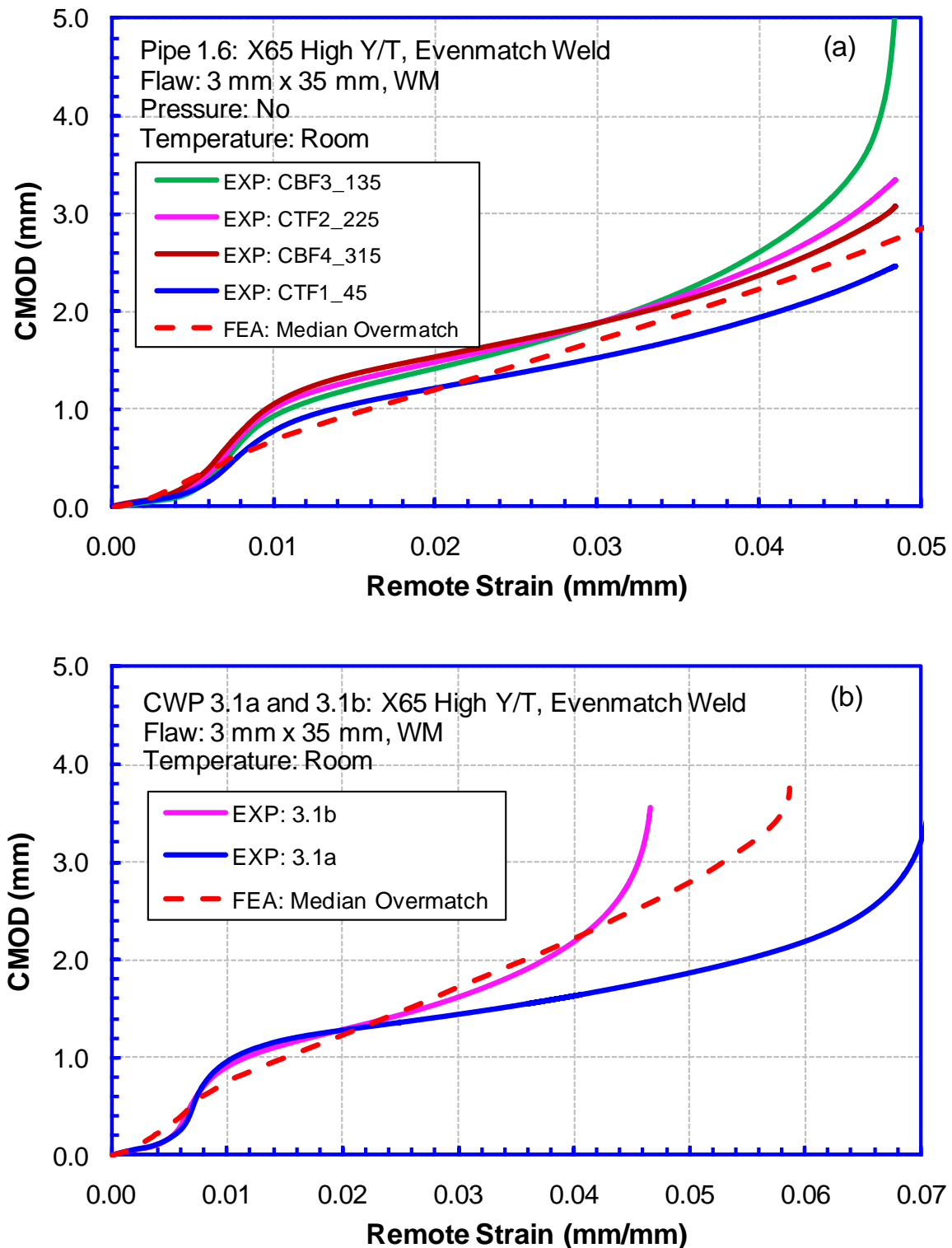


Figure 7.13 Effect of specimen size on CMOD (Pipe: X65 High Y/T; Weld: evenmatch; Flaw: 3 mm x 35 mm, WM; Pressure: No)

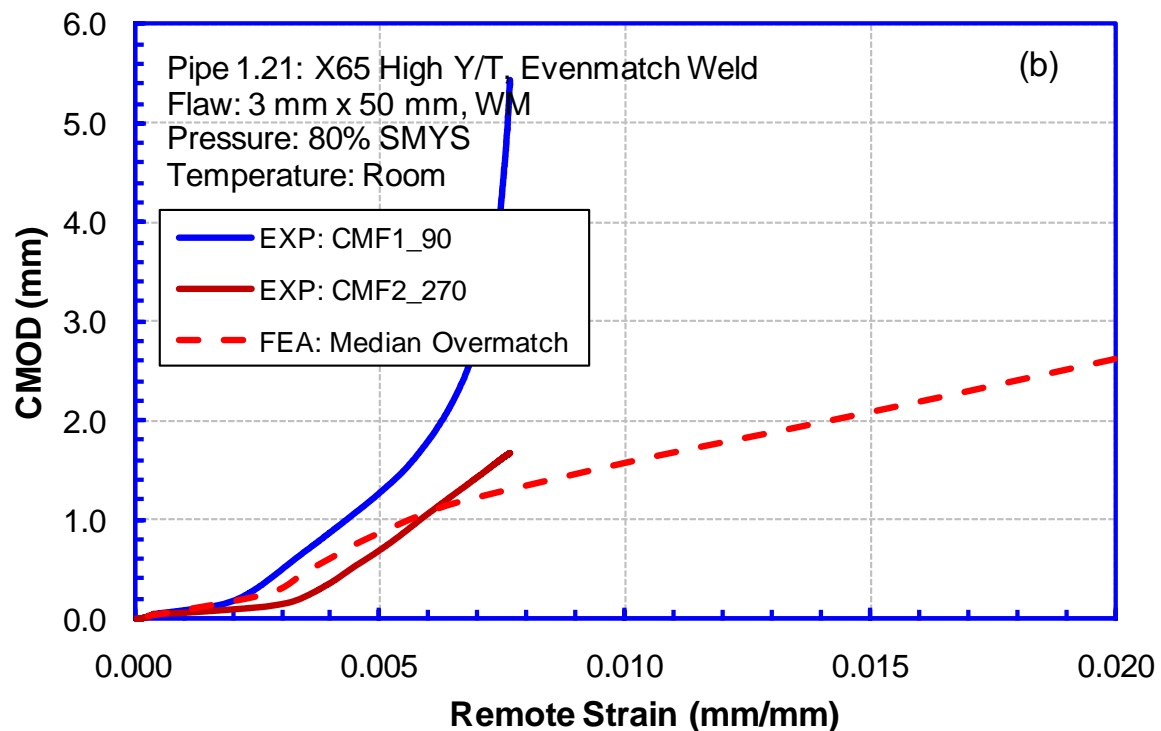
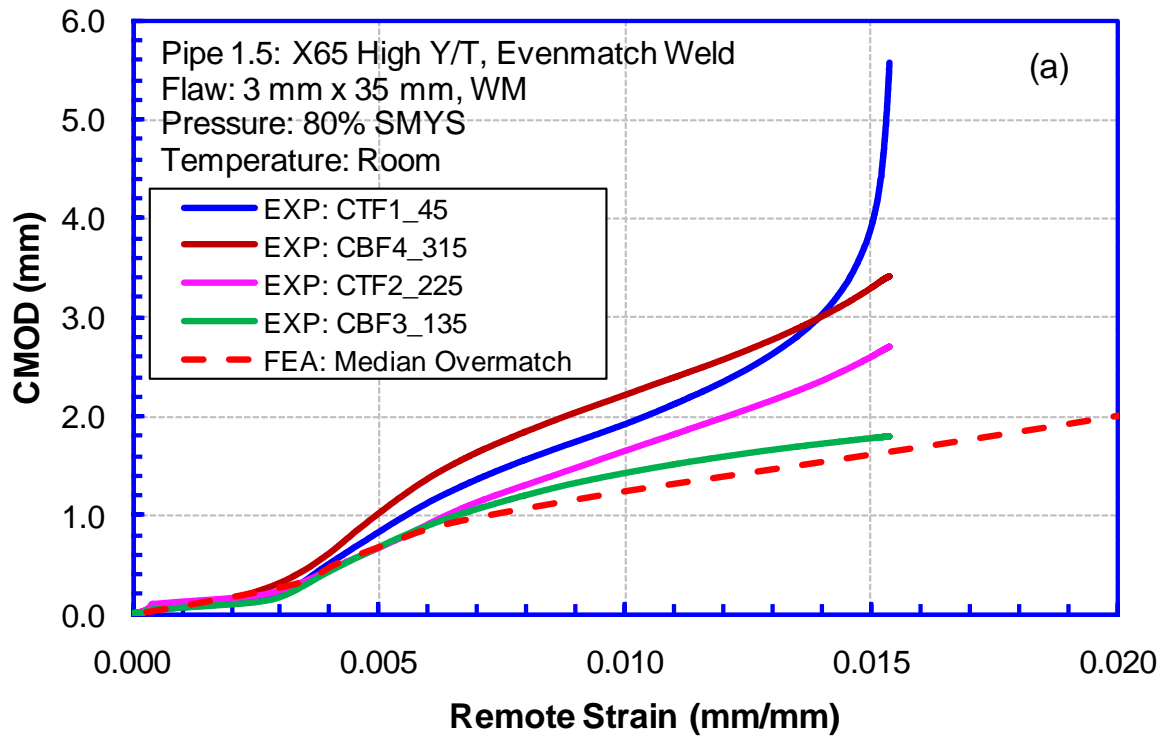


Figure 7.14 Effect of Flaw size on CMOD (Pipe: X65 High Y/T; Weld: evenmatch; Flaw: WM; Pressure: 80%SMYS)

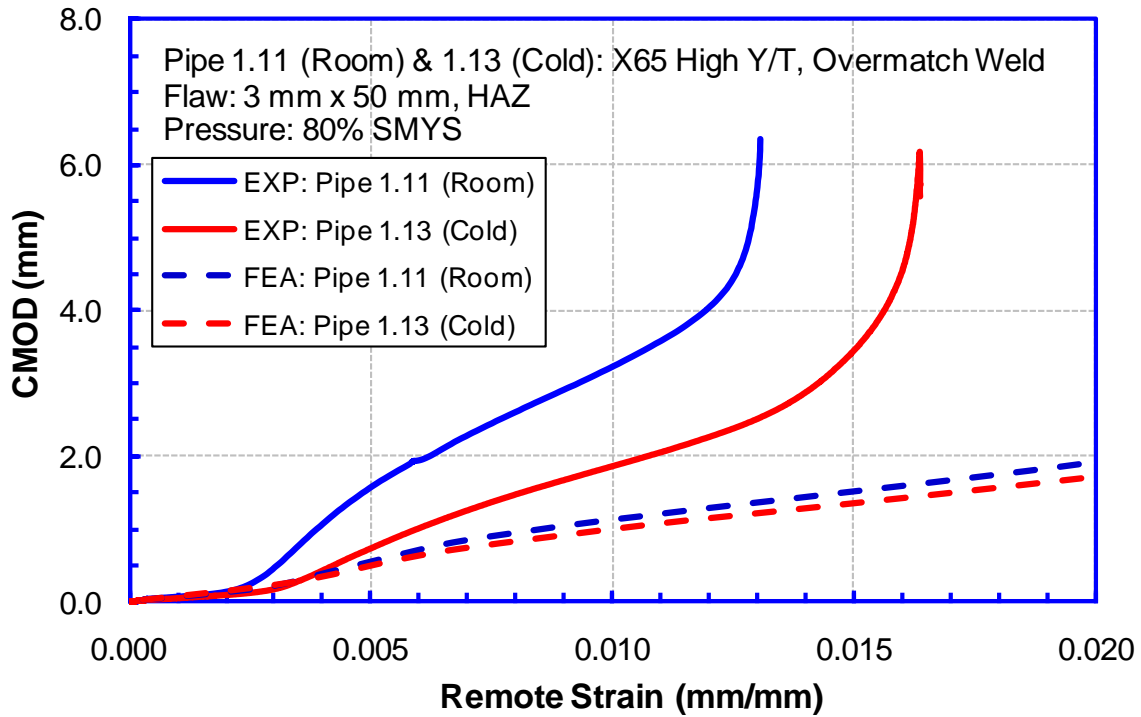


Figure 7.15 Effect of temperature on CMOD (Pipe: X65 High Y/T; Weld: overmatch; Flaw: 3 mm x 50 mm, HAZ; Pressure: 80%SMYS)

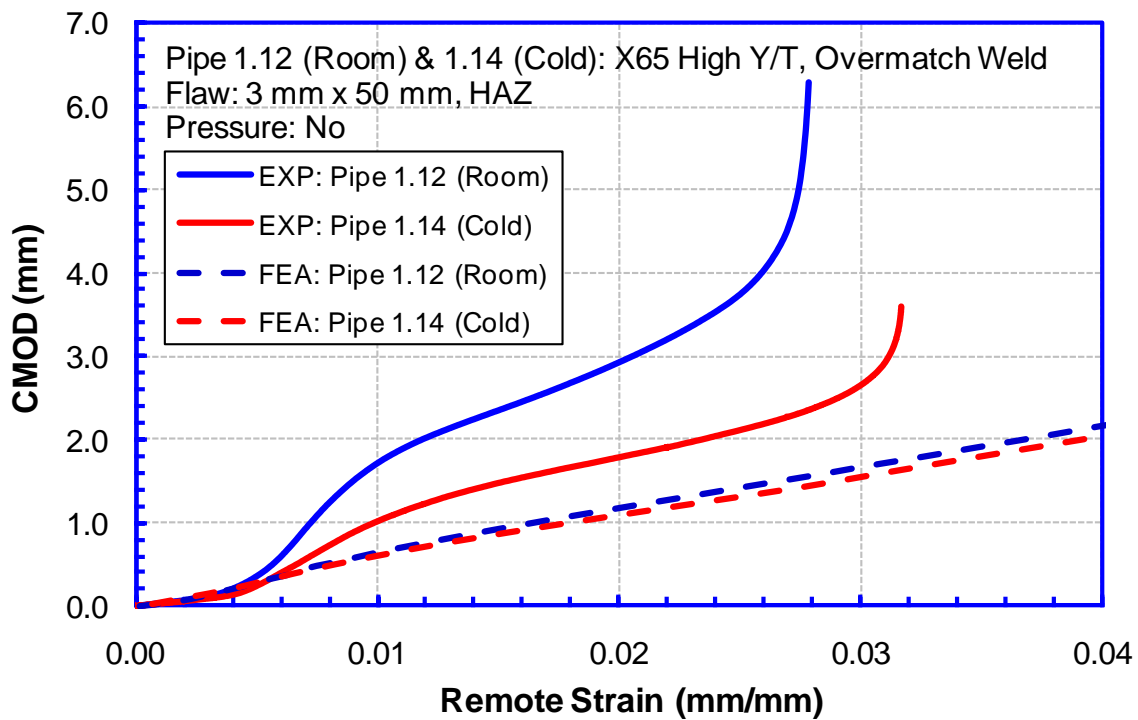


Figure 7.16 Effect of temperature on CMOD (Pipe: X65 High Y/T; Weld: overmatch; Flaw: 3 mm x 50 mm, HAZ; Pressure: No)

7.7 Effect of Stress-Strain Curves on Simulation Results

The difference between the measured and FEA simulated CMOD curves, is at least partially attributable to the variation of the stress-strain curves. To examine the extent of the effect of material property variation, selected tests were analyzed with the paired stress-strain curves which give the highest and lowest weld overmatch as shown in Figure 7.3. It should be noted that those highest and lowest pairs don't necessarily represent the full range of variations due to the limited number of small-scale tests conducted to obtain those stress-strain curves.

The comparison of the test and simulated results is shown in Figure 7.17 and Figure 7.18 for the evenmatched and overmatched weld of the X65 high Y/T pipe, respectively. It should be noted that the measured nominal stress vs. the remote strain curves in the CWP and FSP tests can be used to approximate the stress-strain curve of that section of the pipe material. The measured CMOD curve, on the other hand, depends on both pipe and weld properties.

Figure 7.17 indicates that the paired stress-strain curves giving the highest overmatch for the X65 high Y/T pipe with evenmatched weld could be very close to the full-scale pipe and weld properties used in this particular test. Both the simulated nominal stress vs. remote strain curves and the CMOD curves match the test data very well.

The results in Figure 7.18 indicate that the full-scale pipe property in the test 1.12 is likely between the upper and lower bound pipe properties. However, the simulated CMOD is much lower than the CMOD measured in the full-scale test 1.12. Furthermore, by comparing test 1.22 (see Figure 7.7) with test 1.11 (see Figure 7.10), it can be seen that the measured CMOD of the flaw in the evenmatched weld is lower than that in the overmatched weld under similar test conditions. One of the possibilities is that the weld strength of the overmatched weld of full-scale test specimen could be lower than what was used in the simulation (i.e. measured from small-scale tensile tests).

7.8 Effect of Flaw Growth on Simulation Results

Stable flaw growth before the final failure is believed to be another cause which contributes to the difference in the measured and simulated CMOD curves. To measure flaw growth, unloading compliance measurement was performed in four CWP tests (3.3a, 3.3b, 3.4a, and 3.4b) for the X65 high Y/T pipe with overmatched weld. All flaws are 3-mm deep and 50-mm long. CWP 3.3a and 3.3b are duplicate tests where the flaws are in weld center and CWP 3.4a and 3.4b are duplicate tests for HAZ flaws.

The experimentally measured compliance vs. strain relations (the zip-zapping solid curves) are shown in Figure 7.19 for four CWP tests (3.3a, 3.3b, 3.4a, and 3.4b). The strains at the maximum load were indicated by the vertical lines.

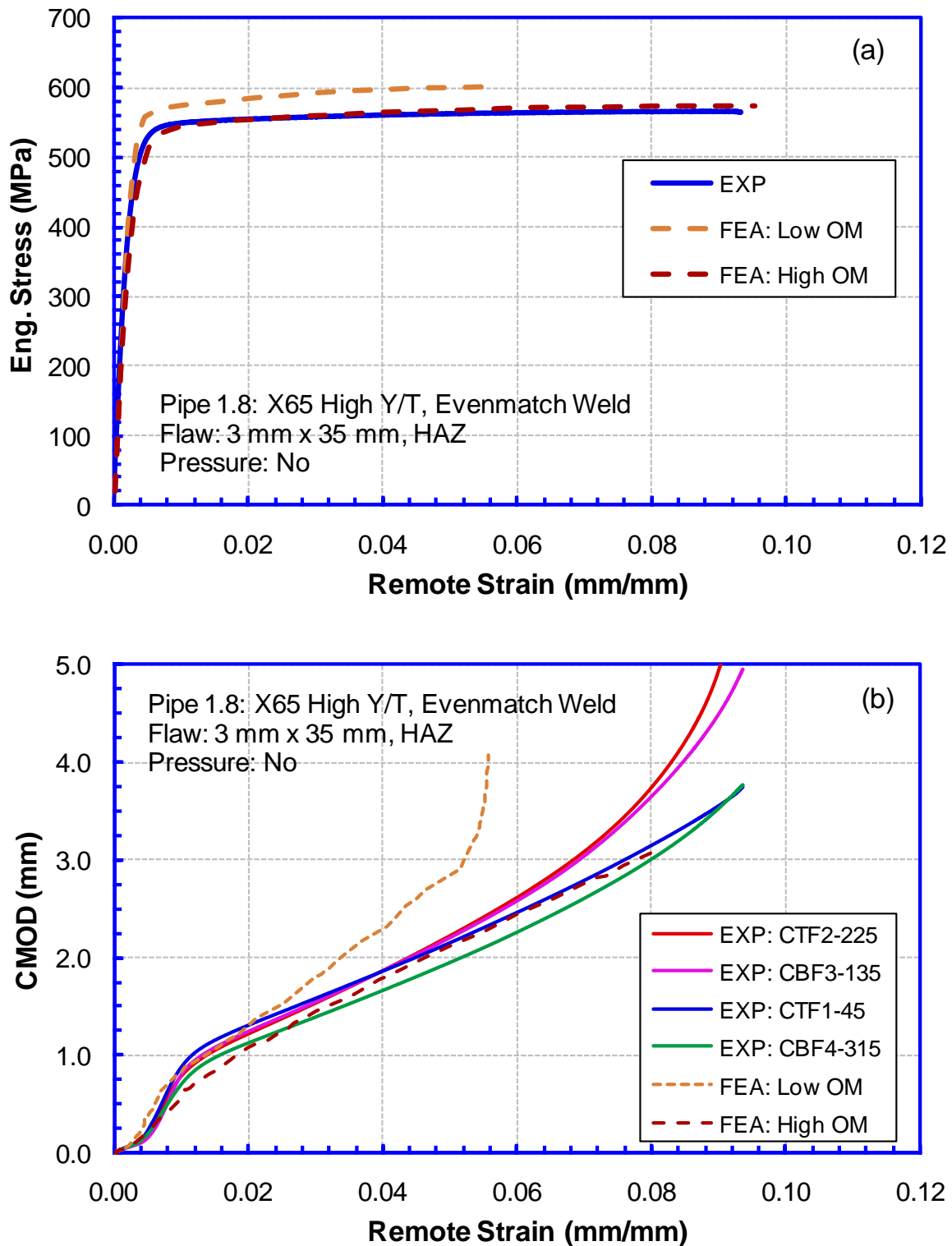


Figure 7.17 Effect of stress-strain curve variation on simulated experiment results (Pipe 1.8)
 (a) stress vs. strain; (b) CMOD vs. strain

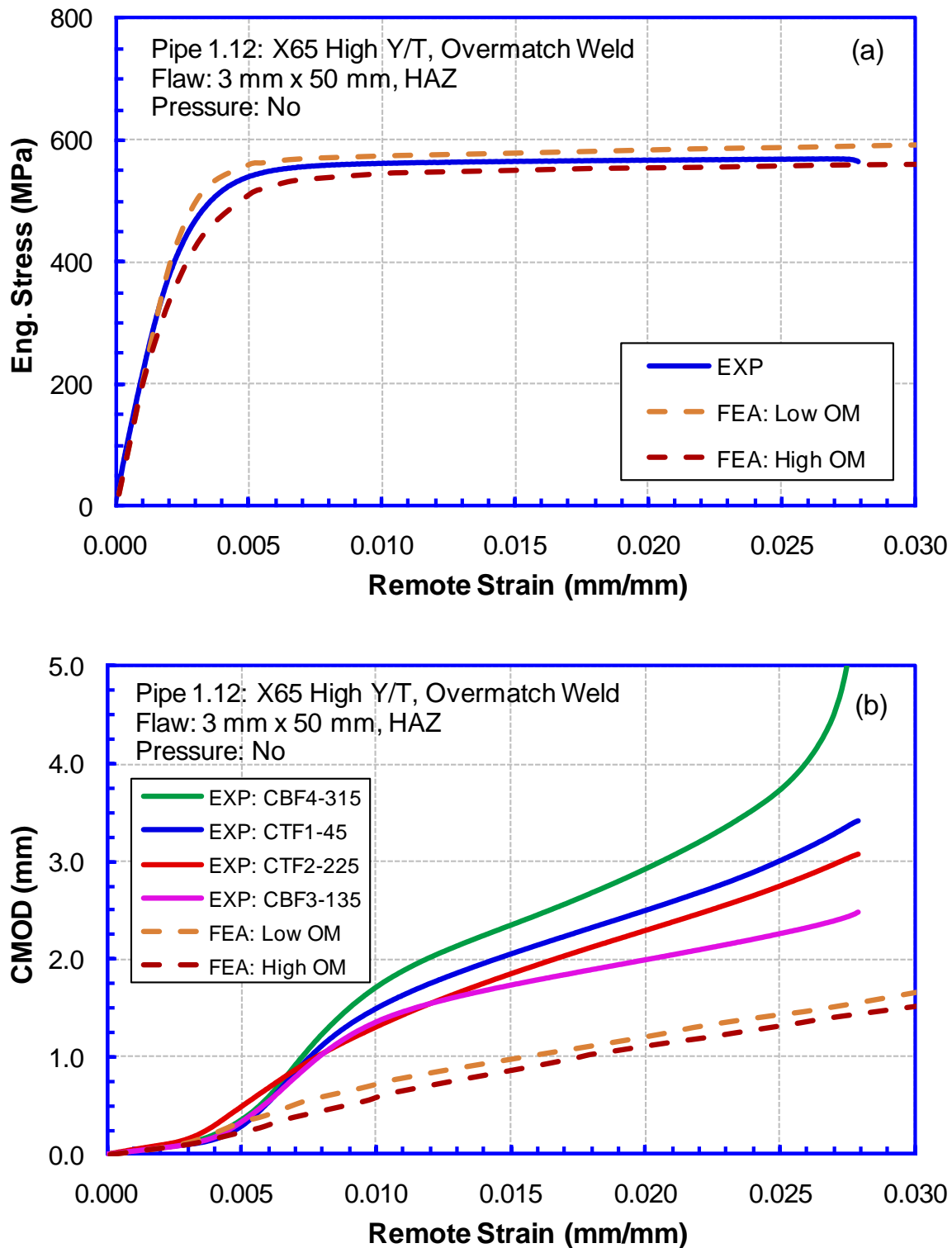


Figure 7.18 Effect of stress-strain curve variation on simulated experiment results (Pipe 1.12)
(a) stress vs. strain; (b) CMOD vs. strain

Finite element analyses were performed to calculate the compliance for various flaw depths, where the flaws were assumed to be static (i.e., no flaw growth). The flaw depths in the FEA were varied from 3.0 mm to 5.0 mm and the flaw lengths were fixed at 50 mm. The FEA calculated compliances of different flaw depths are shown as dotted (black) lines in Figure 7.19. The compliance is usually believed to be an elastic property of the system and independent of the magnitude of applied load. However, due to plastic deformation, the calculated compliance value decreases slowly as the applied strain increases. The intersection of the measured and FEA calculated compliance curves shows the amount of flaw growth.

The result shows that the flaw growth at the strain of maximum load is about 1.5 mm in the four tests. In addition, the flaw grows relatively slowly until the applied strain approaches the strain corresponding to the maximum load. For example, in test 3.3b, the flaw grew about 0.6 ~ 0.8 mm from 0% strain to 2.6% strain. The flaw grows another 0.6 ~ 0.8 mm between 2.6% strain and 2.8% strain (i.e., strain at max load).

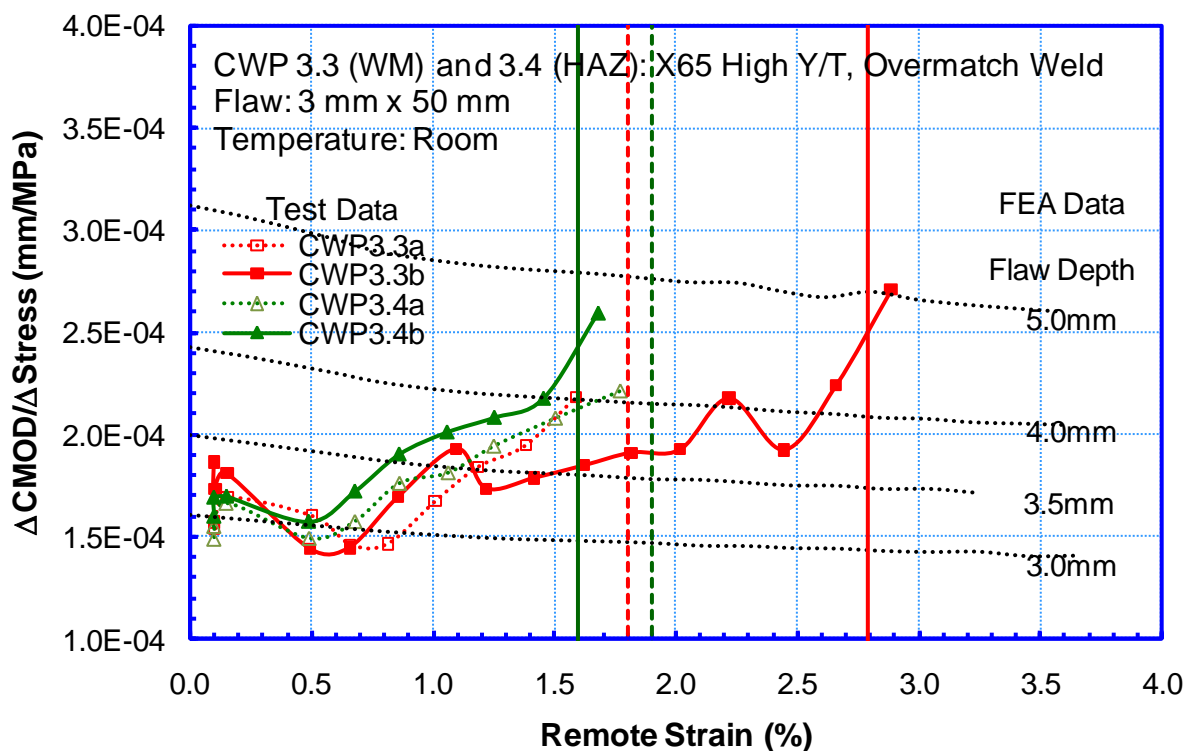


Figure 7.19 Measured and simulated compliance of CWP tests

7.9 Summary of Post-Test Analysis

FEA were performed for all CWP and FSP tests using the median stress-strain curves of the pipe and weld to obtain the CMOD curves (i.e., CMOD vs. remote strain curves). Selected tests were further analyzed, with paired stress-strain curves which can give the highest and lowest weld strength mismatch, based on the distribution of the stress-strain curves obtained from small-scale tensile tests, to study the effect of stress-strain curve variations on simulated CMOD

curves. The FEA results were compared with the experiment data. The agreement between the test and FEA simulated results varies by the material groups analyzed.

- (1) The FEA results reasonably match the experiment CMOD curves for the material groups (the FEA results usually follow the lower bound of the measured curves):
 - X65 low Y/T pipe with overmatched weld (Figure 7.6);
 - X65 high Y/T pipe with evenmatched weld (Figure 7.7, Figure 7.11, Figure 7.13, and Figure 7.14); and
 - X80 pipe with overmatched weld (Figure 7.8).
- (2) The majority of the FEA results predicts lower CMOD than the measured one for the material groups:
 - X65 pipe body (low and high Y/T, no welds) (Figure 7.9);
 - X65 high Y/T pipe with overmatched weld (Figure 7.10a, Figure 7.12, Figure 7.15, and Figure 7.16).
- (3) The unloading compliance results indicate that the flaws grow slowly as the strain increases before reaching the failure strain. The flaw growth rate increases rapidly when the strain approaches the final failure strain.
- (4) The observed difference between the FEA and experiment results was postulated to be attributable to the variation of the material properties and stable flaw growth. When there are appreciable differences between the experimental and simulated CMOD vs. remote strain response, the difference starts early at a strain level around the yield strain (0.5%). At this strain level, the amount of flaw growth, as indicated by the unloading compliance, was minimal. At an even higher strain level, around 1% strain, the flaw growth is still less than 0.5 mm. Therefore, for the tests conducted in this project, the material property variation, namely the tensile property variations, appears to be more influential than the flaw growth.
- (5) The variation of material behavior is particularly striking when the test results of Specimens 1.11 and 1.24 are viewed, see Figure 7.10. These are “identical” flaw at test conditions. The final failure strains differ by a factor of more than two. Even at lower strain, e.g. 1%, the measured CMOD between the lower and upper bound responses varies by a factor of 3.
- (6) Only a small number of tensile tests were conducted for some material groups. It is not surprising that only a small variation of material properties is recorded for those groups. The actual property variation could have been greater. When such variations are not recorded from the small-scale tests, there is a possibility that the numerical analysis will not capture the large-scale behavior, as the actual property of the large-scale specimen may not be reflected by the small-scale tests.

- (7) The FEA and test results showed that the crack driving force curves (e.g., the CMOD curves) were greatly increased (more than a factor of two) by the internal pressure. The magnitude of the increase depends on the flaw size and material properties.
- (8) The CWP and FSP tests showed similar results for the 3 mm × 35 mm flaws. However, for the 3 mm × 50 mm flaws, the CWP tests showed smaller strain capacities than the FSP tests.
- (9) The CMOD curves are found to decrease greatly as the testing temperature decreases from room temperature to -20°C. The decrease in CMOD cannot be explained by the increase of the strain hardening capacity of the materials alone. It is possible that the weld strength mismatch is increased at low temperature.

8 Concluding Remarks

8.1 Overview of the Project

The tensile strain limit state is an ultimate limit state and exceeding it can lead to the loss of lives and properties, damage to the environment, and disruption of pipeline operations. This research program was undertaken to supply high-quality test data for the development of tensile strain design models. One of the major focuses of the test program was the effect of internal pressure on tensile strain capacity. Preliminary work, prior to the start of the project, indicated that the tensile strain capacity could be reduced by the application of internal pressure. Until that point, uniaxial tests, such as CWP tests, had been thought of as the benchmark for determining the tensile strain capacity. No conclusive public domain test data existed on the internal pressure effect on tensile strain capacity. A large number of paired tests, full-scale pipes with and without pressure, were conducted to investigate the effect of internal pressure. In order to ensure that high-quality and consistent results can be obtained from the large-scale tests, extensive analyses were conducted to determine appropriate specimen dimensions, flaw placement locations, flaw sizes, instrumentation plans, magnitudes of internal pressures, and post-test data analysis procedures. The large-scale tests were accompanied by extensive small-scale material characterization tests. An exhaustive post-test physical examination of the full-scale specimens was conducted to provide corroborative evidence of the behavior of flaws. The large-scale tests were also simulated numerically to establish the correlation between the small and large-scale behaviors.

8.2 Major Observations of the Tests

A few major observations of the tests are given below.

- (1) The experimental test results conclusively demonstrated that the internal pressures equivalent to Classes 1 and 2 designs (60% ~ 80% of SMYS) could reduce the strain capacity of pipelines with circumferential planar flaws by as much as 50% or more.
- (2) When a large number of tensile tests were conducted on several joints of pipes of the same order (high Y/T pipe in this case), the yield strength exhibited large variations. Such large variations were not observed when only a small number of tests were conducted on other pipes of different manufacturers. It is not clear if the observed large variations are manufacturer-specific or a reflection of the number of tests conducted. It is possible that large variations of yield strength could exist, but a small number of tests may not capture such variations.
- (3) In a few instances, different strength levels between the procedure qualification welds and the production welds were observed.
- (4) In the majority of the large-scale tests, large variations were found for nominally “identical” flaws. These variations were clearly demonstrated by the differences in the

residual CMOD and the amount of flaw growth indicated from the cross-section of the flaws. The “identical” flaws exhibited similar behaviors only in a minority of cases.

- (5) Due to the asymmetrical nature of weld profile and the variation of weld cap width, making notches into HAZ can be a considerable challenge if the weld cap profile is used for creating reference scribe. The cross-sectional view of the flaws showed that in some cases, the HAZ notches landed at the intended zone, while in other cases they were either in the weld metal or far away from the fusion boundary.
- (6) With other conditions being the same, the specimens with internal pressure showed smaller residual CMOD than the specimens without internal pressure. The specimens with internal pressure failed at lower remote strains, thus experienced less deformations in the flawed area, than the specimens without pressure.
- (7) Post-test finite element analyses were conducted to simulate all large-scale tests. Various combinations of pipe and weld properties were selected within the experimentally measured ranges to give varying levels of strength mismatch. For the global load vs. deformation relations, there is almost always a good conformity. For the CMOD vs. remote strain behavior, the conformity depends on the particular group of welds being analyzed.
- (8) When there are differences between the test results and the numerical analyses in the CMOD vs. remote strain relations, such differences usually start early, at a strain level around the yield strain (0.5%). At the yield strain level, all indications, including the compliance measurement from the CWP tests, are that the ductile flaw growth is minimal, if any. Even at higher strain, 1.0% for instance, the flaw growth is typically small from the compliance measurement. Therefore, the difference in the experimentally observed behavior and the numerical simulation is primarily attributable to material tensile property variations.
- (9) With the variation of material properties and flaw locations (with respect to local microstructure), the experimentally measured tensile strain capacity from “identical” flaws can vary as much as a factor of two or more, in some cases.

8.3 Discussion of a Few Important Features

8.3.1 Effects of Test Temperature

A limited number of CWP tests were conducted at -20°C in addition to their counterpart tests carried out at room temperature. A comparison of two corresponding tests (both tests were done with unloading compliance measurement) is shown in Figure 8.1. The overall stress-remote strain response clearly followed the trend seen in the small-scale tensile tests where the cold temperature stress-strain curves showed enhanced strain hardening capacities and increased uniform strains. The increased strain hardening capacities and uniform strains are believed to be responsible for the increased tensile strain capacity of the CWP at low temperature.

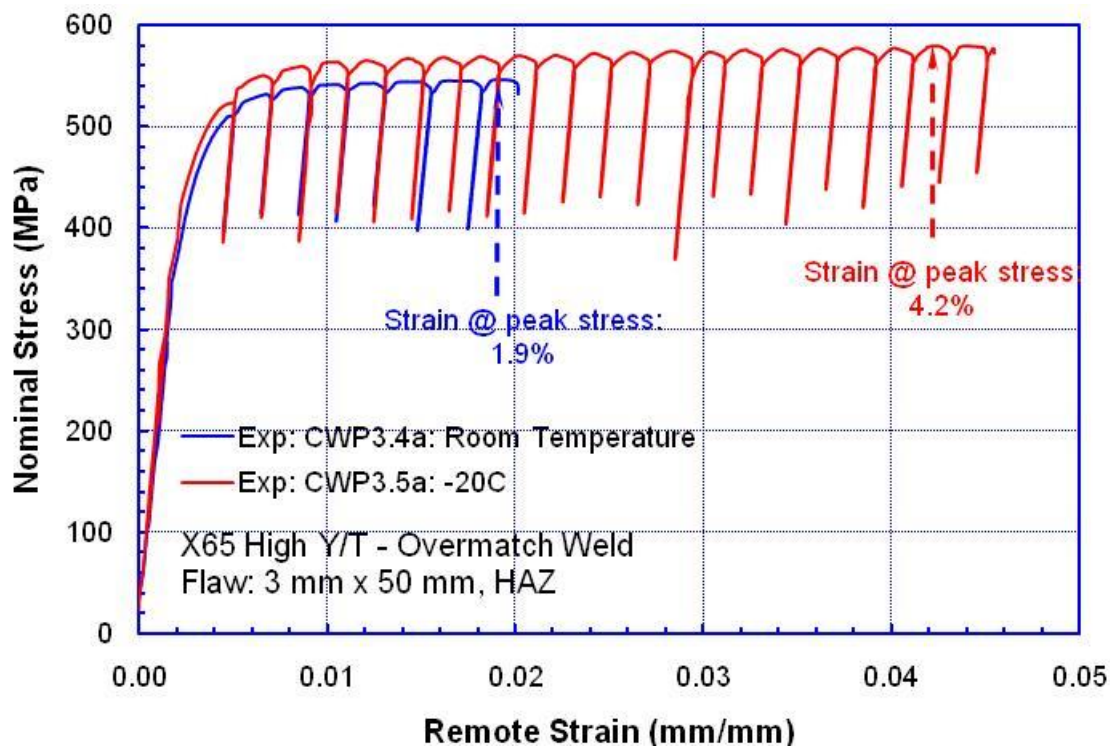


Figure 8.1 Comparison of stress-remote strain response of two CWP specimens at two different temperatures

8.3.2 Tensile Property Variations

The need for adequate weld strength mismatch (overmatch) for strain-based design requires tight control of the spread (standard deviation) of pipe tensile properties. Some of the observed tensile property variations within this project were somewhat of a surprise. A review of other sources indicates that such variations may not be unique. A ~2005-vintage 36-inch OD and $\frac{3}{4}$ -inch wall thickness X100 pipe was tested at CANMET [64]. The room-temperature stress-strain curves, from round and strap specimens cut from different clock positions of the same ring of the pipe, showed that the variation in yield strength within the given section of pipe, is in the range of 80-90 MPa, or 11-13% of the nominal strength level. Tsuru, et al. [65] reported the yield strength (at 0.5% total strain) variation in the range of 50-60 MPa, or 9-11% of the nominal strength for X80 pipes. At the same time, testing data published by Ishikawa, et al. [66], seemed to suggest much smaller variations.

Strength variations at a smaller magnitude can dramatically affect strain distributions. The strain distribution of an X100 CWP specimen is shown in Figure 8.2 by a photo-elastic image [67]. The corresponding remote strains in the base pipe sections (above and below the girth weld) are given in Figure 8.3. It is evident that the strains in the top and bottom pipe sections start to deviate upon yielding. The difference is attributable to small variations of the line pipe properties as shown in Figure 8.4. The strength difference between the top and bottom pipe sections is 10 MPa (1.45 ksi) and 20 MPa (2.9 ksi) at 0.5% and 2.0% strains, respectively. At the

termination of the test, the strength is at 823 MPa (119.4 ksi) on both sides, but the remote strains in the top and bottom pipe sections differ by a factor of approximately 1.5 (3.34% vs. 2.04%), see Figure 8.5. The variation in strength in this range can be considered small and quite reasonable. Due to the flat stress-strain relation in the plastic range of the stress-strain curves, the small difference in the stress-strain curves results in a large difference in strains when both sides are at the same applied stress level.



Figure 8.2 Photo-elastic image showing the non-uniform deformation on both sides of the girth weld [67]

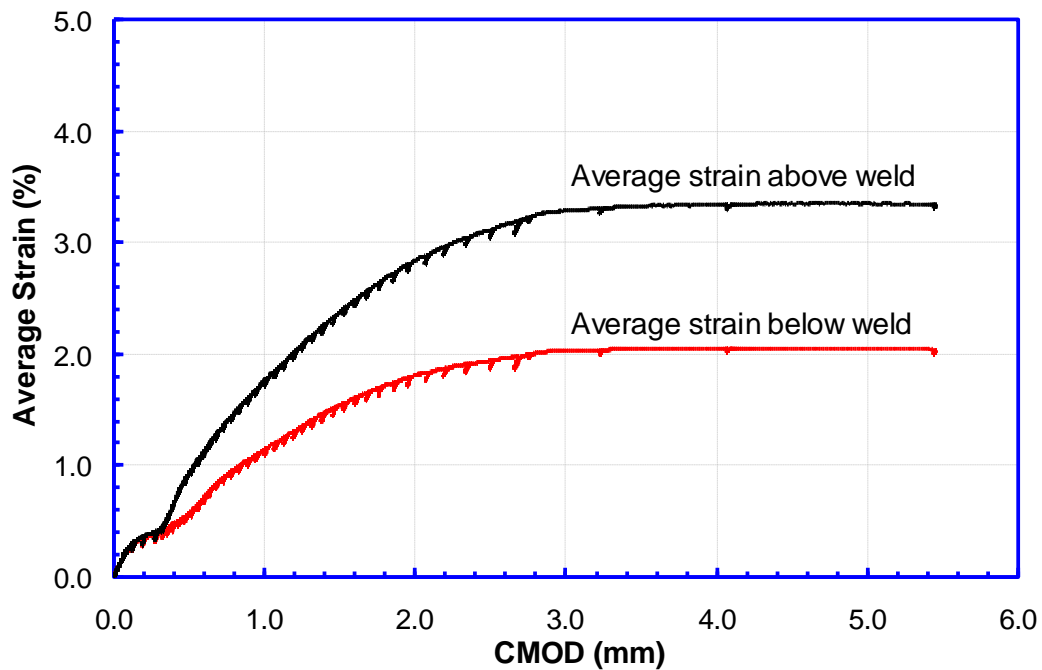


Figure 8.3 Development of strains above and below the girth welds as a function of crack mouth opening displacement (CMOD) [67]

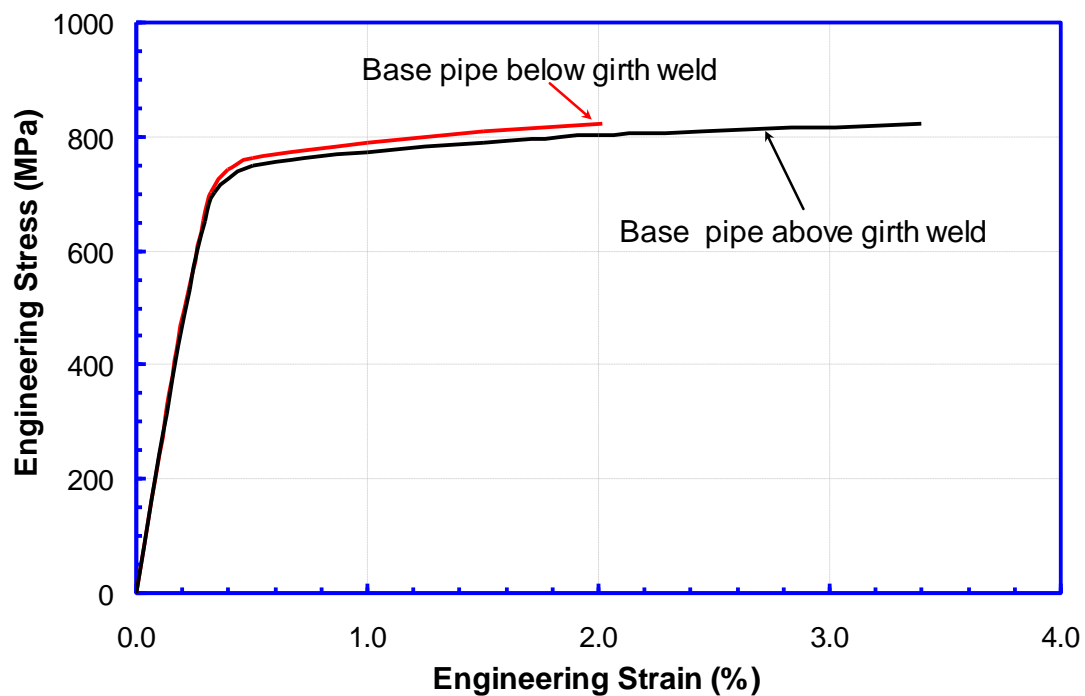


Figure 8.4 Engineering stress-strain curves constructed from the LVDTs located on the base pipe at the top and bottom part of CWP [67]

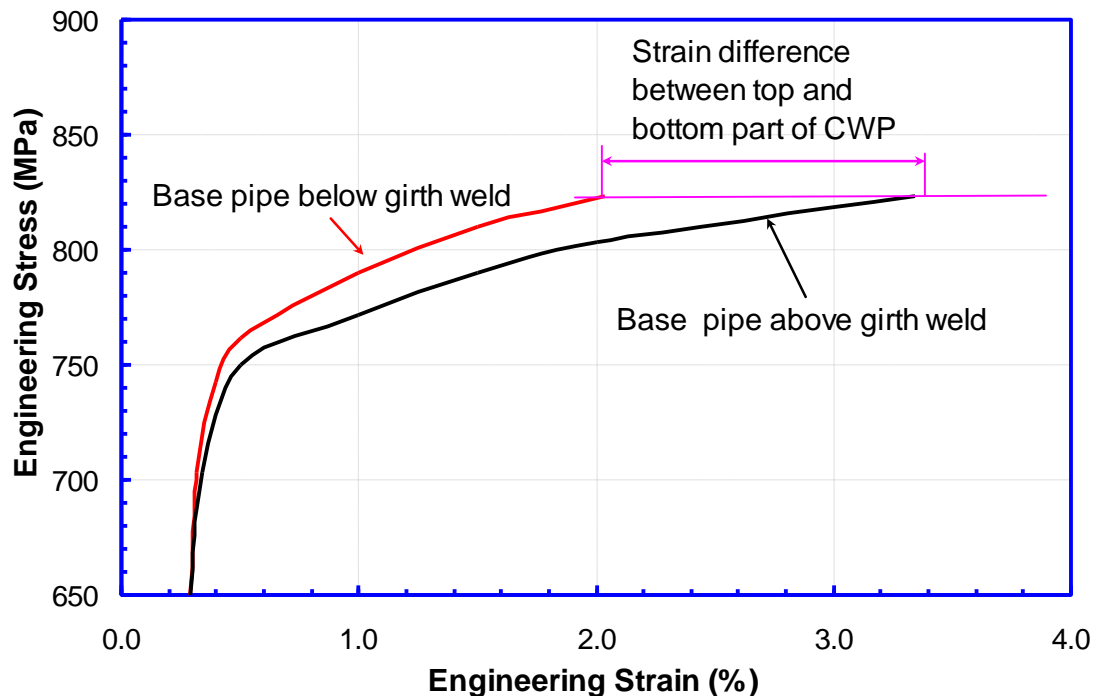


Figure 8.5 Tip portion of the stress-strain curves of Figure 8.4 showing the difference in measured strain between the top and bottom part of the CWP [67]

8.4 Practical Considerations for SBD

Practical steps may be taken to achieve sound strain-based design.

- (1) *Reduce strain demand.* This may be accomplished through the judicious selection of pipeline routes which impose low strain demand, using specially designed trenches and backfill, and other strain reduction methods.
- (2) *Select appropriate line pipes.* A few features which are beneficial to strain capacities are (1) high strain hardening capacity and (2) an upper bound of strength distribution that is as low as possible for manufacturing and yet still meets the minimum specifications. Rigorous specifications and verifications throughout the line pipe manufacturing processes are necessary to ensure the expected properties are achieved.
- (3) *Minimize the likelihood of gross strain concentration at welds.* When there is gross strain concentration at a weld, i.e., the weld experiencing higher strains than pipe body, the overall strain capacity is typically below yield strain (0.5%) because the most applied displacement is imposed on the weld. The leading causes of gross strain concentration at the welds are high levels of high-low misalignment and low weld strength overmatching. It is necessary to ensure sufficient weld overmatching for expected high-low misalignment to prevent gross strain concentration.

- (4) *Ensure upper-shelf toughness behavior.* To have a sufficient level of tensile strain capacity at the expected service temperatures, it is necessary to ensure that the material behavior is ductile.
- (5) *Balance the selection of pipe grade and pipe wall thickness.* Pipes of thicker walls are beneficial to both tensile and compressive strain capacity. For the same pressure containing capacity, a thicker wall would allow the use of lower grade of pipes. Lower grade pipes can more easily be made to have higher strain hardening capacity. However, the increased strain hardening capacity cannot be automatically assumed for lower grade pipes. Rigorous specifications and verifications are still needed.
- (6) *Control flaw size and distribution.* Weld flaws, particularly planar flaws, are detrimental to tensile strain capacity. The flaw size and distribution need to be controlled with appropriate welding and NDT procedures. It should be emphasized that overly aggressive flaw size limits may lead to unnecessary repairs. Since repair welds typically have more inferior properties than mechanized welds, there needs to be a proper balance between flaw size limits and repair rates.
- (7) *Follow a rigorous program on material qualification, including consistent and robust experimental test procedures for material property characterization.* Strain-based design is significantly more sensitive to material properties and their variations than traditional stress-based design. It is necessary to ensure that all test data are generated using a consistent set of test procedures among all labs, including specimen extraction and preparation, instrumentation, data reduction, and reporting.

8.5 Limitation of the Current Project

A large volume of test data has been produced within this project. A few limitations were also discovered in the course of this project:

- (1) The full-scale test matrix consists of X65-grade pipes from two manufactures. Both pipes are of 12.75" OD and 0.5" wall thickness. The Y/T ratios of both pipes are close to 0.90 (i.e., 0.88 and 0.92, respectively).
- (2) The tested line pipes have very flat stress-strain curves after the initial strain hardening (e.g., after approximately 2% strain). Such flat stress-strain curves can lead to large variations in the reported tensile strain capacity from essentially the same behavior.
- (3) Girth weld high-low misalignments have been shown to be a major influencing factor for tensile strain capacities. The test program does not include weld misalignment.

8.6 Future Work

Despite the variability of the test data identified in this report, the development of predictive tensile strain design models should continue, as such models are the only practical tools for large-scale pipeline projects. Obtaining tensile strain capacity from large-scale tests beyond a limited number of verification tests is impractical. Through thorough design consideration, adoption of appropriate line pipe product specifications, and the application of suitable

construction process monitoring, predictive tensile strain design models can be effectively applied on pipeline projects.

In order to better assist the development of tensile strain design models, it is recommended that the focus of future tests include the following:

- (1) Pipes of different grades and strain-hardening rates should be tested. Ideally, the stress-strain curves should have reasonable slopes at relatively high strain values.
- (2) Pipes of different diameters and wall thicknesses need to be tested. It is believed that the pipe wall thickness has a greater impact on the tensile strain capacities than the diameter. Therefore, the priority should be given to pipes of different wall thicknesses.
- (3) The magnitude of the misalignment in field welds is not, in general, precisely known. To fully understand the effect of misalignments on strain capacities, full-scale tests with realistic misalignments need to be conducted.

9 References

- 1 Thenhaus, P. C., and Campbell, K. W., “ Seismic Hazard Analysis,” *Earthquake Engineering Handbook*, Wai-Fah Chen and Charles Scawthorn Ed.,CRC Press, 2003.
- 2 Wells, D. L., and Coppersmith, K. J., “New Empirical Relationships among Magnitude, Rupture Length, Rupture Width, Rupture Area, and Surface Displacement,” *Buttetin of the Seismological Society of America*, Vol. 84, No. 4, August 1994.
- 3 Audibert, J. M. E., Nyman, D. J., and O’Rourke, T. D., “Differential Ground Movement Effects on Buried Pipelines,” *Guidelines for the Seismic Design of Oil and Gas Pipeline Systems*, ASCE Technical Council on Lifeline Earthquake Engineering, 1984.
- 4 Kenny, S., Barret, J., Phllips, R., and Pipescu, R., “Integrating Geohazard Demand and Structural Capacity Modelling within a Probablistic Design Framework for Offshore Arctic Pipelines,” *Proceedings of the 17th International Offshore and Polar Engineering Conference (ISOPE 2007)*, Lisbon, Portugal, July 1-6, 2007.
- 5 Hukle, M. W., Horn, A. M., Hoyt, D. S., and LeBleu, Jr., J. B., “Girth Weld Qualification for High Strain Pipeline Applications,” *Proceeding of the 24th International Conference on Offshore Mechanics and Arctic Engineering* , June 13-17, Kalkidiki, Greece.
- 6 Denys, R., Lefevre, A., and Baets, P. D., “A Rational Approach to Weld and Pipe Material Requirements for a Strain Based Pipeline Design,” *Proceedings of Applications & Evaluation of High-Grade Line pipes in Hostile Environments*, Pacifico Yokohama, Japan, November 7-8, 2002, pp. 121-157.
- 7 Wang, Y.-Y., Liu, M., Chen, Y., and Horsley, D., “Effects of Geometry, Temperature, and Test Procedure on Reported Failure Strains from Simulated Wide Plate Tests,” *Proceedings of 6th International Pipeline Conference*, Paper No. IPC2006-10497, September 25-29, 2006, Calgary, Alberta, Canada.
- 8 Denys, R.M. and Lefevre A.A., “Urgent guidelines for curved wide plate testing”, *Pipeline Technology Conference*, Paper number Ostend2009-110, Ostend, Belgium, October 12-14, 2009.
- 9 “Update of Weld Design, Testing, and Assessment Procedures for High Strength Pipeline,” project funded by the U.S. Department of Transportation Pipeline and Hazardous Materials Safety Administration, Contract No. DTPH56-07-T-000005.
- 10 DNV OS-F101, “Submarine Pipeline System,” 2000.
- 11 BS 7910:1999, “Guide on Methods for Assessing the Acceptability of Flaws in Metallic Structures,” British Standards Institution, 1999.
- 12 DNV-RP-F108, “Fracture control for pipeline installation methods introducing cyclic plastic strain”, 2006.
- 13 Wang, Y.-Y., Cheng, W., McLamb, M., Horsley, D., Zhou, J., and Glover, A., “Tensile Strain Limits of Girth Welds with Surface-Breaking Defects Part I an Analytical Framework,” in *Pipeline Technology, Proceedings of the 4th International Conference on Pipeline Technology*, Edited by Rudi Denys, Ostend, Belgium, May 9-13, 2004.

- 14 Wang, Y.-Y., Horsley, D., Cheng, W., Glover, A., McLamb, M., and Zhou, J., “Tensile Strain Limits of Girth Welds with Surface-Breaking Defects Part II Experimental Correlation and Validation,” in *Pipeline Technology, Proceedings of the 4th International Conference on Pipeline Technology*, Edited by Rudi Denys, Ostend, Belgium, May 9-13, 2004.
- 15 Horsley, D. and Wang, Y.-Y., “Weld Mismatch Effects on the Strain Limits of X100 Girth Welds,” in *Pipeline Technology, Proceedings of the 4th International Conference on Pipeline Technology*, Edited by Rudi Denys, Oostende, Belgium, May 9-12, 2004.
- 16 Wang, Y.-Y., Cheng, W., and Horsley, D., “Tensile Strain Limits of Buried Defects in Pipeline Girth Welds,” *Proceedings of the International Pipeline Conference 2004*, Calgary, Alberta, Canada, October 4-8, 2004.
- 17 Burdekin, F. M. and Dawes, M. G., “Practical Use of Linear Elastic and Yielding Fracture Mechanics with Particular Reference to Pressure Vessels,” *Proceedings of the Institute of Mechanical Engineers Conference*, London, May 1971, pp. 28-37.
- 18 BRITE EURAM Project: Structural Integrity Assessment Procedure for European Industry – SINTAP, Procedure Document, British Steel (now Corus Group) Swinden Technology Centre, Rotherham, UK, November 1999.
- 19 Wang, Y.-Y., Rudland, D., and Liu, M., “Experimental Validation of Constraint Effects,” GRI report GRI-04/0147, February 2005.
- 20 Wang, Y.-Y., Liu, M., and Horsley, D. “Apparent Fracture Toughness from Constraint Considerations and Direct Testing,” *Proceedings of 7th International Offshore and Polar Engineering (ISOPE) Conference*, Paper No. ISOPE-2007-7, July 1-6, 2007, Lisbon, Portugal
- 21 Liu, M., Wang, Y.Y., and Long, X., “Enhanced apparent toughness approach to tensile strain design”, *Proceedings of 8th International Pipeline Conference*, Paper No. IPC2010-31386, September 27-October 1, 2010, Calgary, Alberta, Canada.
- 22 CSA Z662, “Oil and Gas Pipeline Systems,” Canadian Standards Association, 2007.
- 23 Wang, Y.-Y., Liu, M., Horsley, D., and Zhou, J., “A Quantitative Approach to Tensile Strain Capacity of Pipelines,” *Proceedings of 6th International Pipeline Conference*, Paper No. IPC2006-10474, September 25-29, 2006, Calgary, Alberta, Canada.
- 24 Wang, Y.-Y., Liu, M., Rudland, D., and Horsley, D., “Strain Based Design of High Strength Pipelines,” *Proceedings of the 17th International Offshore and Polar Engineering Conference (ISOPE 2007)*, Lisbon, Portugal, July 1-6, 2007.
- 25 Østby, E, “New strain-based fracture mechanics equations including the effects of biaxial loading, mismatch and misalignment”, *Proceeding of the 24th International Conference on Offshore Mechanics and Arctic Engineering*, Paper No. OMAE2005-67518, June 12-17, 2005, Halkidiki, Greece.
- 26 Sandvik, A., Østby, E, Naess A., Sigurdsson G., and Thaulow, C., “Fracture control – offshore pipelines: probabilistic fracture assessment of surface cracked ductile pipelines using analytical equations”, *Proceeding of the 24th International Conference on Offshore Mechanics and Arctic Engineering*, Paper No. OMAE2005-67517, June 12-17, 2005, Halkidiki, Greece.

-
- 27 Nyhus, B., Østby, E, Knagenhjelm, H.O., Black, S., and Røstadsand, P.A., “Fracture control – offshore pipelines: experimental studies on the effect of crack depth and asymmetric geometries on the ductile tearing resistance”, *Proceeding of the 24th International Conference on Offshore Mechanics and Arctic Engineering*, Paper No. OMAE2005-67532, June 12-17, 2005, Halkidiki, Greece.
 - 28 Minnaar, K. Gioielli, P.C., Macia, M.L., Bardi, F., Biery, N.E., and Kan, W.C., “Predictive FEA modeling of pressurized full-scale tests”, *Proceedings of the 17th International Offshore and Polar Engineering Conference*, July, 1-6, 2007, Lisbon, Portugal, P3114.
 - 29 Fairchild, D.P., Cheng, W., Ford, S.J., Minnaar, K., Biery, N.E., Kumar, A., and Nissley, N.E., “Recent advances in curved wide plate testing and implications for strain-based design”, *Proceedings of the 17th International Offshore and Polar Engineering Conference*, July, 1-6, 2007, Lisbon, Portugal, P3013.
 - 30 Kibey, S.A., Minnaar, K., Cheng, W., and Wang, X., “Development of a physics-based approach for the predictions of strain capacity of welded pipelines”, *Proceedings of the 19th International Offshore and Polar Engineering Conference*, June, 21-26, 2009, Osaka, Japan, P132.
 - 31 Kibey, S., Issa, J.A., Wang, X., and Minnaar, K., “A simplified, parametric equation for prediction of tensile strain capacity of welded pipelines”, *Pipeline Technology Conference*, October 12-14, 2009, Paper No. Ostend2009-039, Ostend, Belgium.
 - 32 Otsuka, A., et al., “Effect of Stress Triaxiality on Ductile Fracture Initiation of Low Strength Steel,” *J. of the Society of Material Science*, Japan, Vol. 29, No. 322, pp. 717-723, 1980.
 - 33 Toyoda, M., et al., “Criterion for Ductile Cracking for the Evaluation of Steel Structure under Large Scale Cyclic Loading,” *Proc. Of 20th International Conference on Offshore Mechanics and Arctic Engineering*, OMAE 2001-MAT-3103, 2001.
 - 34 Igi, S. and Suzuki, N., “Tensile Strain Limits of X80 High-Strain Pipelines,” *Proceedings of the 17th International Offshore and Polar Engineering Conference*, Lisbon, Portugal, July 1-6, 2007.
 - 35 Sadasue, T., Igi, S., Kubo, T., Ishikawa, N., Endo, S., Glover, A., Horsley, D., and Toyoda, M., “Ductile cracking evaluation of X80/X100 high strength line pipes,” *Proceedings of 5th International Pipeline Conference*, October 4-8, 2004, Calgary, Alberta, Canada.
 - 36 Gresnigt, A.M., “Plastic Design of Buried Steel Pipelines in Settlement Areas,” *Heron*, vol. 31, no.4, 1986
 - 37 Dorey, A., Murray, D.W., Cheng, J.J.R., “Material Property effects on Critical Buckling Strains in Energy Pipelines,” *Proceedings of IPC’02 – 4th International Pipeline Conference*, Calgary, 2002
 - 38 Suzuki, N., Ishikawa, N., Kondo, et.al., “Effects of Geometric Imperfection on Bending Capacity of X80 Line pipe,” *Proceedings of 6th International Pipeline Conference*, Paper No. IPC2006-10070, September 25-29, 2006, Calgary, Alberta, Canada.
 - 39 Sen, M., Cheng, J.J.R., et.al., “Mechanical Properties of Cold Bend Pipes,” *Proceeding of 6th International Pipeline Conference*, Paper No. IPC2006-10436, September 25-29, 2006, Calgary, Alberta, Canada
-

-
- 40 Fukuda, N., Yatabe, H., "Effect of Changes in Tensile Properties due to Cold Bending on Large Deformation Behaviour of High-Grade Cold Bend Pipe, *Proceedings of 4th International Pipeline Conference*, Paper No. IPC2002-27129, Calgary, 2002
- 41 Zimmerman, T., Timms, C., et.al., "Local-buckling and post-buckling behavior of high-strength line pipe," *Pipeline Technology Conference*, Ostend, 2004
- 42 Das, S, Cheng J.J.R., and Murray, D.W. "Wrinkle behavior under cyclic strain reversals in NPS12 pipes". *Proceedings of 2001 pipeline symposium*, IBP-OMAE, Rio de Janeiro, Brazil, OMAE2001-4010, 2001.
- 43 Das, S, Cheng J.J.R., and Murray, D.W. "Prediction of fracture in wrinkled energy pipelines subjected to cyclic deformations". *International Journal of Offshore and Polar Engineering*, Vol.17 (3), pp 205-212, 2007.
- 44 Zhang, Y.H. and Das, S. "Failure of X52 wrinkled pipeline subjected to monotonic bending deformation and internal pressure". *International Journal of Offshore and Polar Engineering*, Vol.18 (1), pp 50-55, 2008.
- 45 Suzuki, N., and Igi, S., "Compressive Strain Limits of X80 High-Strain Line Pipes," *Proceedings of the 17th International Offshore and Polar Engineering Conference (ISOPE 2007)*, Lisbon, Portugal, July 1-6, 2007.
- 46 Shitamoto, H., et al., "Evaluation of Strain Limit of Compressive Buckling by FE Analysis," *Proceedings of the 17th International Offshore and Polar Engineering Conference (ISOPE 2007)*, Lisbon, Portugal, July 1-6, 2007.
- 47 Mohr, W. C., "Strain-Based Design of Pipelines," final report to MMS, October 2003.
- 48 Mohr, W., "Weld Area Mismatch and Pressure Effects in Strain-Based Design," *Proceedings of the 4th International Conference on Pipeline Technology*, Edited by Rudi Denys, Ostend, Belgium, May 9-13, 2004, pp. 279-290.
- 49 Liu, M., Wang, Y.-Y., and Horsley, D., "Significance of HAZ Softening on Strain Concentration and Crack Driving Force in Pipeline Girth Welds," *Proceeding of the 24th International Conference on Offshore Mechanics and Arctic Engineering*, OMAE 2005, June 13-17, Kalkidiki, Greece.
- 50 Ostby, E., and Hellesvik, A., "Fracture Control of Offshore Pipeline JIP: Results from Large Scale Testing of the Effects of Biaxial Loading on the Strain Capacity of Pipes with Defects," *Proceedings of the 17th International Offshore and Polar Engineering Conference (ISOPE 2007)*, Lisbon, Portugal, July 1-6, 2007.
- 51 Wang, Y.-Y., Stephens, M., Horsley, D., "Preliminary Analysis of Tensile Strain Capacity of Full-Scale Pipe Tests with Internal Pressure," *Proceedings of the 18th International Offshore and Polar Engineering Conference (ISOPE 2008)*, Vancouver, Canada, July 6-11, 2008.
- 52 Shen, G., Tyson, W. R., Glover, A., Horsley, D., 2004, "Constraint Effects on Line pipe Toughness," 4th Intl. Conf. Pipeline Technol., 2, Scientific Surveys Ltd, Ostend, Belgium, pp. 703–720.
-

-
- 53 Nyhus, B., Østby, E., Knagenhjelm, H. O., Black, S., Rostadsand, R. A., 2005, “Experimental Studies on the Effect of Crack Depth and Asymmetric Geometries on the Ductile Tearing Resistance,” *Proc. Intl. Conf. Offshore Mechanics and Arctic Eng.*, OMAE2005-67532.
- 54 Drexler, E., Wang, Y.-Y., Sowards, J. and Dvorak, M., “SE(T) Testing of Pipeline Welds,” *Proceedings of the 8th International Pipeline Conference*, Paper No. IPC2010-31325, September 27 – October 1, 2010, Calgary, Alberta, Canada.
- 55 Shen, G., Gianetto, J. A., Tyson, W. R., 2009, —Measurement of J-R Curves Using Single-Specimen Technique on Clamped SE(T) Specimens,|| *Proc. 19th Intl. Offshore and Polar Eng. Conf.*, ISOPE, pp. 92–99.
- 56 Denys, R., De Waele, W., Lefevre, A., and De Baets, P., “An Engineering Approach to the Prediction of the Tolerable Defect Size for Strain-Based Design,” *Proceedings of the 4th International Conference on Pipeline Technology*, Edited by Rudi Denys, Ostend, Belgium, May 9-13, 2004, pp. 163-181.
- 57 Denys, R., De Waele, W., Lefevre, A., and De Baets, P., “Plastic Straining Capacity of Axially-Loaded Pipelines: Experimental Facts and Critical Considerations,” *Proceedings of the 4th International Conference on Pipeline Technology*, Edited by Rudi Denys, Ostend, Belgium, May 9-13, 2004, pp. 183-207.
- 58 Denys, R., Lefevre, A., De Baets, P., and Degrieck, J., “Effects of Stable Ductile Crack Growth on Plastic Collapse Defects Assessments,” *Proceedings of the 3rd International Pipeline Technology Conference*, Brugge, Belgium, May 21-24, 2000.
- 59 Liu, M. and Wang, Y.-Y., 2007, “Significance of biaxial stress on the strain concentration and crack driving force in pipeline girth welds with softened HAZ,” *Proc. of 26th Int. Conf. Offshore Mechanics and Arctic Eng.*, OMAE2007-29415.
- 60 Liu, M. and Wang, Y.-Y. 2007. Significance of Biaxial Stress on the Strain Concentration and Crack Driving Force in Pipeline Girth Welds with Softened HAZ. *Proceedings of the 26th International Conference on Offshore Mechanics and Arctic Engineering*, Paper No. OMAE2007-29415, San Diego, June 10-15.
- 61 Wang, Y.-Y., Liu, M., Chen, Y. and Horsley, D. 2006. “Effects of Geometry, Temperature and Test Procedure on Reported Failure Strains from Simulated Wide Plate Tests.” *Proceedings of the 6th International Pipeline Conference*, Paper No. IPC2006-10497, Calgary, September 25-29.
- 62 Gioielli, P.C., Minnaar, K., Macia, M.L. and Kan, W.C. 2007. Large-scale Testing Methodology to Measure the Influence of Pressure on Tensile Strain Capacity of a Pipeline. *Proceedings of the Seventeenth (2007) International Offshore and Polar Engineering Conference*, ISOPE, Lisbon.
- 63 Østby, E. and Hellesvik, A.O. 2007. Fracture Control – Offshore Pipelines JIP: Results from Large Scale Testing of Biaxial Loading on the Strain Capacity of Pipes with Defects. *Proceedings of the Seventeenth (2007) International Offshore and Polar Engineering Conference*, ISOPE, Lisbon.
- 64 Wang, Y.-Y., Liu, M., Gianetto, J., and Tyson, B., “Considerations of Line pipe and Girth Weld Tensile Properties for Strain-Based Design of Pipelines,” *Proceedings of the 8th International*
-

-
- Pipeline Conference*, Paper No. IPC2010-31376, September 27 – October 1, 2010, Calgary, Alberta, Canada.
- 65 Tsuru, E., Shinohara, Y., and Asahi, H., “Evaluation of Precept of Strain Capacity of High Strength UOE Line Pipes Used in Strain-Based Design Applications,” *Proceedings of the 17th International Offshore and Polar Engineering Conference (ISOPE 2007)*, Lisbon, Portugal, July 1-6, 2007.
- 66 Ishikawa, N., Okatsu, M., Shimamura, J., Endo, S., Shikanai, N., Muraoka, R., Kondo, J., and Suzuki, N. “Material Development and Strain Capacity of Grade X100 High Strain Line pipe Produced by Heat Treatment Online Process,” *Proceedings of 7th International Pipeline Conference*, September 29-October 3, 2008, Calgary, Alberta, Canada.
- 67 Wang, Y.-Y., Liu, M., McColskey, D., Weeks, T., and Horsley, D., “Broad Perspectives of Girth Weld Tensile Strain Response,” *Proceedings of the 8th International Pipeline Conference*, Paper No. IPC2010-31369, September 27 – October 1, 2010, Calgary, Alberta, Canada.